Stony Brook University

Development of the First Comprehensive Neural Connectivity Map of the Mouse

A Dissertation Presented

by

Vadim Pinskiy

to

The Graduate School

in Partial Fulfillment of the

Requirements

for the Degree of

Doctor of Philosophy

in

Biomedical Engineering

Stony Brook University

May 2012

Stony Brook University

The Graduate School

Vadim Pinskiy

We, the dissertation committee for the above candidate for the

Doctor of Philosophy degree, hereby recommend

acceptance of this dissertation.

Partha P. Mitra, Ph.D., Advisor
Professor
Cold Spring Harbor Laboratory

Emilia Entcheva, Ph.D., Committee Chair
Associate Professor
Department of Biomedical Engineering

Richard A. F. Clark, Ph.D.
Professor
Department of Biomedical Engineering

Joshua Dubnau, Ph.D., External Member
Associate Professor
Cold Spring Harbor Laboratory

Kathleen Rockland, Ph.D., External Member
Senior RIKEN Research Fellow
Picower Institute for Learning and Memory, Massachusetts Institute of Technology

This dissertation is accepted by the Graduate School

Charles Taber
Interim Dean of the Graduate School

Abstract of the Dissertation

Development of the First Comprehensive Neural Connectivity Map of the Mouse

by

Vadim Pinskiy

Doctor of Philosophy

in

Biomedical Engineering

Stony Brook University

2012

Brain function is dictated by its circuitry, but currently we know comparatively little about how the mammalian brain is connected: only 10% of all mesoscale connections in the most studied mammal (rat) have been catalogued and only perhaps one third have been probed at all. To address this knowledge gap, this dissertation is focused on the development of a semi-automated pipeline to enable high-throughput neuroanatomy in mouse, and the use of that pipeline to assemble the first brain-wide connectivity map in mouse. The pipeline was assembled in its entirety as part of this dissertation work, in a top-down design approach of five principle subsystems: (1) Tracer Injection; (2) Brain Fixation and Freezing; (3) Brain Sectioning; (4) Section Staining; (5) Whole-slide Section Imaging and Data Analysis. For each subsystem, conventional neuroanatomy techniques were innovated to facilitate pipeline integration and maximize efficiency. Key innovations include: computer guided stereotactic neurosurgery using a skull scan, a method of freezing mouse brains in stereotaxic coordinates and tape-transfer assisted cryosectioning. Along with whole-slide imaging, these innovations allow for accurate injections to be placed throughout the regions of the brain, in a uniformed manner, across thousands of animals and for the brain of each animal to be finely sampled and imaged in its entirety. The result is an unprecedented view of each injection and each brain, made available to the community through a public web portal. Instead of a few images per experiment, that are

published in literature, all the sections of a given experiment (~500 per brain) can be accessed through this portal by anyone. All brains have roughly the same number of sections and span the entire brain. Comparing specific structures in all brains is possible. This work has the potential to transform neuroanatomy in the same way that the Allen Mouse Brain Atlas changed rodent neurogenetics.

To Alexandra and Marc Benjamin Pinskiy

Engineering ... it is a great profession. There is the fascination of watching a figment of the imagination emerge through the aid of science to a plan on paper. Then it moves to realization in stone or metal or energy. Then it brings jobs and homes to men. Then it elevates the standards of living and adds to the comforts of life. That is the engineer's high privilege.

The great liability of the engineer compared to men of other professions is that his works are out in the open where all can see them. His acts, step by step, are in hard substance. He cannot bury his mistakes in the grave like the doctors. He cannot argue them into thin air or blame the judge like the lawyers. He cannot, like the architects, cover his failures with trees and vines. He cannot, like the politicians, screen his shortcomings by blaming his opponents and hope the people will forget. The engineer simply cannot deny he did it. If his works do not work, he is damned....

On the other hand, unlike the doctor his is not a life among the weak. Unlike the soldier, destruction is not his purpose. Unlike the lawyer, quarrels are not his daily bread. To the engineer falls the job of clothing the bare bones of science with life, comfort, and hope. No doubt as years go by the people forget which engineer did it, even if they ever knew. Or some politician puts his name on it. Or the credit it to some promoter who used other people's money ... but the engineer himself looks back at the unending stream of goodness which flows from his successes with satisfactions that few professionals may know. And the verdict of his fellow professionals is all the accolade he wants.

(Herbert Hoover)

Table of Contents

List of Figures

List of Tables

List of Abbreviations

µL	Microliter
µm	Micrometer
10G	10 Gigabit Ethernet
ABC	Avidin Biotin Complex
ARA	Allen Reference Atlas
BDA	Biotinylated Dextran Amines
CCD	Charge-Coupled Device
Co	Cobalt
$CoCl_2$	Cobalt Chloride
CT	Computed tomography
CTB	Cholera Toxin, Subunit B
DAB	3,3'-Diaminobenzidine
ETOH	Ethanol
EVOP	Evolutionary Operations
GB	Gigabyte
GUI	Graphical User Interface
HC	Histochemistry
HCl	Hydrochloric Acid
HRP	Horseradish Peroxidase
IHC	Immunohistochemistry
LED	Light-emitting Diode
LIMS	Laboratory Information Management System
MBA	Mouse Brain Architecture Project
MRI	Magnetic Resonance Imaging
N	Nissl Stain
NA	Numerical Aperture
NEG50	Embedding Medium, Richard Allan Scientific
Ni	Nickel
$NiSO_4(H_2O)_6$	Nickel Ammonium Sulfate
OCT	Optimal Cutting Temperature Embedding Medium, Tissue-Tek Corporation
PBS	Phosphate Buffered Saline
PCB	Printed Circuit Board
QC	Quality Control
r	Optical Resolution
RGB	Red-Green-Blue
ROI	Region of Interest
SLA	Stereolithography
SNR	Signal-to-noise Ratio
SOP	Standard Operating Protocol
TB	Terabyte
TBS	Tris-buffered saline
TDI	Time Delay and Integration Sensor
UV	Ultraviolet Light

PROLOGUE:

In this dissertation, an engineering approach is applied to help answer fundamental neuroanatomy questions. An industrial scale machine was designed as part of this effort. Much of the work was focused on designing the machine from the ground-up and optimizing the performance of each element. To gain an appreciation for this work and the need for this engineering approach, it is best to first look at the material produced by this system. Therefore, the reader is encouraged to first look at *Chapter 5* and then through the rest of the dissertation document. This chapter presents a short tutorial on the data generated by this engineering system for the mouse connectivity project. A Technical White Paper on this project, can be found in Appendix A. Auxiliary projects are extensively described in the tutorial, as a means of illustrating the broader applications of this system to many neuroanatomical questions. The tutorial shows sample data from around two-dozen different brains - representing just *2%* of the total number of brains processed as part of this work. In terms of volume, over the last year, 1300+ mouse brains have been cut into 650,000+ sections (at a thickness of 20µm) and mounted onto over 100,000+ glass slides. These slides have been digitized into 300+ Terabytes of raw data.

This engineering system is referred to as a "pipeline" throughout this dissertation, is a tool which facilitates scientific analysis. It is not itself an answer to a fundamental question, but is the means of using current technologies to help answer those scientific questions. The pipeline was constructed to help answer the question: "what is the whole brain connectivity of the mouse?". Chapter 1 of this dissertation aims to establish the need for this engineering system and the significance of a whole-brain connectivity map. Chapter 2 focus on the designed and assembly of the system. Chapters 3 and 4, describe novel methods that resulted from this work.

CHAPTER 1: Introduction

1.1. The Missing Circuits

Long-range neuronal projections connect populations of nerve cells to each other across the whole brain and thus orchestrate all high-level cognitive and sensorimotor functions of an organism. Though the importance of these projections has long been established, surprisingly little is known about them. For example, in the most-studied mammal (rat), only 10-30% of all connections have been probed[1]. In the human, even less is known about neural connectivity--almost no long-range projections have been mapped, and most of the brainwide histological studies that were performed are more than a century old. These knowledge gaps in mammalian neuroanatomy are a substantial barrier to understanding how the brain executes its functions.

If it were necessary to map every synaptic connection between every neuronal pair, every gap junction, and the spatial geometry of diffusely released neuromodulatory substances from every neuron, then mapping nervous system connectivity would be an unrealistically difficult task. Moreover, since brains show individual variation at these microscopic scales, one would have to map many brains at this impractical scale in order to gain a sense of the individual variations and invariances – an even more prohibitive task. Such microscopic mapping has not been done for even a small brain such as the fruit fly, about a quarter of a millimeter in size. The full electron microscope based neuronal process mapping of the fly brain is a large scale, ongoing experimental project at the Janelia Farms research campus of the Howard Hughes Medical Institute, and even data for the optic lobe of the fly has not yet been released.

However, there is an intermediate scale of organization at which the whole brain connectivity architecture can be meaningfully mapped today. This is because the brain has non-random organization at an intermediate *mesoscale*, consistent with classical neuroanatomical atlases in which nuclei, layers, and different cytoarchitectonic regions are defined. Mapping the circuit architecture of the entire brain at this scale can be done using injection based tract tracing methods described in more detail in the following section. Enabling the mapping this mesoscale circuit architecture, for the first time, is the driving scientific goal of this dissertation. The rationale for such a project has been extensively discussed elsewhere (see the position paper by Bohland et al, “A Proposal for a Coordinated Effort for the Determination of Brainwide Neuroanatomical Connectivity in Model Organisms at a Mesoscopic Scale”, PLOS

computational Biology (2009)). Briefly, these include: (i) enabling comparative and evolutionary studies of the circuit architecture across species, as was the case for genomes; (ii) elucidating the phenotype-genotype relationship for behavior, and therefore addressing the "missing heritability" problem in psychiatric genetics by studying a critical intermediate phenotype, (iii) enabling better theoretical treatment of brain function and improving experimental design in neuroscience. Since the commencement of the project, interest in mapping neuronal circuitry has only grown, as shown by numerous articles in both the scientific and popular press.

1.2. Tract Tracing Methods

Systematic dissection of the brain is the precursor to all modern neuroanatomy methods. The works of Vesalius[1], Steno[2] and others, showed that careful dissection of the brain can be used to differentiate white and grey matter and that large fiber bundles can be traced through the brain. Nissl, Golgi, Weigert, Marchi[6, 7] and Gudden[8], advanced this science by providing the ability to identify specific organelles (the endoplasmic reticulum, the Golgi apparatus, etc.) and processes, across the entire brain[9]. Dejerine was able to use these fundamentals to "describe radicular myotomes and dermatomes, the somatotopy and connections of the pyramidal tracts, the aberrant corticobulbar bundles (explaining for example central facial palsy in medullary lesions), the ascending sensory tracts, and the connections between the thalamus and the cerebral hemispheres"[10]. The "Anatomie des centres nerveux" is one of the most comprehensive works of neuroanatomy and is still widely referenced today[11-13]. The major drawback of these methods was the inability to trace individual fibers or even select groups of fibers across the brain.

It was not until the early 1970s that tools became available to perform targeted tractography. These methods were based on active axonal transport. Specific tracer molecules would be injected into live animals (under anesthesia), as part of a stereotaxic surgery. The molecules would pass through the circuit over the course of several days to weeks, after which, the animal would be sacrificed and the location of injected molecules would be determined. The first such tracers were radiolabeled amino acids incorporated into cell proteins and transported in the anterograde direction (cell body → synapse)[14]. Autoradiography would be used to detect the location of the radiolabeled isotopes. The main limitation of this method was the lack of resolution compared with antibody based tracers. One such tracer, which is still extensively used,

is the enzyme horseradish peroxidase (HRP), which can be detected using diaminobenzidine(DAB) as the substrate[15-17].

coarser ↓ finer

Procedure	Used in	Spatial specificity	Brief Description
Gross dissection (1543)	postmortem human	major fiber bundles	classical "hands on" anatomy
Myelin stains (1882)	any species	large and fine myelinated axon bundles	ferric chloride and hematoxylin stain myelinated fibers deep blue
Degeneration Methods (1885-1950's)	any species	degenerating axon bundles	e.g. silver impregnation selectively labels degenerating fibers from a lesion site
Diffusion-based MR imaging (1990 -)	primates including human	major fiber bundles	MR imaging of water diffusion direction + reconstruction
Neuronal tracers (1968 -)	rodents, primates, postmortem human	Single neurons and/or fibers down to neural processes	active or passive transport of injected substances
Transgenesis (1990 -)	mice, drosophila	fiber bundles down to neural processes	selective expression of genes to label specific cells
Viral gene transfer (1998 -)	rodents, non-human primates	fiber bundles down to neural processes	selective expression of genes to labels specific cells
SPIM / Ultramicroscopy (2007)†	rodents	single cell	planar imaging of whole sample
Volume EM reconstruction (2004 -)†	any species	nanometer resolution; single boutons, spines, receptors and other subcellular organelles	serial scanning of ultrathin sections, or block-face scanning of three-dimensional volumes

Table 1: Techniques for determining neuroanatomical connectivity
Imaging methods that can be used in conjunction with dyes and tracers, etc. for detailed reconstruction of micro circuitry.[18]

Horseradish Peroxidase was an enabling factor, which opened the door to localized tract tracing. The main problem with HRP was speed of tracing and lack of neurite resolution. Retrograde tracing with HRP gave way to more sensitive antibody based methods: Cholera Bacterial Toxin subunit B (CTB) and Biotinylated Dextran Amines (BDA). CTB is predominantly a retrograde tracer (synapse → cell body) that has been used extensively to label fine processes throughout the brain and has been shown to be one of the most stable tracers for routine tractography[19]. Depending on the molecular weight, BDA can be used either as an anterograde (≈10kDa,) or retrograde tracer (≈3kDa). Unlike other tracers, BDA is already conjugated with biotin, so the best way to detect the tracer is through a simple two step procedure: (1) Incubation in avidin-biotinylated HRP (ABC)[20], followed by (2) a DAB reaction. This procedure is significantly more robust, than that of other anterograde tracers, such

as PHA-L[21]. A summary of the other common neuronal tracers and the methods used to visualize them are described in Table 1 [18].

The application of the methods described above has mostly, been limited to individual brain regions and targeted connectivity studies, answering questions, such as: what are the projection patterns of a given nucleus of the thalamus? Application of these methods on the whole brain-level even in small rodents, was, until recently, deemed unfeasible because the downstream technology needed to process the data, did not exist. As an example, though massive slide collections of neuroanatomical material exist, they are rarely used, even by those who know about them. Occasionally there is a study which has used material from the Yakovlev-Haleem collection[22], for clinical comparison, but these instances are quite rare. *The bulk of the slides have remained untouched since their production.*

It is only in the last decade, that advances in automated light microscopy and computer hardware/software have converged to allow for a means to convert these massive slide collections into digital, high-resolution image data, which can be used throughout the community. Dr. Edward Jones, is one of the pioneers that has led the effort to "digitize" neuroanatomy, and has produced one of the most comprehensive sources for neuroanatomy material on the internet: www.brainmaps.org[23]. By using an Aperio whole-slide microscope, Dr. Jones was able to produce high-resolution datasets (up to .5µm/pixel) of various species, as a function of multiple experimental conditions.

Though successful at reaching a broad audience and provide high-resolution data that can be used for a range of neuroanatomy studies, www.brainmaps.org lacks overall data cohesiveness. This database was amassed from existing slides collections, donated by different laboratories, which used different processing techniques to produce the slides. As an example, for Mus Musculus, out of the twenty-three series displayed on the website, only four series (same sectioning plane) have the same number of slides. As such, digitizing existing slide collections is best suited to provide a broad historical view of neuroscience, and also to provide comparative studies across species that are not normally available to neuroscientists working on major model organisms and may in cases be endangered.

To answer focused "big picture questions", an approach that combines experiential data gathering with modern imaging technology, is needed. One of the most successful applications of this integrated approach to whole-brain data collection was performed by the Allen Institute

for Brain Science. Though the institute has diversified its focus in recent years, its first major effort was generating the "Genome-wide atlas of gene expression in the adult mouse"[24]. This effort involved the use of several thousand 56 day-old C57BL/6 mice. For a series of target genes, a mouse brain was sectioned and stained, for both cell body morphology (Nissl) and gene expression (in situ hybridization), across the entire brain. The processed slides would then be digitized using several Leica DM6000B (.95μm/pixel) microscopes, and posted on a public data portal. The resulting database, is one of the most expensive digital anatomical collections on the internet and an excellent resource for gene expression studies.

Though successful, the Allen Institute did not place a focus on method development. Instead, they used commercial technologies, without customization and overcame native limitations with a large budget. The approximate budget for the gene expression atlas was in the neighborhood of $50M. Investigators outside the institute do not have access to such a sum and therefore, cannot directly replicate or further the work of the institute. Because of this, and known discrepancies within the atlas (gene expression mismatch between coronal and sagittal planes), one of the biggest criticisms of the institute data set is the lack of replicates in the data.

To address these problems, an engineering based approach to high-throughput neuroanatomy must be taken. Unlike previous efforts, this approach should not focus directly on a given scientific question, but rather focus on the design of a platform that allows for broad use across neuroscience. As it is becoming clear that genetics alone cannot be used to fully understand disease states or general workings of biology[25], this industrialization of modern neuroanatomical methods will an invaluable asset. As part of this project, we aim to assemble such a pipeline and use it to develop the first comprehensive neural connectivity map of the mouse. Similar in principle to the recent work in Drosophila[26], the resolution and scope of this map will be proportional to the size of the animal and the complexity of the wiring network.

CHAPTER 2: High-Throughput Histology System Design

2.1. An Engineering System's Approach to the MBA Pipeline

A major component of this dissertation was to construct a high throughput pipeline for automated histology, which was then used for a number of scientific projects, primarily the Mouse Brain Architecture (MBA) project to map the neural circuit architecture of the brain. The creation of this pipeline was an exercise in engineering systems design and implementation. The system thus generated represents a next generation of systems neuroscience research, in which the efficiencies and standardization of engineering will be brought to bear on challenging neuroscientific questions for which the methods have so far been of a significantly more ad hoc, labor intensive nature.

In designing and implementing the MBA pipeline, theoretical engineering concepts were employed at the level of the overall system design, in addition to the more detailed engineering work involved in the individual components of the pipeline. In this chapter, we present both the big picture motivations, as well as details of the individual components of the MBA pipeline. Therefore, this chapter constitutes the core of this dissertation. Some of the sections of the chapter are further expanded in subsequent chapters and meant to be published as independent manuscripts.

2.1.1. Overall Specifications of the MBA Pipeline.

In the usual “black box” approach, an engineering system is composed of discrete elements, each with a well defined purpose (usually characterized by an input-output relationship). These are integrated to produce a single system, also characterized by an overall input-output relationship. While this may seem a conceptual triviality, it is in fact useful to guide our thinking of what is in fact a rather complex object.

We may think of the MBA pipeline as a system set up to answer specific neuroscience questions. The primary question of interest to us has been: "What is the whole-brain connectivity diagram of the mouse?". To answer this question, the pipeline was given some inputs, and specific outputs are expected; however, as we will see later, the pipeline is also useful in answering other neuroscience questions (e.g. cell density of inhibitory interneurons).

For the MBA connectivity mapping project, inputs to the pipeline were: (1) a specific mouse strain/age/sex: 56 day old male C57BL/6 mouse; (2) injection grid and tracer choices. In making the choices of the animal model (in 1) we were influenced by the Allen Brain Institute for and the high throughput neuroanatomical study produced by them of the mouse brain. The choice of the grid-based approach to neuronal tractography (in 2) originated through discussions organized by our group at CSHL since 2006 (and has been adopted by other competing projects, at the Allen Institute and UCLA). The specific injection scheme is to follow a grid-like approach, with a total of 250 sites, evenly distributed across the brain. In choosing the grid algorithmically, regional borders were avoided [27]. Further, the choice was made that each site be injected with four tracers, in four different mice, namely a classical anterograde and retrograde tracer (BDA and CTB respectively, with subsequent histochemical processing and brightfield imaging), and a viral anterograde (AAV 1/9) and viral retrograde (modified Rabies virus) tracer, with subsequent fluorescent imaging. This approach allows for a comprehensive study of the inputs and outputs of each injection site, distributed over the whole-brain.

The outputs of the system are: (1) a searchable and browsable catalog of brainwide projections in individual mice for each tracer, and (2) a unified dataset, obtained by co-registering these individual brains together, so as to provide the desired brainwide connectivity atlas. This second output requires co-registration of project brains onto a single reference atlas. The Allen Reference Atlas has been chosen for this purpose for the MBA project.

Given the nature of the project, the pipeline parameters and even the injection grid have undergone evolution based on intermediate results from the pipeline, so that the pipeline design has not been entirely static. One may regard this as a result of a feedback process in which system output has caused adaptive changes to the system as well as to its control inputs. In addition to this overall feedback on a relatively slow timescale, there have been also faster feedback loops around the individual stations of the pipeline, to fine tune or to improve individual pipeline components. Three classes of performance criteria have been utilized to improve the system: (1) maximize system reliability; (2) maximize data quality; (3) maximize system throughput.

2.1.2. Functionality and Performance of the System

The MBA pipeline essentially transforms a mouse into a large data cube. The pipeline contains five stages and has three important transformations: (1) Mouse → Extracted Brain with Tracer Injection; (2) Brain → Sections on Slides; (3) Sections → Digital Image Stack. These transformations jointly determine the rate limiting steps as well as overall data quality. Overall performance of the system can be assessed on the basis of data quality and rate of data production at each of these transition points. Optimal performance of the system occurs when the maximum data rates of each system component are matched, and when the final data quality is determined by the injection placement (rather than process issues).

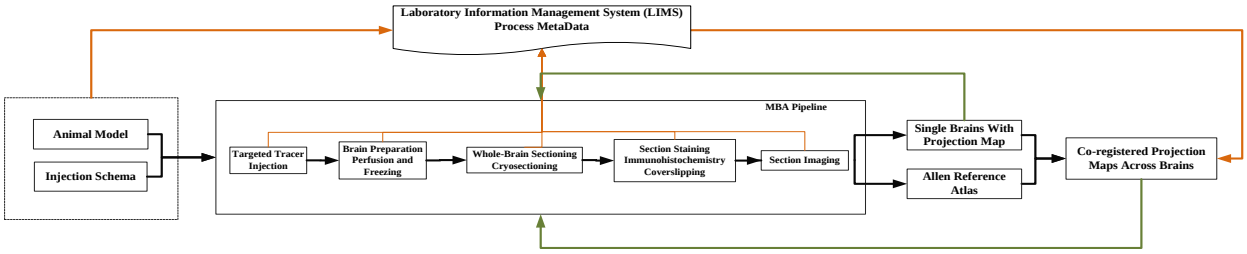

Figure 1: System Workflow Diagram

Data quality is measured along two axes: (1) biological quality and (2) process quality. The biological quality depends on whether labeled neuroanatomical connections can be adequately identified and characterized based on the experimental design. The process quality deals with the ability of the system to correctly process the brains without distortion or damage, with adequate histological labeling, with correct imaging, etc. The goal of the system is to obviously maximize both of these quality factors, but in terms of system design the focus is on process quality.

2.1.3. Component Relations and Dependencies

The five principle stages of the MBA pipeline are each governed by a set of control variables. These variables define the individual performance of each component and also contribute to the overall performance of the pipeline. Therefore, the collection of these control variables should be thought of as a joint set of experimental parameters, and the relationship between these components needs to be carefully examined and monitored.

A primary relationship, between the different stages of the pipeline, are that of a linear dataflow and the need for matching data rates for optimal performance. Downstream components need to have a data rate, equal to or greater than that of upstream components, or the system will

be inefficient and bottlenecked. If this is the case, it is vital to either improve the data rate of the downstream components (by increasing number of units) or to reduce the rate of upstream components. The latter strategy can be advantageous, because it allows for the improvement of upstream data quality or a better distribution of resources, system wide. The other option is to give up the linear flow through the system and create material/data holding areas - these are points in the system where material/data can accumulate without expiration (reduction in quality). When these intermediate data buffers or reservoirs are full, upstream processes have to be stopped so that the reservoirs can be partially emptied out by downstream processing. Since the upstream processes may naturally fluctuate in rate, due to different causes (e.g. reagent stock depletion), these buffers act like capacitors in an electrical circuit, and therefore smooth out temporal fluctuations.

A convenient insertion of these holding areas is immediately following a change in the material/data state (transition state). In our case, there are three such buffers: a store of frozen brains, a store of slide collections, and a store of digitized data sets. It is important that the material/data do not degrade in time in these reservoirs, for example, we have prioritized the processing of fluorescent brains over histochemically stained ones since the former have a significant decay rate over the experimental timescales).

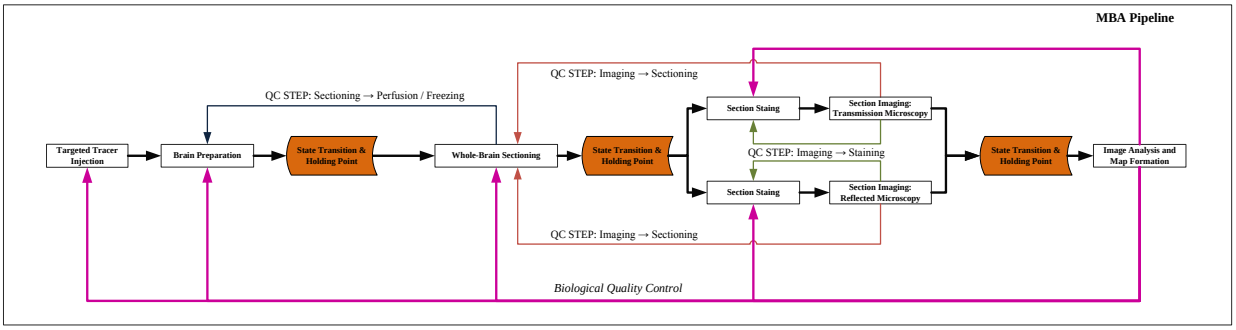

Figure 2: Organization and data flow of the MBA Pipeline

In addition to throughput rates, another constraint governing the system is the relation between the parameters of whole-brain sectioning, with parameters for the downstream components (section staining and imaging). One primary parameter in this regard is "section thickness.".This determines: (1) the staining rate, as any stain needs to penetrate through the entirety of the tissue and (2) the imaging resolution, by setting the spacing between physical sections. This parameter is determined by combining the experimental requirements with the system performance (e.g. processing rate).

The above relationships are static in nature - once optimized for the system, they should not be altered, unless there is feedback from final data quality assessment, which governs the final selection of all variables. The system, however, also contains intrinsic dynamic relationships, which are the local feedback loops that are mentioned above. These feedback loops are essentially Quality Control steps that validate that the previous step was performed according to specifications. This local Quality Control is not a substitute for or even an analog to the final assessment of the data, but rather serves as a means of improving the performance of the individual components of the system.

The MBA pipeline can be thought of as a simple dynamical system, with inputs and outputs as well as local feedback loops, and designing the pipeline presents an exercise in process control engineering. While we have not employed formal control theoretic methods in engineering the system, or constructed a simulator, we have encountered multiple issues that are amenable to control and dynamical systems analysis. We have employed qualitative insights from feedback control systems in the process of designing and developing the pipeline. In the future, it should be possible to further formalize the design and analysis of the MBA pipeline as an engineered dynamical system.

2.1.4. Appropriate Level of Automation

Robotic automation of a complex process is a double-edged sword. On one hand, it brings the promise of greatly improving the overall efficiently of a process, by improving throughput and minimizing variability. On the other, robotic automation can increase the number of failure modes and complicates real-time debugging (as opposed to an investigator performing bench top experiments). For components that do not have established robotic solutions, commercial or otherwise available, the development cycle of a fully working robotic system needs to be considered. This development cycle is obviously dependent on the complexity of the action to be automated. For this reason and in consideration of finite resources (i.e. time and money), full robotic automation could not be applied to the MBA pipeline as a whole, although this remains a desirable future outcome. Rather, robotic automation is currently an ergonomic enhancement to the previously fully manual laboratory process for these experiments. As such,

the system can be considered semi-automated; it contains automated stages, but manual control and intervention are required between the stages.

We were able to adopt existing solutions to largely automate two stages: section staining and section imaging. Automated whole-brain sectioning is not currently available and will require significant technology development. Due to the manual dexterity required in the current procedure, we kept it manual, with standardization introduced by the Tape Transfer technique, described in a later chapter of this dissertation. Section staining and imaging are appropriate for automation because in each case, a human agent does not interact with the fragile biological material directly, but rather with the support media, the glass slides on which the sections are mounted during the whole-slide sectioning. This allows standard robotic techniques to be applied.

In terms of staining, this means that the robotics just need to apply controlled amounts of reagents, each for a finite period of time. The solutions to be applied, the incubation time and the solution volume are all process specific (stain specific). In terms of imaging, the optics of a conventional microscope are constrained for both transmitted and reflected light, to a relatively small field-of-view that is governed by the magnification and numerical aperture of the optics. For neuroanatomical applications to whole mouse brain sections (or larger brains), this conventional microscopy field-of-view is significantly smaller than the size of a single section. For this reason, the main element of robotics in the imaging component, is to allow for in-plane translation of the section, around the fixed optics. This results in the entire section being imaged, in discrete images (discrete tiles). These tiles can then be combined into a unified mosaic, representing the entire section. For both components, the essential requirement is that the robotics must be able to perform the given task not just for one section or one slide, but rather for a large number of slides. The whole-brain sectioning component produces ~200 sections per brain.

The recording of process meta-data and the process knowhow is an integral aspect of the system design. The design and implementation of the LIMS (Laboratory Information Management System) is key to effective automation of the components. In the spirit of semi-automation, the LIMS system was designed to facilitate data-entry into a common database, by the human operators of the different stages of the system. We have also produced an extensive

set of Standard Operating Protocols that have served both to standardize operation of the laboratory by individual technicians, and to provide training to incoming technicians.

2.1.5. Comparing Our Systems Approach to Existing Practices

In neuroanatomy, much like in many biological fields, the laboratory protocols are rarely subjected to engineering style optimization. These methods have been developed over time, at individual laboratories, for "optimal performance" and are essentially "written in stone". The result is often protocols that are fixed by historical accident, but not necessarily optimal. This technical expertise/knowhow is also investigator/technician dependent. The expression: "magical hands", is sometimes used to describe a particular technician responsible for generating a good dataset. As a result, there is little formal quality control feedback in the system and process inefficiencies remain unresolved. The system's approach presented in this dissertation, is an attempt to address this fundamental problem, by employing an engineering design techniques for the system. By treating all of the components, as part of a single system, instead of as stand-alone elements, we tried to optimize the overall global performance of the MBA pipeline. As part of this re-evaluation of involved engineering methods, one is able to critically examine the choice of "accepted" optimization parameters and document the selection accordingly.

Our approach allows for better process scalability. This is not just a matter of increasing the number of animals that the established pipeline can support, but also ensuring that economies of scale occur. Per-sample marginal cost for supplies and personnel should ideally decrease with the total number of animals to be processed. We indeed obtained such economies of scale by paying attention to process efficiency and automation.

Another consideration is the scaling of brain sizes. As the field advances towards whole-brain connectivity mapping of larger brains, process complexity will increase. The fundamental elements of processing mouse tissue may be scaled up to rats and primates. In fact, we have processed rats through the MBA pipeline, with minor modifications to our process. Human tissue may also be processed by the same procedures, with the caveat that injection based tractography is inapplicable to human since it has to be done in a live organism. For all post-mortem neuroanatomical work, the fundamental elements are: whole-brain sectioning, section staining and section imaging. As a result, the system used to process mouse tissue can be directly

adapted to handle larger brain samples by adjusting the specifics of each component. The interaction/integration of the components remains unchanged.

The main advantage of the system's approach, is that by standardizing the methodology and improving the *process quality* of the data, an efficient platform was created to improve *biological data quality*. In the terms of connectivity, this takes the form of investigating different neuronal tracers and comparing their whole-brain effectiveness. As an example, viral tracers, though extensively cited in literature, have not been validated on the whole-brain level. In particular, our project provides the first whole-brain study utilizing the retrograde Rabies virus as a neuronal tracer.

2.2. System Design and the Industrialization of Neuroanatomical Methods

2.2.1. Design Approach: "Do not reinvent the wheel, change the lug nuts and the rubber"

The system's approach discussed above, calls for a re-evaluation of the methodology at each component of the process, to maximize efficiency. This re-evaluation must be performed in the context of practical considerations for development time, cost and available manpower. For this reason, a ground-up redesign of any component will not be feasible. Commercial equipment needs to be used for each required redesign and optimization. Commercial equipment intended for clinical applications - clinical pathology - can be adapted for neruoanatomical applications. Clinical equipment is generally designed for low-failure and high-reproducibility of process, which makes it ideal for this application. Clinical pathology is a mainstream medical field, and many companies have developed specialized commercial equipment to address specific needs. The general problem with clinical equipment is that the above advantages come at the expense of functional versatility, cost (initial and reoccurring) and component integration. This makes the adaptation of clinical equipment non-trivial but still offers the ability to use equipment that would otherwise be unavailable.

For each component of the engineering system, the basic design and system integration procedure is: (1) evaluate existing neuroanatomy procedures and equipment; (2) identify possible process inefficiencies and limitations of method; (3) explore means of addressing the process problems; (4) design, manufacture or purchase, test and implement the solution. If the existing

Neuroanatomy methodology is acceptable, replicate setup from literature; (5) Validate optimal integration of the component into the system as a whole. Innovation should not be performed for the sake of innovation, but rather to solve a concrete methodological problem.

For components that require extensive redesign and retooling, it is vital to minimize the manufacturing cost and lead time. Conventional manufacturing techniques are not ideal for low-volume production of specialized equipment. Emphasis should be placed on utilizing rapid manufacturing methods, such as stereolithography (SLA). SLA is "3D printing", in which a resin and support material are placed in a recursive manner, layer-by-layer, until a given part is created. The resin is than "hardened" through a curing step, the support material is removed and the part can be used. As a printing process, SLA production is fully automated and very fast - the cost of material is the only expenditure per part and the cost is per volume of material, not by the complexity of the part. For low-volume components, SLA costs around 10X less than conventional manufacturing. Most parts can be "printed" in the matter of hours. Recent developments in SLA technology have increased the strength of available materials, reduced the degradation of the resulting parts and improved the manufacturing resolution. SLA is not appropriate for the production of load bearing parts (extended term durability is significantly lower than that of machined plastics or metals), but is very suitable for all other type of parts. Besides a reduction in lead-time and manufacturing cost, SLA offers the ability to produce parts that would otherwise be impossible to create. A classic example is the creation of a solid cube, with a hollowed center, or a solid rectangle with a complex network of embedded hollow channels[28, 29].

2.2.2. Tracer Injections

2.2.2.1 Component Function and Basic Requirements:

This system component integrates the Animal Model, with the Injection Schema, by targeted injection of a neuronal tracer into a specific region in the brain. This is a survival surgery, which means the well being of the animal is of the upmost importance and proper animal handling procedure needs to be followed. It is also vital to establish a standardized environment for the animals and ensure that the surgical procedure does not condition the animal's behavior. The effectiveness of the procedure is the main determinant of the overall

biological data quality of the system. The role of the downstream components of the system is to detect the signal from the cells/fibers that are labeled as part of this process.

To support the specified injection schema, this component must allow for injections to be placed throughout the regions of the brain and for different tracers to be used in the system. To ensure whole-brain coverage of injections, it is vital to maximize the accuracy and repeatability of injections, by maximizing the precession of the mechanics of the system and the volume control of the system. Volume of injection is a critical variable, with direct relation to the efficacy of the tracer. By maintaining tight tolerances on the volume of injection, and maintaining consistency in the titer of the tracer, one can standardize the injection region. For retrograde tracers (CTB and Rabies virus), one can standardize the number of cells that are labeled.

This system component integrates the Animal Model, with the Injection Schema, by targeted injection of a neuronal tracer into a specific region in the brain. This is a survival surgery, which means the well being of the animal is of the upmost importance and proper animal handling procedure needs to be followed. It is also vital to establish a standardized environment for the animals and ensure that the surgical procedure does not condition the animal's behavior. The effectiveness of the procedure is the main determinant of the overall biological data quality of the system. The role of the downstream components of the system is to detect the signal from the cells/fibers that are labeled as part of this process.

To support the specified injection schema, this component must allow for injections to be placed throughout the regions of the brain and for different tracers to be used in the system. To ensure whole-brain coverage of injections, it is vital to maximize the accuracy and repeatability of injections, by maximizing the precession of the mechanics of the system and the volume control of the system. Volume of injection is a critical variable, with direct relation to the efficacy of the tracer. By maintaining tight tolerances on the volume of injection, and maintaining consistency in the titer of the tracer, one can standardize the injection region. For retrograde tracers (CTB and Rabies virus), one can standardize the number of cells that are labeled.

2.2.2.2 Established Methodology and Equipment:

Tracer injections into mouse brain are performed as part of a stereotactic surgery, in which the animal in anesthetized, and then secured in the stereotaxic frame [30, 31]. This fixation, creates a stable work surgical work environment and a fixed coordinate system, in which to localize specific brain regions. The stereotaxic frame is equipped with a movement arm that allows for controlled movement to specific targets in the brain. For tracer injections, either a syringe or a similar apparatus is attached onto the movement arm and provides direct volume control of the tracer to be injected. For this reason, the stereotaxic frame and the injector need to be discussed separately, as they are independent entities that contribute differently to the overall efficacy of the injection. The stereotaxic frame governs the spatial accuracy of the system, while the injector governs the volume accuracy and tracer efficacy of the system.

The most popular stereotaxic frames, such as the Kopf Model 900 are based around a u-frame design. These systems are designed with the notion that precise injections can be performed using the same platform, for a wide range of different applications. The U-frame allows for mice, rats and other small animals to be secured, via ear-bars, onto the same frame. Ear-bars are species and size specific. The base is light weight, so it can be easily positioned. Controlled spatial movement is provided by individual X, Y and Z screw-drives. Accuracy/ precession/repeatability are not metrics that the manufacturer uses. Position resolution is on the order of ten's of microns. Angle rotations can be performed around any axis - individually, or in combined rotation. There are locking screws to enable/disable the rotation around each axis. The Y-motion of the system is the load bearing axis. It is designed as a reinforced dovetail, to maximize orthogonality, with respect to the Y axis. The other two axis (X and Z), consist of screw driven actuators, each supported by two guide shafts. Orthogonality of the X and Z axis is assumed, but difficult to validate, for the full range of motion.

Though versatile and easy to use for a broad range of applications, this system suffers from several critical design flaws, which limit its effectiveness for high-throughput applications:

Figure 3: Kopf model 900 Stereotaxic Instrument
The Kopf model 900 is one of the most widely used stereotaxic instruments in neuroscience. This unit is very adaptable and can be used for a wide range of procedures. The main downside is the limited mechanical repeatability of the unit. David Kopf Product Catalog is source of image[32]

1. *Mechanical Repeatability*: The accuracy and precession of this system are quite poor. On average, a variable offset of several hundred micrometers is typical, as judged by empirical testing on the model 900. The source of the error is found in several design elements: (1) The drive screws are not of the finest quality. The screw drives are used across the full length of the screw, without an encoder or any references as to the native irregularities in the screw. (2) The locking screws to control the rotation around each axis are mechanically unstable. Rotational drift and non-orthogonal movement are often experienced. (3) The base is very light and prone to vibrations, which can cause deflections of several hundred microns, if not more, depending on the magnitude of the vibration. Due to this mechanical instability, the system is very difficult to use for specific targeting of brain regions.

2. *Lever Arm Stability*: In order to allow for open access to the animal, the stereotaxic employs a lever arm configuration (single point on contact to the frame). This means that the weight of the tool (i.e. Injector), directly affects the loading on the unit and thus the mechanical performance of the lever arm. As a lever arm, the mechanical performance of the system is not uniform as a function of distance from the vertical base - meaning that the spatial accuracy of the system is different throughout the brain [33, 34].

3. *Offset between Tools:* This stereotax is designed as an open system - any tool set, can be positioned onto the distal end of the lever arm (x-axis of system) through the use of an attachment fixture. The tools are rarely concentric with each other - which forces the user to recalculate the anatomical position for each tool to be used. As a consequence, the average user often finds it easier not to have the drill mounted (used to bore through the skull) mounted on the stereotax, but prefers to use a handheld drill[30]. This allows the user to have the injector always mounted on the stereotax and to use the injection needle (or a disposable needle) as the means of locating the ROI on the skull. It is optimal, however for the drill to be mounted inline (or close to) to the injector. This way, the user is guaranteed that the drilled bore hole is in the correct area. This also minimizes damage to the skull by isolating hand tremors, away from the tools that are applied to the animal, such as the drill.

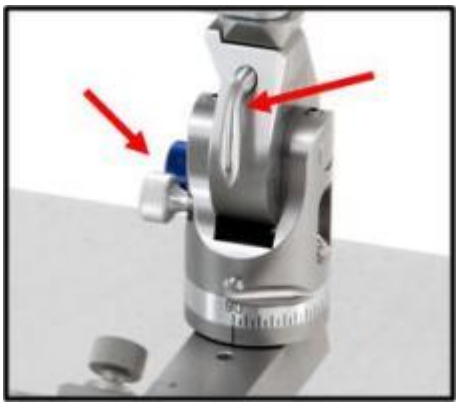

Figure 4: Model 900 Lever Arm Base In terms of mechanical movement reproducibility, one of the biggest problems with the Kopf model 900 and similar units is that the rotation around the axis is controled by a single set of locking screws (red arrows). Because of this, rotational drift and non-orthogonal movement is often experienced[32].

4. *User Feedback:* This system employees vernier scales on all axes. Though these are accurate, they are often slow and difficult to read, especially for technicians without an engineering or mechanical background. Worse yet, there is no feedback loop in the system, thus the user can easily make a calculation or position reading error of several hundred microns, if not larger, without knowing.

In terms of the injector, the two most common methods for tracer delivery are: (1) Hamilton syringe injector or (2) pneumatic based system. Both approaches are based around the use of a glass capillary, pulled to a fine tip (≈20-30μm), filled with the tracer to be injected and a passive liquid. Direct pressure is used to control the movement of the tracer. The principle difference between the two methods is that the Hamilton syringe (Hamilton Company) is typically used in conjunction with oil as the passive liquid, and the pneumatic system uses air. The Hamilton syringe allows for linear volume control, as regulated by the depress of the plunger, with precession on the order of hundreds of nanoliters. The pneumatic, in the form of a

Picospritzer or similar instrument, has an input of pressurized air to a valve (that is normally closed) and allows the operator to control the duration, frequency and total number of air bursts (i.e., valve opening) that enter the glass capillary and thus control the volume of the tracer. The discrete precession of this method is on the order of ten's of nanoliters[35, 36].

The main problem with the Hamilton syringe approach for brain-wide injection into mouse is that injection volumes are hard to control. Volume for the tracers to be used in this project is on the order of 1-25 nanoliters. Also, the plunger is very easy to rapidly press, without a feedback loop. The picospritzer solves both of these problems, as it has tighter volume control and offers discrete volume release (one press of the button = one opening of the valve = one discrete volume release), but it has a fundamental problem of compressibility. Air is a gas, and it is compressible, meaning that the amount of air required to force the release of a finite amount of tracer is a direct function of the resistance of the tracer (liquid viscosity) and the mechanical resistance at the injection site. As such, for precise tracer injections, this system is fundamentally flawed, as it is impossible to measure the resistance at all injection sites. Besides the equipment issues discussed above, the surgical techniques for performing injection into mouse brain are well established and can be directly followed from the literature[30, 31, 37]. These techniques include the method of handling animals, applying anesthetic (type and dose), creating a bore hole in the skull and the safe recovery of the animal. One procedural element that lacks overall standardization is the means of registering the animal space onto the reference atlas[38, 39]. In other words, how does the operator align the coordinate systems (origin) of the reference atlas, to that of the actual animal to be injected. The classical method is to locate one or more landmarks on the skull, assume a one-to-one relationship and perform a rigid transformation in each axis. This is a very simple procedure but has the obvious problem of ignoring the tilt and pitch of the skull - which can be quite significant, depending on the placement of the animal into the ear bars. Also, the spatial error in finding landmarks on the skull, can be on the order of a hundred micrometers[40].

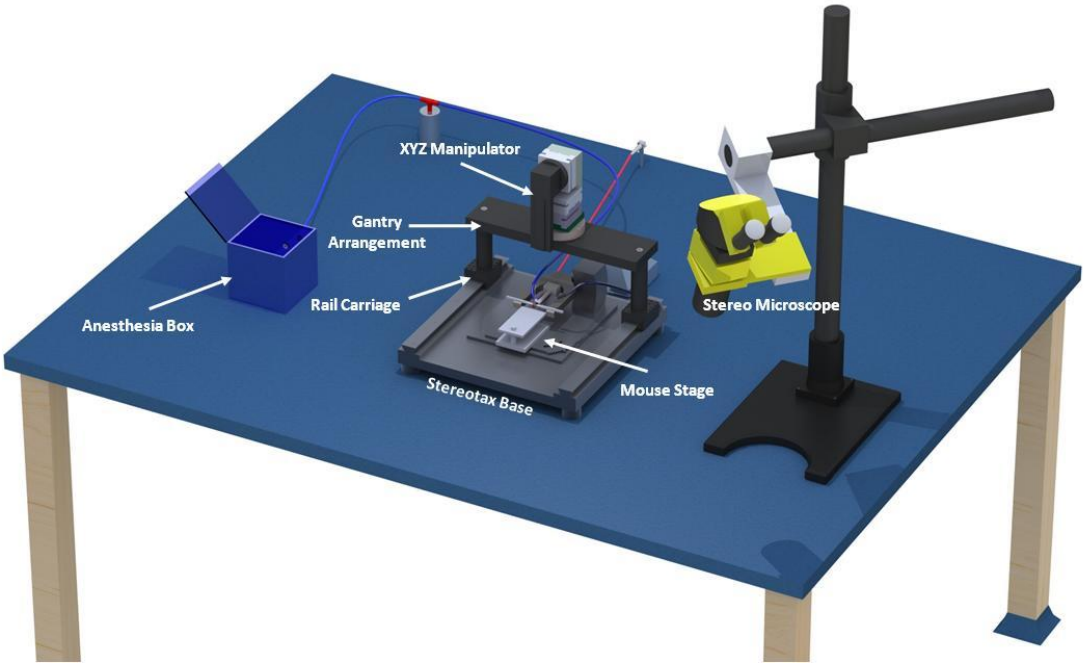

Figure 5: Animation of the assembled stereotax station
The stereotax station consists of three primary elements: (1) the stereotax frame, with a gantry arrangement and motorized motion controller; (2) a direct connect anesthesia system, to allow for the use of a oxygen/isoflurene mix, to be used as the primary anesthetic; (3) a stereo microscope that is used by the operator to visualize the procedure.

2.2.2.3 Design Implementation and Innovation:

To address the limitations discussed above, a novel stereotax was designed and constructed, specifically for the purpose of performing injections into the mouse brain, per the injection schema. This stereotax is designed to maximize mechanical stability of the system, while ensuring maximum spatial accuracy/precision, without sacrificing usability or increasing procedure time. The setup is assembled from commercial components that are integrated in a novel fashion, to provide enhanced performance. Figure 5, shows the assembled stereotaxic component.

The main attributes of this system are as follows:

1) *Mechanical Stability*: To solve the mechanical problems of the conventional stereotax, a heavy metal base (Kopf model 1900) was used in conjunction with a motorized XYZ manipulator, suspended in a gantry crane arrangement. The heavy base ensures that the frame

performs as a rigid body, whose mechanical properties could be easily mapped and accounted for in function. As a rigid body, the frequency response is uniform to any outside vibrations, instead of part specific. This greatly reduces the mechanical instability of the system; that is, the movement arm does not act independently of the base[33, 34]. Besides a heavy base, the Kopf model 1900 is equipped with two parallel, full-length, dovetail rails. The carriages that ride on these rails were used to support two heavy steel posts, onto which an X95 rail was mounted. Onto this gantry arrangement, a motorized XYZ manipulator (Sutter Co, MP-285) is mounted. The manipulator is digitally controlled and allows for precise movement to within 40-200nm, in a travel window of 25mm, in all three axes. The front faceplate of the manipulator was redesigned to support a standard Kopf dovetail. This allows for direct integration with all stereotax "tools" and is directly concentric to the path of the glass pipette to the injection.

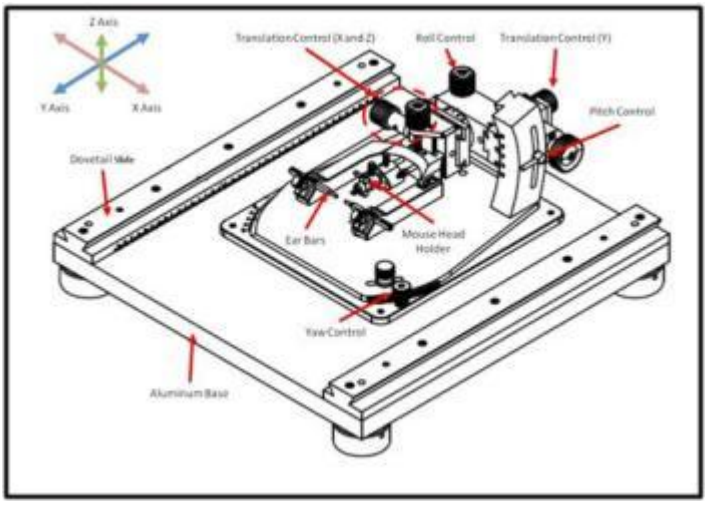

Figure 6: Kopf model 1900 stereotaxic instrument base
The Kopf model 1900 stereotaxic instrument base is comprised of a heavy metal base, with parallel dovetail rails on either side of the base. The base is integrated with independent translation and rotation controls for the mouse holder. This allows for controlled movement of the animal, after it has been fixed in the ear bars, relative to the stereotax base. The critical elements of the stereotaxic base are labeled in the diagram, along with the reference axis.

The main advantages of this system are (1) The movement of the system is divided between coarse and fine, which allows for large travel while retaining high-accuracy. Coarse motion (>25mm in any axis) is manual, but needs to be performed very rarely - only at the onset of the surgical procedure. Fine control (<25mm of travel) is fully motorized and the precision (40-200nm) is validated by the manufacturer. After the initial coarse movement, all other motion in a given surgical procedure is governed by this fine control. (2) The operator's only interaction with the actual manipulator is to load and unload the stereotax tools. All other movement control is guided by a digital controller. (3) Orthogonality is ensured, because the manipulator is fixed to the gantry rail using right-angle braces, and the gantry is orthogonal to the base because the dovetail rails, on which it is suspended on, are parallel. Furthermore, the system is static during the procedure. The only elements that move are internal to the manipulator, validated by the

manufacturer. (4) The mechanical performance of the manipulator is identical, regardless of the position within the travel range. This performance is identical for all stereotax tools, regardless of weight. (5) The system can be used to support all stereotaxic tools, including the drill, and since the components are all assembled using an identical dovetail based clamp, they can be tuned to be concentric. This minimizes overall system error.

2) *Feedback Control*: The movement of the XYZ manipulator of this system is performed through a digital controller (ROE-200, Sutter Co). The controller allows the user to move each axis independently or simultaneously, by turning a specific knob. The controller also displays the absolute position of the manipulator. This eliminates the need for vernier scale interpretation and thus leads to a lower failure rate. By separating the human operator from the actual movement of the manipulator, errors due to hand tremors are eliminated.

The ability of the operator to directly visualize the absolute position of the manipulator and thus the loaded tool allows for much more direct and fluid interaction with the procedure. In the case of drilling the bore hole through the skull, the user can keep track of the displacement of the drill through the skull and compare that value to the approximate thickness of the skull. When the user is near the distal edges of the skull, the user can reduce the advance rate, so as to be sure not to damage the dura or the cortex of the brain. Similar benefits apply to guiding the glass capillary into the brain for the tracer injection.

3) Animal Care and Positioning: Besides a rigid base, one the main advantages of the Kopf model 1900 is that the mouse fixation holders are at the center of the frame. The ear bars and head holder are suspended such that once the animal is secured, the user is able to easily control the pitch, yaw and roll of the animal's head position, in the range of ±10-15°. This is a major advantage over conventional systems, because it allows the operator to easily control the rotation of the animal's head without repositioning the animal in the ear bars. This feature also removes the need to place the animal "perfectly" in the ear bars, relative to the horizontal. Rather, the operator just needs to place the mouse in the ear bars in a way such that a firm mount is achieved; the actual rotation can be adjusted afterwards. In practice, this facility feature is used in conjunction with a two-pronged alignment indicator. This is mounted as one of the stereotaxic

tools on the manipulator and allows the operator to assess the relative depth of two points simultaneously. The operator can then make needed pitch and yaw changes to ensure that the coordinate axis of the animal is parallel to the horizontal and the vertical in stereotax space.

The head-holder for this setup is a critical component that further simplifies the positioning of the animal into the frame. Unlike in other systems, which employ a clamp-like means of securing the nose/head of the animal in the frame, the model 1923 (Kopf) head holder, consists of a metal bar that fits into the mouth of the animal. The bar has a center hole into which the front tooth of the animal is expected to fit. The bar can then be slightly retracted, away from the body of the animal, to create tension in the system and make for a stable fixation. The other major advantage of this head holder is that it allows for the use of a gas anesthetic, which can be pumped across the nose of the animal, instead of one that is injected into the animal (intraperitoneal injection). This is a major procedural advantage, as anesthetization using injectable substances (for example, Xylazine/Ketamine mixture) is one of the principal causes of animal fatalities in conventional procedures. By using an inhalable anesthetic (Oxygen + Isoflurane) the dosage is very small, but sustained over time - Therefore the likelihood of over dosage is significantly reduced.

4) *The Injector*: Due to the problems with the Hamilton syringe approach (lack of precision) and the pneumatic system, (where volume control is uncertain, due to the compressibility of the passive liquid), a direct drive injector was used. The so-called Nanoject (Drummond Corporation) utilizes a servo controller attached to a metal plunger - on to which, a glass capillary, filled with oil, is attached and secured in place through a plastic gasket. This forms a "closed system" where the movement of liquid at the distal end of the glass capillary is controlled by the movement of the plunger at the proximal end. This is a modification of the Hamilton syringe approach; but due to the use of a servo motor, instead of manual control of the plunger, the device is able to deliver much better volume control. The Nanoject is advertized to allow for volume injections in the range of 2.5nl to 60nl per pulse, with variable speed and user-defined number of pulses. The Nanoject is a stand-alone device (aside from the controller), and is cylindrical in shape, meaning that it can be directly retrofitted into the standard Kopf dovetail toolset and directly attached onto the manipulator.

From extensive empirical testing, it has been found that one of the main drawbacks of the Nanoject and of all similar systems, is native hysteresis in the system. In other words, after loading the pulled glass capillary into the Nanoject, if one attempts to remove trapped air bubbles in the distal end of the tip, by evacuating the oil (Empty Button) through the tip, there is a significant time delay between the movement of the plunger and the equalization of pressure across the pipette. This is not a fundamental to the Nanoject, but rather a native fluid dynamics problem - i.e. reduction in diameter of a cylinder from 1000µm to 15µm (tip diameter of the pulled pipette, used in the Nanoject), a reduction of 66X, will cause an increase in the pressure drop, per unit length, of around 1.2 million times (33^4). This significant pressure difference manifests itself in the form of a significant time delay for the pressure to equalize with the atmosphere (the glass capillary is assumed to be a rigid body and no significant stress is caused by this pressure difference). Therefore, one is forced to wait 5-10 minutes, sometimes longer, until the pressure equalizes. This only occurs after prolonged release of solution. This element of the system adds a procedural layer of complexity - but to our knowledge, this is the only practical solution to this fluid dynamics problem.

2.2.2.4 Procedure Standardization/Industrialization:

At a conventional neuroanatomy laboratory, an average of several animals per week are injected, per operator. To meet the goals of the Injection Schema (i.e. 250 injection sites, with 4 tracers per site = 1000 animals per year), the setup must be able to accommodate close to 20-40 animals per week, with a single operator. Given this, major procedural changes had to be enacted, to reduce the procedure time per animal and improve the overall throughput. Critical procedural changes were: (1) Use of the inhalable anesthetic; (2) Application of 30% H_2O_2 to enable the swift identification of bregma and lambda skull landmarks; (3) Standardization of animal housing that minimized animal-to-animal variations; (4) Pre-procedure Quality Control of pulled glass-pipettes, to ensure consistent size of the tip; (5) Use of surgical glue to close the skin around the skull, as opposed to sutures; (6) Pre-procedure preparation of tracers and selection of injection targets. The most significant procedural change, was the creation of a Standard Operating Protocol for Stereotaxic Injections. This protocol provides the operator, usually a technician or student, with a step-by-step guide to performing injections and aims to address common failure modalities.

2.2.2.5 Downstream integration and upstream feedback:

This is the first component of the Engineering System and the principle determinant of downstream biological quality of the data. This is one of two system components that interact directly with the live animal (the other being Brain Preparation) and the only component in which the animal survives. For these reasons, this component of the system does not need to directly integrate with the rest of the system, in terms of equipment or process. Rather, this component needs to result in a high rate of successful injections and a standardized meta-data flow. Since this is the first component of the engineering system, it is also where an animal, following a successful injection, officially enters the Laboratory Information Management System (LIMS). As part of this process, the animal is a assigned a unique identification number - which is written on the housing cage (animals are individually housed). As a further safeguard, a metal identification ear tag is also attached to the animal and recorded in the LIMS system. This allows for animal identification in the event the cage card is lost or the cages are mixed. As part of the LIMS process, all procedural meta-data, concerning the injection, is recorded into the system: injection type, injection tracer, injection volume, injection coordinates, observations, animal health, et. All downstream processing is performed related to the date of injection. Brain preparation is performed 7 days after injection, for most tracers. LIMS is described at length in Section 2.2.7.2.

2.2.2.6 System Evolution:

This component of the system underwent significant evolution through the time course of the project. This development was aimed to further refine the equipment and the process to maximize the ability of the system to target a specific region in the brain. To accomplish this, improvements in the mechanical movement of the system would not be sufficient, as the problem was not the lack of mechanical resolution, but rather the animal-to-animal variability and the intrinsic inefficiency in identifying skull based landmarks. To address this problem, we developed a practical means of quickly acquiring a point cloud dataset, representing the skull surface of the individual animal. We then developed a Matlab based program to allow for the direct registration of that dataset onto a co-registered skull/brain atlas. This reference atlas is

developed based on three datasets: Computed tomography (CT) scan of the skull and Magnetic Resonance Imaging (MRI) of the brain from a C57BL/6 mouse[41], Allen Reference Atlas (ARA) [39], and a brain variability map of 40 male mice[42]. Registration to this atlas, allows the location of detailed brain regions, as annotated on ARA, to be extrapolated from the skull data of the animal to be injected. This is a practical procedure, that takes only minutes to perform and results in high-accuracy injections, especially in cases where the ear-bar placement of the animal is not optimal and when the target region is small.

2.2.3. Brain Preparation Component

2.2.3.1. Component Purpose:

This system component encompasses (1) the extraction of the tracer injected brain from the animal and (2) preparation of that brain for whole-brain sectioning. As part of this component, the animal undergoes a perfusion process, in which the brain tissue will be "fixed," meaning that the proteins will be cross-linked to prevent tissue deterioration. After undergoing post-fixation, the brain is frozen in embedding medium and stored for sectioning. Prior to and during the freezing process, the brain is very susceptible to damage. Therefore, this is the most process dependent (manual) component of the system. This is also the last time the brain appears as and is treated as a single physical entity. Once it is frozen, the actual brain is, is obscured within the opaque embedding medium. For this reason, a critical procedural outcome from this component is the "proper" orientation of the brains, relative to a fixed plane of the block. This allows for standardized sectioning of the brains, without blocking the brain or otherwise distorting the whole-brain structure.

2.2.3.2. Established Methodology and Equipment:

The process of preparing a brain for whole-brain sectioning is well documented in the literature and fairly well standardized. The process has four steps: (1) perfusion of the animal; (2) extraction of the brain; (3) post-fixation and (4) brain freezing. The only machine that is required for this process is a standard peristaltic pump - which is used to actively pump the fixative through the circuit of the intact animal. A standard array of surgical tools is also required - scissors, forceps, scalpels, retractors, clamps, hemostats, etc.

(1) Perfusion Process: The basic protocol for perfusion of the animal is to: (1) anesthetize the animal with a lethal dose of anesthetic; (2) secure the animal on a raised platform by the extremities, inside of a chemical fume hood; (3) open the chest cavity to expose the beating heart; (4) insert and clamp a primed needle into the left ventricle of the heart. The needle should be connected by a tubing through a peristaltic pump to a solution of saline. The pump should be activated for forward flow, through the needle, at a specified rate of 10 ± 2ml/minute; (5) The right atrium of the heart should be cut to allow blood to escape. (6) Depending on the animal, about 25-50ml of solution should pass through the circulation, until only saline is seen flowing from the atrium; (7) The pump should be stopped. The solution should be changed to fixative, and the pump should be activated for forward flow; (8) As with saline, about 25-50ml of the fixative should pass through the circulation. The animal will stiffen, as the muscles undergo fixation, and some extremities, like the tail, will twitch and move. (9) The pump should be stopped. The needle should be removed from the heart of the animal and the animal specimen can proceed to brain extraction[44, 45]. The protocol affirms the minimal role of equipment in this process. Although there are several vendors that claim to have optimized the perfusion process (Perfusion One[46], Leica Corporation), derivatives from the classic perfusion pump approach are minor, with few practical advantages. In some approaches, the perfusion pump can be replaced by a gravity driven flow or by a manually controlled syringe. Though these approaches are slightly easier to implement, the results are less consistent and they make the process harder to regulate, especially for a large number of animals[47].

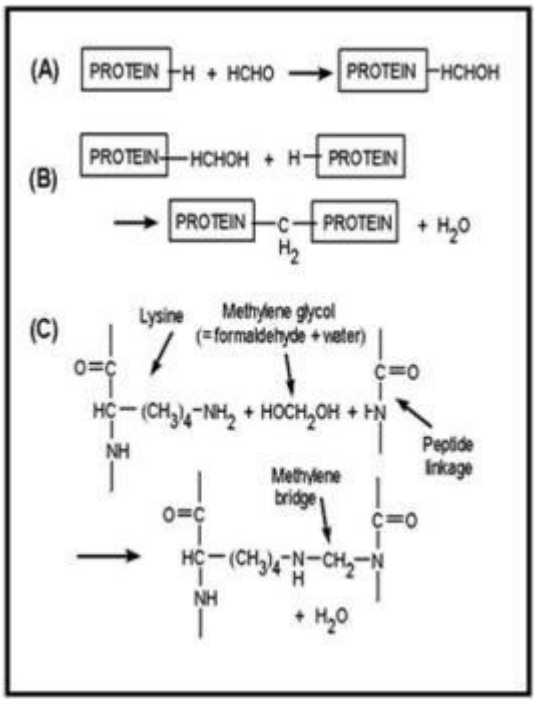

Figure 7: Reactions involved in fixation by formaldehyde

(A) Addition of a formaldehyde molecule to a protein. **(**B) Reaction of bound formaldehyde with another protein molecule to form a methylene cross-link. (C) A more detailed depiction of the cross-linking of a lysine side-chain to a peptide nitrogen atom[43]

The choice of fixative solution is dependent on the intended downstream use of the tissue. In this system, the main determinant factor is the injection schema, which calls for the use

of viral (fluorescent) and conventional tracer. The latter requires enzyme-histochemical detection of the injected tracer. The tissue will also be used for basic neuroanatomical staining of neuronal cell bodies and fibers. For this application, the most common fixative is paraformaldehyde (4% PFA).

Paraformaldehyde is the highly-polymeric form of formaldehyde. A typical solution of 4% PFA is made by diluting formalin in water by 10X. Formalin is a 40% formaldehyde solution; a 10X dilution results in a 10% formalin solution or 4% PFA. Formalin also contains 10% methanol; a 4% PFA solution, therefore, contains 1% methanol. Paraformaldehyde can also be made directly from powder (JT Baker, S898-07). In the first stage, formaldehyde molecules combine with various parts of protein molecules, especially the side-chain amino group of lysine and the nitrogen atoms of peptide linkages. The resulting cross-links, known as methylene (—CH2 —) bribdges, are stable and account for the insolubility and rigidity of protein-containing tissues that have been fixed by formaldehyde. Paraformaldehyde is preferable to other fixative (Glutaraldehyde, Acetone, Alcohol, ect.) because it does not impair enzyme histochemistry of most antigens, the rate of fixation is fast (cross-linking is complete within 24-48 hours) and the tissue/operator is not exposed to organic solvents[49-52]."Formaldehyde causes less shrinkage than any of the other fixatives... It is relatively cheap and stable fixative and allows more special staining techniques than any of the other fixative reagents. The morphologic criteria used for diagnosis have been established primarily on formalin fixed tissues."[51].

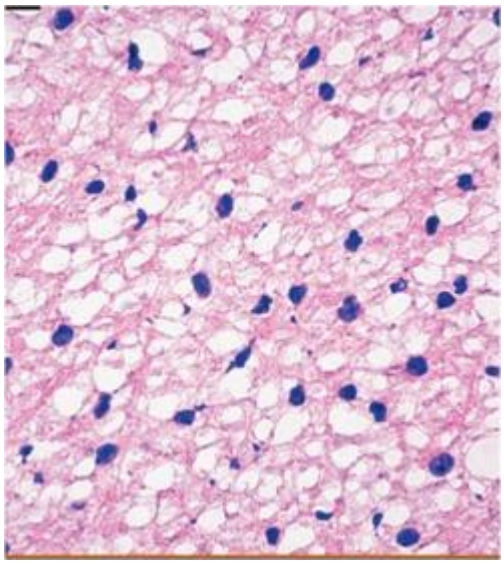

Figure 8: Tissue damage due to improper freezing technique

To properly freeze biological tissue, for histological staining, the tissue must be frozen rapidly, so that "water [in the tissue] does not have time to form crystals and remains in a vitreous form that does not expand when solidified". If the rate of freezing is slower, water molecules will expand when frozen, causing fractures in the tissue. Depending on the material and the region, either the extracellular matrix will be damage (as is seen above) or the cells, or both. Regardless, the damage will be widespread and the tissue will appear as "Swiss cheese" [48].

(2) Brain extraction: This is a fully manual process, in which the user: (1) severs the head of the animal from the body (this step can be skipped, depending on the preference of the user) ; (2)

cuts the skin above the skull and then (3) using either forceps, rongeur or a similar tool, begins to peel away the skull, piece by piece, until (4) the brain is completely exposed. Exposing the olfactory bulb, without damage, is the hardest. To free the olfactory bulbs, one is usually forced to fracture both orbits of the skull, to allow for easier access. (5) a spatula or a similar flat tool is used to lift the brain from the skull and place it into solution[44]. Most macro damage to the brain, in the form of physical nicks and scratches, occurs as part of this process. The most practical solution to minimize brain damage, is increased user practice and increasing personal skill with the surgical tools. Other approaches, such as decalcification of the skull, prior to brain extraction - appear promising, because the skull would be "softer" and thus easier to remove, without damaging the brain. However, this is a lengthy process and involves strong acids, with can damage the tissue and affect downstream staining of the tissue.

(3) Post perfusion and extraction: After extraction, the brain needs to undergo a post-fixation process. This processing is intended to further reinforce the fixation of the tissue, and rescue any areas of the brain that were not thoroughly perfused. This process entails placing the brain in the fixative solution, the same used for perfusion, and allow for passive diffusion into the tissue. This post-fixation process will not correct major procedural errors that might have occurred during perfusion and cannot be used as a substitute for perfusion. Post-fixation is intended to address circuit related issues, like the local blockage of a capillary network, that can prevent adequate amounts of fixative from penetrating that area.

Following the post-fixation of the tissue, it is necessary to adjust the water content of the tissue to facilitate proper brain freezing. If tissue is frozen in its native form, the water molecules inside of the cells and the extracellular matrix will freeze at a different rate than the rest of the tissue, resulting in burst cells and ice crystals within the tissue. To prevent this, and ensure anatomical integrity of the tissue, it is vital to perform a cryoprotection step, by immersing the tissue in a solution of sucrose. Sucrose acts as a partial dehydrant and freezes at approximately the same rate as tissue, and to the same hardness. The optimal concentration of sucrose is tissue specific - as a function of fixation and contents of the tissue.

The need to equalize not just the rate of freezing, but also the resulting hardness of the tissue, is vital to ensure uniform sectioning of the tissue. If the hardness of the tissue is heterogeneous, the sectioning of the tissue will introduce not only global stresses on the tissue,

but also local stresses. These internal mechanical forces will cause the cellular structure of the tissue to deform and should be minimized. The tissue has native composition heterogeneity; namely, the white matter, which consists mostly of highly-lipid myelinated axonal fibers, and the grey matter, which consists mostly of neural cell bodies. Therefore, the ideal cryoprotectant solution acts to minimize these differences by maintaining mechanical properties (i.e., hardness) that is between the two extremes. For most neuroanatomical applications, the use of 30% sucrose solution as the cryoprotectant has been shown to result in a satisfactory uniform rate of freezing and uniform tissue hardness.

(4) Brain Freezing: Following cryoprotection, the tissue needs to be actually frozen. To minimize freezing damage, the tissue needs to be rapidly frozen, in a uniform manner. This is typically performed by: (1) embedding the tissue in support medium in a metal block. The embedding medium, facilitates the freezing of the brain, minimizes damage to the edges of the tissue due to freezing and supports the brain during sectioning. The metal block serves as mold for the medium and provides optimal heat transfer; (2) Once the brain is embedded, the metal block is submerged into a solution of isopentane (2-Methyl Butane), which is surrounded by a beaker containing crushed dry-ice. The metal block is slowly lowered into the solution, as to not to "shock the system". Such thermal shock (caused by the dropping of the block into the solution) would result in block wide fractures. The two beaker freezing method - dry-ice in the outside beaker, cooling isopentane in the inside beaker - is preferable to the use of liquid nitrogen or similar cryogenic compounds, because the temperature can be adjusted to match the optimal freezing rate of the embedding medium and the tissue. For most applications, the temperature of the isopentane solution is on the order of -40°C. At this temperature, the freezing process takes only a few minutes. (3) Post freezing, the brain can be stored in -80°C for extended periods.

One critical step that is overlooked in the above protocol is the importance of orienting the brain in the embedding medium. Once frozen, the embedding medium is completely opaque. Therefore, this is the last opportunity to fix the orientation of the brain, relative to a fixed edge of the mold. The effectiveness of this process determines the symmetry of the brain during sectioning - which is a critical element for downstream registration of the sections to a reference atlas. This process is typically performed under a stereomicroscope and the operator attempts to

align the midline of the brain with the corresponding edge of the mold. This process is obviously slow, error prone, as the brain can shift after alignment (during freezing) and difficult to standardize. The other drawback of this technique is that it is not suitable for freezing several brains in a single block. Two brains will not fit in a given metal mold, and increasing the size of the metal mold is not desirable, as this will affect the overall freezing rate of the brains.

A few commercial ventures, like the Brain Block One Encasement Gels[53] (Leica Corporation) have attempted to address this problem, by providing a gel-based mold with a precast cavity to receive the brain. The midline of the cavity is parallel to the corresponding edge of the mold. The main problem with this system is: (1) the gel does not freeze at the same rate as or to the same hardness as the tissue, and thus causes mechanical stress onto the tissue during sectioning and (2) price, as these molds cost about $10 per brain. This is considerable, as the cost of the embedding medium is typically negligible. The use of these molds also does not solve the problem of freezing multiple brains in a single block, and there are procedural problems with maintaining the two halves of the molds during freezing and sectioning.

2.2.3.3. Design Implementation and Innovation:

As discussed above, this component of the system is not equipment centric, but rather process centric. As a result, the implementation of the first three steps of the brain preparation process (i.e. animal perfusion, brain extraction and post-fixation)were performed based on standard practices as described in the literature, with only minor adjustments. Anesthetic type and dosage, volume of fixative, ratio of pre-flush to fixative, flow rate of perfusate, exact extraction technique, post-fixation solution and incubation times, were all adjusted for the in-house environment and for use with C57BL/6 animals.

The main development of this component focused on standardizing the orientation of the frozen brains. To address this problem, we developed a system of creating customized freezing molds that are composed of just host embedding medium. These molds are created by positioning a stereolithographic (SLA) model of an MRI reconstructed mouse brain in the center of a standard rectangular metal chamber, filling the chamber with embedding medium and freezing the set in -80°C. After the embedding medium has fully hardened, the brain models are removed. This results in a rectangular mold with a center cavity that is a negative of the brain. These molds can then be used to envelope a mouse brain and ensure that it will be frozen in a

standard reference frame relative to the host metal chamber. These molds can be made in bulk and stored indefinitely in -80°C. The consumable cost of this system is just the cost of the embedding media, which in the case of NEG50 or comparable media is on the order of $.30 per brain mold, versus the $10 cost for similar gel based molds[53].

In terms of thermodynamics, this system has lower thermal resistance than comparable gel molds, since the tissue is in contact only with the embedding medium, without an intermediary material. Since the resulting brain molds consist of only two components, embedding medium and tissue, there is no worry about mold splitting or similar breakage of the mold. In terms of downstream image analysis, one of the advantages of these molds is global consistency from mold-to-mold and animal-to-animal. The center cavity of the molds is always formed in the same location, relative to the fixed edges of the base mold, through the use of a rigid cast; and therefore the embedded brain is always in the same location. For serial sectioning, this means that the same brain region should appear in the same slide range, for all sectioned brains.

One of the advantages of this method, versus conventional molds, is the ability to freeze two mouse brains in a single brain block. This is possible by adjusting the casting apparatus to house two brain models, so that the resulting mold has two cavities available for brains. Both brains would be frozen in standard stereotaxic coordinates, relative to the fixed planes of the mold. Adequate spacing between the two brains is incorporated into the system, as not to introduce distortion during cryosectioning. The freezing dynamics are unchanged versus freezing of a single brain and the overall freezing time is the same, 3-5 minutes per mold. The resulting advantage of this system is a two-fold increase in overall cryosectioning throughput, as both of the two brains can be sectioned simultaneously. Chapter 3 describes this method and the development process in extensive detail.

2.2.3.4. Procedure Standardization/Industrialization:

As discussed above, this component is process centric. It is the most labor-intensive component of the entire system. As such, it was also one of the most difficult to standardize. As with the Tracer Injection component, the key to this standardization was the development of a Standardized Operating Protocol (SOP) for each step of the component.

2.2.3.5. Downstream Integration and Upstream Feedback:

The integration of this component and the rest of the system, mainly the Brain Sectioning component is ensured through the standardization of the brain positioning and orientation in the frozen block. This frozen block is the principle input the Sectioning component and this standardization of brain placement, allows for the standardization of sectioning plane and the sectioning angle (knife angle). There is also direct feedback between the two components, in terms of design development and data production. In terms of design, the main feedback is the fine tuning of the hardness of the brain, relative to the regional structures and the embedding medium. As part of this feedback, it was shown that brains frozen in nominal embedding medium (O.C.T - "Optimal Cutting Temperature", Tissue-Tek Corporation), with 30% sucrose as the cryoprotectant, tended to have both "micro" damage (cellular) and "macro" damage - whole section. This damage emphasized the need to tailor the preparation of the brain to the specifics of the sectioning methodology. This tailoring was performed empirically and resulted in changing the cryoprotectant process from a single incubation in 30% sucrose to a two-step process: (1) first an incubation in 10% sucrose for ≈ 24 hours, followed by (2) an incubation in 20% sucrose for another 24 hours. The embedding medium was also changed from O.C.T (a standard in modern histology) to NEG50 compound (Richard Allan Scientific). The latter has a consistency and resulting hardness that is a closer match to the tissue, and thus results in less distortion of the tissue, during sectioning.

In terms of dataflow, the main feedback is a validation of the brain orientation in the block, which is assessed by the technician at the time of sectioning as noted in the appropriate LIMS field. Importantly, this allows for rapid diagnosis of possible process problems. As part of this feedback, it was determined that under certain circumstances a temperature gradient can be created in the isopentane freezing solution, which causes uneven freezing of the brain and results in macro tissue distortion. This gradient is created when an excess amount of dry-ice is inadvertently placed on one side of the isopentane solution, usually the bottom of the beaker. This side is therefore colder than the others, and the rate of freezing of the tissue closer to this side is faster than that of the other sides of the tissue, a situation which causes deformation of the brain. To address this problem, modifications were made to the SOP to ensure that the temperature of the solution was sampled throughout the liquid, not just at a single point.

As with the other system components, all process information is recorded in LIMS. A unique feature of LIMS, with regard to this component, is informing the user to perform post-perfusion solution changes. This feature, ensures the consistent treatment of brains and further ensures that a technician does not forget to change a solution for a given brain. Each solution change is specified in the system. In terms of processing rate, this component is not rate limiting. All steps of the processing are low bandwidth and can be adjusted to handle an extended quantity of animals, as determined by the Tracer Injection component. In terms of individual processing steps, the average time per animal is 30-45 minutes for perfusion and brain extraction, 2 days (no significant technician time) for post-fixation and cryoprotection (passive), only <10minutes of active technician time and ≈10-15minutes for brain freezing.

2.2.4. Brain Sectioning

2.2.4.1. Component Purpose:

This system component is responsible for transforming the frozen brain(s) into a set of cut sections, mounted on glass slides. This is a critical transformation of the brain and one of the main determinants of the process quality of the system. This component of the system is the first "industrial" element of the system, as a single brain will be converted into several hundred sections, as part of a standardized procedure. All downstream interaction with this tissue will be slide centric and based on the placement of the sections at this system component. To facilitate enzyme histochemical processing and light microscopic imaging, the sections need to be cut very thin, on the order of <10-100μm. At this thickness, the sections are assumed to function as static objects, but are in fact, non-negligibly dynamic. The sections tend to stretch, compress, fold, and are highly sensitive to temperature and other environmental variables. For whole-brain sectioning, as is required in this system, there is an intrinsic need to minimize section distortion and number of damaged sections. This facilitates optimal 3D reconstruction of the brain, and the post-sectioning steps of staining and imaging. To match the production rate of the upstream components (Tracer Injection), this component needs to be capable of processing at least 4 brains per day, which corresponds to 1000 brains per year.

2.2.4.2. Established Methodology and Equipment:

The conventional method of cryosectioning of mouse brain tissue calls for a fully manual process, in which the operator: (1) mounts the frozen block onto the chuck of the cryostat; (2) adjusts the angle (pitch and yaw) of the block and the clearance angle of the knife, relative to the block; (3) trims the block to expose the region-of-interest(ROI), by rotating the hand-wheel (clockwise), which forces linear motion of the block across the knife. With each complete half-turn of the wheel, the block completes one pass through the knife. With each complete-turn, the block is returned to its original position and the stage is advanced by the pre-set "section thickness". For block trimming, this value is on the order of >100μm. At this stage, sections will not be collected, but the block is “trimmed” to approach the ROI. (4) Once the desired location is reached, the operator lowers and adjusts the anti-roll plate of the cryostat, such that the edge of the plate is slightly offset from the knife, in-plane. This offset is empirically determined, by the operator, on the basis of "feel". The main objective is to ensure that as the block passes across the knife, the cut section passes between the anti-roll plate and the body of the knife (or body of the knife holder) and rests intact, without curling or other deformations. If the anti-roll plate is either ahead of the knife or behind the edge of the knife, by too large of an offset, the section will curl and be difficult to collect[44, 54].

Temperature of the stage and the specimen are critical elements of the process (discussed below) and significantly contribute to the production of a properly cut section. (5) Once a given section is cut from the block, the section is either (A) transferred via a paintbrush (camel hair) to a buffer solution, to be stained and mounted onto glass slides, in a downstream procedure or (B) directly mounted onto glass slides, by gently pressing the slide onto the section and allowing the temperature gradient to facilitate the adhesion of the section onto the slide. (6) Following the transfer of the section, the operator cleans the stage, readjusts the anti-roll plate and repeats the process for all sections to be cut from the block, up to 600 times per block, if the section thickness is 20μm.

The critical elements of the above process are: (1) temperature of the specimen and the chamber, which determines the relative hardness of the block/section and also the tendency of the section to curl; (2) the position of the anti-roll plate, relative to the knife; (3) the clearance angle; (4) the sectioning angle and position of the block, relative to the knife (5) the transfer of the section into buffer or onto a glass slide. Chamber and specimen temperatures are a function of the local environment in which the cryostat is housed and the properties of the tissue block.

Specimen temperature needs to be adjusted relative to the chamber temperature to ensure optimal hardness of the block, so that the section can be cut by the knife without "chattering" (fracturing due to excess cold) or melting (when conditions are too hot). Chamber temperature needs to be adjusted so as to maintain the cut section in a frozen state, thereby facilitating its easy transfer onto the slide or pickup with the paintbrush. An optimal temperature range is empirically determined for the type of tissue to be sectioned. Adjustments in the range of ±3-4°C need to be made on a case-by-case basis.

The clearance angle, for optimal sectioning is usually set to around 10-12° and is locked in place, so as not change during the process. The orientation of the block, relative to the knife - which determines the exact plane of sectioning is harder to set, because both the pitch and yaw of the block need to be simultaneously adjusted - as a function of the placement of the block onto the chuck. In most instruments, this adjustment is very coarse and empirically determined - on a case-by-case manner. As noted in section 2.2.3.2, because the embedding media is opaque, one cannot visualize the orientation of the brain within the block and must make adjustments either based on the edges of the block or based on the blackface. The latter is the best measure, but has the drawback of losing sections, while the adjustment is made.

The position of the anti-roll plate and the transfer of the section, after being cut from the block, are the two most difficult adjustment elements of the process. Both are made as a function of the downstream use of the sections, and this is a main bifurcation point in the process. Sections that are intended for free-floating staining (staining to be performed with sections floating in solution) are collected with a paintbrush and transferred to buffer. For these sections, the process is independent of the curling of the sections. The role of the anti-roll plate is minimal; it usually acts as merely a point of reference for the collection. Some operators prefer not to engage the anti-roll plate at all. The collection of the section with the brush is also very direct. With practice, this collection can be streamlined with low failure. Though optimal for sectioning, this process has the problem of downstream inefficiency. For post-sectioning staining, each section needs to be manually mounted onto slides, a very tedious, variable, and error prone process. For this reason, and because of the overall need to minimize distortion of the sections (as a function of manual manipulation of the sections), it is desirable to mount cut sections onto the glass slide directly. All downstream processing is therefore performed as a function of the slide, not the section. However, this process is much more elaborate than the

collection of free-floating sections and requires the constant adjustment of the anti-roll plate and the standardization of the section collection onto slides.

The difficulty in the use of the anti-roll plate to control the curling of the cut sections is evident in the loose use of the word "offset" in the process description above, where there is no firm measurement of the offset. The optimal value of the offset is equal to the set section thickness, plus 1-2µm, to allow for thermal expansion. However, the mechanical standardization of the plate to these tolerances is very difficult to do, in the context of the dynamics of the cryostat. For this reason, the classic approach to this problem is to make it operator controlled - "adjustment through feel." In this case the operator actually guides a finger across the knife and the plate (normal to the knife) and adjusts the offset of the plate until the position appears optimal. This process is obviously error prone, but in the standard cryostat it is difficult to improve. The same can be said for the transfer of the cut section onto the glass slide. This process entails the operator placing the slide on top of the section, and allowing the thermal gradient between the knife block and the glass slide, to drive the adhesion. If the position of the slide relative to the section is not in tune with the movement of the section due to the thermal gradient, the section will either fold on the slide or possibly tear. In optimal fashion, the operator needs to curl the slide around the section, such as to ease the tension on the section and thus minimizing folding and tearing of the section. This process is further complicated when multiple sections are placed on the slide as the operator is limited by the range of motion that is possible without damaging the sections already mounted on the slide.

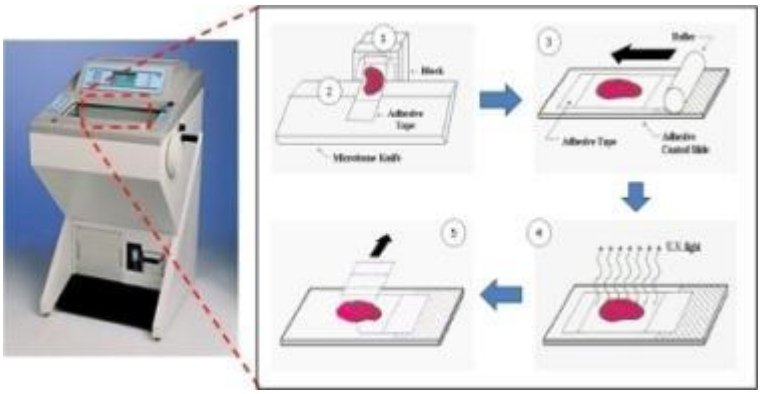

Figure 9: Tape-transfer sectioning method
The tape transfer method of sectioning is a departure from convention. The steps involved in this process are as follows: (1) An Adhesive Tape is attached to the tissue block surface; (2) The tissue [with the tape attached] is sectioned; (3) The tape+tissue is transferred onto a polymer coated slide; (4) A high-intensity UV light cures the polymer and adheres the section onto the slide; (5) The tape is removed from the slide and can be used for conventional downstream processing.

Due to the intrinsic difficulties in the cryostat methodology, several add-on technologies have emerged to facilitate the process and make it more compatible with high-throughput processing of tissue. The most widely used add-on system is vacuum based stretching of

sections. In this system, a vacuum pump is configured into the cryostat, such that a pneumatic vacuum is created between the engaged anti-roll plate and the knife block. This vacuum facilitates the stretching of sections as they pass through the anti-roll plate and helps to prevent curling of the sections. The use of this system, allows for greater flexibility in the exact position of the anti-roll plate and also helps to ease the transfer of the sections onto the glass slide, by maintaining the slides in a stretched position. This and similar techniques make the process easier but do not address the inherent inefficiencies in the system, nor do they have a great impact on the overall quality of the resulting sections.

In recent years, an effort has been underway to completely eliminate the need for the anti-roll plate and greatly increase the quality of cut sections, by minimizing spatial distortion of the sections through the use of a carrier to ferry the cut sections from the knife onto slides. This tape-transfer based sectioning was first commercialized in the form of the CryoJane system (Instrumedics Corp)[55-57]. This system relies on the use of an adhesive kapton tape that is manually adhered onto the blackface, using a roller. As the block passes across the knife, the tape remains adhered to the surface of the resulting section, and the adhering of the tape, prevents the section from deforming. Post-sectioning, the tape+section complex is placed onto a coated glass slide and adhesion is achieved by using Ultraviolet Light (UV). The slide is pre-coated with a UV polymer, such that when UV light is applied, the polymer is polymerized, resulting in a firm adhesion of the section onto the slide. This adhesion is greater than that of the kapton tape, allowing the operator to peel the tape away without damaging the section. After removal of the kapton tape, the glass slides can directly be used for any downstream staining. This process is repeated for all sections cut from the block. The polymerization reaction is performed once per slide, after all sections have been adhered onto the slide. As shown in Figure 10, the quality of staining performed on sections cut using the CryoJane system is equivalent to that of sections processed by conventional paraffin-based sectioning.

This system eliminates the need for the anti-roll plate and greatly simplifies the process of mounting sections onto the glass slide, while reducing distortion of the sections. In addition to improving section quality, the CryoJane system, offers the main advantage of making section production operator independent. This is a major benefit for the overall process quality of a high-throughput system. One of the inherent drawbacks of the system, however, is per-section cost: the cost of the adhesive kapton tape and UV-activated solution. The consequent average per-brain cost increase is on the order of $50. This makes the system an expensive addition, but the ability to streamline the sectioning process, without sacrificing processing rate or section quality, is worth the extra cost.

Though promising in the abstract, empirical testing of the CryoJane system at the pilot phase of the development, was very disappointing and resulted in the conclusion that the system practically "did not work". In the histopathology field, the use of the CryoJane system is mostly reserved for clinical tissues or bone[57-59]. To our knowledge, there were no published accounts of the use of this system for neuroanatomical or high-throughput applications. One of the main differences between clinical tissue/bone and tissue for neuroanatomy applications is the fixation method. Clinical tissue is usually either unfixed at the time of sectioning (fresh-frozen) or is lightly fixed. Neuroanatomical tissue undergoes heavier fixation, through a perfusion process (section 2.2.3.2), which changes the chemical and material properties of the tissue. It was found that sectioning

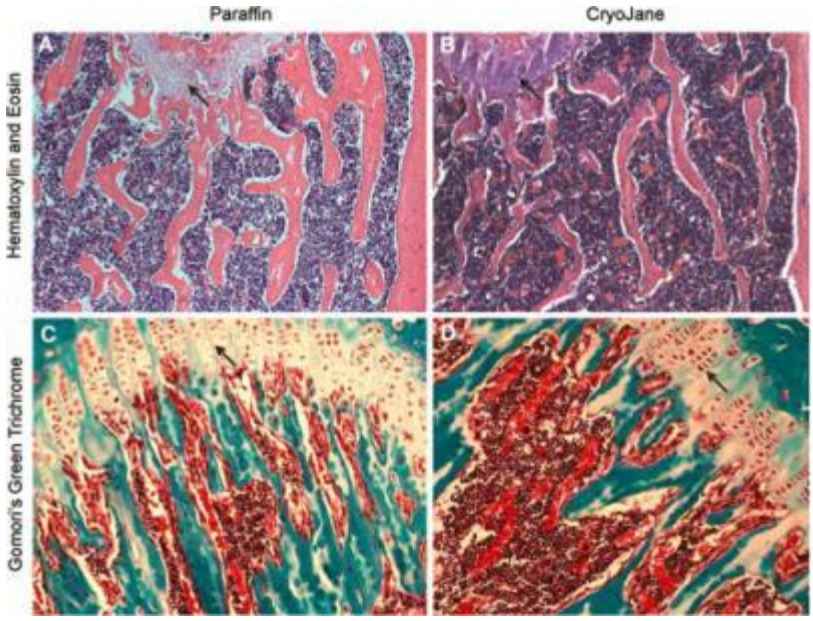

Figure 10: Morphology of paraffin vs. cryojane sectioned tissue
"Paraffin sections (A, C) and cryosections (B, D) were stained with H&E (A, B) or Gomori's green trichrome (C, D)". "Paraffin sections (A, C) have a very similar, high-quality morphology compared to sections cut on the CryoJane system (B, D). Hematoxylin/eosin (H&E) staining of both types of sections (A, B) revealed intact trabecular bone (pink) as well as minimally distorted bone marrow (purple). Chondrocytes of the growth plate were also well preserved (arrow). Staining intensity of H&E is greater in cryosections. Gomori's green trichrome staining (C, D) also showed excellent morphology in both paraffin and cryosections. Intact trabecular bone (green) was apparent in both sectioning methods, as were the columns of proliferating and hypertrophic chondrocytes (arrow)" [57]

perfused brain tissue using the CryoJane system resulted in sections that were morphologically damaged, either by mechanical factors, thermal factors or both. The two most common artifacts would be either be the "window blind effect," in which the tissue would have periodic line damage throughout the tissue, parallel to the edge of the knife, or the "Swiss cheese effect," in which the tissue would have widespread thermal damage.

The sources of this damage were pinpointed to both process problems (workflow) and design problems. Process problem originated from lack of proper instruction from the manufacturer, due to the lack of a thorough analysis of the system. As an example, the optimal sectioning chamber and specimen temperatures were not provided; and the logical assumption that the system could optimally function with temperatures calibrated for conventional cryostat sectioning proved false. These process problems were surmountable through a proper system diagnostics and extensive empirical testing.

The design problems of the CryoJane were pinpointed to the method of applying UV light onto the slides. The CryoJane utilized a capacitor-based system to apply a pulse of UV onto the slides. The problem with this approach is that the charging time of the capacitor is relatively long (30-60seconds) for a singular discharge that would produce a UV pulse of just a few microseconds. This long charging time, practically limits the number of pulses that can be applied onto a slide to ensure full cure of the polymer. Furthermore, the system would often require the changing of a power fuse, especially if the operator accidently triggered multiple pulses in succession. The system also had a single curing chamber. This means that for processing that involved multiple series of sections (i.e., alternating sections placed on different slides), the operator would have to shuttle the slides on-and-off the platform, to adhere the sections and then cure the slides individually. The other disadvantage of the design was that the applied UV light was not evenly distributed across the entire length of the slide, which limited the number of sections that could be placed on the slide and also forced the operator to change the orientation of the slide between multi-pulses. The entire process was very slow, not robust and resulted in poor quality sections.

2.2.4.3. Design Implementation and Innovation:

To address the problems discussed above, a novel tape-transfer based method and apparatus was designed and constructed, to meet the specific requirements of the overall

pipeline. Despite the problems with the CryoJane system, the fundamentals of the tape-transfer method were well founded in engineering and physics principles. Therefore, optimization of the method was worthwhile. The industrializing of tissue sectioning steps is the cornerstone of this system component and essential for the streamlined processing of the entire system. This development focused on overcoming the central limitation of the CryoJane system; namely, the inefficient application of UV light to cure the polymer coating of the slides. Instead of using a capacitor based means of applying UV light, the so-called "CryoJane 2.0" utilizes an array of ultraviolet light-emitting diodes (LEDs)[60]. The main advantages of the UV-LEDs (Nichia Corporation, Model NSPU510CS) is that: (1) the output power is voltage regulated; (2) the LEDs can be arrange in any array configuration, using a common power source; (3) the pulse duration can be quite long, governed by the application of current across the LED; (4) the steady-state operating life is on the order of 1000hours; (5) the LEDs are stable at low temperatures (up to -30°C); (6) the LEDs are inexpensive, on the order of $5 per LED. The drawback of the UV LEDs, is that the native power of each LED is significantly less than that of the capacitor based system.

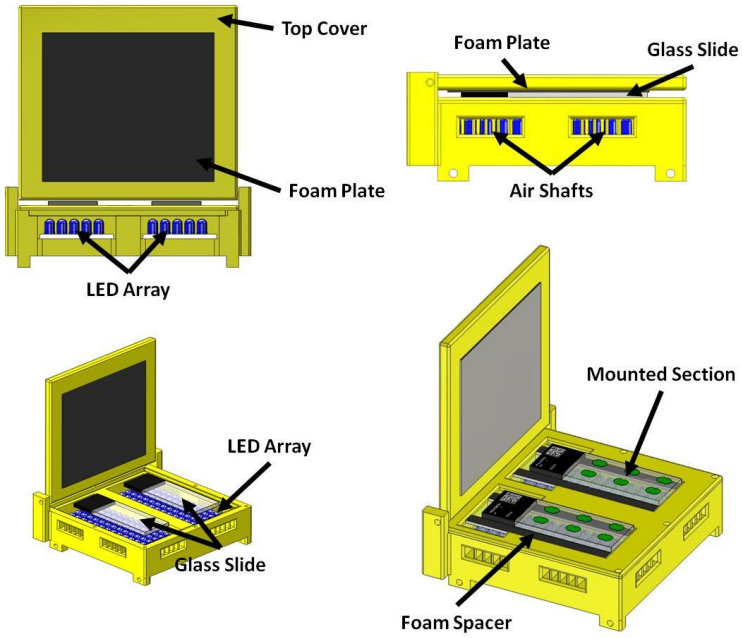

Figure 11: Model view of CryoJane2.0 tape-transfer system

In the CryoJane system, the average irradiance is on the order of 5mW/cm2, for a duration of approximately 25ms. This irradiance was determined from empirical testing, using a PM100 Optical Power Meter, with aS121B sensor and an NE01A filter (ThorLabs Corporation). The power sensor was placed at the center of the curing chamber, representing the center of the exposed surface of the slide. With the use of UV LEDs, an irradiance of 2.5mW/cm2 - .250mW/cm2 can be achieved per LED, as a function of distance from the surface of the LED, as

shown in

Figure 12. This limitation in power, can be overcome by increasing the duration of pulse activation to several seconds. At a practical application of 10 seconds, the total wattage applied per LED is on the order of 200-20X higher than that of the CryoJane system. In a 2D array, the spacing of the LEDs can be adjusted, such that the resulting irradiance is made uniform (linear range of each LED) and can cover a large area. Such an array is shown in Figure 13. This array is comprised of 65 individual LEDs, which are arranged in a parallel resistor network on a printed circuit board (PCB). The PCB (Figure 13A) is a four-layer board, which allows for all the necessary connections to be premade into the board, including the power and ground terminals. In this parallel network configuration, each LED (model resistor) has a voltage potential equal to the applied DC source (Figure 13B). Since the LEDs are of high-tolerances, the resistance across each LED is approximately equal, meaning that the forward voltage will also be equal ($V = I * R$). In most such arrays, it is common to include a serial resistor (100 Ohm, or similar) for each LED, as shown in Figure 13B; but in this implementation, the resistor was not needed. Instead, a DC source was selected that would produce a regular output (Omron Corporation, model S8VS-03005) without any erroneous spikes. The incorporation of resistors into the circuit was also logistically challenging, since this had to be accomplished without increasing the LED-to-LED spacing.

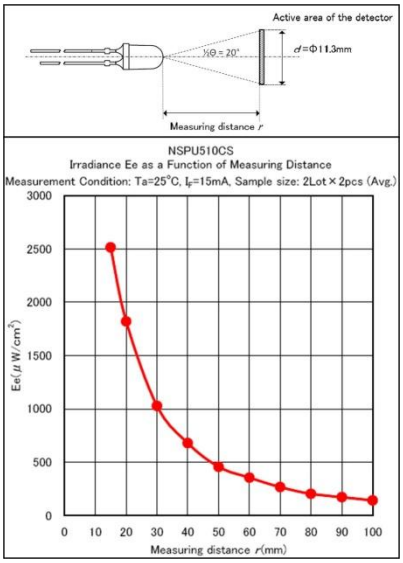

Figure 12: Irradiance of the UV-LEDs, NSPU510CS
Irradiance of the NSPU510CS UV-LEDs, as a function of distance from the top point of the LED. The Irradiance ranges from of 2.5mW/cm^2 to .250mW/cm^2. The irradiance half-angle is 20°.

This array was used as the basis for the CryoJane 2.0 design. The complete system is shown in

Figure 11. The main attributes of this system, are: (1) two parallel, slide curing platforms, each with a uniform LED array that allows for even irradiance of the entire slide area; (2) a foam cover that presses sections against the slide during curing and helps to prevent air bubbles. The cover also helps to localize the applied UV light and reduce exposure to the operator; (3) foam based spacers that prevent the slide from moving while sections are attached.

The main highlight of the CryoJane2.0 system is its simplicity. It is an SLA built body, with interchangeable pre-assembled LED array. If and when (>1000 hours of use) the LEDs stop working, the board can easily be removed and a new one added. The power source (3V, 2A) is external to the apparatus; it is equipped with a serial switch (latching) that is used to control the application of UV light. There are no fuses or similar failure points in the system (a fuse is only a failure point when its triggering is part of normal system use), meaning that it is quite robust and does not require much maintenance. The only maintenance that is required is the periodic (bi-monthly) cleaning of the glass above the LEDs. This tends to accumulate moisture and foreign contaminants (dust, glass fragments, et.), which reduce the intensity of the transmitted light. The overall cost of the system (low-volume manufacturing) is around two thousand dollars ($2,000), about 1/4 the cost of the commercial CryoJane system, but with the added benefit of having two curing chambers. Essentially, twice the system, for a quarter of the price.

In conjunction with the procedural changes discussed below, this design proved quite superior to the commercial CryoJane. The underlining improvement was in terms of tissue quality. Both the "window blind effect" (prevalent mechanical damage) and the "Swiss cheese" effect (thermal damage) were eliminated. The resulting tissue quality was equivalent to that produced through conventional sectioning, but with significantly less spatial distortion and much higher section-to-section reproducibility. The rate of sectioning was also greatly improved, by approximately

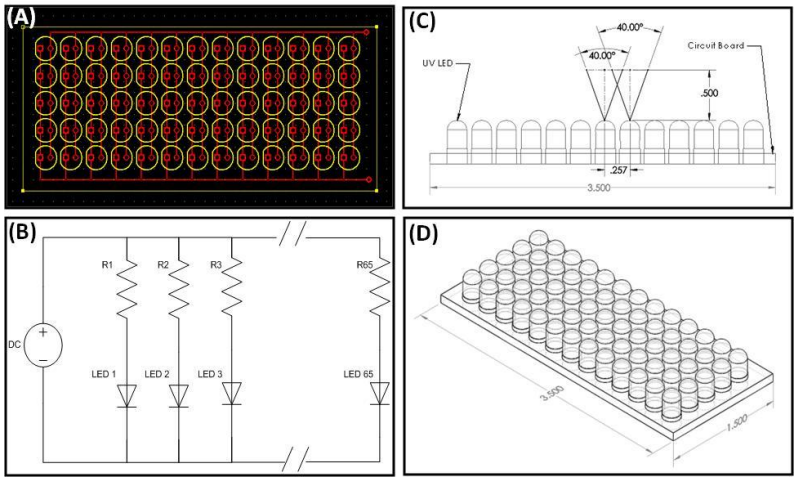

Figure 13: Printed circuit board of the UV-LED array
The PCB used as the basis for the UV-LED array of the CryoJane2.0 system is composed of parallel arrangement of 65 LEDs. (A) The schematic of the PSB board shows the connections between the LEDs, in relation to the common power terminal and ground terminals. As a diode, the LEDs are directional, meaning that the relation between positive to negative terminals, must be maintained for all LEDs. (B) The electrical schematic for the parallel LED array. The inclusion of the serial resistor, per LED, is common, but was not implemented, due to the tolerances of the LEDs and that of the DC power source. (C) The LED-to-LED distance is illustrated on the side-view of the array, as a function of the irradiance angle and the overall PCB board. (D) An isometric view of the PCB board, showing all 65 LEDs and the relative size of the board.

3X. At a section thickness of 20µm, a technician is able to routinely complete a brain block in 4-5hours, producing 200 slides, split into two series. As discussed in section 2.2.3.3, through the use of the novel means of freezing mouse brains, a given block can contain up to two brains, meaning that a technician can section the equivalent of two brains per day. Four brains per day can also be obtained, but the rate is not sustainable without additional support personnel to perform the background duties; that is, slide coating, cryostat maintains, etc.

Additional details about the system, including validation of the claim made above ("less spatial distortion and higher section-to-section reproducibility") are discussed at length in Chapter 4. Overall, this was a very successful design, one that was expanded to a second cryostat -to be operated in parallel with the first, for a combined daily throughput of 2 blocks (1 per technician) = 4 brains per day = 20 brains per week = 1000 brains per year (250 working days per year). In terms of design performance, once standardized, CryoJane2.0 has had no major problems or lead to any significant downtime (downtime of more than a few hours). In fact, both CryoJan2.0s have been more reliable than the cryostats in which they were placed. The cryostats have required periodic upkeep and have had continuous problems with internal components. The most common failure is the peltier specimen cooling, which has been failing on the average of once every 2-3months. Overall, with CryoJane2.0, the rate of 1000brains/year, has been achievable.

2.2.4.4. Procedure Standardization/Industrialization:

As discussed earlier, the CryoJane1.0 system, was found to have both process and design problems. The design problems were addressed through the creation of CryoJane2.0, which increased the amount of UV irradiance that can be easily (efficiently) applied onto the slide. This design feature helped to reduce the loss of tissue due to uncured polymer, when the kapton tape is peeled away from the slide. Other failure points would need to be solved through process changes. The main enacted process changes are: (1) changing the type of rollers that are used to adhere the kapton tape onto the surface. For the adhesion of the kapton tape onto the blackface, a hard roller is used (polycarbonate). This is because the block is frozen and one needs to ensure that the kapton tape is firmly adhered. Maximum pressure (within reasonable application by a technician) can be applied, without damaging the block. For the adhesion of the kapton tape + section (post removal from the block), a soft silicone roller needs to be used. This is because the

section is now only a few microns in thickness; it is fragile and will develop cracks under extreme compression. This soft roller was also found to do a better job at removal of air bubbles, than a hard roller. In practice, the technician applies relatively the same amount of force for both applications and the hardness of the rollers accounts for the differences in process. This makes the process very reliable.

(2) Once the section are is cut from the block and adhered onto the kapton tape, the complex is very susceptible to thermal damage. Any increase in temperature will cause the section to expand; but since it is adhered to the kapton tape, the adhesive will counteract this expansion and thus lead to mechanical damage. The solution to this problem is to maintain the section+tape complex at a stable temperature, away from any air currents. The standardization of this process took the form of outlining the concrete path that the section+tape should travel within the cryostat (within the cold stream of the cryostat) and maintaining a stable environment around the cryostat. This environmental stability, took the form of actively regulating both the humidity and temperature in the room housing the cryostats; and regulating the airflow in the room such that it did not directly impact the open surface of the cryostat. Cryostat operating temperature, chamber and specimen were also standardized to within 1-2°C.

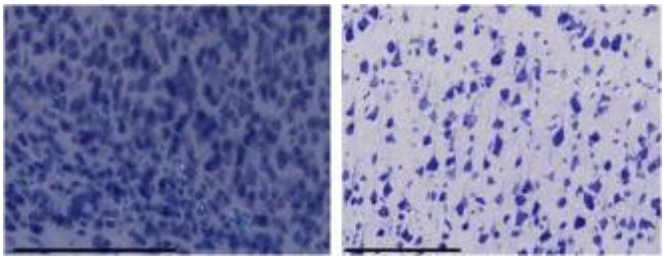

Figure 14: Cell-body identification as a function of section thickness
(Left) Coronal section (40µm), of a Giemsa stained slide (www.brainmaps.org)[23]. Overlapping cell bodies are evident throughout the section, which hinders downstream processing. (Right) A coronal section (20µm), Nissl stained. There are fewer instances of overlapping cell bodies. Scale bar is 100µm.

As with other system components, the most significant procedural change was the creation of a Standard Operating Protocol for Cryostat Sectioning. This protocol provides the technician with a step-by-step guide to sectioning mouse brains and aims to address common failure modalities.

2.2.4.5. Downstream Integration and Upstream Feedback:

The integration of this component and the rest of the system, was ensured through the standardization of the sectioning process and the placement of the sections onto the slide. The integration with upstream components, mainly the Brain Sectioning component, is discussed in section 2.2.3.5. Throughout the life of the system, this feedback from the upstream component

(brain orientation and other preparation steps) has been essential for maintaining consistency and identifying and erroneous process changes. In terms of integration with the Section Staining component of the system, the three main integration elements are (1) the separation of cut sections into distinct slide series; (2) ensuring optimal adhesion of the sections onto the slides; (3) achieving optimal section thickness to allow suitable antibody penetration. The organization of tissue sections into series, is critical because all downstream staining is performed on the entire slide basis, not the section basis. Regardless of the upstream processing of the brain (i.e. tracer type), the sections cut from the block are separated into two series - one series to be used for cell-body staining and the other for tracer detection, either through enzyme histochemistry[1] (HC) or direct fluorescence imaging. This schematic is a function of the need to register the resulting brainwide data onto the ARA. The sections are arranged in an alternating manner, between the two series, such that the section-to-section spacing for any series, is 2X the section thickness. To help facilitate downstream identification of the series, each slide is labeled with the appropriate case information and also the series identification, as shown in Figure 15.

Section thickness is one of the critical determinants of data quality, in two senses: (1) the number of cells that are present in any section, as shown in Figure 14 and (2) for enzyme histochemical, the penetration success of the antibodies. As discussed in section 2.2.5.2, the antibody reaction is subject to the laws of passive diffusion, meaning that as a function of time, the penetration distance of the antibody is finitely limited. As discussed earlier, classical neuroanatomy staining is based on the use of free-floating sections. This is advantageous from the perspective of antibody penetration, because the reaction can take place from both sides of the tissue, and thus can cover a larger thickness. In this system, the sections are directly mounted onto slides, which means that the reaction will be unidirectional. For this reason, the baseline section thickness selection, was 20µm - half that of classical neuroanatomy (40µm).

1Throughout this dissertation, the phrase "enzyme histochemistry" or histochemistry (HC) for short, will be used to refer to the chemical process of labeling a specific molecular antigen in tissue. The nature of the HC reaction, is specific to the type of antigen. For Cholera Toxin subunit B, an antibody based reaction is required. For this reason, the reaction is termed "immuno"- histochemistry or IHC. For Biotinylated Dextran Amine (BDA), an antibody is not required, because BDA can be directly reacted by Biotin to form a stable complex (ABC method). Therefore, the term HC is correct. However, since the two methods overlap in all other technical aspects (staining instrumentation, reagents, ect.), the two terms are occasionally used reciprocally (mostly in supporting material).

In terms of adhesion of sections onto the slide, sections that undergo enzyme histochemistry, will encounter significantly more tension, from solution rinses and similar processing, than those intended for either bulk staining or direct fluorescence imaging. To adjust for this, sections intended for enzyme histochemistry are placed on different slides than other sections. The coating of these slides has been optimized to maximize adhesion strength, at the slight penalty of reduced SNR (at high magnification, >60-100X). To standardize this process and ensure that the technician is aware of the material to be sectioned, this bifurcation point is integrated into the LIMS. At the start of the process, the technician logs into LIMS and retrieves a sectioning list, that is prepared ahead of time by the laboratory manager. For each brain on the list, there is a dedicated column that specifies the "stain paradigm." This alerts the technician as to the type of slides to be used for the sectioning. All other processing is identical for all stain paradigms.

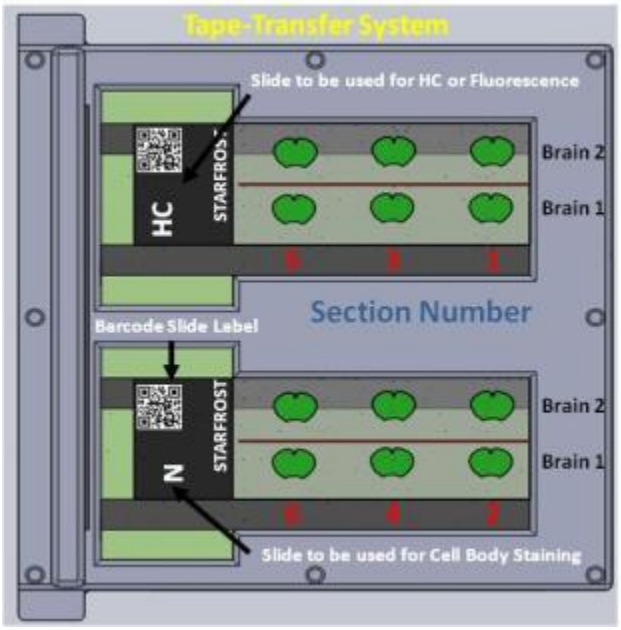

Figure 15: Labeling and placement convention on the CryoJane2.0

The CryoJane2.0 allows for sections to be placed on alternating slides, for the creation of two distinct series. In this system, one set of slides is intended for cell-body staining - labeled "N" for Nissl staining. The other set is intended for either histochemical staining or direct fluorescence imaging, labeled "HC" or "F". In this alternating arrangement, the section-to-section spacing, in a given slide set, is twice the section thickness. Two brains can be sectioned per block, the nomenclature is standardized such that "Brain1" position always refers to the brain on the bottom of the slide, when orientated as shown above. Three tape segments can be placed per slide. The first segment is placed at the edge of the slide, the furthest point from the slide label.

In terms of integration with the Section Imaging component of the system, the main integration element is the spatial placement of the sections on the slide. The width of the kapton tape used in this component is fixed at 15 mm, meaning that a maximum of 3 parallel segments of tape can fit onto a standard glass slide. The slide is 75mm total length, but 25mm is reserved for slide label, so that the effective surface is 50mm. Nevertheless, the exact position of the tape segments is not inherently controlled by the system. It is advantageous to standardize this placement, so as to allow the tissue detection algorithms of the Imaging component to have a localized search area. This

standardization was performed by instructing the technician to place the tap segments onto the slide, so as to align the midline of the tape with the midline of the slide This helped to reduce variations in the X-axis placement, parallel to the width of the slide. To standardize the placement of sections along the Y-axis, or length of the slide, the technician was instructed to align the first segment of tape with the edge of the slide (edge to edge) and then adjust position of the other segments accordingly. This did not completely eliminate the problem, but did help to improve the overall success rate of the tissue-finding algorithms.

2.2.5. Section Staining

2.2.5.1. Component Purpose:

This system component is responsible for the preparation of sectioned tissue, on glass slides, for section imaging. This preparation is a direct function of the upstream processing - i.e. the type of tracer that was injected into the animal. For animals injected with HC based tracers (CTB and BDA), this preparation entails the application of a tracer specific staining protocol, to reveal the location of the injected tracer. The duration, number of steps, type of solutions and the resulting SNR is exclusively tracer specific. Post-staining, the slides undergo a coversliping process, in which mounting media is sandwiched between the glass slide and a thin piece of coverglass - creating a homogenous index of refraction - which facilitates optimal imaging of the sections. For animals injected with viral based tracers, the preparation of the tissue is localized to the just the coverslipping process - because the location of the tracer will be determined upon fluorescent imaging. For both types of tracers, one of the series of slides (cut sections are separated into two series, section 2.2.4.5) is used for cell-body staining, which facilitates in the 3D reconstruction of the brain. Unlike other components of the system, these three processing steps are not applied linearly, or uniformly on all input material - which means that the processing rate of the component is a function of the material to be processed.

This component is a critical determinant of the signal-to-noise ratio of the data, and thus affects both the *biological quality* of the system and the *process quality*. The biological quality is affected because the interpretation of the injection label - determining where/what on the slide, can be categorized as "label" - is directly associated with the SNR of the label and thus the staining process. Of the three types of processing involved in this component - histochemical, cell-body staining and coverslipping - the latter two are most established in principle and

application. Both processes do need to be industrialized for high-throughput, but since the founding methodology is robust, this industrialization is direct. The protocols used for histochemical staining of tissue, vary widely between laboratories and are almost always, manually performed, on a small subset of sections. Whole-brain histochemical staining is quite rare - especially in high-throughput fashion. Therefore, the critical requirement of this component is to industrialized this process and ensure that the resulting label in the tissue is of high SNR and that the sections do not sustain damage while staining.

2.2.5.2. Established Methodology and Equipment:

As discussed above, this component of the system has three processing steps: (1) Histochemical (HC) staining; (2) Cell-body staining and (3) Coverslipping. For each step, there are two elements to consider: (A) the method of performing the staining and (B) the parameters of the staining protocol. It can be said that the first determines the biological quality (independent of this system), while the latter governs the process quality (specific to this system). A discussion of both elements for each processing step follows below:

(1) Histochemical (HC) Staining: The injection scheme of this system calls for two primary histochemical tracers to be used: Cholera Toxin (CTB - retrograde tracer) and Biotinylated Dextran-Amine (BDA - anterograde tracer). Classically, the HC staining for both of these antigens, is performed on free-floating sections. In this method, the sections are submerged in the staining solution in a petri dish or a multi-well, cell culture plate. The sections are initially submerged in a buffer solution and then the solutions are manually changed, as per the protocol. For each solution change, great care is taken as not to damage the section. The main advantage of this method is that the antibody reaction occurs from both sides of the tissue and thus the effective distance that the antibody needs to penetrate is ½ that of a unidirectional reaction, as per sections mounted on slides. More important than the rate of diffusion, is the actual rate of antibody-antigen reaction, through the entire thickness of the tissue. It is not enough for the antibody to just penetrate the tissue, but the antibody-antigen reaction must take place, so that the antigen (tracer) can actually be identified. On the molecular level, this reaction is governed by the antibody-antigen affinity, the association and the dissociation coefficients, and the relative concentration of antibody and antigen, and environmental factors (temperature, pH, etc.). This

relationship can be summarized as the number of antigen-antibody reactions/per unit time, which is a direct function of surface area. In this bi-directional method, the surface area is maximized, and thus the overall reaction rate.

The other practical advantages of the traditional, free-floating method is that: (1) the SNR of the product is higher compared to other methods, because the buffer washes are more efficient; the entire sample is washed and there are no "pockets" of antibody residue left on the sample; (2) the antibody-antigen reaction can be maintained for a long period of time, without much consideration for evaporation; (3) The antibody can be reused for many reactions (some addition of stock solution is advisable, between reuses). The main disadvantage of this method is that post-staining, the sections need to be manually mounted onto glass slides. This is a very tedious and error prone process. In many cases, especially in the high-throughput framework, the high-SNR of the HC staining is distorted and reduced by the artifacts introduced during the mounting process. The other less serious disadvantage, is uneven staining , which occurs when the tissue curls together, so as to result in uneven contact with the antibody. This curling can also lead to a high rate of false-positives. This which occurs either when antibody molecules are not properly washed away or if there is erroneous and prolonged contact between two areas of the tissue.

To overcome this limitation, the common alternative to the use of free-floating slides is to perform the HC reactions directly on mounted sections. This method has the obvious advantage of avoiding the need to mount the sections, post-staining, and is distinctly preferable for tape-transfer based cryosectioning (section 2.2.4.2). The main disadvantages of this method are that: (1) The antibody-antigen reaction is unidirectional on the section surface and thus the rate of diffusion and the overall reaction rate are slower than for the free-floating method; (2) the logistics of maintaining fixed quantities of solution onto the slide are significantly more complicated, as one needs to consider the effects of temperature, humidity (evaporation), surface leveling and physical movement of the slides. The reagents used in the HC process are quite expensive, therefore there is a need to minimize volume per slide. For this reason, it is not practical to simply submerge the entire slide in a beaker of solution, as is done in cell-body staining. On average, the HC process is around 20-50X more expensive than a common cell-body stain. (3) Maintaining the sections on the slide, without introducing mechanical damage, is also a difficulty - as each application of solution, introduces mechanical stress on the adhesion.

For these three reasons, HC staining on-the-slide is reserved for either very expensive HC reactions, which are performed on individual sections, or for clinical based purposes.

For clinical applications, the disadvantageous of on-the-slide staining are addressed through the use of automated staining machines, which control the volume, incubation, number and type of reagents that can be used to treat the slides. This automation allows for minimal manual intervention and therefore an increase in slide-to-slide staining consistency. This automation is not possible for free-floating sections, because of the high-risk of damaging the sections during solution changes. On-the-slide staining is more amenable to automation, because the sections are firmly adhered on the slide and the slide+section complex can thus be treated as a rigid body.

In the most common form of these clinical automated stainers, the slides are arranged in a horizontal array, such that the top surface of each slide (each section) is exposed. A computerized dispensing pump is attached to a two-axis translation arm/stage that is used to move between each slide and apply the appropriate solution. The dispensing pump is usually configured such that it can both take up the solution and dispense it, depending on the need. Therefore, the workflow for the system is that once the operator inserts the slides and provides all of the required reagents in individual vials, the system automatically goes through the process of up-taking the solution from the vial and then dispensing the user-specified volume onto the slide. The system repeats this for as many processing steps as specified by the user. The system usually has a separate pump for buffer (connected to a appropriately sized reservoir). Buffer is applied between each processing step. The incubation time per solution is specified by the user, as are most of the other general elements: start time, wait time, number of dispensing zones on the slide (middle of slide, edge of slide, etc.), name of solutions and their location in the vial rack, so that the machine has a map of the solutions; and means of error notification/response (if "not enough solution in vial", then ...). The use of these automated systems, helps to greatly standardize the entire HC process and reduced the failure mode of an operator accidently dispensing the wrong amount or the wrong solution onto a given set of slides. These systems, also allow for the continuous overnight operation - the technician just needs to load the slides and the reagents for an overnight batch-run and depending on the incubation times, the process can be complete by morning. As such, the overall throughput of the component, can improve by 2X.

These systems are not without fault; the biggest problem is that despite advertisement, the performance of the system is protocol dependent. This means that there is an inherent limitation on total incubation time per volume dispensed. This is because of the considerations mentioned earlier - temperature and humidity, which both govern the rate of evaporation of the solution from the slide. On a year-round average (20±2°C Temperature, 30±10% Humidity), a solution of <=1ml can remain on a slide without drying for 4-5hours. A given 1X3" glass slide cannot accommodate more than 1.2ml of solution without spillover, assuming that it is leveled to the horizontal. Therefore, the only two ways of prolonging this incubation time are to either increase the humidity in the chamber to 70-80% or to reapply a given solution multiple times, in discrete incubation times of 4-5hours. The latter choice is undesirable, as it will increase the disposable cost per batch-run by the number of dispenses required; for example, up to 6X for a 24 hour incubation. For these reasons, these machines should be integrated into the section staining component of the system, only as a direct function of the antigen detection protocol to be performed. These machines are not universal and cannot be treated as fully versatile machines.

Figure 16: Standard histochemical protocol for the detection of injected CTB

The HC protocol for the detection of injected Cholera Toxin Subunit B (CTB) and similar antigens, calls for a multi-step process, that is summarized in Figure 16. This protocol is a derivative of the "Standard Immunohistochemical Protocol", from J. A. Ramos-Vara[52]. Steps that are not appropriate for frozen sections (those produced using a cryostat) are excluded.

The main elements of this protocol, are (1) Permeabilization & Protein Blocking: is required to reduce the background (reduce noise) from erroneous interaction of the antibody with tissue proteins. This entails the treatment of sections with serum from the host of the secondary antibody or other blocking proteins, such as bovine serum albumin (BSA). During this step, the

sections are also treated with Triton X. This helps to make the cell membrane permeable to antibody penetration. The incubation time for this step is usually on the order of hours (.5-2 hour(s) is typical). (2) Primary Antibody: this is the central step of the process, and involves the treatment of sections with the primary antibody solution, usually prepared with a derivative of the blocking solution.

For CTB, this antibody would be Goat anti-CTB (List Biologics Corp) or a similar antibody, in a different host species. This is the most "direct" reaction in the protocol, meaning that the applied antibody is targeting the specific antigen (injected CTB) in the tissue The concentration of the antibody is usually in the range of 1:2,000 - 1:20,000. The range is narrowed through empirical testing. This is typically one of the longest incubation steps of the process: "overnight," meaning 12-24 hours is the most common interval. (3) Secondary antibody: Unlike the primary antibody, which is selected to target the antigen in the tissue, this antibody targets the primary antibody. This secondary antibody is tagged (labeled) with a detection probe. This probe is typically biotin or a fluorophore, like fluorescently conjugated Alexa. The conjugate determines the downstream imaging that will be required to visualize the signal, brightfield (for biotin) or fluorescence (for fluorophore). Though the issue is widely debated, the main advantages of biotin (brightfield) base reactions are: (A) the ease and cost of performing brightfield imaging versus fluorescence imaging; (B) the reaction is

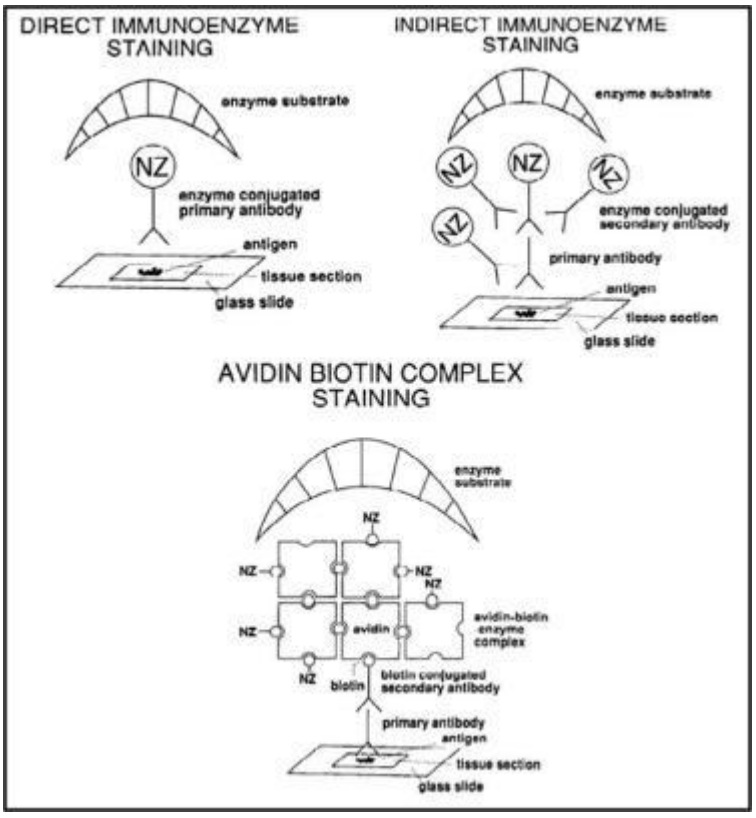

Figure 17: Diagrammatic representations of three enzyme histochemical staining methods.
(A) Direct immunoenzyme stain. (B) Indirect immunoenzyme stain. (C) Avidin-biotin complex (ABC) immunoenzyme stain. The principle advantage of the ABC method is the high affinity of avidin to biotin and the four binding sites that avidin has for biotin. Avidin is conjugated to horseradish peroxidase**(**HRP), which when reacted with H_2O_2 in DAB solution, produce much higher quality of label (SNR) than through other methods[61].

permanent and does not degrade easily with imaging (photobleaching); (C) the reaction is more sensitive for the detection/identification of fine processes. The downside of biotin is that it requires further chemical processing; namely, two more reactions (ABC, step 12 and DAB, step 14), while a fluorophore-conjugated reaction, concludes with the incubation in the secondary antibody .

For CTB, the secondary antibody would be Biotinylated Rabbit anti-Goat (Vector Laboratories), at a concentration of around 1:100- 1:500. The host species, rabbit, is not very relevant, as long it is not mouse (tissue source) and is against the host of the primary antibody (goat). The incubation time is typically shorter than that of the primary antibody, on the order of two to four hours. (4) Avidin-Biotin Complex Formation: To increase the sensitivity of the detection of the biotinylated secondary antibody, the biotin is reacted with horseradish peroxidase (HRP) conjugated to avidin. Avidin has a very high affinity for biotin, with a very low reaction dissociation rate, which makes the reaction "permanent". "Avidin has four binding sites for biotin, and most proteins including enzymes can be conjugated with several molecules of biotin. These properties allow macromolecular complexes (ABC's) to be formed between avidin and biotinylated enzymes"[17, 62].

Unlike other steps of the process, ABC is most commonly used in the form of a manufacturer's prepared kit (Vector Laboratories), and as such, the concentration is predetermined. In the case of the Standard ABC kit from Vector, the concentration is on the order of 1:60 and requires a short incubation time, of 30 minutes. (5) Reaction Development: The final step in this process is developing the reaction products and forming a stable precipitate. This is most commonly done through the use of with diaminobenzidine tetrahydrochloride (DAB) as a chromogen. When DAB is mixed with H_2O_2, in the presents of HRP, a dark brown precipitate is formed, meaning that the HRP-ABC complex turns dark brown. This is a redox reaction, in which HRP is the enzyme, H_2O_2 is the substrate; H_2O_2 is reduced to H_2O and the oxygen molecule combines with DAB to form a brown precipitate. Metals, such as Nickel Ammonium Sulfate ($NiSO_4(H_2O)_6$) and Cobalt Chloride ($CoCl_2$), can be added to the DAB reaction, to form a black precipitate, which is advantageous from a detection perspective. The incubation time for DAB is quite short, on the order of a few minutes. The concentration of DAB is typically .05%, same for the metal additives; the H_2O_2 concentration is around ⅓ that of the

DAB concentration. Proper safety considerations need to be followed for the disposal of the DAB solution, as it is highly toxic.

The five critical steps discussed above, represent the principal components of the reaction. Between each step, it is vital to extensively wash the sample with buffer solution and to keep the sections hydrated at all times. The DAB reaction product is very pH sensitive; the pH must be maintained between 7.2-7.6 to ensure proper staining intensity, without increasing the background (noise).

The HC protocol for the detection of injected Biotinylated Dextran-Amine (BDA), is significantly simpler than that of CTB for the sole reason this antigen, is natively biotinylated, meaning that the treatment of the sections with the primary and secondary antibody is not need. As such, the HC protocol for BDA is reduced to three steps: (1)Protein Block, which only contains a detergent like triton, no serum is needed because no antibody reaction will occur; (2) ABC incubation - which is performed similar to that of CTB, but incubation time is significantly longer - on the order of "overnight", meaning 12-24hours. This longer incubation time is needed to allow for the ABC reaction to take place in the context protein crosslinking performed by the tissue fixation. In the case of CTB, this is not needed, because the primary antibody already account for this "direct reaction". (3) Reaction Development - following ABC, the reaction is developed, through the use of DAB, in a identical manner (same concentrations) to that of CTB.

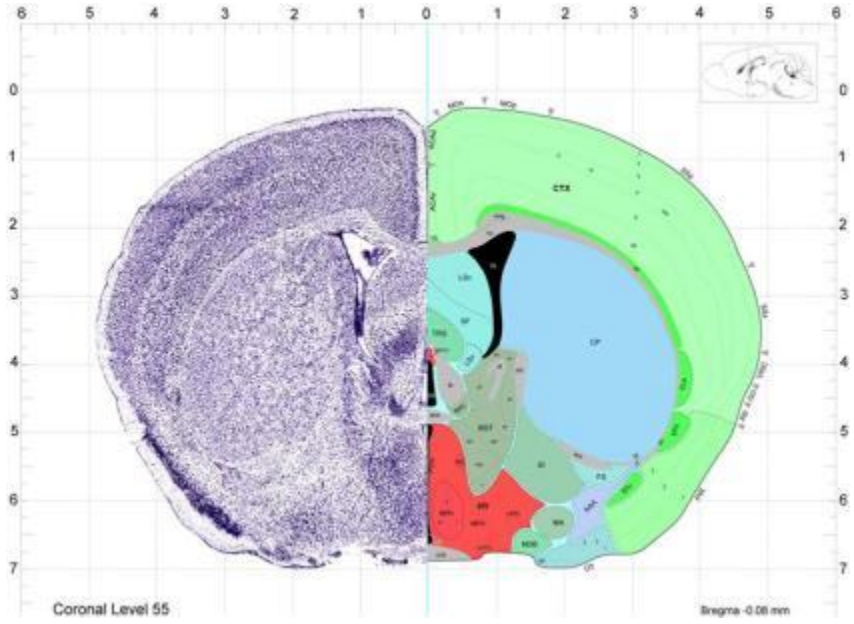

Figure 18: A coronal Nissl/atlas section of the mouse
One of the principle applications of the Nissl stain is to identify and segment regions in the brain sections. This segmentation, allows for the development of a regional brain atlas. Above, an extract from the Allen Reference Atlas[39], coronal level 55, is shown. The regional segmentation was performed for only the left hemisphere, which is shown on the right in the above image.

As is evident from the above, the HC process is "simple," borne out by an extensive literature, going back over 30 years; but it is quite "complex" in terms of implementation and, conspicuously, in terms of standardization. Besides the logistics of introducing and maintaining the solution on the slide, there are batch-to-batch effects that need to be considered for high-throughput processing of tissue. Though manufacturers claim to implement rigorous internal quality-control measures, empirical evidence has shown that entire lots of antibody solution can be defective ("dead on arrival") or lead to sub-optimal staining. For long-term storage of these reagents, one needs to consider safeguards in refrigeration and making sure that if one system (refrigeration or facility power system-) fails, the entire stock of antibody is not lost.

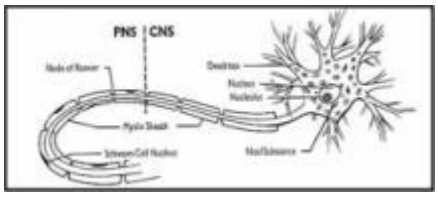

Figure 19: The neuron with its various structural components
A representative neuron: cell body and processes. The image above shows a cell body with prominent clumps of Nissl substance (rough endoplasmic reticulum), which are visualized by Nissl stains. Also indicated are the dendrites and part of the myelinated axon[51].

(2) Cell-Body staining: Unlike HC staining, where the molecular target is localized to a small subset of neurons (or axonal fibers) of the tissue section, cell-body staining is intended to label a target that is common to the majority, if not all, neurons in the brain. The most common such "antigen" target is the Nissl substance (Figure 19), which is primarily composed of large aggregates of rough endoplasmic reticulum, that contain lots of ribosomal RNA. Because of RNA content (i.e., acidic pH), the Nissl substance is strongly stained by basic aniline dyes, such as thionin and cresyl violet. Nissl substance varies in form, size and distribution in different types of neurons. By varying the pH and the degree of differentiation, either the Nissl substance and/or the nucleus can be labeled [51]. Since this stain labels all of the neurons in a given section, one is able to easily develop a global view of the section and its nuclear or cortical laminar organization. This regional organization is well annotated and illustrated in whole-brain anatomical atlases of the mouse[38, 39]. One such section with annotations is shown in Figure 18. The use of the Nissl stain allows for direct registration of the sections onto an anatomical atlas, which is critical for reporting the exact location of connections. The Nissl stain should not be assumed to be "neuron" specific as it does label other cell types, most notably, glial cells (Figure 20).

The classic method of performing the Nissl stain, is to: (1) hydrate the tissue in buffer, if sections are dehydrated from earlier processing; (2) incubate sections in the basic aniline dye, either a 0.1% Cresyl violet solution or 0.25% Thionin solution, for a few minutes (1-2 minutes); (3) wash the sections in distilled water, for two separate rinses, to remove the dye from the sections surface (1-2 minutes per wash); (4) dehydrate and differentiate the tissue, by progressing through increasing grades of ethanol (50%, 75%, 90% and then 100% ethanol) . Incubation time in ethanol determines the differentiation of the stain; i.e., the background color, with respect to that of the labeled cell bodies. The average time is on the order of 1-3 minutes per ethanol grade. Typically, two washes per grade are applied. (5) Following the last step in 100% Ethanol, the sections are processed through two solutions of xylene, for 1-3 minutes each. This is an intermediate step, that removes any excess ethanol from the sections and prepares them for coverslipping with a xylene based mounting medium.

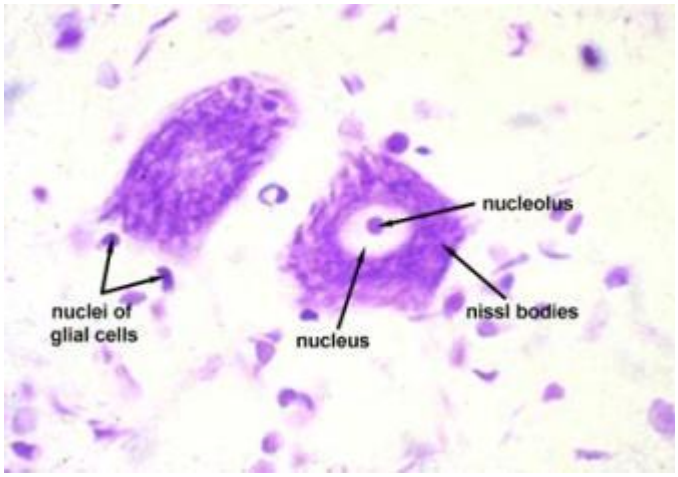

Figure 20: Nissl stain of neurons and glial cells
Two Motoneurons from the ventral horn of the spinal cord stained with a Nissl stain are shown. Glial cells are labeled at the same intensity, but can be differentiated from neurons by relative size.[63]

Compared to the HC staining protocol, the Nissl protocol is significantly easier, not only because of the order of magnitude faster processing time (<30 minutes), but also because the reagents are inexpensive and can be prepared in bulk. The typical volume for each reagent is on the order of 500-1000ml. This is prepared in large beakers, and several dozen slides can be stained simultaneously. The Nissl stain is less sensitive to tissue preparation in terms of slide-to-section adhesion, thickness of the sections (above a certain point, the processing times need to be modified); and method of sectioning. The tissue processing is also independent of the environmental variables (within a margin); temperature and humidity variations in the laboratory do not affect the stain quality. The only environmental variable that needs to be monitored in the pH of the reagents.

The classical approach to performing the staining is to simply prepare the solution in designated (labeled) beakers, and then manually regulate the incubation time of slides in each solution. Slides are typically loaded into a holder with a handle, to allow for easy handling. An obvious point of failure, in the context of high-throughput, is maintaining consistency in time of processing steps for all reagents, over a large volume of slides. The use of a laboratory timer is a simple means to achieve this;, but factors such as small variations in technician response time to

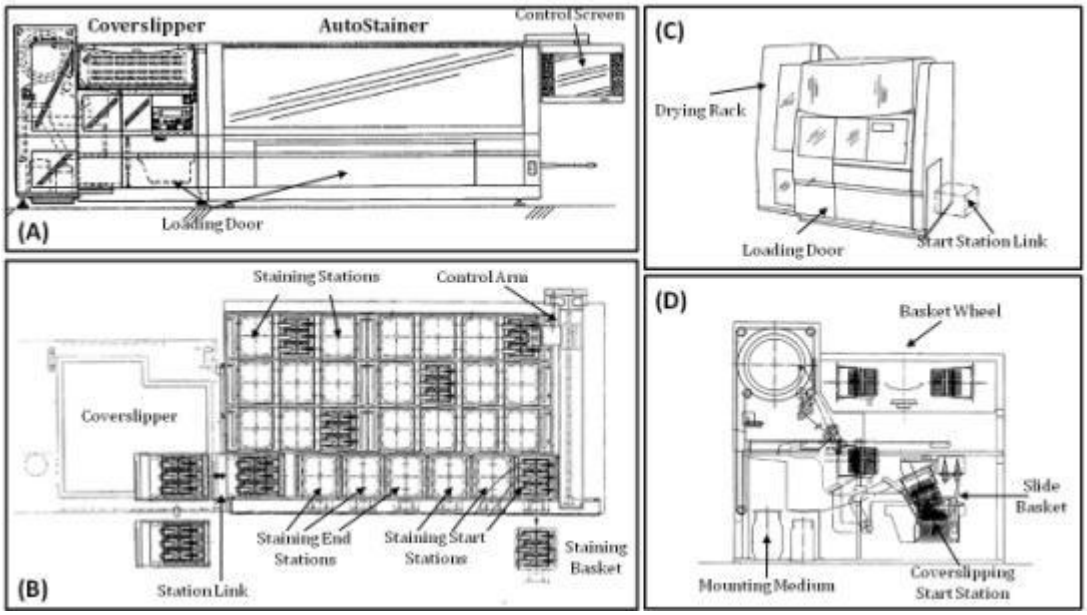

Figure 21: Perspective view of the Automated Slide Stainer and Coverslipper
A model view of the Sakura Automated Slide Stainer and Coverslipper is shown in (A). The two components are integrated into a single unit, such that stained slides can be automatically coverslipped, without further manual intervention. A top-view of the autostainer component is shown in (B) - the unit is comprised of 3 start station basks; 3 end station baskets and 21 staining baskets. Each basket can accommodate 60 slides. Staining can be done continuously - following a predefined staining paradigm. (C&D) The coverslipper is a mechanically intensive unit - consisting of many moving parts, but is calibrated to produce consistent results, with minimal downtime[64].

the beeper can cause significant batch-to-batch differences. Since the average time for each step is on the order of 1-2minutes, a 10% variation is 6-12seconds; and if a technician is otherwise engaged, even momentarily, variation could be larger. For this reason, it is desirable to automate this process, again through the use of clinical systems. As in the case of HC staining, this automation is only possible because the staining is performed on the entire slide. These stainers are similar to those used for HC staining, except that they are significantly simpler machines and are not prone to the protocol based constraints. This is because the single biggest problem with HC stainers - i.e. maintaining solution on the slide over prolonged periods of time - is not an

issue in this method. The processing times are very short and, more importantly, the entire slide is submerged in solution. The main determinant of batch-to-batch consistency is not the mechanics of the system, but rather the preparation of the solutions that are loaded into the system. The machine can be relied upon to deliver consistent performance, as its sole purpose is just to ferry slides from beaker to beaker, at specific times, based on a preset protocol. Maintaining high-consistency in reagent preparation is a matter of protocol standardization, as discussed in section 2.2.5.4. Though primarily intended for cell-body staining, these machines can be used for other bulk-style staining - such as hydration and dehydration of tissue. A diagram of such a stainer is shown in Figure 21(A&B). This stainer is integrated with an automated coverslipper (discussed below), such that stained slides can be automatically coverslipped, without manual intervention.

(3) Coverslipping: Biological tissue, even fixed tissue, degrades in over time. For this reason, and for the microscopy considerations discussed below and in section 2.2.6.2, all slides need to be coverslipped, post staining. In this process (1) a liquid suspension, mounting medium, is applied onto the sections, (2) the suspension (section+medium) is sealed on top by the addition of a cover-glass (coverslip), and then, (3) the sides of the "sandwich" are sealed either by the drying of the mounting medium (hard set) or the use of lacquer (nail polish) to create a perimeter around the edges of the coverglass. The result is that the sections are preserved in an air-tight suspension, such that they can be stored for prolonged periods and properly imaged. The two critical factors in this process are the mounting medium and the cover-glass. The basic requirements for both elements are: (1) an index of refraction that is well-matched to each other and to the glass slide, so as to minimize the amount of light that is refracted as it passes through each medium boundary; (2) optical, chemical and physical properties that do not distort the SNR of the specimen. The second requirement refers to possible quenching of fluorescence due to the interaction with the mounting medium and the presence of artifacts on the coverglass that will impede transmitted light imaging.

The cover-glass is specimen independent, but is a critical determinant of the imaging resolution that one can achieve. Most microscope lenses are tailored to a specific thickness of coverglass, that will result in optimal resolution, usually in the range of .17mm (#1.5, Corning). Coverglass with these specifications is readily available from manufacturers like Corning, with

tight thickness (.16-.19mm) and refractive index (1.5255 ±0.0015) tolerances. The footprint of the coverglass is such that the entire useable area of the glass slide can be covered (25X50mm). The coverglass needs to be handled with care, as it is quite thin (7X thinner than the glass slide), but can nevertheless be reliably used in large volume applications, without a concern for failure rate (breaking coverslips). Though ignored in most applications, the surface of the coverglass cannot be assumed to be artifact free, as dust, glass particles and other foreign material are known by-products of the manufacturing process. As such, Because of this, the coverglass should be washed in either ethanol or a similar liquid and allowed to air dry, prior to use. This is a simple process, but greatly reduces the issues of artifacts in the resulting image of the specimen.

The mounting medium has a similar role to that of the coverglass, but with the caveat that it interacts significantly more with the tissue, as it is the suspension medium. The refractive index matching of the mounting medium is a critical element of the system. The mounting mediums, and the corresponding refractive indices, are shown in Figure 22[65]. The two common base forms of the mounting medium are xylene and water based. This distinction is critical, as xylene is classically thought to quench certain fluorophores and is commonly not used for fluorescence microscopy. For brightfield imaging, xylene based mounting mediums are the norm and present give major advantages in terms of automation and general handling. This is because many xylene based mounting mediums, such as DPX, DEPEX, etc. are truly "hardset". That is, once the coverglass is applied onto the mounting medium (with specimen), the medium will dry and harden within a short period (initial cure in 10-20minutes, full cure within several days). This makes the entire coverslipping process significantly easier, as the "sealing step" with lacquer is not required. Xylene based mounting mediums are also more homogenous than water-

Mounting Media	Refractive Index[a]
Gel/mount (Biomeda)	1.3641
Methyl salicylate (Sigma)	1.5409
Dimethyl sulfoxide (Sigma)	1.4836
VectaShield (Vector Labs)	1.4577
DPX (Fluka)	1.5251
50% glycerol/PBS/DABCO	1.4159
Water	1.3381
Cargille index of refraction liquids	1.460–1.700[b]
5% *n*-propyl gallate/0.0025% *p*-phenylene gallate (PPD) dissolved in glycerol	1.4739
0.25% PPD, 0.0025% DABCO, 5% n-propyl gallate dissolved in glycerol	1.4732

[a]Corrected to 20°C.
[b]Can be ordered as a set of liquids with refractive index intervals between each samples as low as 0.002.

Figure 22: Refractive index of common mounting media The refractive indices of common mounting media are shown. The index of the mounting medium should match that of the cover glass. For the case of #1.5 Corning Coverglass, the refractive index is in the range of 1.5255 ±0.0015. DPX is a close match and offers the advantage of a hardset [65].

based mounting mediums, which is a critical factor for whole-slide imaging, in that the overall image will be more homogenous. Color fluctuations in the whole-slide image are a common, undesired attribute of water-based mounting mediums.

As suggested above, the two main drawbacks of water-based mounting mediums are: (1) the need for lacquer (nail polish) sealing of the medium, post coverslipping, a manual process that is quite tedious. Though some water-based medias are advertised as "hardset", this property depends on the tissue thickness, and rarely holds for 20μm sections. (2) lack of uniformity in the chemical/optical properties of the solution over the entire slide. Nonetheless, the use of water-based mounting medium is standard practice in most neuroanatomy laboratories, because of the common belief that the degradation of fluorescence is reduced, compared to xylene based mounting mediums. This belief is strongly supported through the claim that commercial mediums, such as Vectashield (Vector Laboratories) and Fluoromount-G (Southernbiotech Corporation), have anti-fade and photo-bleaching resistant properties. However, empirical evidence suggests that these vendor claims are specimen and preparation dependent, and cannot be assumed to be universal. Vectashield, as an example, is known to "become fluorescent over time and quenches CyDyes"[66]. For these reasons, and in the context of high-throughput and standardization, it is best to use xylene-based mounting mediums with proper sample preparation changes (reduced time in ethanol/xylene), if possible[67, 68]. The main point here is that the effects of the mounting medium on the preservation of the specimen has more to do with the preparation of the specimen, than does the actual media. The main role of the mounting medium, especially in the context of high-throughput processing, is just to match the index of refraction to that of the coverglass. Reduction in fluorescence, as a function of time, should be addressed through rapid imaging of the sections post coverslipping and storage of the sections in dark, at a temperature of 4°C.

Xylene-based mounting mediums are standard in clinical pathology, which means that automated solutions are available for the streamlining of this process. These automated coverslippers, are very precise instruments, consisting of many motorized components, but are calibrated to function as reliably as a "Swiss made watch". As in the case of automated stainers for cell-body staining, the system performs repetitive motion; and though the process requires fine motion and the movement of thin glass, the entire process is well within the tolerances and capabilities of modern robotics. A diagram of such a stainer is shown in Figure 21(C&D).

Extensive empirical testing of these instruments, from vendors such as Leica Microsystems, Sakura Finetek, Richard Allen Scientific, etc, have shown them to be quite reliable for several thousand slides, with minimal maintenance required. These instruments can be used with a wide range of tissue types and tissue thickness, as long as the dispensing volume is within the range of 50-200ul and is xylene-based. One of the reasons that these systems work only with xylene based mounting medium is that these mediums have a significantly higher viscosity than that of water and thus are easier for the system to handle. In terms of throughput, these systems can perform, as empirically tested, at a rate of about 5X faster than that of a technician, coverslipping manually.

2.2.5.3. Design Implementation and Innovation:

As evident in the above discussion, this component is the most elaborate in terms of technical detail. Unlike the Sectioning component, which consisted of a single major element of departure from conventional methodology - i.e. tape-transfer based cryosectioning - this component contains many elements of departure, each of marginal magnitude, but together, representing a major leap in methodology. As directly suggested in the above section, the general goal and novelty is automation, through the adaptation of clinical systems for neuroanatomy applications. Therefore, the main focus of the implementation process was the selection, purchase and deployment of the appropriate clinical system. Batch staining (cell-body staining) and coverslipping machines, were deployed with no significant design changes, just modifications of the classical, manually based staining protocol (manual) to optimally integrate with each machine. For HC staining, significant changes were made to the hardware of the machine, to improve performance while minimizing the amount of reagent used per batch (and the associated cost per batch).

(1) Histochemical (HC) Staining: The clinical machine selected as the backbone of the HC staining for the system, was the Labvision 720 (Thermo Scientific). A diagram of this system, is shown in Figure 23. The key attributes of this machine, compared to the Leica Bond (Leica Microsystems), the Benchmark ULTRA (Ventana Corporation) and other products, are: (1) staining protocol is open-ended and driven exclusively by the user's configuration. There are no intrinsic constraints on the processing time per reagent, the type of reagents that can be used, or the number of times a day that a given protocol can be run on the system; (2) reagents used in the

system are independent of the system; thus, the user can switch the antibody vendor, without considering compatibility with the machine; (3) capacity of the machine is 84 slides, which are arranged in a horizontal array of 7 racks, with 12 slides per rack. In terms of general staining quality, reproducibility and overall adaptability, this system is significantly superior to other commercial HC stainers.

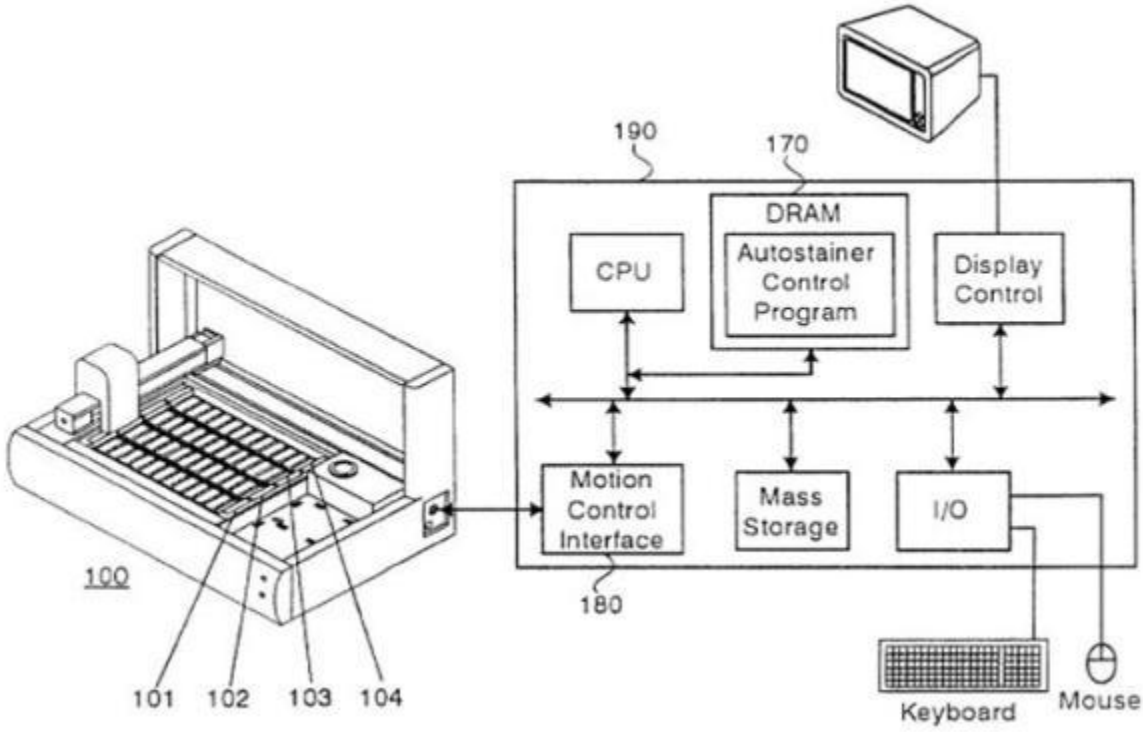

Figure 23: Perspective view of the autostainer apparatus
A model view of the Labvision Autostainer is shown. The relation of the robotic arm to the slide racks is shown, as is the schematic view of the computer control of the system. (100) The autostainer; (101-104) Slide racks, each capable of accommodating 12 slides. (190) The computer Control System; (180) The Motion control interface card; (170) The Autostainer Control Program.[69]

As discussed in the previous section, though optimal for clinical staining, this machine was fundamentally incompatible with the staining protocols for CTB and BDA. The maximum incubation time, per reagent, that could be achieved with the dispensed volume of 800ul per slide was on the order of 4 hours, with slight variability as a function of the humidity/temperature in the room. To address this problem, two design changes were implemented: (1) A custom fixture was designed and adapted to fit onto the slide racks of the Labvision720. This fixture allowed for the leveling (pitch) to be adjusted per slide, by rotating a screw that was positioned underneath each slide. This was a very simple fixture, but one that ensured that each slide can be leveled to

the horizontal. The basic protocol for the use of this fixture is for the operator to periodically (weekly/monthly) place a ball-level on top of a blank slide positioned in the holder and then to adjust the screw, until the slide is leveled, repeating the process for all positions in the rack. (2) To address the lack of environmental controls in the staining chamber, a steam humidifier (Skuttle Corporation, Model 60-BC1) was connected in series with the staining chamber of the system. The humidifier was connected to a controller (TruelAQ, Honeywell Corp) that was placed inside of the chamber. Weather stripping insulation was placed on the perimeter of the chamber door, such that when the door was lowered, a closed system would be formed, with the humidity controlled directly by the TruelAQ humidistat. The humidistat was programmed to maintain an average humidity of 80%. This which was empirically shown determined to allow for a dispensed volume of 800ul to remain on the slide, without evaporation, for at least 18 hours.

One of the challenges with humidifier control was preventing excessive condensation from forming inside of the chamber and precipitating onto either the electronics of the system or onto the glass slides. This "biosphere effect" was solved by carefully monitoring the humidity in the chamber and maintaining it below the critical condensation point (90%). The location of the humidistat was adjusted, such that it would represent record the average humidity in the chamber and not a local minimum or local maximum. The sensor is calibrated monthly.

In addition to the above two modifications, the use of the PAP-pen (Manu Corporation) was incorporated as standard for all HC staining. The PAP-pen is used to draw a hydrophobic perimeter around the exposed surface of the glass slide. This raised surface perimeter helps to adjust for minor differences in leveling from slide-to-slide, and also minimizes the amount of solution that is lost due to the dispensing process (i.e., the actual release of solution, by the syringe pump, onto the slide). The Pap-pen is toluene based, meaning that it "self" removes when immersed in xylene, during the last steps of the coverslipping process.

With the implementation of the above design modification, the Labvision720 could be effectively and routinely used, for both CTB and BDA based staining. One of the remaining problems with this system was that the throughput was maxed at 1 series per day. This was not a machine limitation, but a protocol limitation (processing time requirements). This limitation was addressed through the deployment of multiple staining systems. Instead of using the Labvision720, which has a base price of $80,000 (Spring 2010), smaller, refurbished units were

purchased from a 3rd party and integrated into a configuration similar to that of the 720. These refurbished units were identical in form and function to that of the 720, aside from having half the slide capacity (4 rack of 12 slides each = 48 slides per machine). Notably, they were a fraction of the cost. Four such machines were acquired, rebuilt and deployed, with similar humidifier and slide rack modifications, for a combined cost of $15,000. This resulted in a slide capacity increase of 192 slides. With this addition, three series could be stained simultaneously, a rate higher than that of the sectioning upstream components.

Anti-CTB Immunohistochemistry Staining Protocol:			
Step	**Station Name**	**Concentration**	**Time (min)**
1	Protein Block	5% Normal Rabbit Serum 1% Triton in PBS	30
2	**Primary Antibody**	**Goat anti-CTB, 1:7500 Dilution**	**840**
3	Secondary Antibody	Biotinlyated Rabbit anti-Goat, 1:200 Dilution	120
4	**ABC Incubation**	**1:1 Ratio of Solution A to Solution B** **1:62.5 Dilution of each in PBS**	**180**
5	DAB Development	.05% DAB, .05% Co, .05% Ni, .015% H_2O_2	5

Table 2: Histochemical staining protocol for the detection of injected CTB

BDA Immunohistochemistry Staining Protocol:			
Step	**Station Name**	**Concentration**	**Time (min)**
1	Protein Block	1% Triton in PBS	60
2	ABC Incubation	1:1 Ratio of Solution A to Solution B 1:62.5 Dilution of each in PBS	1080
3	DAB Development	.05% DAB, .05% Co, .05% Ni, .015% H_2O_2	5

Table 3: Histochemical staining protocol for the detection of injected BDA

The above development was focused on maximizing the efficiency of the technical HC process. This development was performed in parallel to the optimization of the actual label detection protocol. Much of this protocol development was performed through empirical testing. The finalized protocols for CTB and BDA are shown in and Table 3, and the detailed protocols are shown in Figure 25 and Figure 26.For both CTB and BDA, the goal was to maximize the SNR of the label. For CTB, the concentration of the primary antibody was increased from 1:10,000 to 1:7,500 and the incubation time for the primary antibody was increased from the original baseline of 8 hours to 12 hours. The incubation in ABC was increased to 3 hours from 2 hours. For BDA, the incubation in ABC was increased from a baseline of 6-12 hours to 18 hours. The incubation time for DAB was fixed at 5 minutes, per the concentrations shown. Cobalt Chloride ($CoCl_2$) and Nickel ammonium sulfate (Nickel Ammonium Sulfate ($NiSO_4(H2O)_6$)) were added

to the DAB solution to maximize SNR and to result in a black reaction product. This is easier to detect through automated algorithms than gray, brown or other color shades. The fixed incubation time for DAB is a departure from convention, in which the DAB process is typically observed under the microscope real-time and the incubation time is adjusted as needed. Since the tissue processing and all related reagents are standardized in this process, the observation under the microscope is not needed, as the DAB reaction is a function of the tissue, the labeled antigen and the other used reagents.

(2) Cell-Body Staining and Coverslipping: The clinical machine selected as the backbone of this process was the Tissue-Tek Prisma® & Glas™g2, automated stainer and coverslipper. The advantages of this machine, compared to the Leica Autostainer XL / Leica CV5030 (Leica Corporation), Gemini Autostainer / Shandon ClearVue (ThermoFisher Corporation) and other machines that were evaluated, are: (1) Multiple start stations, each capable of handling 60 slides; (2) Ability to initiate several simultaneous staining process, following the same, or different programs; (3) Ability to perform variably timed processing steps, from several seconds (>5 seconds) to several hours; (4) Ability to directly program the entire staining protocol, without any intrinsic limitations (Vadim: meaning is unclear); (5) Ability to initiate coverslipping directly after the completion of the staining process, without manual intervention; (6) Ability to control the volume of mounting medium dispensed, the pressure applied on the slide (during the lowering of the coverglass) and the drying of the slides; (7) Ability to treat the coverglass and the mounting medium is also as independent of the machine. The other main attribute of this machine is that the rate of processing is protocol dependent and not machine dependent; the datasheet specifies the rate as "330 slides per hour" for the coverslipping.

Nissl Staining Protocol:			
Step	**Station Name**	**Concentration**	**Time (min)**
1	Thionin	2.50g / 1000 mL dH_2O	1:30
2	dH_2O - Deionized Water	-	0:30
3	dH_2O - Deionized Water	-	1:30
4	50% Ethanol	50% / dH_2O	1:30
5	70% Ethanol	70% / dH_2O	1:30
6	95% Ethanol	95% / dH_2O	2:00
7	Absolute Ethanol	-	2:30
8	Absolute Ethanol	-	2:00
9	Xylene	JT9490	2:00
10	Xylene	JT9490	2:00
11	*End Station (Xylene)		-

Table 4: Nissl staining protocol for cell-body labeling

This machine, unlike the other's that were evaluated, is designed to operate under negative pressure and vent all exhausts through a carbon filter. This feature helps to minimize the

exposure to xylene and other hazardous staining chemicals by the technicians operating the equipment. To further minimize the chemical exposure from the machine, the exhaust was directly connected to a nearby fume hood, so as to guarantee that all chemical fumes are safely removed from the laboratory.

The machine was configured to routinely perform Nissl staining, dehydration of fluorescent sections, and direct coverslipping of both types of slides. The parameters for the Nissl stain are shown in Table 4. The time values of each processing step were empirically optimized to maximize the intensity of the cellular label and differentiation between brain regions. The stain quality was equal to or better than that of manual staining. In terms of coverslipping, DPX was used as the universal mounting medium, for both brightfield and fluorescence slides.

Maintaining a uniform index of refraction for the mounting medium and the coverglass is a critical, to achieve optimal image resolution and a uniform whole-slide image. Mounting media distribution and coverage on the slide are the main optimization parameters. Prior to the application of the mounting media, the slides are immersed in xylene; and when the xylene-based DPX mounting media is applied, the residual xylene on the slide (slides are shaken and undergo a 90° rotation) mixes with the applied mounting media. Depending on the ratio of residual xylene to applied mounting media volume, the average index of refraction of the entire slide surface will vary. The mounting medium is applied as a line, down the midline of the slide and then the coverslip is applied onto of the slide, so as to cause the lateral spreading of the mounting media. If the mounting medium to residual xylene ratio is low, the center of the slide will have more mounting media than the edges of the slide, and thus the index of refraction will vary along the same gradient. The obvious solution to the above is to maximize the amount of applied mounting medium; but the downside to this approach is that the excess mounting medium will squeeze out of the side of the sandwich and pollute the top of the coverslip and the bottom of the slide. Excess mounting medium will increase the drying time for the slide and, more importantly, interfere with subsequent imaging (another refractive layer). Also, the removal of this medium will have to be done manually, on a slide by slide basis. This will severely decrease the overall efficiency of the coverslipping process.

In manual coverslipping, the mounting medium is applied onto the slide, either in the center of the slide or as a line, depending on individual preference, and then the coverslip is

lightly lowered onto the slide. The weight of the glass, with some application of minor force, is used to spread the mounting media. The main difference between this and the automated process is that the coverslip is not dropped onto the glass but rather pushed onto the slide in a concave motion. This is done to control the lateral position of the coverslip (relative to the edges of the slide) and to reduce air bubbles on the slide. This concave application motion pushes air bubbles to the edges of the slide. The resulting thickness of the mounting medium is therefore significantly less in the automated process than in the manual process.

To address the above issues and ensure optimal mounting medium coverage, the settings on the coverslipper were modified, such that the distance from the coverglass to the surface of the slide was increased. The amount of force applied by the machine remained unchanged (as this is hardwired into the motion system); but since it is applied further away from the surface of the slide, the actual impact on the mounting medium is greatly reduced. This modification allowed for an increase in the amount of applied mounting medium volume from 40µl to 100-120µl. This translates into a thickness increase of approximately 26-35µm. The entire applied volume remains on the slide, after the application of the coverslip, without leakage from the sides. It was found that for reflected microscopy, a more uniform whole-slide image would result through the higher volume of mounting media. Image uniformity was judged based on ease of focusing, achievable resolution and color/contrast across the entire surface of the slide.

2.2.5.4. Procedure Standardization/Industrialization:

The operation of this component is a major departure from conventional neuroanatomy, and as such, required a complete overhaul of the operating procedure. This overhaul focused on standardizing the use of the autostainers and coverslipper, and maximizing their efficiency. Since the autostainers were configured to perform the main interaction with the actual slides (i.e., applying the reagents of the staining protocol), the main responsibility of the technician was to prepare the solutions and load the slides into each machine. In the case of cell-body staining, the reagents are prepared in bulk. In this case, measuring is easy, since tolerances are larger (±1% of 1000 ml = ±10ml), but the consequent downside is that a large number of slides can be stained (>60) before a reagent problem is identified. For this reason, and to account for other reagent preparation issues, the following procedural changes were enacted: (1) Thionin solution (the main staining solution of the Nissl stain) would be freshly prepared from powder, 24 hours

before use. The parameters of the powder(manufacturer's batch number and lot number, date of arrival at facility and other aspects of the products) would be recorded in LIMS, as part of the preparation. The solution would be stored in the dark, in a designated bottle. Distilled water (dH2O) directly from a water purifier system (Milli-Q, Millipore Corporation) was used as the solvent. This "aging" procedure helps to normalize the solution over many batches, and allows for the solution to become homogenous. The same volume of the solution would is always be prepared; (2) All ethanol grades for the protocol would be prepared from a common stock. (3) All solutions would be prepared in designated containers, which would not be used for other types of reagents. The requisite concentrations of ethanol (50%, 75%, 90% and 100%) would be prepared by diluting the stock (95% Ethanol) with dH2O. The inherent bias of 5% caused by using 190proof ethanol, instead of 200 ethanol, as the stock, was– overlooked, as 190 proof alcohol is significantly easier to obtain, is significantly cheaper and is more stable, in large volumes. Dehydration/differentiation times, at each grade, are shown in Table 4.

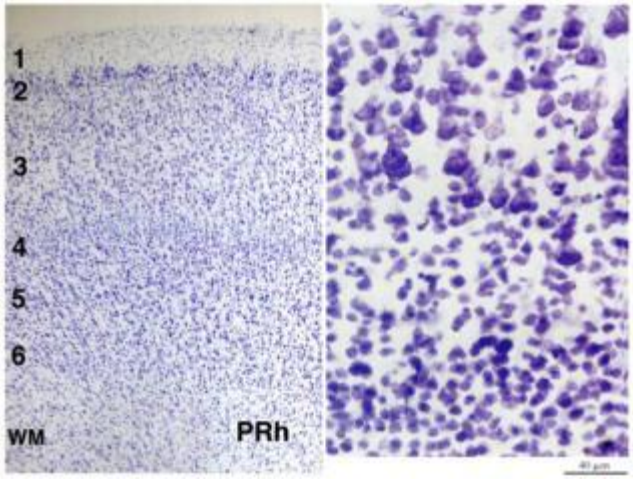

Figure 24: Nissl stain of cortex, with identified layers
A proper Nissl stain, should allow for the differentiation of cortical layers, as is shown above. Layer1 of the cortex, which has very few neurons, should appear to be white or off-white[70, 71].

(4) Xylene baths for both the Nissl stain and the coverslipping process were routinely examined for possible contamination. This results if the tissue sections are not thoroughly dehydrated; residual water turns the xylene from clear to milky. (5) Once prepared, all reagents are treated as a single lot. Each lot is used for a maximum of four slide batches, each of 60 slides, for a total of 240 slides per batch. If fewer slides are processed, each lot is nevertheless changed after 48 hours. (6) Prior to running an entire slide series through a new lot of solutions, 2-3 test slides from that series, usually posterior sections of a coronal series or far lateral sections of a sagittal series, are used for trial validation.

The trial involves running the slides through the entire staining process, including coverslipping. As a final step, the technician examines the slides under the microscope for

quality. For Nissl stains, the main optimization variable is differentiation of the cell bodies (neurons) against the background (extracellular matrix). In "textbook" Nissl stains, the background should be white or off-white and the cell bodies should be blue, as is shown in Figure 24. For example, in the case of cortical areas, one should be able to resolve the individual layers. The main objective of this process is to validate that the prepared reagent solutions are of proper quality and that the resulting stain will match expectations. The full criteria for this examination are shown in Table 5. The first two columns of the table refer to the general appearance of the tissue. If there are processing problems in the preparation of the slides, these need to be immediately identified, since in the high throughput context, the alternative is to generate a large number of inferior slides.

Verification is also needed that the proper amount of mounting medium is dispensed on the slides. Since the technician does not physically handle the medium, and the color of the mounting medium is clear, it is often difficult to distinguish is mounting medium and what is xylene underneath the coverslip (section2.2.5.3). Large differences can easily be noticed, but a difference of 20% (20µl of solution) is often difficult to spot initially. Over time, the difference becomes quite apparent, in that, in the case of excess xylene, air bubbles form at the distal edges of the slide. To address this problem, technicians are instructed to "watch" the actual dispensing of mounting medium by the machine and to report if they notice any irregularities in the dispensing. Slides are also allowed to dry for 20-30minutes and then rechecked for proper mounting medium coverage. If no problems are spotted, the technician starts the staining of the entire series. The same standards are used for the processing of fluorescent series.

Slide Number	Macro Tissue Damage? (2-5X Obj)	Sections Peeling from Slides? (2-5X Obj)	Cell Body Rupture? (20-40X Obj)	Lack of Nissl Differentiation in Deeper Structures? (20-40X Obj)	Lack of Nissl Differentiation in Cortex? (20-40X Obj)	Focus or other imaging problems, at high-magnification (40-60X Obj)?
TBD	True or False	True or False	True or False	True or False	True or False	True or False
TBD	True or False	True or False	True or False	True or False	True or False	True or False
TBD	True or False	True or False	True or False	True or False	True or False	True or False
TBD	True or False	True or False	True or False	True or False	True or False	True or False
IF True?	Notify sectioning technicians to perform a system check. The knife angle, humidity in the chamber and alignment of the block, should be verified	Verify that the correct slides were used for staining and validate the slide coating solution. The operation of the CryoJane2.0 system, should also be checked.	Verify the preparation of the staining solutions. "Osmotic shock" is most likely cause, if no macro damage is evident.	Concentration of Thionin solution is higher than protocol or, the first few ethanol solutions (50% and 75%) are weak. Solutions should be prepared from stock.	If only cortex is undifferentiated, verify freezing procedure. Cortex could have undergone "thermal shock" that would affect differentiation	Volume of dispensed mounting medium should be verified. Slides should be allowed to dry for an addition 20 minutes, and then rechecked.

Table 5: Quality Control (QC) criteria for Nissl Staining

In terms of HC staining, the role of the technician is to: (1) prepare the reagents, (2) load the slides, while ensuring that each slide is leveled and (3) validate that the correct program is set to operate and that the humidity of the staining chamber is within the appropriate level. Unlike cell-body staining, in which the reagents are prepared in large volumes, reagents for HC staining are prepared in very small amounts. From the initial prototyping of the process, we found that one of the main failure points of the process occurs while the technician calculates the amount of reagent that is needed for a given staining process. A simple calculation mistake can lead to the preparation of the wrong concentration of antibody solutions. To address this problem, all the "guess work" was removed from the process, and an active worksheet (Microsoft Excel) was created for each staining protocol. Figure 25 and Figure 26 show the protocol for CTB and BDA. The inputs to this worksheet are: (1) The concentration of the primary, secondary and ABC reagents, if different from the SOP; (2) The number of slides to be stained and the amount of solution per drop zone (1 slide = 3 drop zones), if different from SOP; (3) The start time of the

process. With these inputs, the worksheet calculates the exact amount of each solution that needs to be added to correctly make-up each reagent. This is a very simple implementation, but greatly expedites the reagent preparation process and ensures consistency across technicians.

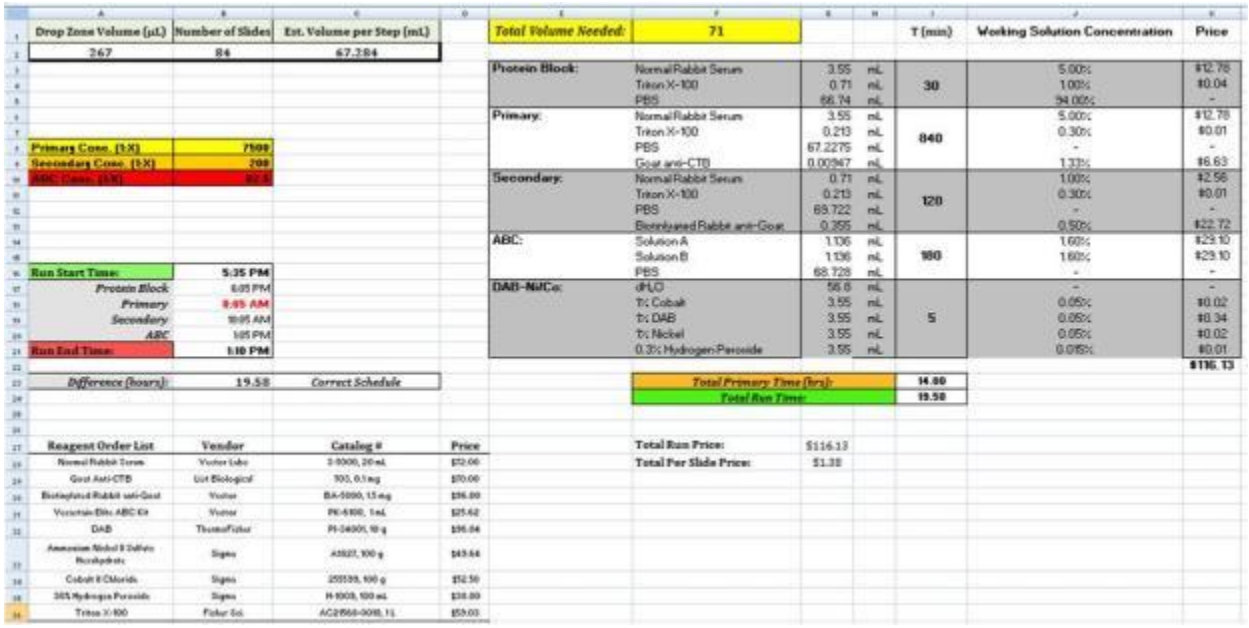

Drop Zone Volume (µL)	Number of Slides	Est. Volume per Step (mL)
267	84	67.284

Total Volume Needed:	71			T (min)	Working Solution Concentration	Price
Protein Block:	Normal Rabbit Serum	3.55	mL	30	5.00%	$12.78
	Triton X-100	0.71	mL		1.00%	$0.04
	PBS	66.74	mL		94.00%	-
Primary:	Normal Rabbit Serum	3.55	mL	840	5.00%	$12.78
	Triton X-100	0.213	mL		0.30%	$0.01
	PBS	67.2275	mL		-	-
	Goat anti-CTB	0.00947	mL		1.33%	$6.63
Secondary:	Normal Rabbit Serum	0.71	mL	120	1.00%	$2.56
	Triton X-100	0.213	mL		0.30%	$0.01
	PBS	69.722	mL		-	-
	Biotinylated Rabbit anti-Goat	0.355	mL		0.50%	$22.72
ABC:	Solution A	1.136	mL	180	1.60%	$29.10
	Solution B	1.136	mL		1.60%	$29.10
	PBS	68.728	mL		-	-
DAB-NiCo:	dH2O	56.8	mL	5	-	-
	1% Cobalt	3.55	mL		0.05%	$0.02
	1% DAB	3.55	mL		0.05%	$0.34
	1% Nickel	3.55	mL		0.05%	$0.02
	0.3% Hydrogen Peroxide	3.55	mL		0.05%	$0.01
						$116.13

Run Start Time:	5:35 PM
Protein Block	6:05 PM
Primary	8:05 AM
Secondary	10:05 AM
ABC	1:05 PM
Run End Time:	1:10 PM
Difference (hours):	19.58 Correct Schedule

Total Primary Time (hrs):	14.00
Total Run Time:	19.50
Total Run Price:	$116.13
Total Per Slide Price:	$1.38

Reagent Order List	Vendor	Catalog #	Price
Normal Rabbit Serum	Vector Labs	S-5000, 20 mL	$52.00
Goat Anti-CTB	List Biological	703, 0.1 mg	$70.00
Biotinylated Rabbit anti-Goat	Vector	BA-5000, 1.5 mg	$96.00
Vectastain Elite ABC Kit	Vector	PK-6100, 1 mL	$25.62
DAB	ThermoFisher	PI-34001, 10 g	$96.04
Ammonium Nickel II Sulfate Hexahydrate	Sigma	A8027, 100 g	$49.64
Cobalt II Chloride	Sigma	255599, 100 g	$52.50
30% Hydrogen Peroxide	Sigma	H-1009, 100 mL	$38.00
Triton X-100	Fisher Sci	AC21568-0010, 1 L	$59.03

Figure 25: Protocol worksheet for histochemical detection of injected CTB

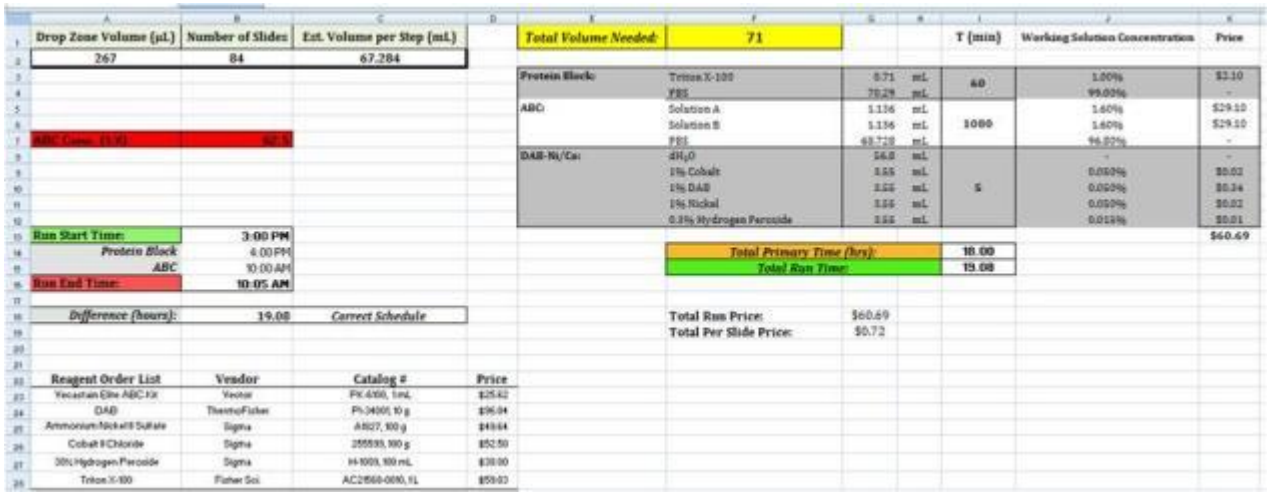

Drop Zone Volume (µL)	Number of Slides	Est. Volume per Step (mL)
267	84	67.284

Total Volume Needed:	71			T (min)	Working Solution Concentration	Price
Protein Block:	Triton X-100	0.71	mL	60	1.00%	$2.10
	PBS	70.29	mL		99.00%	-
ABC:	Solution A	1.136	mL	1080	1.60%	$29.10
	Solution B	1.136	mL		1.60%	$29.10
	PBS	68.728	mL		96.82%	-
DAB-Ni/Co:	dH_2O	56.8	mL	5	-	-
	1% Cobalt	3.55	mL		0.050%	$0.02
	1% DAB	3.55	mL		0.050%	$0.34
	1% Nickel	3.55	mL		0.050%	$0.02
	0.3% Hydrogen Peroxide	3.55	mL		0.015%	$0.01
						$60.69

Run Start Time:	3:00 PM
Protein Block	4:00 PM
ABC	10:00 AM
Run End Time:	10:05 AM
Difference (hours):	19.08 Correct Schedule

Total Primary Time (hrs):	18.00
Total Run Time:	19.08
Total Run Price:	$60.69
Total Per Slide Price:	$0.72

Reagent Order List	Vendor	Catalog #	Price
Vectastain Elite ABC Kit	Vector	PK-6100, 1 mL	$25.62
DAB	ThermoFisher	PI-34001, 10 g	$96.04
Ammonium Nickel II Sulfate	Sigma	A8027, 100 g	$49.64
Cobalt II Chloride	Sigma	255599, 100 g	$52.50
30% Hydrogen Peroxide	Sigma	H-1009, 100 mL	$38.00
Triton X-100	Fisher Sci	AC21568-0010, 1L	$59.03

Figure 26: Protocol worksheet for histochemical detection of injected BDA

As with other system components, the most significant procedural change was the creation of a Standard Operating Protocol for each element of the staining process.

2.2.5.5. Downstream Integration and Upstream Feedback:

The integration of this component with the imaging component of the system was ensured through the standardization of the staining intensity and the refractive index of the slides. Uniform staining intensity for the for the HC-stained slides, Nissl-stained slides allowed for optimization of light source brightness, image contrast and focus plane determination. For the HC-stained slides, the quality was such that there was minimal background of the sections. This is highly desirable for interpretation of the data, but undesirable for automated focus algorithms, as there is minimal contrast in the image, although this is necessary for a proper focus plane to be computationally determined. Since the signal (CTB or BDA label) is natively sparse, one cannot focus just on those regions. For this reason, a counterstain was incorporated into the staining process, and would be applied to all HC-stained sections. Counterstaining is commonly performed in neuroanatomy, and in the context of HC, is usually performed as a bulk-staining process, analogous to cell-body staining (thinion based Nissl staining). The main difference between the "counterstaining" of tissue and "staining," is that the counterstain is a second procedure, additional to the base "stain." The counterstain must not "block" or otherwise degrade the quality of the HC label. For this reason, we used a modified Wright-Giemsa stain. Giemsa is classically used to stain hematopoietic tissue, such as bone marrow[51], but can also be applied to DAB-stained tissue, without degrading the intensity of the label[52, 72]. An example of such staining is shown in a sagittal mouse section in Figure 27[23]. Giemsa stained cell bodies are easily visible in combination with retino-thalamic projects, anterogradely labeled by an injection of CTB in the retina.

The protocol for performing the "classic" giemsa stain, involves the incubation of sections in the Giemsa solution (Modified Azure Blend, which is commercially acquired from vendors such as Sigma-Aldrich and EMD Chemicals) at a elevated temperature of approximately 60°C. This increase in temperature facilitates the penetration of the stain into the tissue, but at the same time, disadvantageously increases the stress on the adhesion between the sections and the slide. The

Giemsa Staining Protocol:			
Step	**Station Name**	**Concentration**	**Time (min)**
1	Giemsa	50% / 1X PBS	10:00
2	1X Phosphate Buffer Saline	-	0:30
3	Ammonium Molybdate	1% / dH_2O	1:00
4	1X Phosphate Buffer Saline	-	0:30
5	70% Ethanol	70% / dH_2O	5:00
6	70% Ethanol	70% / dH_2O	5:00
7	95% Ethanol	95% / dH_2O	5:00
8	95% Ethanol	95% / dH_2O	5:00
9	Absolute Ethanol	-	5:00
10	Xylene	JT9490	5:00
11	*End Station (Xylene)		-

Table 6: Giemsa counterstaining protocol of HC sections

classic giemsa stain is well known to be highly problematic and very variable, with problems such as sections detaching from the slide or sustaining significant damage, as part of the staining process. To prevent these problems and ensure consistency of the counterstain process the staining protocol was modified through extensive empirical testing, and designated "cold giemsa staining". The parameters of the staining process are given in Table 6.

The advantages of this protocol are that: (1) the staining is performed at room-temperature; (2) the staining can be performed in an autostainer, similar to Nissl staining, as all solutions can be prepared in bulk and (3) the stability of the stain is on the order of 1 day, meaning that the solution can be used to stain a large batch of slides uniformly. As with the Nissl solution, the Giemsa solution would be aged for 24 hours, prior to use. The downside to the "cold giemsa" protocol is that the penetration of the stain is reduced, which results in less defined cellular staining. But in the context of this system, the main purpose of the counterstain is not to label individual cells (as this can be done for alternating nissl sections), but to increase the contrast of the section so that it can be adequately imaged. The latter goal is routinely and easily met using this staining protocol. The rate of "out-of-focus" sections was reduced by 40%, through the application of the cold-giemsa stain.

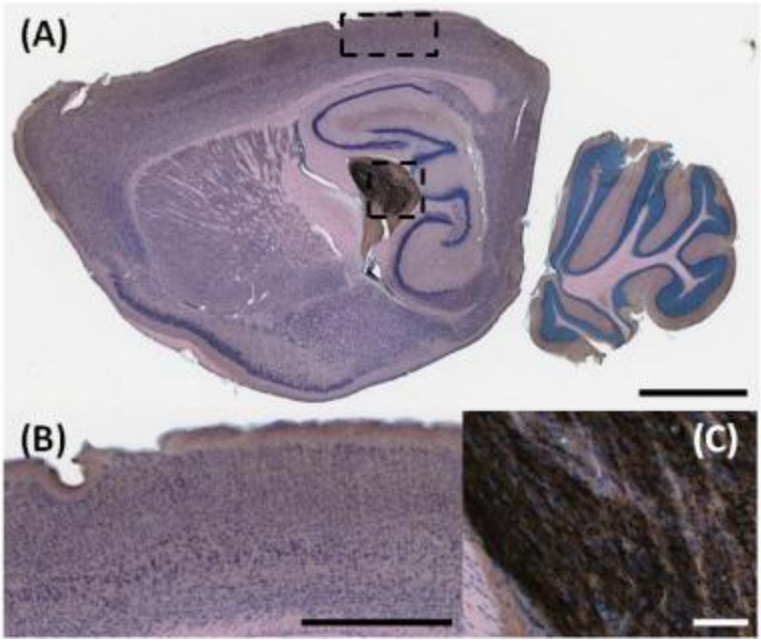

Figure 27: A CTB injection into the retina of mouse, with Giemsa counterstain.
A sagittal section of a CTB injection, with a Giemsa counterstain is shown. Giemsa does not reduce the SNR of the DAB reaction product, while allowing for the identification of cell-bodies. Cortical layers are difficult to differentiate - Giemsa is not a replacement for Nissl. The retrograde projections of the retinal CTB injection, are clearly seen in the Thalamus. Scale bars are 1cm, 300um, and 300um[23].

2.2.6. Section Imaging

2.2.6.1. Component Purpose:

This system component is the terminal end of the system and is responsible for the transformation of the physical slides into digital data. This transformation is performed through light-microscopic imaging of all sections of a given mouse brain, in their entirety, regardless of the location of the biological signal. By imaging each section as a whole-entity through the entire brain, one is able to apply computation algorithms to transform these 2D images into a 3D stack. This stack can be used to visualize the complete connectivity pathway, in the context of the entire 3D structure of the brain. This is a major departure from conventional neuroanatomy, in which only selected ROIs (typically injection sites and selected targets) are imaged and reported in the literature. This sampling of data has several inevitable consequences. Most minor, but nevertheless a factor, the investigator will often close to present optimal data, More importantly, this selective sampling bars the reader or viewer from a full appreciation of the pattern and density of the total connectivity. Digitizing the entire section and the entire brain provides public access to raw digital data, which can then be used for either manual or computerized analysis by individual users.

The underlining requirement for this component, is to perform both transmitted (brightfield) and reflected (fluorescence) light microscopy, to produce high-quality data, that is an adequate representation of the physical material, at a practical throughput rate. The latter is a vital requirement, because light microscopy is traditionally a fully manual process and the prospect of imaging all of the sections (at a thickness of 20µm) of 1000 brains per year, would be impossible, without extraordinary resources. An obvious balance between image quality and throughput, would need to be established. The resulting data would also need to be in a format that is applicable for downstream software processing, and also fits within the practicalities of storing large volumes of digital data ($/TB).

2.2.6.2. Established Methodology and Equipment:

Two types of imaging need to be performed as part of this component: (1) transmitted light microscopy (brightfield) to image sections that have undergone Nissl staining or HC staining (with or without counterstain), and (2) reflected light microscopy (fluorescence) to image sections that were injected with a fluorescent tracer (viral tracer). The conventional

approach calls for the use of a research grade microscope, similar to the one shown in Figure 28 (Olympus America Inc). The microscope allows for the visualization of the image through either the eyepiece or through the use of the camera that is attached to a trinocular head. Modern digital cameras are self-contained and easier to use, compared to the film camera setup that is shown in the diagram. The conventional microscope is an open-ended research tool; it allows coarse and fine adjustments to be made for each type of imaged sample.

For brightfield imaging, the main adjustments are: (1) Illumination intensity, which determines the brightness of the image and is adjusted through either the regulation of the halogen lamp power or through the field diaphragm; (2) Condenser aperture, which determines the numerical aperture of the condenser and the angle of light that is concentrated on the sample; (3) Selection of the magnification objective. The standard objectives are: 5X, 10X, 20X and 40X; (4) Selection of region-of-interest, which is performed by using the XY manual control knobs to move the stage, until the ROI is within the approximate field-of-view of the objective; (5) Focus plane determination. While looking through the eyepiece of the microscope, the focus knobs (coarse and fine) are used to adjust the distance between the sample and the objective until the sample appears in focus and can be properly resolved. The user continues to make fine adjustments, varying magnification and changing the XY position of the stage, until the desired area is found and the appropriate image is obtained. Once this image appears through the eyepiece, the light path can be directed to the camera and an image can be acquired. For brightfield imaging, a color camera is preferable. The pixel resolution of the camera should be higher than or equal to that of the microscope optics or the image will be downsampled.

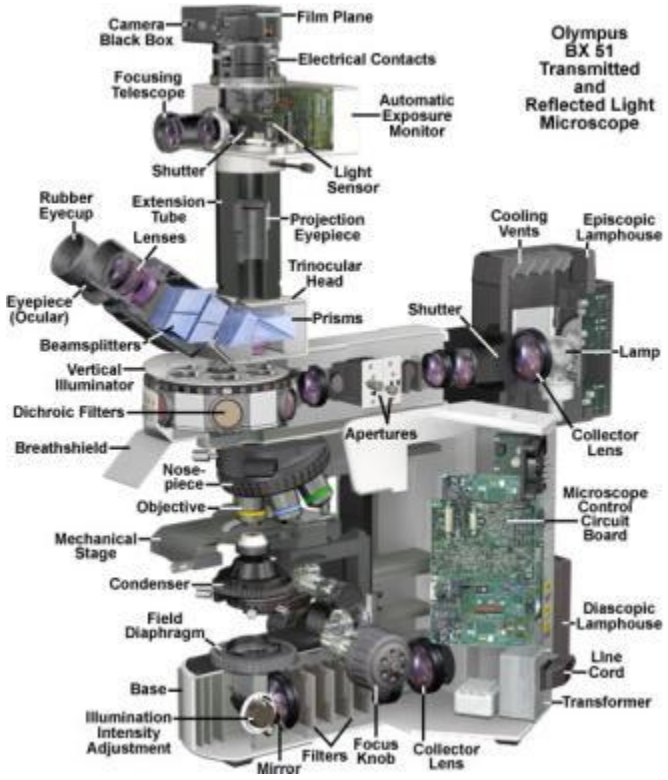

Figure 28: A standard research microscope
Components of a standard research microscope are shown in the image above. This microscope can be used for either brightfield (transmitted light) or fluorescence (reflected light) microscopy. The light from the objective can be directed to either the eyepiece for direct viewing, or to the camera. Modern digital cameras are self-contained and easier to use, compared to the film camera setup that is shown in the diagram.

For fluorescent imaging, the main adjustments are similar to that of brightfield imaging, except that a specialized light source is used in the form of a 200W mercury lamp, or similar. The user adjusts the intensity and wavelength of the light by controlling the shutter position and selecting an appropriate filter cube. The filter cubes are pre-installed into the microscope, and contain the excitation and the emission bandpass filters, which are tuned to the specific fluorophore to be imaged. The most common filters are: FITC (Green Channel), with an excitation bandpass of 470-490nm and an emission bandpass of 520-560nm; Texas Red (Red Channel), with an excitation bandpass of 540-580nm and an emission bandpass of 600-650nm; and DAPI (Blue Channel), with an excitation bandpass of 340-380nm and an emission bandpass of 435-485nm. These filters can either be used individually with a monochrome camera, or in combination, as is shown in Figure 29. A color camera can be used in conjunction with the latter, to image all three channels simultaneously. However, most cameras use a Bayer Mask (filter), which calls for a (2:1:1) ratio of Green: Red: Blue pixels in the detector. Thus, the camera and the resulting image are more sensitive to the green fluorophore than to the two others.

Both types of imaging, as done conventionally, are very labor intensive and the quality of the image is as much a function of the microscope optics and the imaging camera, as it is the technique and knowhow of the operator. For fluorescence imaging, the operator must take great care (especially for dim fluorophores) as not to photo-bleach the samples, which will occur from

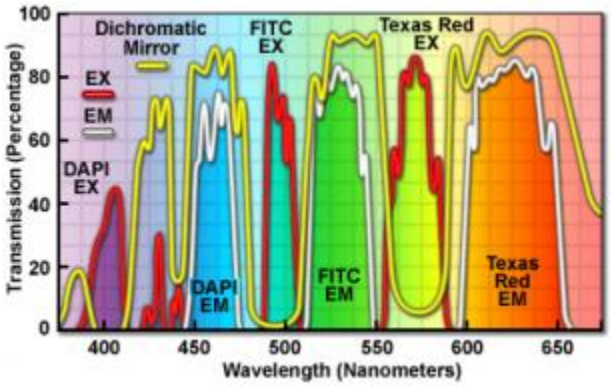

Figure 29: Transmittance profile of a DAPI-FITC-Texas Red triple band filter
Ultraviolet and visible transmission spectral profiles for the DAPI-FITC-Texas Red filter combination. This filter set is designed for optimal detection of DAPI, FITC, and Texas Red probes when applied in combination (triple) staining techniques.[73]

prolonged exposure of the sample to light. For optimal image quality, the operator must adjust the microscope settings and camera acquisition settings, for each ROI to be imaged. The focus plane can vary extensively across the section, depending on the sectioning and mounting methods used to prepare the sample. Exposure will vary based on the intensity of the signal. For connectivity studies, the site of injection and terminal projections will typically be brighter than intermediary sites and will require shorter exposure times. Imaging of cell bodies will also require less exposure than imaging of fine axons or dendrites.

To image an entire section or an entire slide by conventional methods, one would need to either image at a lower magnification, where the field of view captures a large portion of the slide, or to image at high-magnification to acquire a large subset individual images ("tiles"), that can later be stitched as an unified image. Imaging at low magnification results in obvious loss of spatial resolution, due to the lower NA of the objectives. Resolution is on the order of .37µm for 20X, but only 1.375µm for 4X and 2.5µm for 2X. The problem of collecting high-resolution tile images for an entire section is that the operator needs to manually align the tiles during acquisition and gauge the appropriate amount to move the stage for each tile. This process is obviously error prone and leads to stitching artifacts in the form of "black lines" between the tiles. Furthermore, a single coronal section of the mouse can require up to 50 tiles at 20X and 200 tiles at 40X. This is very time consuming and not practical for most applications. Scanning all sections (20µm thickness), through an entire mouse brain, borders on the impossible with conventional methods.

In recent years, an effort has been underway to automate this process. As with the automated stainers and coverslippers, this development is focused on clinical pathology. What are called whole-slide microscopes are simple in description, but complex in detail. The hardware of the system has four basic components: (1) Slide loader, which is a three-axis

manipulator that ferries the slide from a loading area onto the motorized stage. This loading area can accommodate multiple slides, on the order of five to several hundred. This allows the operator to load a large batch of slides at once, so that the subsequent imaging of this batch proceeds continuously without need for further reloading. Once the slides are loaded and the scanning parameters are confirmed, the imaging can perform autonomously, without any manual intervention. (2) Motorized stage, which is a two-axis linear manipulator that contains a mechanism for fixing the slide onto the stage and controls the position of the slide throughout the imaging process. The movement of the stage is fully computer controlled and optimized to be in sync with the acquisition system. The spatial accuracy and repeatability of the stage position are inherent properties of the system and are designed so that any discrepancies in motion are overcome by the overlap of the tile images. This overlap is on the order of 10% in each axis and is one of the limitations in acquisition time for the sample. (3) Optics and camera, aside from the lack of eyepieces, the light path and the basic optics of the microscope are unchanged from that of the research microscope (Figure 28). Some elements, like the selection of filter cubes, are automated through the use of a filter wheel, but the band-pass of the filters is unchanged. Shutter and illumination settings are also automated. For brightfield, the numerical aperture of the condenser is typically fixed. A motorized aperture for the condenser can be used, but due to technical problems, is rarely incorporated into commercial instruments. The objectives are typically similar to those used in research microscopes; but in most whole-slide microscopes, a single primary objective is used. The imaging camera is of critical importance to the overall performance of the instrument. Two types of sensors are typically used, a CCD (Charge-Coupled Device) or a TDI (Time Delay and Integration) sensor. Both use the Bayer Mask, but the difference is that the TDI sensor is essentially a CCD sensor with an internal clock that is synchronized to spatial movement.

The TDI sensor allows for the motion of the motorized stage to be synced to the shutter of the camera, such that the image can be acquired without the need for the stage to be stopped. This so-called "lane-scanning" technique allows for significant improvements in data acquisition rates. Since the lane is collected in a single pass, it is generally treated as a single entity, which is than stitched to form the resulting image. This results in fewer stretching artifacts than if a traditional tilling approach was used. (4) Software. Aside from orchestrating the robotics of the system, the software also allows for determination of the optimal imaging parameters. The focus

surface is determined on the basis of sampling several points throughout the tissue. These tissue points are either selected by the user or automatically selected by the system. Per point, the system finds the optimal focus plane by sampling through the thickness of the tissue and then, from these individual planes, constructs an optimized focus surface, that used for the high-resolution scans. An algorithm for excluding point outliers and other compensations (coverslip and foreign contaminants) are incorporated into the algorithm. Image stitching is also automatic; at the conclusion of each scan, the user is provided with a single stitched image that represents the entire scanned surface. Depending on the model, the user-interface of the software will vary, as will the range of features that are available. A schematic view of a typical system is shown in Figure 30.

The use of these whole-slide microscopes makes the prospect of scanning sections, in their entirety for a large number of slides, technically feasible. The average scan time for a brightfield slide is on the order of 1-3 minutes and 5-10 minutes for a fluorescent slide, depending on exposure time, as determined by the magnification (optical and/or software equivalent) and the general settings of the instrument. These rates are an order of magnitude faster than can be accomplished by the classical tiling method by a single operator. The results are also more standardized and have fewer imaging artifacts.

As with the HC staining component of the system, the direct application of these instruments for high-throughput connectivity research is not without problems. The three biggest problems are: (1) Workflow and throughput. Whole-slide microscopes are in their infancy and as such, much of the machine optimization that one would expect from a sophisticated microscope is missing. In the clinical setting, these instruments are rarely used to full capacity, and if they are, it is usually for a short period of time. Therefore, these instruments have inherent inefficiencies in terms of the setup procedure: loading/unloading of slides and configuring the imaging parameters per slide. From empirical testing, we found that these inefficiencies contribute to a practical imaging throughput that is around 60% of the maximum potential. Adding on downtime, due to mechanical and software problems, the true practical imaging rate is about 50% of the maximum. To achieve even this efficiency, a full-time technician needs to be dedicated to the task of loading/unloading slides and setting imaging parameters, obviously not the most efficient use of a technician. Many of the problems are software based and can be resolved; others, such as the need to maintain perfect alignment between the slide and the

coverglass and to prevent any residue mounting medium from sticking on the slide, are inherent to the process and are difficult to resolve.

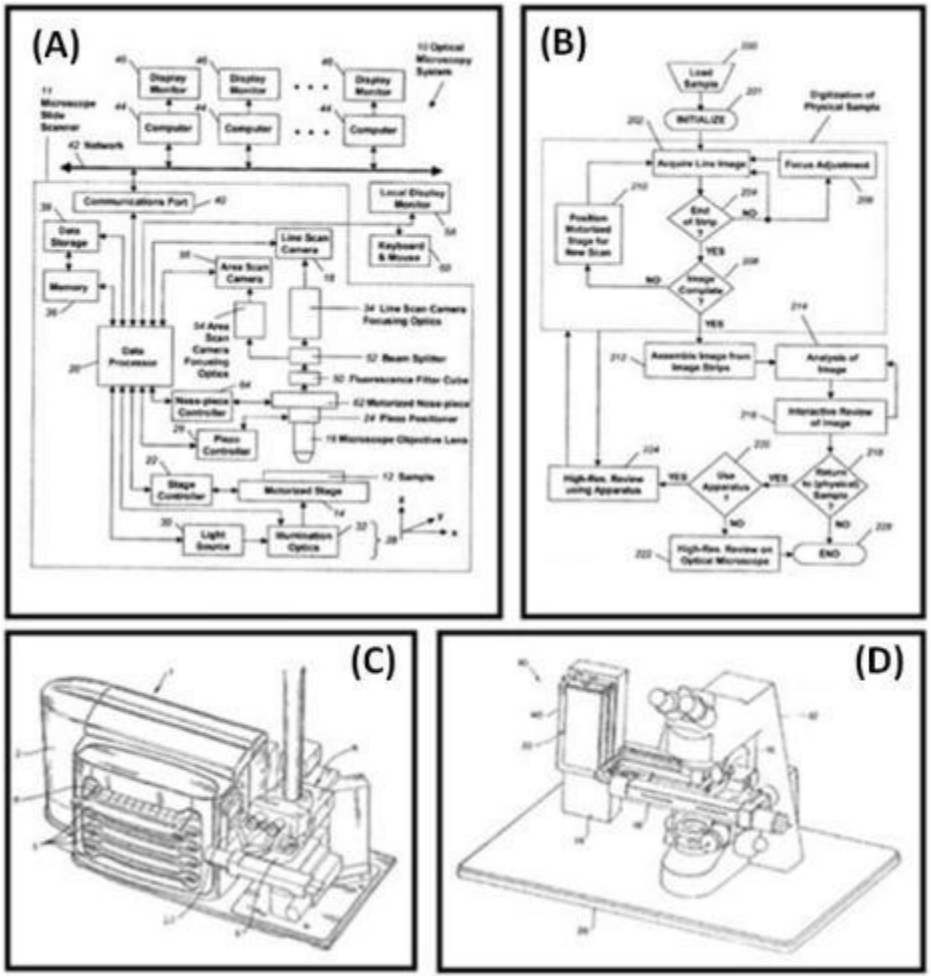

Figure 30: Schematic and block diagram drawing of various whole-slide microscopy instruments
Whole-slide microscopy is a general term, used to refer to any instrument that is used for the imaging of an entire glass slide (1X3" or larger). The most common form of these microscopes is as an attachment, in the form of a motorized stage and a slide loader, onto an existing microscope, as is shown in (C) and (D). More sophisticated solutions, in the form of integrated instruments, that offer advantages in throughput and overall image quality, are described in (A) and (B). (A) A block diagram of a optical microscopy system[74]. (B) A flow chart of the operation of an optical microscopy system[74]. (C) Perspective view of a slide loader adjacent a microscope arrangement incorporating a motorized translation stage[75](D) A perspective view of the automated slide loader cassette instrument, mounted to a microscope;[76]

(2) Image quality and reproducibility. Clinical standards for microscopy are generally lower than those for laboratory research. In terms of brightfield, one of the main problems with most whole-slide microscopes is that the numerical aperture of the objective(s) does not match that of the condenser. This reduces the overall "sharpness" of the image, and thus the maximum resolution

that can be achieved. The numerical aperture of the condenser, in clinical usage, is generally lower than that of the objective in order to intentionally reduce the amount of light that enters the detector and to facilitate the determination of the focus plane of the tissue. At a high numerical aperture, the amount of light that enters the condenser is maximized, but at the same time, the sample is saturated with light. This makes it difficult for computational algorithms to decipher the optimal z-plane for the focus plane.

For fluorescence, the main problem is that these instruments use a mercury based lamp (the same light source as the research microscope). These lamps have a useable lifetime of 200hours. For a research microscope, this is sufficient for several months, if not a year, of periodic use; but for a high-throughput microscope, that is operated continuously (24hours/day), this is a lifetime of 8 days. Besides the inherent workflow problems, introduced by the need to switch the light source weekly, there is the issue of standardizing the output power of a given lamp through its lifetime and that of multiple different lamps. Exposure time is a direct function of the lamp intensity; and to ensure that a sample can be scanned at the same exposure settings, with the same image quality (same SNR and max intensity of signal), the lamp intensity needs to be closely calibrated[77, 78]. This is generally overlooked in these whole-slide instruments because only a small subset of clinical samples are fluorescent (as, fluorescent in situ hybridization). Those that are will most likely not be used for quantitative, but only for qualitative analysis.

(3) Post-acquisition use of data. This is by far the most serious problem with these instruments. Acquired image data are written into a propriety image format. This is optimized for initial viewing of the data, to allow the pathologist rapid access to the data and to easily pan/zoom through the image. The downsize to this optimization is that it usually results in "locking the data." In the case of a JP2000 format (the common base of these proprietary formats), the decompression time (i.e., the amount of time required to load the image into computer memory, so that image processing algorithms can be applied) is on the order of 6 minutes for a 30 GB file. This means that the total "scan time" for a brightfield slide is on the order of 15minutes (10 minute scan + 5 minute conversion). This 50% increase in the scan time poses a significant limitation on throughput processing rates. Furthermore, in most uses of the JPG2000 format, lossy compression ("quality factor") is applied, which constitutes manipulation of the data and results in loss of fine resolution. Though the above four issues are significant

shortcomings, whole-slide microscopes are the only practical means of imaging whole sections, over a large number of slides, without extensively compromising resolution and image quality.

		Aperio			Olympus/Bacus Labs/Hamamatsu	Zeiss	BioImagene / Roche
		ScanScope XT	ScanScope CS	ScanScope FL	NanoZoomer HT	Mirax Scan	iScan Coreo Au
Intended use		Research	Research	Research	Clinical: Pathology	Not for Clinical	Clinical: Pathology
Cost [Thousands]	Basic Model ($ Thousands)				150	180	
	Fluorescence ($ Thousands)				65		
	Software License ($ Thousands)				6.2		
	Estimated Total ($ Thousands)				221.2	180	250
Camera Specifications	Bit Depth			8/10-bit	12 bit	8 bit	10 bit
	Camera Type	Basler L301 kc CCD	Basler L301 kc CCD			Allied Vision, Marlin F-146C	
Scanning Method		TDI	TDI	TDI	TDI	Tile Scanning	Tile Scanning
Imaging Type		Brightfield	Brightfield	Fluorescence	Brightfield + Fluorescence	Brightfield + Fluorescence	Brightfield + Fluorescence
Slide Loading		120, 1 x 3"	5	5	210	300	160
Slide Orientation		Horizontal	Horizontal	Horizontal	Horizontal	Vertical	Horizontal
Scan Time Whole Slide [25 X 75 mm]		<16 min @ 20X	<16 min @ 20X	<16 min @ 20X	<14 min @ 20 X	< 15 min @ 20 X + stitch	<40 min @ 20X
Glass Slide Dimensions	Footprint	25 X 75 mm	25 X 75 mm, or 2 x 3"	25 X 75 mm, or 2 x 3"	26 X 76 mm		25 x 75 mm
	Thickness [+ coverglass]	1mm	1mm	1mm	0.9-1.2 mm		
Scanning Region [H x W]	Standard Format	23,4 x 55 mm	26.3 X 54 mm		25 X 52 mm	27 x 50 mm	
	Larger Format	50 x 55 mm (single slide)	50 X 54 mm		NA	NA	None
Objective	Mag	20X	20X	20X	20X	20X & 40X	Olympus, 4X, 10X, 20X, 40X
	NA	0.75	0.75	0.75	0.75	0.95, 0.8	0.1, 0.3, 0.5, 0.75 NA
	Notes	40X with 2X mag changer	40X with 2X mag changer	40X with 2X mag changer	Equvalent of 40X possible through camera		Turret Objective Change
Resolution	Low Mag [20X]	0.5 um/pixel	0.5 um/pixel	0.468 um/pixel	0.46 um/pixel	0.23 um [with 1x Adapter]	0.46 um/pixel
	High Mag [40X]	0.25 um/pixel	0.25 um/pixel	0.234 um/pixel	0.23 um/pixel	0.12 um/pixel	0.23 um/pixel
Fluorescence	Lamp	EKE 150 W, Internal	EKE 150 W, External	Mercury	Mercury	Mercury	Intergrated LED, 200W Mercury
	Filter	NA	NA	6-position motorized filter cube turret and a 6-position motorized filter wheel Quad multi-bandpass filter set [DAPI, FITC, TRITC, and Cy5]	Three Filter Cubes: B excitation G excitation Triple Band [UV, B, G]	10 position filter wheel	
	Notes	NA	NA	LED Illumination to help find tissue sample on slide	L10387 Option		
Image Files	Formats	TIFF[SVS], CWS	TIFF[SVS], CWS	TIFF, SVS, JPG2000	JPEG compressed imaged + slide information	BMP, PNG	TIFF, BIF, JPEG2000
	Compression	JPG2000, JPG	JPG2000, JPG	JPEG2000, JPG	JPEG compression	JPEG compression	JPEG2000, JPEG
Barcode Support		2-D Data matrix	2-D Data matrix	2-D Data matrix	2-D Data matrix [optional]	2-D Data matrix	2-D Data matrix [optional]
		1-D 2-of-5	1-D 2-of-5	1-D 2-of-5	1-D 2-of-5	1-D 2-of-5	1-D 2-of-5
Dimensions [W x D x H]		597 X 406 X 648 mm	318 X 465 X 502 mm	318 X 465 X 502 mm	860 X 590 X 637 mm	742 X 452 X 531 mm	457 x 457 x 432
Weight [lbs]		105	55	55	206		75
Warranty [months]		12	12	12			12

Table 7: Feature-matrix of the commercially available whole-slide microscopy instruments

2.2.6.3. Design Implementation and Innovation:

To address the problems discussed above, and implement a whole-slide scanning solution that would be robust and capable of matching the processing rate of upstream components, extensive empirical testing of all commercially available systems was performed. Instruments from Aperio Technologies, Carl Zeiss Inc, Hamamatsu Photonics/Olympus Corporation, Bioimagene Inc and DMetrix, Inc, were evaluated. The feature-matrix of the different systems is shown in Table 7[79]. Of these systems, the NanoZoomer HT (Hamamatsu/Olympus) was

selected as the principle imaging platform. The advantages of the NanoZoomer were: (1) ability to perform both brightfield and fluorescence imaging, in a single platform; (2) a large slide capacity (210 slides), such that once fully set, the instrument can run autonomously for 24+hours, depending on scanning parameters; (3) a sustainable spatial resolution of .23-.5µm/pixel, depending on the type of digital sampling that is used. The system uses a single 20X lens, with an NA of .75, that is able to achieve a maximum optical resolution of .46µm. The camera of the microscope can be configured to sample either one or two pixels per the optical resolution, resulting in either a .46µm/pixel or .23µm/pixel.

(4) For fluorescence imaging, the main advantage of the Nanozoomer is the ability to use a tri-pass filter (Figure 29) for the simultaneous imaging of multiple fluorophores. This is possible because the TDI sensor of the instrument, is actually three identical monochrome sensors, each of which is dedicated (using a dichroic single band pass filter) for a specific RGB (red-green-blue) color channel. The data from these three sensors, which are synchronized to the same clock frequency, is overlaid to form a unified image. The practical advantages of this approach, is that for samples with multiple fluorophores, the effective scan rate is 2-3X faster than if a single sensor was used.

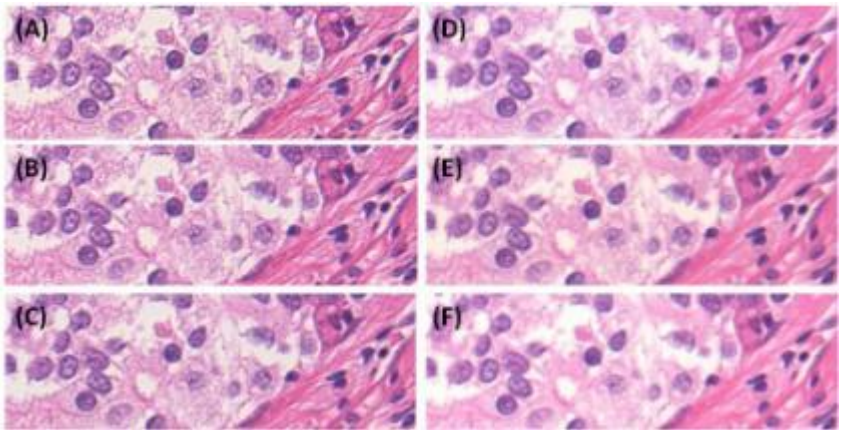

Figure 31: Effects of the numerical aperture of the condenser, on image quality

In relation to a fixed objective (20X, .75NA), the effects of six different condensers, with an NA ranging from .17 to .70 (A-F), are shown in the image above. At the extremes, an NA of .17 (A) results in highest image contrast, but worst resolution and sharpness; an NA of .7 (F) results in lowest contrast but highest resolution and sharpness. The effects of NA are more distinct for samples with lower native contrast, such as unstained tissue samples.

The NanoZoomer, much like the other instruments tested, is not without fault. A year-long process was undertaken, with collaboration from engineers at Hamamatsu Photonics, to address these problems and improve the efficiency of the system. The following were the most significant design changes that were implemented: (1) Optimization of Optics: A condenser, with an NA of .33 was chosen as the default for both brightfield and fluorescent scanning. For brightfield scanning, sacrifice in resolution - sharpness of the image, was made to accommodate

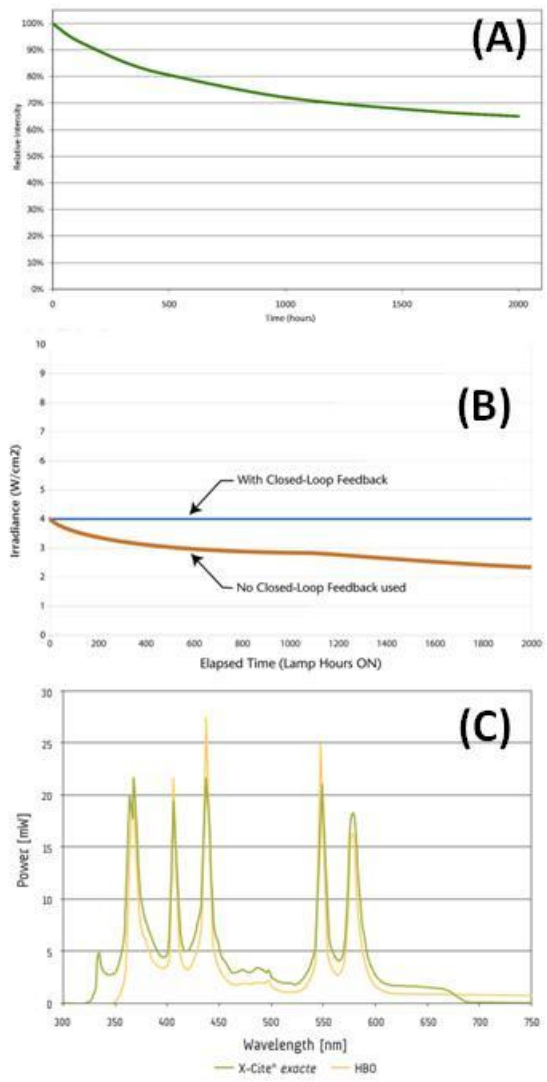

Figure 32: Properties of Metal Halide Arc Discharge Reflector Lamps (EXFO X-Cite)
The Exfo X-Cite light source (Lumen Dynamics Corporation), offer a ten-fold increase in effective lamp hours, predictable and controllable irradiance degradation as a function of lamp hours and equivalent wavelength distributions to that of a traditional mercury lamp source. (A) Irradiance Degradation of the X-cite exacte light source[55]; (B) Degradation of the light source, when operated in closed-loop feedback, using the model XR2100 optical meter[56]; (C) Spectral Comparison to the standard mercury light source[55].

the fluorescent imaging. Figure 31, shows the effects on image quality, as a function of the condenser's numerical aperture (the same 20X objective, with an NA 0f .75 was used for all testing). The primary reason that the above sacrifice was required, is that the determination of the focus plane for both brightfield and fluorescence imaging, was performed using transmitted light (brightfield imaging). Since fluorescence samples are unstained, their contrast is significantly less than that of stained samples, and thus the NA of the condenser needs to be reduced, to allow for the detection of these samples. Reflected light could not be used for the focus plane determination, because fluorescence in these samples is very sparse (limited to the connectivity pathway) and thus for most points, the fluorescence would be only background. The use of this condenser, in conjunction with a 20X objective (.75NA), limits the optical resolution of the microscope to .447µm for fluorescence and .621µm for brightfield, as the formula: $Resolution(r) = \frac{1.22\,\lambda}{Na(Obj) + Na(cond)}$ with 550nm as the average wavelength of light (λ).Therefore, the average resolution is .5µm. The CCD/TDI sensor of the NanoZoomer oversamples the optical resolution by a factor of 2, which allows for a maximum resolution of half the optical resolution or .25um/pixel. In the interest of preventing digitization artifacts and the inflation of file size, it was decided to maintain the pixel resolution at a 1:1 relation to optical resolution, thus.5µm/pixel. These scanning parameters were set as the default for all scanning.

(2) Fluorescent Light Source: To address the lack of uniformity and limited life span of the mercury-lamp, a Metal Halide Arc Discharge Reflector Lamp was used, in the form of the EXFO X-cite light source (Lumen Dynamics Corporation). This illumination source, allows for a usable life span of 2000hours (83 days of continuous use) per lamp, and a smooth decline in illumination, within the life span(Figure 32). To further normalize the illumination power, the light source was configured in "closed-loop feedback" mode. Every 100 hours, the light source would be connected to a serial radiometer (Lumen Dynamics Corporation) and the unit would adjust the diameter of the aperture, to account for degradation in the native lamp output (Figure 32, B). The baseline illumination power was set at an aperture of 70%, which would be increased as a discrete function of the lamp's degradation. This procedure was very fast and efficient, requiring less than 10minutes of technician time. In terms of spectral output, the EXFO covers the same useable range of wavelengths (as a function of common fluorophores) as the mercury lamp (HBO 100), with higher intensity (10-25%) at some wavelengths (Figure 32, C). The latter increase, was not significant to allow for a major decrease in the exposure time.

(3) Software changes and output file format: One of the biggest problems with the early version of the NanoZoomer control software (circa 2009) was the amount of technician time required to configure the scanning per batch. This was on the order of 5-6 hours per batch, with the majority of the time spent setting cropping boxes (these determine the location of the tissue on the slide), setting focus points within the boxes and configuring the slide name per slide. Though the NanoZoomer is advertised with an ability to automatically place focus points on the slide, as a function of the detected contrast on the slide (i.e. sections), the native algorithm is highly error prone. The algorithm does not account for the type of tissue on the slide, but is designed to accommodate all types of samples. The algorithm normalizes the detected contrast and places the "best fit" box around the tissue so as to minimize the size of the cropping box, which usually clips the lateral and ventral parts of the coronally sectioned mouse brain. The mouse brain can be approximated as an ellipse and the cropping box as a rectangle. Thus the clipping occurs when one tries to minimize the size of the rectangle, while capturing majority of the entire section. This problem was addressed through a static area offset of 20%.

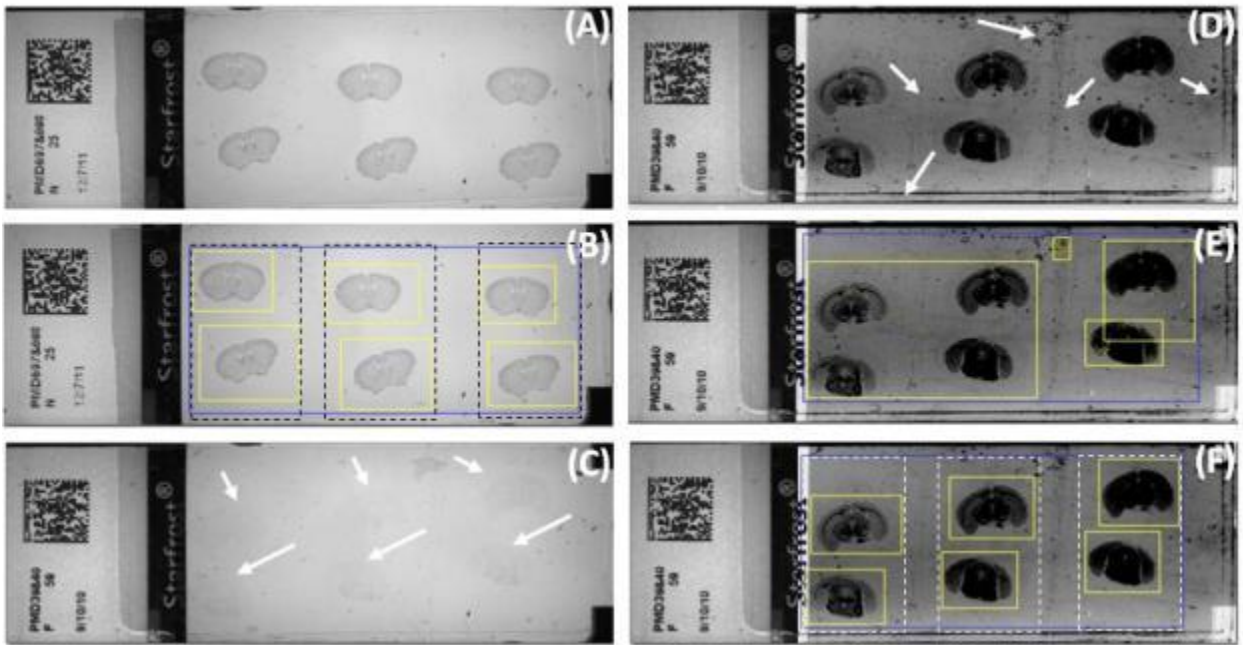

Figure 33: Macro NanoZoomer images of brightfield and fluorescence Slides
NanoZoomer acquired macro images of brightfield (Nissl stained) and fluorescent slides are shown. These macro images are acquired as part of the pre-scan, which is performed for all slides in a given batch, before the high-resolution imaging. These macro images are used to locate the ROI (the sections) and set the focus points per slide. (A&B) show the macro image of a typical brightfield slide. (B) shows the automatically detected (contrast based algorithm) ROIs, in yellow. The success rate of this ROI detection is on the order of 80%. The black dotted lines show the lane groups that will be scanned as part of this configuration. In the resulting byte-stream file, the space between the lane groups will be identified by a stream of zero's. (C-F) shows the macro image for a typical fluorescence slide. (C) shows a brightfield image of the slide. Since the sections are unstained, the contrast is low and the sections are difficult to detect (white arrows). (D) shows the same slide but imaged through side-illumination darkfield, which allows for clear identification of the sections. As a drawback, impurities and other artifacts on the slide are illuminated to the same intensity as the sections (white arrows), which causes the automatic ROI detection algorithm to fail (E). (F) shows the manually placed ROIs for each section; the resulting lane groups are highlighted by white dotted lines.

The software was configured, through the manipulation of registry based settings, to inflate the calculated cropping boxes by 20% in both axis. For brightfield sections, this change, accounted for most of the clipping and increased the success rate of the automatic detection algorithm, to around 80% (Figure 33B). To further increase the consistency of the cropping box placement, the intensity of the macro-brightfield lamp (different than that used for high-resolution imaging) was adjusted to maximize the detection of the nissl stained sections. The number of focus points per section (area within the cropping box) was configured to 9-12, and these were automatically positioned within the box. Though a technician would still review all settings, the required time setup time for brightfield scanning was reduced by an order of magnitude.

For fluorescence sections, the automatic tissue finding algorithm is applied on a darkfield macro image of the slide, which is acquired in parallel (time delayed) with the brightifeld macro image, using side-illumination. Though dakfield microscopy is a very efficient way of illuminating thin sections that would otherwise be undetectable (especially in terms of macro-imaging). Figure 33C shows the macro-brightfield image of a fluorescent slides; Figure 33D, shows the same slide under darkfield. Darkfield image allows for clear identification of the sections, but also results in the illumination of all impurities in the slide (mounting media) and on the slide (dust). The resulting image, is noisy and it is difficult to differentiate the tissue from the noise (Figure 33E). Therefore, instead of instructing the technician to "fix" detection of the algorithm per slide, the NanoZoomer was configured to rely solely on manual input for fluorescent sections. Once a technician was trained in the process, they were able to set all cropping boxes and focus points within 2 hours per batch. Since the sections are placed in approximately the same location, slide-to-slide, the process is very repetitive and performance improves through the repetition. This is not an ideal solution, but the best that can be implemented under the system constraints.

In terms of slide naming, the main problem is that the 2D barcode (Data Matrix) reader of the NanoZoomer does not utilize all of the redundancies in the data matrix and therefore, has a natively high failure rate. The automatic completion of the slide data field, from the interpretation of the data matrix on the slide, was empirically found to be very sensitive to any minor artifacts on the slide label. This detection, overwhelmingly underperformed that of a commercial barcode scanner, such as the Honeywell 4600g. For this reason, the barcode based system, was abandoned for a tradition array approach, which called for a technician to populate a text file with the exact names of each section. This array ($\leq$210 elements) was then correlated directly with the slides loaded into the system. This text file would be compiled by the technician, per batch, after the slides were loaded into the NanoZoomer racks. Since the series are standardized, the same baseline file could be used for most series, with minor adjustments made for missing slides (damaged through previous processing). Overall, this process required an investment of 10-20minutes of technician time, but significantly reduced nomenclature problems to near zero. In cases where the slide name was difficult to interpret, a manual scan of the data matrix, using a handheld scanner, was performed.

(4) Data Flow, to facilitate downstream use of the data, the output file was altered from the native JPEG2000 based format(*.ndpi) to a raw 12-bit byte-stream (*.ndpi) format. This file format, allowed for the separation of the image data, from slide meta-data. For each slide, a separate folder would be created, which would contain: a main meta-data file (*.vmu) - which would contain all the relevant information about the slide; the byte-stream file (*.ngr), a macro image of the slide (*.jpg) and several related configuration files (*.txt). Therefore, all information needed to parse the image data, was written into these files, that could be accessed through any configured program. As a byte-stream, the main image file would be written as the scanning was progressing and not at the conclusion of the scan - this allowed for an optimal use of the hard-disk. To further optimize the output, a new software module was installed, with the help of Hamamatsu Corporation, which allows for scanning to be performed and collected in distinct groups of lanes, separated by null lanes (byte stream of zero value). The significance on this, is that lane groups can be extracted from the byte-stream file, without the need to load the entire image (all of the groups) into memory at once. The data within the lane, is still treated as a single entity, so for instances if two sections are placed within the same lane group, a downstream cropping step is required to separate the data of the two sections. Since the TDI sensor collects data in a single pass, of a predefined length, it is not efficient, nor was it possible at the time, to automatically segment the data into distinct data streams, separated by null space. This cropping is performed through a custom Matlab interface (Figure 34).

As discussed in section 2.2.4.3and illustrated in Figure 15, the brain sectioning component was standardized to allow for the simultaneous sectioning of two brains and the placement of 3 tape segments (6 sections), on a given slide. This Matlab program, was designed to directly interface with this schema, by assuming that each lane group = 1 tape segment = 2 brain sections and that the two sections would be approximately at the same coronal level, with the same spatial area. This assumption allowed for the efficient and rapid parsing of each lane group into two distinct ROIs, with 1 ROI=1 tissue section. A standard contrast based threshold algorithm was used for the tissue detection, with a 20% enlargement (as discussed above) - this application was equally efficient for brightfield and fluorescent tissue. In cases where an artifact

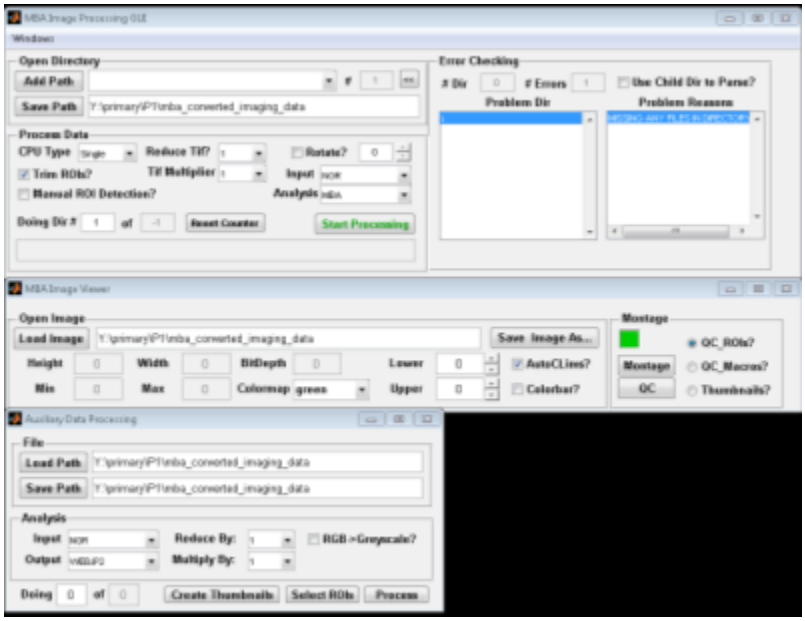

Figure 34: Image processing GUI
The two panel, "MBA Image Processing GUI" is the primary program page, on which the user selects the source and target directories for the conversion, along with the file types. Per input directory, the program verifies the file structure and reports any errors (top right). The "MBA Image Viewer" allows for dynamic viewing of all data types and is the primary means of performing Quality Control to determine if automatically placed cropping boxes are correct. The "Auxiliary Data Processing" window, allows for data to be converted into non-standard data types.

or noise, resulted in the detection of cropping boxes that are disproportionate to each other, in area, the algorithm would just split the lane in half - thus separating the sections. The latter is undesirable due to disk usage, as there would be more "whitespace" saved than if a tight bounding box was placed. To account for potential failures in the automatic algorithm, a manual review process was initiated. A technician would quickly, using the Matlab interface, glance through all of the cropping windows, and adjust those that have failed. This process would be repeated, for all the slides of a given series and result in two folders, one for each of the brains on the slide, with all the cropped sections placed into each folder. Each section would be annotated with the slide number from which it originated and the approximate section number. $SectionNumber = (SlideNumber - 1) * 3 + (SectionPostiononslide[1, 2\ or\ 3])$.

For each section: (A) a meta-data file (*.txt) would be create created and would contain all the relevant information from the Matlab processing and also a copy of the NanoZoomer scanning metadata; (B) a byte-steam of the cropped ROI, saved in a binary format (*.bin); (C) a downsampled (32X in each axis) byte-stream, saved also in a binary format (*_small.bin). The primary reason for selecting the binary format as the principle means of saving the data, is to allow for rapid access of the data, for downstream computation. In comparison to JPEG2000, the access time for the same size file, is around 10 faster. The increase in disk footprint is significant

(3X larger, than lossless JPEG2000 compression). To address this, a linux process was setup to autonomously compress all binary data (using a gzip algorithm) that is larger than 100MBs. Using this compression, the footprint was reduced by an average of 40%. Table 8 shows the relative footprint of the data, at each stage of the software processing pipeline. The decompression time for gzip (linux) is on the order of 15 second, for a 2 GB file - making the entire process faster than JPEG2000, with the added benefit of using parallel/distributed computing for the gzip compression and decompression.

	Fluorescence Series Nissl+Fluorescence			HC Series Nissl+HC			Average
	Nissl	Fluorescence	Combined	Nissl	HC	Combined	
Number of Slides per Series	100	100	200	100	100	200	
Raw Data Size Per Slide (Direct from NanoZoomer, *.ngr Format) [Gb]	12	25	37	12	12	24	
Total Size of Raw Data [TB, per Series]	1.2	2.5	3.7	1.2	1.2	2.4	
Total Size of Raw Data [TB, per brain]	0.6	1.25	1.85	0.6	0.6	1.2	1.53
After Cropping + Conversion to Binary [GB, per Section]	1.3	2.1	3.4	1.3	1.3	2.6	
After Cropping + Conversion to Binary [GB, per Slide]	7.8	12.6	20.4	7.8	7.8	15.6	
After Cropping + Conversion to Binary [TB, per Series]	0.78	1.26	2.04	0.78	0.78	1.56	
After Cropping + Conversion to Binary [TB, per Brain]	0.39	0.63	1.02	0.39	0.39	0.78	0.90
After Cropping + Conversion to Binary + Gzip Compression [GB, per Section]	0.5	1	1.5	0.5	0.5	1	
After Cropping + Conversion to Binary + Gzip Compression[GB, per Slide]	3	6	9	3	3	6	
After Cropping + Conversion to Binary + Gzip Compression[TB, per Series]	0.3	0.6	0.9	0.3	0.3	0.6	
After Cropping + Conversion to Binary + Gzip Compression[TB, per Brain]	0.15	0.3	0.45	0.15	0.15	0.3	0.38
Number of Brain per Storage Node (24TB/per)	64						
After Conversion for WebPosting [GB, per Section]	0.125	0.5	0.375	0.125	0.125	0.25	
After Conversion for WebPosting [GB, per Slide]	0.75	3	3.75	0.75	0.75	1.5	
After Conversion for WebPosting [TB, per Series]	0.075	0.3	0.375	0.075	0.075	0.15	
After Conversion for WebPosting [TB, per Brain]	0.0375	0.15	0.1875	0.0375	0.0375	0.075	0.13
Number of Brain per Storage Node (24TB/per)	183						

Table 8: Disk usage, at each stage of the software processing pipeline

Since image acquisition (NanoZoomer scanning) is the rate limiting step of this component, it was critical to ensure maximum efficiency of the NanoZoomer computer. This computer and it's hard disk would be dedicated to image acquisition. All image processing and data storage would be performed by other systems. The NanoZoomer computer would be connected to this distributed network, as discussed in section 2.2.7.3, via a 10G copper network, which allowed for a maximization of transfer speeds. A linux script was implemented to allow for the autonomous

transfer of acquired data to a central repository. This configuration ensured that the NanoZoomer scanning would not be halted, due to lack of available disk space.

This element of the component is the most elaborate but also the most significant in terms of workflow optimization. Once fully operational, the above changes allowed for the whole-slide imaging to be solely limited by the scanning rate. The performance improved from 50% of the theoretical maximum to the current level of 80%. Once the image are gather (per series), they are immediately processed (cropped) and transferred to a central repository and available for Quality-Control to be performed, using a web-interface. The latter allows for dynamic access to the data - the user can modify the dynamic range of each color channel, zoom/pan, annotate image regions and also rapidly switch between neighboring sections. There is also an option to view all of the sections of the series, as tiles, in a large mosaic view.

2.2.6.4. Procedure Standardization/Industrialization:

As discussed above, the primary challenge of performing whole-slide imaging on a large scale, was implementing the design changes to the NanoZoomer hardware/software and data workflow. As with other components, an SOP was compiled for the proper use of the NanoZoomer and the Matlab cropping program. Unlike other SOPs, this protocol focused heavily on troubleshooting the NanoZoomer hardware. This was because the Olympus/Hamamatsu technical support was found to be ill-equipped for rapid troubleshooting of problems. Therefore, empirical problem solving solutions were thoroughly documented, for every problem encountered through the extended use of the NanoZoomer.

The critical procedure changes that were implemented as part of the SOP, were (1) Slide cleaning - all slides loaded into the NanoZoomer would be extensively cleaned using 70% ETOH, on both surfaces of the slide. This process helped to minimize the amount of dust and other foreign contaminants on the slide; (2) Any slide with a misaligned coverslip, was excluded from the scanning. The slide would need to be re-coverslipped before scanning could take place. The NanoZoomer has very tight tolerances on the parameters of the slide and therefore any change in shape (caused by an overhanging coverslip), can result in a failure of the mechanism and require manual intervention to reload the slide; (3) As discussed in section 2.2.6.3, output of the EXFO light source would be normalized using the radiometer, every 100 hours. The brightfield and fluorescence settings of the NanoZoomer would also be calibrated, against

"standard slides" every 100-200 hours. (4) The resulting images would be sampled at random to verify proper illumination and expected SNR. The output of this system component, more so that others, was made virtually operator independent and thus very uniform.

2.2.6.5. Downstream Integration and Upstream Feedback:

This is the terminal component of system, and therefore, a critical process feedback step. The appearance of the tissue in the digital images is the final determinant of both the biological and process quality factors. The major feedback was: (1) Adjustments to viral tracer injection volume, to prevent saturation of signal at the injection site. Even though the NanoZoomer was configured with a dynamic range of 12-bits, pixel saturation would occur for concentrated injections of viral tracers. The saturation was acceptable, as long as it did not interfere with the interpretation of the injection - i.e. identifying the injection site, projection site and the connectivity in-between. To allow for this, the injection volume for viral tracers was limited to 2.3-4nl - which helped to localize the injection site and to limit the saturation to just the primary infected cells; (2) To further control the saturation of the label, the exposure time was fixed at around 16ms (equivalent of 4X on the NanoZoomer), for all fluorescent samples. This setting was empirically determined to result in the optimal label intensity through injection and the projection site. This exposure was selected in conjunction, with the normalization of the light source output at 2.5W. (3) As discussed in section 2.2.5.5, due to the inability of the NanoZoomer to focus on unstained sections, a counterstain, in the form of a Giemsa Stain was added for HC processed tissue. The Giemsa stain produced a "Nissl like" appearance and allowed for optimal determination of the focus plane; (4) The coverslip procedure and the "drying" of the slides was altered to minimize the number of slides with misaligned coverslips that were loaded into the NanoZoomer.

Post-coverslipping, the slides would be manually examined for proper mounting media coverage and to verify that the coverslip was aligned with the edges of the slide. The slides would be placed on a drying rack and allow to dry for at least 24hours, prior to imaging. This process added a time-delay to the system, but greatly improved the performance of the NanoZoomer, as the rate of slide handling related errors, was reduced by an order of magnitude; (5) Volume of applied mounting media (DPX) was also altered to allow for maximum coverage of the slide, while allowing for sections to be detected on the brightfield macro image. Through

empirical testing, a volume of 100ul was selected as an optimal amount. Depending on the purity of the slides (dust and other foreign contaminants), air bubbles would still occasionally form on some slides, at an average rate of about 1 in 20 (10 per a standard series of 100 slides). The use of this volume, guaranteed that a suitable image can be resolved, with detectable sections, from both the brightfield and darkfield macro imaging modes (Figure 33). (6) The elements of the HC staining, were altered to maximize the intensity of the label and ensure high SNR. For both CTB and BDA, the type of DAB used for the exposure of the label, was modified from 3,3'-Diaminobenzidine Tetrahydrochloride (Fisher Scientific, Product #PI-34001) to 3,3′-Diaminobenzidine (Sigma-Aldrich, Product #D8001), which resulted in higher intensity of fine processes. Hydrochloric Acid (HCl), at a volume of around 50µl, would need to be added to this DAB to allow for the power to dissolve in the solution. Incubation time for DAB was fixed at 5 minutes.

2.2.6.6. System Evolution:

The most significant evolution of this component, occurred with the increase in the number of NanoZoomer units that comprised the imaging station. Originally, a single NanoZoomer was used for all scanning and had a throughput of approximately 4 brightfield series, or 2 fluorescent series per week. Since this rate is approximately 3-5 times less than the full capacity of the system, which is 10 series per week (tracer independent), an additional NanoZoomer was purchased and configured to operated in parallel with the existing unit. This addition doubled the scanning capacity of the system. To further increase imaging throughput, a third and for a few months, a fourth NanoZoomer was "leased" from Olympus America and installed in parallel with the two primary units. Besides and increase in the overall imaging rate, this seamless addition of units, is a testament to the robustness of the system design. As the number of NanoZoomer units increased, the amount of data acquired daily, increased by the same proportion. The data network was able to handle this added loaded without creating a bottleneck in the dataflow. The Matlab conversion program was able to facilitate the rapid cropping of all incoming data and the transfer of that data to a central repository. Furthermore, the entire imaging component was staffed by a single technician - who was able to perform the scanning for all 2-4units and facilitate the proper management of the resulting data.

2.2.7. Support Infrastructure:

In addition to the primary system components discussed above, the system is comprised of several support components. These components function as the "glue of the system" and help to ensure that the system functions as a single entity. The three principle support elements are: (1) the laboratory space, which houses the components; (2) the Laboratory Information Management System (LIMS), that stores and manages process meta-data and (3) the Data Network of the system, which stores the resulting image data from the system and allows for downstream analysis to be performed on the data. All three support elements were specifically engineered for this system.

2.2.7.1. Laboratory Space Design:

In order to maximize efficiency and ensure an ergonomic process, the arrangement of the system components, is as important as the elements of each component. One of the main problems in most high-throughput process implementations, is that existing laboratory space is used to house the system and as such, intrinsic ergonomic inefficiencies lead to decreased performance of the system. As a common example, rodents are typically housed in an Animal Facility that is not directly connected to the laboratory space, where the tracer injection is to be performed and as a result, a technician can spend 10-15 minutes just ferrying the animals from the facility to the laboratory. The exact level of inefficiency, is obviously facility dependent, but the underlining issue is that when a generic setup is used to attempt a high-throughput operation, native inefficiencies of each process, will combine to a significant drawback. To address this issue, a specialized laboratory area would be designed to house the components of the system.

As shown in Figure 35, this laboratory space is divided across two physical locations, the "main laboratory space" (A) and the "injection room" (B-C). The "injection room" houses the Tracer Injection component - more specifically, the stereotax stations, that are used by the technician to perform the survival surgery into mouse. This room is part of the animal facility, meaning that the mice are housed in the adjoining room and that the transport time is insignificant. As importantly, the animals are not subject to any unintended environmental conditioning - they are always kept at the same conditions and there are no transport related effects to consider. The animals are kept in the same room before and after injections - different cages, with proper annotations on the cage. Since viral tracers will be used on some of the

animals, the injection room and the animal room are both designed to adhered to Biosafety Level 2 standards. Access to each room and the general area of the Animal Facility are restricted to specific personnel. This animal facility, is located directly beneath the main laboratory space.

The main laboratory space, houses the remaining system components. The critical design elements of this space are: (1) the sectioning and staining components of the system are localized to an isolated part of the laboratory, away from the main entrance, which minimizes environmental variability. The sectioning component is further isolated to a closed area, with a sliding door, and is attached a dedicated temperature/humidity controller - this minimizes rogue air currents flowing through the cryostat and uniformity of environmental conditions in the room.

During normal operation, the door stays closed for the duration of the sectioning. The temperature in the room is set to a stable range of 20±2ºC, with a humidity level of 50%±10%. The quality of the sectioning component is very dependent on environmental temperature and humidity. If temperature is in excess of 24-26ºC, the sections will display thermal artifacts ("Swiss Cheese effect"). If humidity falls below 30-40%, the tissue will begin to flash-dry on the slides, causing macro cracks. If humidity rises above 70%, excessive frost will develop inside of the cryostat, reducing cooling airflow and causing heat artifacts in the tissue.(2) A linear process workflow is assumed: Brain Preparation → Brain Sectioning → Section Staining and → Section Imaging. The staining component is located immediately outside of the sectioning component room, which allows for the technician to directly load the slides into the staining machine, without having to ferry them to a distant location. The slide drying station is located opposite the coverslipper, which allows the technician to easily examine the slides and to place them for drying, again without to ferry them to an distant location.

The imaging component is housed in an adjoining room to the other components, this is to isolate the computer equipment from the wet-laboratory. Both primary NanoZoomers are placed onto a center island. The island is equipped with a 10G switch, which allows it to serve as a regional network distribution hub. All computers that need access to the 10G network, need to be localized to this area. Access to the NanoZoomer is available from all sides - which is quite useful for debugging the instruments and retrieving fallen/damaged slides. The NanoZoomers and computers on the island, can be rearranged to accommodate extra units. Post-scanning, slides are placed back into slide boxes and stored in a 4°C refrigerator, which helps to preserve the fluorescence intensity. This refrigerator is located inside of the Imaging Room, which allows for

ease retrieval of slides, for possible re-imaging or to confirm the imaging results, through manual imaging on an upright microscope. For long term storage, the slide boxes are transferred to a dedicated cold room (4°C).

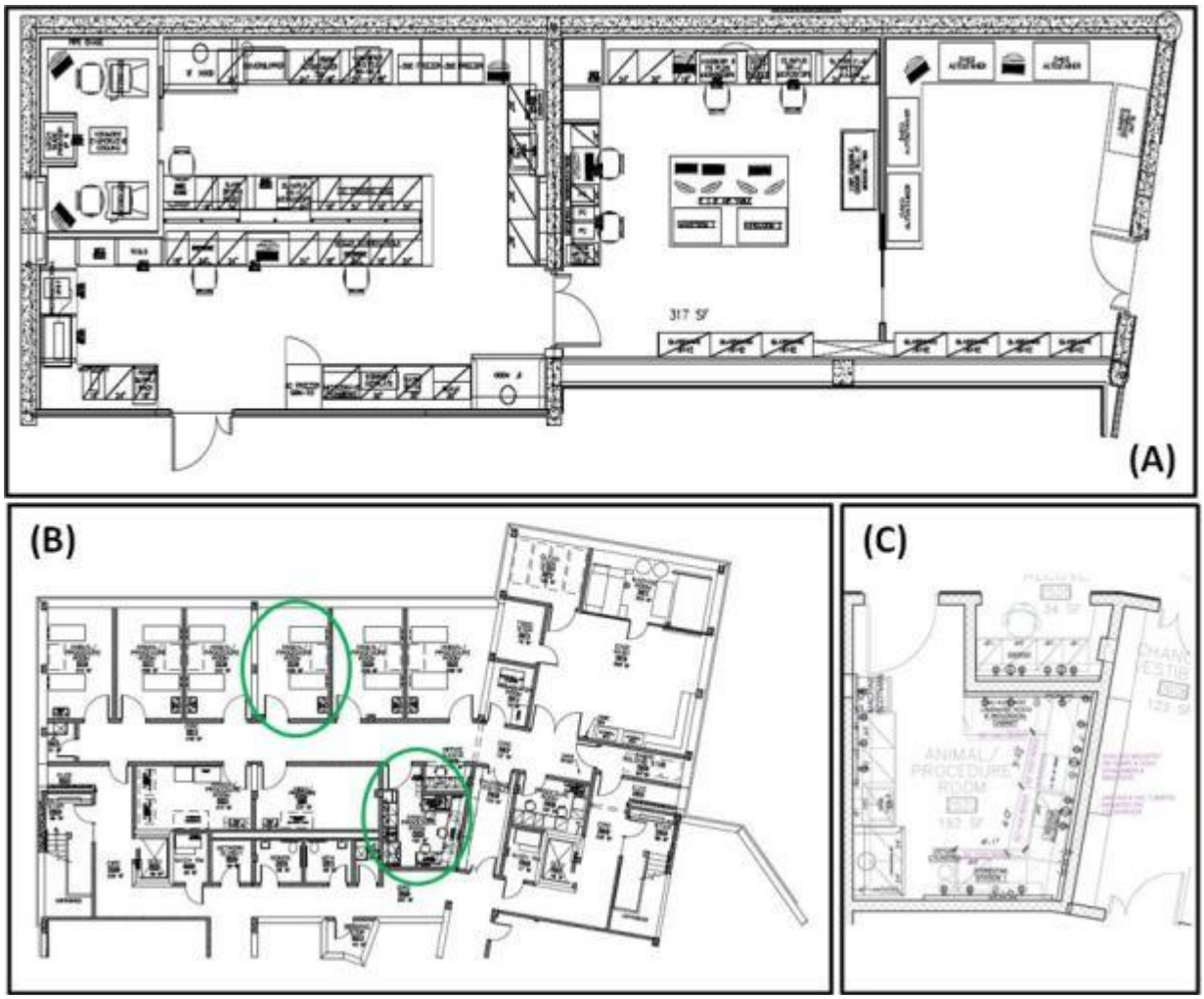

Figure 35: Laboratory floor plan

The laboratory space was optimized specifically to facilitate maximum efficiency of the system. The laboratory space is divided across two distinct areas, the main laboratory space (A) and the injection room & animal housing room (B and C). The main laboratory space is over 1000ft^2, spread over three connected rooms. The cryosectioning room (top left corner) is segregated from the rest of the laboratory by a sliding glass door. The room has a dedicated environmental system (temperature and humidity control). The injection room is located inside of a dedicated animal facility. Access to the facility is controlled. The animal room for this project and the injection room are circled in (B), (C) shows the detailed layout of the injection room.

2.2.7.2. Laboratory Information Management System:

The need to collect and maintain metadata of laboratory and experimental processes is well established in modern industry. In academia, this is not so. For most laboratory groups, the state of art, for metadata collection is Microsoft Excel, Google Documents or similar generic product. Though "efficient" for some purposes, it is highly problematic, at an exponential rate, with the number of specimens (number of mice to be processed). The main problem with these approaches is that they are not process specific and lack transparency, scalability and simultaneous multi-user accessibility - which translate to lose of critical process information. An Excel Sheet (local or web-based) with 200-500 columns and several hundred(or thousand) rows of data, is a simple means of visualizing the complexity of using these generic tools to maintain complex process data.

In recent years, many laboratory specific, information management tools have began to be available from manufacturers like RuRo Corp and Waters Corp. The goal of these laboratory information management software (LIMS) tools is to provide the experimenter or laboratory manager, with a robust database backbone and a customizable frontend, that can be used to create process specific pages with specific data entry fields. These programs are similar in nature, though different in database design/structure and overall effectiveness, to Microsoft Access and similar applications. Though straightforward and adaptable, the problem with this form based approach, is that the result is most often a generic user-specified program and though it is an improvement over Excel, it is still limited in scope and adaptability. One does not have the ability to fully tailor the application to meet the unique needs of each laboratory process. Most often, the ability to directly interface the LIMS software with a specific laboratory instrument is also missing. The LIMS is often viewed as a software aid, rather than a firm system requirement, and as such, if a technician experiences prolonged software trouble, they retreat to using either a physical notebook or memory. In either case, the practical result is the loss of valuable metadata, that eventually hampers the efficiency of the laboratory process.

For these reasons, an extensive effort was undertaken to implement a custom web-based LIMS system that would be specific to this laboratory process and allow for the management of all relevant metadata. Ruby on Rails (RoR) (version 1.9 and version 3.0.5) was selected as the platform building this LIMS. RoR is an open source web application framework for the Ruby programming language. RoR employs the Model-View-Controller (MVC) architecture pattern. MVC is a three-tier architecture which separates domain logic from presentation. HOBO, a

collection of open-source gems/plugins for Ruby on Rails that assist in rapid prototyping and development, is also extensively utilized. HOBO is itself written in Ruby and helps to automate various tasks in the creation of a RoR application by relying on conventions, and provides extensions and enhancements for the standard models, views and controllers. HOBO includes an application wizard for initial setup as well as command line tools for the creation of resources and the management of database migrations. The database used for the LIMS is MySQL v.5.0.77, a free open-source relational database management system (RDBMS). Figure 36 depicts the Entity-Relationship (ER) model of the LIMS. Using the HOBO framework, this database model was formed into an extensive series of inter-reliant view pages. The basic design was to devote a single page, a single tab in the LIMS web-interface, to each critical element of the system.

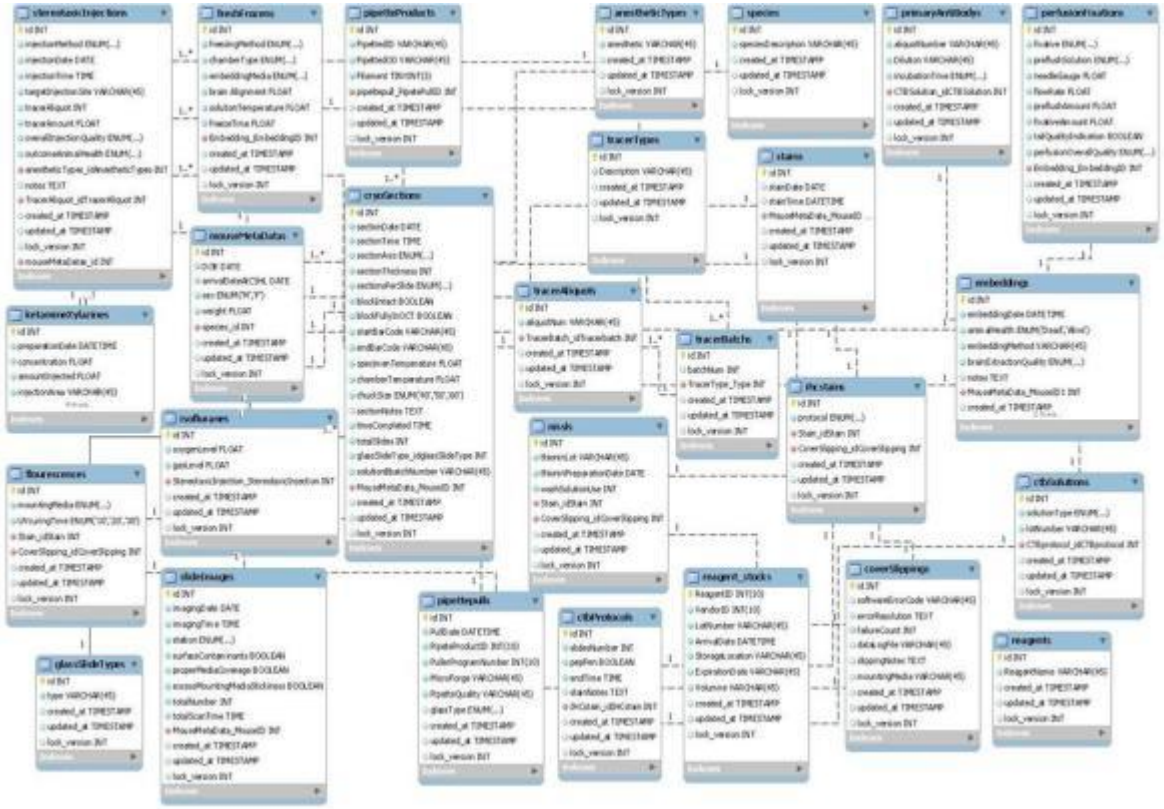

Figure 36: Entity-relationship (ER) model of the LIMS

There are eight principle pages in the LIMS: (1) Steretoax Injection (Tracer Injection component); (2) Brain Embedding (Brain Preparation component); (3) CryoMount(Brain Preparation component); (4) Cryosectioning (Brain Sectioning component); (5) Staining (Section Staining component); (6) Imaging (Section Imaging component); (7) Pipette pulling; (8) Quality

Control. There are also several support pages: (9) Tracers; (10) Injection Plan; (11) Summary and (12) Home. These supporting pages are a means of managing the management software - they are used for reagent supply chain management (9), to predefine a weekly set of coordinates and tracers to be injected by a technician (10). To visualize the data, two key features exist - the home page(12), which shows the table view of the animals and their general status in the queue of each system component - this is used to answer questions such as: has a specific animal been sectioned or imaged? This page is fully searchable - using the provided interface. For more detailed snapshots and to answer questions such as: how many mice were processed at a given component in the last week?, the summary (11) page is used. This page provides a weekly, monthly and historical view of all animals in the system.

The obvious key element of this LIMS is the design and implementation of the fields associated with each component, each page, of the LIMS. The conversion of a given laboratory process into a standardized set of LIMS fields, requires the operator/technician to subdivide the process into key attributes. This is obviously easier said than done. For this reason, we adopted a reverse methodology - given select fields (chosen by the experimenter), can the process be repeated by a different, non specialized experimenter, with identical results? If so, than only these fields should be recorded. If not, the number and type of fields needs to increase until this is so. To allow for an adapted feedback, a notes field was included for several pages. Technicians were instructed to use this field to enter only information that could not be captured by existing page fields. After it was noticed that the same type of critical information would be populated in the notes, a new dedicated field would be added to the page. For prototyping and auxiliary operations, the notes page proved invaluable, as the technician could easily document the specifics of a given experiment, as a function of the animal and glass slides (section staining experiments) on which the experiment was performed.

Unique sample identifiers are a key component of the LIMS structure - they are assigned by the system at the time of entry and noted on the physical samples. In the case of the mice, two sets of corresponding identifiers are used: (1) the animal number and (2) the ear tag number. The former is assigned on a 1-animal per cage basis and the latter is used to tag the actual animal and to account for scenarios in which cage cards are lost. The animal number in LIMS is labeled with a specific experimental designation, such as: PSB = "Practice Series Brains", PTM = "Production Trial Mode", PMD = "Production Mouse DATA"; and MD = "Method Development". This

animal number is treated as a series number, once the tissue is sectioned and mounted onto slides. Upon imaging, each file has a name identical to that of physical slide. To prevent the likelihood that a given brain sample would be mounted onto slides with the wrong sample ID, LIMS was directly interfaced with the slide printer (Thermo Scientific, SlideMate Printer). In order to print a set of slides, per an established SOP, the technician would first need to located the brain sample in LIMS, verify that the sample is to be sectioned on that day (rolling queue), than locate the physical frozen block and once it is confirmed that the block is intact and can be sectioned, the technician would simply press a button labeled "print slides".

Based on the selected sample ID, LIMS would output a standard text file with the relevant fields to be printed on the slide: the sample ID (Unique Identifier + Sample Number), Date of sectioning, followed by the slide type (Nissl or HC/Fluorescence) and the slide number. This information was physically printed on the slide and also encoded into a data matrix (2D barcode). A default of 100 Nissl and 100 HC/Fluorescence slides would be printed per request, with the ability to reprint failed slides due to a printer error or print additional slides. This process is significantly more robust and less prone to mistaken sample identification, than the use of preprinted generic slides. Printing the sample ID text on the slide, and encoding all the information into the data matrix, allowed for identification redundancy.

At present, the LIMS is being used to store information for about 1500+ brain samples. It has been an invaluable organization tool and a critical system support component.

2.2.7.3. Data Network Backbone:

As a byproduct of the enormous volume of data generated by the pipeline, an elaborate network of data-entry computers, data-acquisition computers, data viewing (quality control) stations, data storage nodes and analytical machines was integrated over a 1/10G network to provide a cohesive solution[81, 82]. As illustrated in Figure 37**Error! Reference source not found.**, the network is subdivided based on location within the laboratory and the intended use of each computer station. The network is segmented according to data flow. The data streams from LIMS computers (low bandwidth) and those of the NanoZoomer data-acquisition computers (high bandwidth), are considered independent and integrated only in background processing of the image data - correlating metadata with image analysis. The main data stream from the NanoZoomer computers, is first written onto local drives, and then is automatically transferred,

via a linux process, onto the storage nodes of a Data Viewing Computer. This computer is the central repository for all imaging data. The computer is attached to two direct attached storage (DAS) storage nodes (Promise Technologies, Vtrak M310p and M610p[83, 84]), which are configured as Raid6 devices and provide 24 and 18TB of useable disk space (total of 42TB of local disk storage). This storage space is intended to act as a buffer - for all images, of a given series to be amassed and then hold the data while the Matlab image conversion process can initiate, and be fully complete. At full throughput, each NanoZoomer can generate data at the rate of 2 TB per day. Therefore, this local data cluster, is able to facilitate uninterrupted scanning for 10 days - but if the Matlab conversion is operating at peak, this buffer is just reserved space.

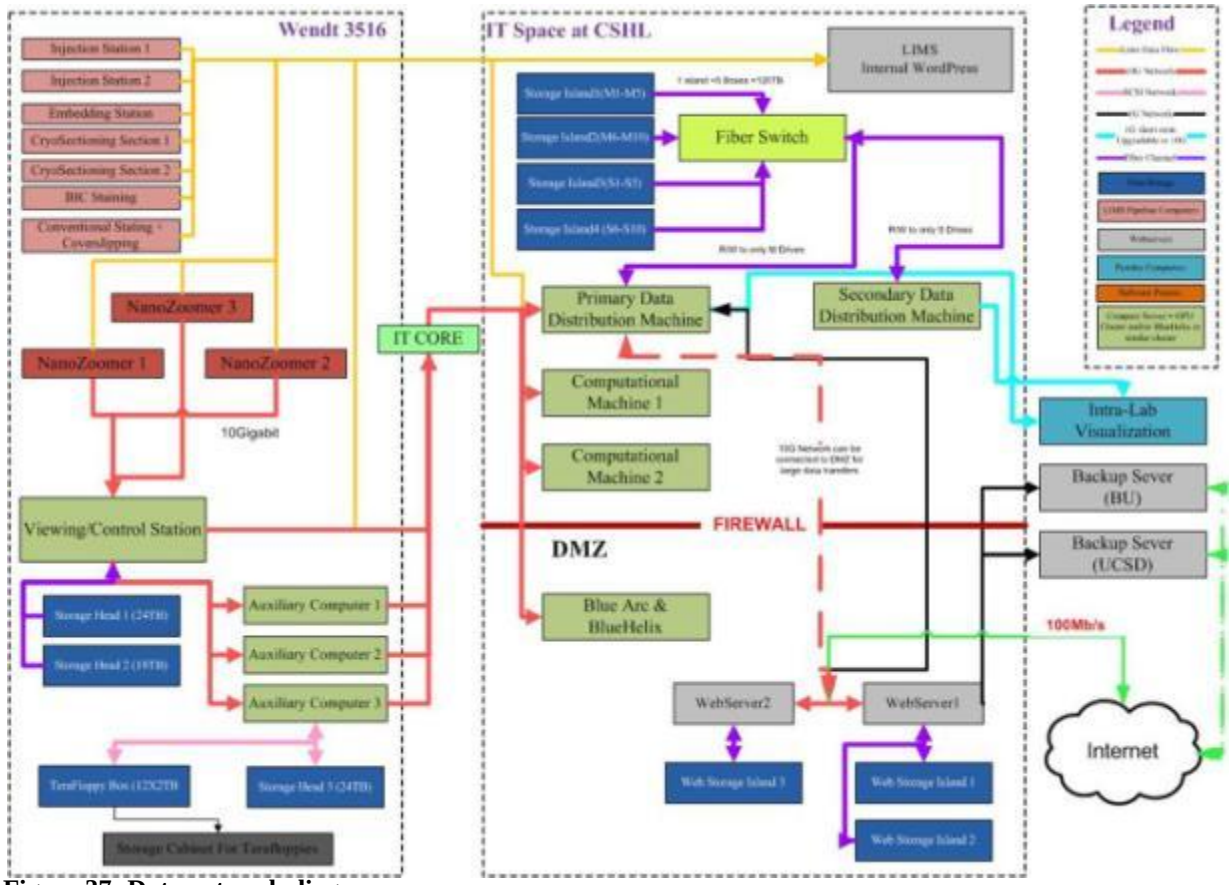

Figure 37: Data network diagram

To facilitate the Matlab conversion process, additional computer nodes are designed to process the data in parallel from this central repository. The NanoZoomer machines, the data viewing machine and these additional computers (auxiliary computers), are all networked via a local 10G switch, which allows for optimal data transfer rates. The network has been configured

for optimal data transfer rates, the average node-to-node transfer rate is on the order of 175 MB/s (empirical rate). The theoretical maximum transfer rate of the 10G network is 1.25GB/s - the 7 fold difference is because the rate limiting process is the hard disk write speed of each computer. This was intended, to account for the active scenario when parallel transfer will be outgoing through the common switch. This local 10G network, is directly networked, through an intermediary fiber optic core (labeled "IT CORE") to another local 10G network. This geographically separated network, is located in a dedicated server room, maintained by the Cold Spring Harbor Information Management (IT) Department. This room is access limited, equipped with backup generators and active climate control systems. The central data repository for the system, is placed into this environment, to allow for maximum performance and data integrity. This repository consists of 12 network attached storage (NAS)nodes (Promise Technologies, Vtrak M610p) which are connected to a common fiber-channel switch. As such, all data that is hosted on these storage nodes, is available to any computer that is connected to the fiber-switch at the same data rate. The reason for this configuration is to prevent the bus of a single computer from acting as a bottleneck for the simultaneous transfer to data to many different nodes.

2.3 Summary:

In this chapter, I have presented the detailed development of a high-throughput histology pipeline for mapping mouse brain circuitry systematically using tracer injection based neuroanatomy. Engineering challenges arose in the very concept of the pipeline, as well as in the development and interface of each element. Conventional techniques were adapted for high-throughput processing and supplemented with novel methodology to improve tissue quality and system performance. Chapters 3 and 4 focus on the development of two such novel methods. A sample of the data produced by this system is shown in Chapter 5.

CHAPTER 3: BRAIN FREEZING METHODS DEVELOPMENT

Significance: This paper presents a method that was developed as part of this dissertation and is critical to the data produced by the pipeline. This method has facilitated the high-throughput sectioning ability of the pipeline and has facilitated the computational registration of the cut sections into a common space.

Contribution: My role in this paper was that of the lead engineer and main author of the paper. I designed, fabricated and extensively tested the method that is presented in this paper. The 3-D model of the brain was provided by the Allen Institute and transformed into a 3-D object by a collaborator. Laboratory technicians (co-authors) contributed empirical observations that were used to optimize the method.

Status of Manuscript: The manuscript is currently in the draft form, and is awaiting submission to a journal.

Previous Work: This work has not been previously presented or published.

Title: A low-cost technique to cryo-protect and freeze rodent brains, precisely aligned to stereotaxic coordinates for whole-brain cryosectioning

Authors: Vadim Pinskiy[1,2], Alexander Tolpygo[1], Jamie Jones[1], KevinWeber[1], Neil Franciotti[1], Partha P. Mitra[1]

[1]Cold Spring Harbor Laboratory, Cold Spring Harbor, New York

[2]Department of Biomedical Engineering at Stony Brook University, Stony Brook, NY

Abstract:

Sectioning of rodent brain tissue parallel to canonical planes of section (coronal, sagittal or horizontal) is an important technique for modern neuroanatomy. Digital re-slicing of data after imaging is possible, but is not a substitute for obtaining physical sections aligned to the canonical coordinate axes. Such alignment facilitates automated computational registration of the sections onto a reference atlas and permits quantification of information present in the imaged brain slices, in the reference atlas frame. With the advent of high-throughput neuroanatomy, where thousands of brains may need to be processed for a given project, a reliable method to obtain physical sections precisely aligned to coordinate axes has become a necessity. Obtaining such aligned sections is a difficult and error prone process. The difficulty stems from the lack of rigid rectilinear edges on the rodent brain that can be used for such alignment. We address this problem by freezing the brain in a pre-cast, age-specific mold that utilizes the native curvature and shape of the brain to obtain the alignment. Unlike previous approaches, these molds are composed of standard embedding medium (Neg-50, O.C.T, TFM, etc.), which enables optimal heat transfer during the freezing process and results in morphologically intact tissue. The disposable cost of the system is solely the cost of the embedding medium. The method is scalable and does not significantly impact processing time. We demonstrate the use of this system with 56-day old, C57BL/6 mice.

Problem Statement: How to freeze rodent brains in stereotaxic coordinates without damaging the tissue or otherwise hampering downstream 3-D reconstruction, using a standardized, high-throughput means?

Introduction:

Alignment of a frozen-tissue sample to a fixed reference frame is an important practical problem in modern rodent neurohistology. This problem is widely known and appears throughout prepared samples. This problem is even evident in the Allen Reference Atlases (ARA)[39] of the mouse, and similar atlases. The rodent brain does not have any rigid edges that can be used for direct alignment to a fixed rectangular plane. Landmarks on the brain can be used for visual alignment, but this is subjective and difficult to standardize. In the case of the ARA, the brain was aligned in the freezing chamber under a dissection microscope, but as shown in Figure 70, the symmetry between the two hemispheres is clearly lacking. The offset is on the order of 2-3 atlas plates, depending on the coronal level.

Why is it important to obtain canonically aligned sections? There are two reasons: firstly, brains are (to a first approximation) symmetric around the mid-sagittal reflection plane, and symmetrically cut coronal sections are significantly easier to interpret than asymmetrically cut coronal sections. For example, one can examine contra-lateral projections for a tracer injection study more easily if the coronal plane is cut in a symmetrical manner. Similarly, sagittal sections that are not parallel to the mid-sagittal reflection plane will intersect this plane and include parts of both left and right brain hemispheres, increasing interpretational difficulties. The second reason is that sections in the histological reference atlas are cut (approximately, modulo the same difficulties discussed here) in planes aligned to the canonical coordinate axes. Therefore, if the physical sections are also cut and imaged in the canonical planes, then they can be more easily aligned to the reference histological sections (for example by using a simple Euclidean distance between intensities or section boundaries). Note that while MR based reference atlases do not suffer from these issues (since they are typically 3D volumetric atlases), these are not that useful for analyzing histological sections since MR atlases do not have high enough spatial resolution to resolve individual cells.

Since the brain sections get eventually digitized into a three-dimensional data set, one might think that digital re-slicing of the data would correct for improper alignment during sectioning. However, this is not the case, due to the large asymmetry in the resulting 3D data set: the in-plane resolution is typically much higher than the between-plane resolution, resulting in highly anisotropic data volumes that cannot be easily re-sectioned into other planes. In principle, it is possible to obtain higher between-plane resolution by obtaining z-stacks within the tissue

sections, but this may be prohibitive in terms of data acquisition times and volumes. Isotropic 3D voxels are only possible using some variant of a serial block-face sectioning method that is integrated with the imaging, but even this method suffers from impractically large data volumes.

Existing approaches:

Besides landmark based alignment of the brain, the other common alignment method is to place the brain back into the skull from which it was extracted, or a rigid mold, and trim the brain parallel to a fixed rectangular edge. For coronal sectioning, it is common for the olfactory bulb or the cerebellum to be trimmed. This fixed edge, would be used as the reference plane for cryostat or microtome sectioning. For whole-brain research, this method has the obvious problem of tissue loss due to the macro trimming of the brain and during alignment of the reference edge to the knife of the cryostat. This method makes alignment easier but does not solve the problem entirely, as the block can still be misaligned with the knife of the cryostat, producing non-symmetrical sections.

The brain can also be sectioned without blocking or landmark based alignment during freezing. Rather, the sectioning angle can be adjusted based on the block-face appearance of the brain. For coronal sections, it is often difficult to gauge the alignment of the brain until after the olfactory bulb (for anterior to posterior sectioning). The number of sections needed to obtain that desired alignment is technician dependent, but can be approximated at around 10-20. This technique is effective, but has the downside of being time consuming, difficult to standardize, and subject to tissue loss until a stable sectioning angle is found.

Neither approach is suitable for high-throughput neuroanatomy because of the lack of reproducibility in the method and the possible inconsistency in the resulting sections. Recent solutions to this problem have included the use of silicone molds (Leica, Model #39417501) to encompass the brain in rectangular coordinates, prior to freezing. This approach is sound in concept, but suffers from the following problems:

(1) An increased thermal resistance, through the introduction of another material, which can result in thermal damage of the tissue during freezing;

(2) A significant increase in the disposable cost, per animal. The average cost of these brain molds is on the order of $6-10;

(3) The silicone material can interfere with sectioning and mounting of the sections onto slides. For these reasons, this system is not widely used in the neuroscience community and is not widespread in the published literature.

To address these issues, we have created a method for easily freezing rodent brains in standard stereotaxic coordinates, without the use of a supplementary support material. Instead, our system allows for the casting of the brain shape directly into standard embedding medium (such as O.C.T). The disposable cost of the system, is solely the cost of the embedding medium - which is around 30cents per brain - 20X less than that of the silicone based system. The system utilizes 3-D printed model of the ARA mouse brain to create a tailored cavity for the placement of the brain in a standard rectangular base-mold. Once frozen, the block is sectioned relative to the fixed edge of the mold, which corresponds directly to the parallel plane on the brain. We demonstrate the use of this technique for coronal and horizontal sectioning of 56 day-old C57BL/6 mouse. The size of brain model can be adjusted for other ages and species. This technique has been extensively used as part of the Mouse Brain Architecture project to freeze over 1000 brains.

Methods:

Approach: In order to freeze a mouse brain in stereotaxic coordinates, we have created a method of freezing a mouse brain in a custom-fitted mold. The mold is pre-cast, such that it is aligned to the rectangular edges of the freezing chamber (base-mold). These edges can be used as reference plane for cryostat chuck adjustments and to ensure that the sectioning of the brain is parallel to the canonical planes. To maximize the curvature contact between the mold and the brain, the mold is prepared by casting a negative of one hemisphere of the brain. To prevent the brain from rotating or otherwise distorting, in this "sagittal mold", a second negative of the opposite hemisphere of the brain, is placed over the brain. This "sandwich" approach, ensures that both hemispheres of the brain are treated identically and minimizes deformation during freezing. Once frozen, the two molds and the brain fuse to form a single entity, and the block can be sectioned through any established protocol. For our testing, we section all material using the Tape-Transfer system. One important advantage of Tape-Transfer method, used in conjunction with this pre-cast-mold system, is that it allows for sectioning and slide mounting of two mouse

brains (coronal sectioning) simultaneous. This results in a two-fold increase in daily sectioning throughput.

Brain Model: A 3-D model of the left hemisphere of a 56-day old, C57BL/6 mouse was derived from the "two-sided" volumetric anatomical atlas, sampled at 200 microns, provided by the Allen Institute. The volume contains integer-valued intensities at each voxel in the left hemisphere, which uniquely identify a brain area to which that voxel belongs. The atlas was computationally mirrored (the original ARA data set is asymmetrically shaped) to create a label in both hemispheres. This label-based atlas was binarized (such that voxels outside the brain were assigned value 0 and voxels in any part of the brain were assigned value 1. The volume was then smoothed with a 3-D gaussian kernel and the outer boundary of the brain was extracted. Software was then used to convert from a MATLAB internal format defining vertex coordinates (in millimeters) and triangular faces (sets of three connected vertices) into the standard tesselationlanguage (STL) format to be used in computer aided engineering software. A volumetric size increase of 10% was applied, to account for animal-to-animal variations, affects of paraformaldehyde perfusion, and the viscosity of the embedding medium. This model of the left-hemisphere was mirrored to create a model of right-hemisphere. A combined brain model of the two hemispheres is shown in Figure 70A.

For the model of each hemisphere (Figure 70C), a rectangular extrusion was created, perturbing from the medial plane, away from the brain (Figure 70B). The purpose of this extrusion is to allow for a convenient means of positioning the brain in the fixture. A model of each hemisphere was required to account for the relative orientation of the two hemispheres (mirror images). If two negative molds, created from one hemisphere are placed on top of each other, the cavities will not align. The discrepancy will be largest at the olfactory bulb (Figure 70C).

Fixture Design: The support fixture for this assembly is a static part that was designed entirely in Solidworks. The purpose of this fixture is to securely position the brain model(s), relative to the base-mold. The part is designed with tight tolerances, so as to minimize erroneous positioning. Thumb-screws are used to lock the position of the base-mold and the brain model, once ready for freezing. As shown in Figure 70D, this part is intended for the simultaneous freezing of two

mouse brains, but can be modified for freezing of a single brain. The part is designed to minimize volume of formed material (primary cost of 3-D printing) by employing an open gantry-frame design. The gantry has two precast grooves, designed to mate to the rectangular extrusion of the brain models. Once inserted into the grooves, the horizontal position of the models is fixed. Vertical position is variable to allow for the easy insertion and removal of the base-mold. The base-mold is designed to be placed in the center opening of the fixture, such that the frame forms around it. Once the position of the base is secured to the frame, using the thumbscrews, the entire assembly is supported by the rigid base-mold. Since the fixture is lightweight (≈45 grams), it does not add any significant stress onto the base-mold. Even a plastic base-mold (Peel-A-Way Embedding Mold, R-30) is fully suitable to support the fixture. The complete assembly is shown in Figure 70E.

Base-Molds: The freezing fixture is intended to be used with the Tissue-Tek® Base-molds for Embedding Rings (Tissue-Tek, Model #4132). This base-mold is stainless steel, which facilitates optimal heat transfer and thus minimizes the possible thermal damage to the brain. This mold has a large footprint that allows for two brains to be frozen side-by-side, and sectioned at the same time. The edges of these base molds are angled, which helps to extract the frozen mold from the base, but creates a problem for alignment. This angle is addressed in the mounting of the block to the chuck of the cryostat. This angle is estimated at around 5°.The system can be used with other base-molds, such as the Peel-A-Way (R-30).We have also created custom base-molds, by using stock brass tubing and soldering a bottom plate. The advantage of these molds, is that the sides are not angled.

Embedding medium:Neg-50 (Richard Allen Scientific, Model #6502) is the principle embedding medium, used for all experiments. The presented method has been tested with other compounds, such as O.C.T and TFM. Neg-50 is preferable, because we have found that its composition is closer to that of tissue (once frozen), than the other compounds.

Fabrication: Both the brain model and the support fixture where manufactured through commercial 3-D printing (Vistatek Corporation). The brain model was printed using polyjet technology, in KryptonGreen. The support fixture was printed using SLA technology, in

VeroWhite. The resolution for both parts was 0.001" (25.4µm). KryptonGreen is preferable for the brain molds over VeroWhite because the brain molds undergo significant stress when being removed from the frozen embedding medium and the higher tensile strength of the material reduces fractures. Post-printing, the only assembly work that is performed on these parts, is the thread tapping of the through holes for the thumb-screws and the insertion of the screws. The thumbscrews (McMaster-Carr, Model#91185A333) have a thread of 6/32 and can be directly attached to the fixture, after the holes are tapped.

Mold Production and Brain Freezing: The steps of the mold casting and general freezing process are summarized in Figure 40. The steps are animated to best illustrate the process. The process consists of two distinct set-of-steps: (1) Mold production, steps I - VIII and (2) Brain freezing, steps IV - XV. The two sets do not need to be performed continuously. Cast-molds can be prepared ahead of time and stored at -80°C, until brains are ready for freezing.

The mold production process entails positioning of the brain models in the fixture (vertical adjustment), relative to the bottom of the base-mold (approximately 4.5mm from the bottom). The accuracy of this positioning is not as important, as repeatability (assured by marking the vertical position on the rectangular extrusion). Once the position is secured, fresh embedding medium, Neg-50, is added to the base-mold, such that it just covers the brain model. Excessive amounts of Neg-50 will make the removal of the brain models difficult after freezing and should be avoided. Approximately 3mL of Neg-50 is required for the casting of one such mold. Any air bubbles in the poured medium should be removed before freezing. The assembly is then frozen, either using the two-beaker method (described below) or simply placed in -80°C for 15+ minutes. The rate of freezing is not a critical factor for the mold production. The molds will harden to the same strength, regardless of the method. To conserve reagents (isopentane) and reduce cost, it is preferred to let molds freeze in the -80°C.

Once frozen, the molds need to be returned to room-temperature (RT) and allowed to acclimate, through mild thawing. The thawing occurs on the outer edges of the block, the edges that contact the base-mold and the brain models. This thawing does not damage the integrity of the cast, but facilitates in removing the cast from the fixture. Once the temperature of the block reaches around -7°C, which at a room-temperature of 20-23°C requires 10 minutes, the thumbscrews of the fixture should be loosened (or entirely removed) and the brain models should

be slowly raised to the highest point in the fixture. This should force the cast block and the base-mold to also raise. The base-mold can then be removed, by carefully rolling it side-to-side. If the mold does not remove easily, additional time (1-2minutes) should be given for the block to thaw. Once the base-mold is removed, exposing the cast-mold, the same motion can be used to remove it from the brain models. This process is shown in Figure 41. The resulting mold, represents one hemisphere of the model and should be placed into an appropriately labeled container and stored at -80°C. In a linear workflow, this model is that of the left-hemisphere, and is termed, the "left-mold". The same process is then repeated for the other hemisphere, producing the "right-mold". As shown in Figure 41E, the molds are structurally sound and the shape of the brain is well cast. The top surface of the mold is typically rough, due to the nature of the freezing process. This surface is made smooth, either by trimming with a razor blade or by mild grinding with a metal file.

Once molds of both hemispheres are cast, the brain freezing process can begin. If the brain is fixed, than it should be cryo-protected through sucrose immersion. We typically pass the brains through 10% sucrose and 20% sucrose, for 24 hours each. The brain should be blotted, to remove moisture, prior to freezing and covered with a thin layer of Neg-50 to prevent a moisture barrier and air pockets. The cast brain molds should be removed from the -80°C and allowed to acclimate for 8-9 minutes at RT (20-23°C) and then fresh embedding medium should be added to the cavities of both molds. An additional 1-2 minutes of acclimation should be allowed. This thawing of the mold is *essential* to prevent thermal damage to the brain. Since the molds are frozen, the brain cannot directly contact the molds because local partial-freezing of the tissue will occur, causing the water molecules in the tissue to crystallize and expand, damaging the tissue. The initial wait of 8-9 minutes ensures that the mold has reached a temperature of at least -2°C, and when the warm embedding medium is added, it will not freeze on contact and alter the cavity. Rather, the addition of the warm medium helps to further thaw the cavity of the mold and make it adequate for brain insertion. The second wait of 1-2 minutes ensures that the temperature of the mold is at least 1°C and that the temperature of the embedding medium is at 5-6°C. Some local freezing of the medium is possible at the contact with the cavity, which can slightly alter the size of the cavity, but this is accounted for, by the 10% volume increase of the mold, relative to the expected size of the brain.

Once both molds have acclimated accordingly, the blotted brain should be added into the left- mold, such that the left hemisphere of the brain is in contact with the entire curvature of the mold. The olfactory bulb of the brain should align with that of the mold. The brain should be orientated such that the midline of the brain, roughly aligns with the edge of the cavity. The brain should not be depressed into the mold. This operation should be repeated for both brains. The position of the brains should be recorded, relative to a labeled edge of the block. We typically denote the anterior and posterior orientation of the brains on the base-mold and the cast-molds with an "A" and "P" using a marker, and have standardized that brain1 is to be placed into the dorsal cavity and brain2 should be placed into the ventral cavity. This can be adjusted per user-preference. The corresponding right-mold should than be placed over the brains, such that the olfactory bulb's are aligned. As the right-mold is being lowered, the edges of the molds should be roughly aligned. Once the top-mold has "sandwiched" the brains, lateral motion should be avoided, as this can damage the brains. The two molds should be carefully pressed together. Residual embedding medium should be removed from the sides of the block. The block should then be quickly placed into the base-mold and frozen using the two-beaker procedure (below). Unlike during mold production, this rate of freezing should be maximized to prevent crystallization of the water molecules in the tissue and associated thermal damage to the tissue. The use of liquid nitrogen to freeze is not recommended, as the block is likely to fracture and damage the brains. The freezing using the two-beaker method, with isopentane, requires approximately 3 minutes for a complete freeze. The block can be stored in -80°C or directly transferred to the chamber of a cryostat for sectioning.

Two-Beaker Freezing Procedure: To adequately freeze the brains in the embedding medium, without thermally damaging the tissue or cracking the block, we freeze using isopentane, which is chilled by dry-ice. The process involves the use of two beakers, one placed inside of the other. The large beaker (VWR, Model #D10898666) has a volume of 1500mL; the smaller beaker (VWR, Model #13977-042) has a volume of 250mL. Either glass or metal beakers can be used; although metal is preferred due to the superior heat transference (McMaster, Model #4352T3). Dry ice is crushed to small chunks (¼ - ½ in diameter) and placed inside of just the large beaker, such that surface area contact with the smaller beaker is maximized and air gaps are minimized. Isopentane (Sigma-Aldrich, M32631-4L) is slowly poured into the smaller beaker. After a few

minutes of acclimation, additional solution is added to the beaker to account for rapid evaporation at the initial pour. Once the surface of the solution is calm (minimal bubbling), a few pellets of dry ice should be added to the smaller beaker. The isopentane solution should be at a temperature of -60°C. A base-mold with embedding medium and tissue is then placed inside of the isopentane, such that the lip of the base-mold is at the surface of the solution. The base-mold should not be submerged into the isopentane, until it has fully frozen. As the embedding medium freezes, its appearance will change from translucent to opaque white. Freezing should occur at a uniform rate from the five sides that are in contact with the isopentane. A standard block that is 32x25x12 mm in size, should freeze in approximately 3 minutes. Thermal gradients in the isopentane are possible, and can lead to macro deformation of the brain. To minimize these, the amount of dry ice around the smaller beaker, should be approximately the same on all sides and on the bottom of the beaker.

Cryostat Mounting and Sectioning: The frozen brain blocks were sectioned using a Microm HM 550, with a fixed cutting angle of 12°, at a section thickness of 20µm. The frozen blocks were removed from the -80°C and placed into the chamber of the cryostat, and allowed to acclimate to chamber temperature of -15°C. After 20 minutes, the blocks are placed on the flat surface of the cryostat and the edge of the block is slightly trimmed until it is normal to the horizontal. This is intended to account for the 5° angle of the base-molds. This trimming is performed with a fine metal file. The block is aligned against the wall of the cryostat to judge if the edge is normal to the horizontal. The block is then mounted onto the chuck of the cryostat by applying fresh Neg-50 onto the chuck and then firmly pressing the block down. The block was orientated according to the required plane of sectioning, relative to earlier marking ("A" and "P"). The peltier chamber of the cryostat was used to speed up the mounting. Once frozen, the chuck was installed and lowered such that the base of the block was near the knife of the cryostat. The yaw (side-to-side rotation) was adjusted such that the leading edge of the block was parallel to the knife. The pitch was adjusted the same way.

The anti-roll plate of the cryostat would be lowered, adjusted relative to the knife position and the first section would be slowly cut. The section would be entirely of Neg-50. If the knife does not appear to be cutting an equal amount from both sides of the block (left-to-right and bottom-to-top)adjustments would be made to the yaw and pitch of the chuck. Since the sections

are composed entirely of Neg-50 at this point, many iterations of this adjustment can be made, without affecting the tissue. Once the alignment is finalized the chuck would be securely locked in place. The section thickness would be changed to 50µm (trim setting) and block should be trimmed until the first indication of tissue is seen, at which point, the thickness would be returned to 20µm and serial sections of the entire block should be collected using the Tape-Transfer system. Regardless of the blockface appearance of the brain, no further adjustments to the block, relative to the knife should be made. All sections would be collected and mounted directly onto slides, per the Tape-Transfer system.

Slide Staining and Imaging: The sectioned material was allowed to dry overnight at 4°C and was then stained for Nissl bodies, using a thionin based protocol and coverslipped using DPX. The staining and coverslipping was performed in a Sakura Tissue-TekPrisma&Glas g2.The Nissl protocol was as follows: 1.5 minutes in 0.25%Thionin Solution, two minutes in two solutions of deionized water; five minutes in three grades of ethanol (50%, 75%, 90%), five minutes in two solutions of absolute ethanol, and 5 minutes in two solutions of xylene. Once coverslipped, the slides were manually examined to ensure proper coverage of the mounting medium and allowed to dry overnight at room temperature.

Imaging of the sections was performed using a NanoZoomer HT system, at a resolution of 0.5µm/pixel. Blockface images were taken at the time of sectioning, using a Nikon D300 camera, with a macro lens (85mm f/3.5G).

Temperature Measurements: Temperature measurements of the frozen blocks were performed using an infrared thermometer (Omega OS423-LS). The temperatures were validated by using an insulated Type-K thermocouple.

3-D Scans of the Brain: The NextEngine Laser Scanner was used to 3-D scan the brains, before freezing and after thawing and removing the embedding medium. The scans were performed with 13 divisions at a resolution of 4,400 points/inch^2. Once scanned, the images were converted to STL and formatted in Solidworks.

Animals: All animals for this testing were acquired from Jackson Laboratories. The animals were 56±3day old mice, C57BL/6, with a weight of 18.8 – 26.4 grams. The animals were treated per IACUC approved protocols. The animals were perfused with 4%paraformaldehyde (PFA)[JT Baker, Model #JTS898-7) through the heart. Avertine (2.5%) was used as the anesthetic. A saline preflush of 50mL was used to remove the blood from the circuit, prior to addition of 4%PFA (50mL). The brains were extracted and post-fixed in a solution of 4%PFA, with 10% sucrose (JT Baker, Model#4072-05) in PBS, for 24 hours. The brains were further cryo-protected in 20% sucrose in PBS for an additional 24 hours.

Results:

Blockface and section images of brains that were frozen using the pre-cast-molds and sectioned on a cryostat, using the Tape-Transfer system, are shown in Figure 42 and

Figure 43. Coronal sections are shown in Figure 42. Horizontal sections of a different brain, are shown in

Figure 43. As evident in the images, the hemispheres of the brains are close in symmetry throughout the block. There is a slight offset between the two brains, seen most prominently in the hippocampal formation of the coronally sectioned brain. The offset is estimated on the order of around 2-3 ARA atlas plates (200-300um), this is consistent with the alignment of the atlas. For the horizontally sectioned brain, the misalignment is on the same order of magnitude. These results are significant because they were obtained under two drastically different conditions. The ARA was likely produced under stringent controls for the production of this atlas data. The material presented here was produced under lighter controls, and in fact was collected under normal processing conditions in the MBA pipeline. Therefore, this level of plane accuracy is reproducible across many samples and different technicians.

The lack of perfect symmetry with this method is due to the difference in size of the brain, relative to the mold, and not the procedure employed by the technician. The molds can be closer tailored in size (by altering the volumetric increase, relative to the ARA) to the brain, which would help to further reduce this variability. The downside of this approach is that for high-throughput processing, the exclusion criteria (brains that cannot be frozen with a given mold) will be relatively high). Besides the above, the macro shape of the brains is undistorted

and appears as expected. No thermal damage is evident on the sections. At high-magnification (Figure 42E), the cells of the cortex appear structurally sound, without any damage that would result from water crystallizing during freezing. The two brains shown in Figure 42, where frozen in a single block and appear to be not only symmetrical, but also at a similar coronal plane, at each level. This correspondence between the two brains, facilitates downstream processing of the data, and in localizing and region-of-interest on the slides.

One of the concerns with this method was that it would cause a deformation of the brain during freezing. To address this, we collected a 3-D point cloud of two brains. One brain was frozen using this mold based system; the other was frozen conventionally without the molds. NEG-50 was used as the embedding medium in both cases. Both brains were then thawed, blotted to remove excess embedding medium and rescanned. The results showed the whole-brain volumetric deformation for the mold system, was equivalent to that of the conventional method. There was also no evidence of any obvious damage to the surface of the brain. The 3-D scans for this experiment are shown in Figure 44.

Discussion:

In this work, we present a method of freezing mouse brains in stereotaxic coordinates, by pre-casting a brain specific cavity in the embedding medium, which is used to secure the position and orientation of the brain relative to a known rectangular edge. We use this system to show that two brains can be frozen in the same block and sectioned simultaneously, in the coronal plane. We also show that the same system can be used to section a brain the in the horizontal plane. In both cases, the brains are processed by simply mounting onto the chuck of the cryostat, aligning the knife to the face of block and then collecting serial sections. The technician *does not* adjust the tilt and yaw of the block based on appearance of the brain (as is typically the case in previous approaches). The resulting sections show that the symmetry between the two hemispheres is similar to that of the ARA, but is reproducible across samples. As shown in Figure 42, the two coronal brains are at approximately the same coronal level (±2) and have a similar tilt angle. We also show that this system does not result in any erroneous deformation of the brain or in damage to the morphology of the tissue (Figure 44).

With the use of this system for processing of many mouse brains, we argue that accurate symmetry between the two hemispheres, is less important than repeatability of obtaining the

same sectioning plane. This is because the lack of symmetry between the hemispheres is a cosmetic problem for manual analysis, but a serious problem for 2-D and 3-D computational processing of the images. The biological data on the sections, is not altered by the lack of symmetry, but visual analysis is hampered because multiple sections need to be examined to understand a single bilateral plane through the region-of-interest. For streamlined computational analysis of the data, the sections across all brains, need to be registered into a common space. This registration is based on identifiable features. The outline of the brain and macro-landmarks, such as ventricles, are used to align similar sections so that the features of the sections overlap. If the two brains to be registered were cut at a radically different sectioning plane, the majority of the features, on the 2-D sections, will not have the same appearance and thus alignment will be poor. As shown in Figure 70, the ARA also has a native misalignment of about 2 atlas plates. Obtaining a perfect registration of brains onto the ARA, would require that the brain be misaligned by the same amount, in the same direction. This is obviously not conducive to research, especially if there is a need to later align the brain onto a different reference atlas, which has a different native orientation. Therefore, we consider it more critical to align brains to each other (precision) rather than to a specific reference atlas (accuracy). Though we present the data for only three brains (two sectioned in the coronal plane and one in the horizontal plane), we sectioned several hundred brains with this technique and have seen consistent results.

In terms of maximizing "accuracy" with this system and obtaining sections that are symmetrical, one needs to maximize alignment between the mold and the brain to be frozen. One way, is to perform a 3-D scan of each brain to be frozen and then manufacture, through 3-D printing technology, a custom mold for each brain. This technique would result in better-aligned sections but has the obvious problem of cost and time. The other method is to assume a misalignment of 1-2 atlas plates as a margin of error. This misalignment of ≈200μm is caused by a tilt of approximately *1°*, when measured from the lateral edges of the coronal brain. This 1° is a combination of the rotation of the brain in the mold (caused by relative size difference) and the manual orientation of the block relative to the knife. Though the former can be optimized, the latter cannot, without extensive changes to the cryostat. Conventional cryostats and microtomes are designed without the ability to precisely orient the block relative to the knife. The block is orientated by visual alignment and adjustments to position are made through manual

manipulation of the chuck. When the first section through the embedding medium is collected, visual inspection is required to ascertain the best rotation of the block relative to the knife.

Unlike other methods that aim to address the alignment problem, this system is inexpensive. The equipment cost is on the order of $200, which can be used to freeze hundreds of brains. The disposable cost is solely the cost of the embedding medium, which is on the order of $.3 per brain. The Leica Brain Blocker One system (Model #39417501) has a cost that is approximately 20X higher and in our testing, does not result in improvement alignment. For these reasons, our method is appropriate for high-throughput applications, where many brains are to be sectioned. This system is also appropriate for applications where a dissecting microscope is not available or the operator cannot easily identify the landmarks on the brain for orientation. This approach to frozen block alignment, can be expanded for use with spinal cords, whole-rodent skulls and any other entity that is of relatively standard size across animals. This technique can also be used for non-standard tissue specimens, but requires the fabrication of a sample specific mold.

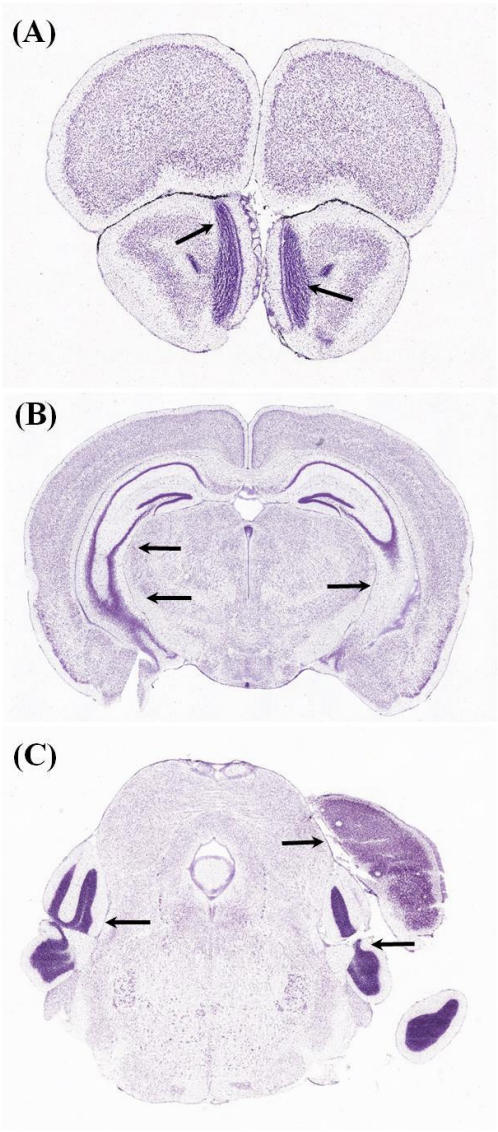

Figure 38: Alignment of Allen Reference Atlas (ARA) coronal plates
Obtaining whole brain sections, parallel to canonical planes of section, is an unsolved problem in neurohistology. As shown in A-C, the lack of symmetry between the two hemispheres of the brain, is clearly evident in the Allen Reference Atlas, which is one of the most commonly used anatomical references. Allen Reference Atlas, coronal Level 27 is shown in (A); level 80 is shown in (B); and level 105 is shown in (C). The black arrows point to the lack of symmetry between the two hemispheres.

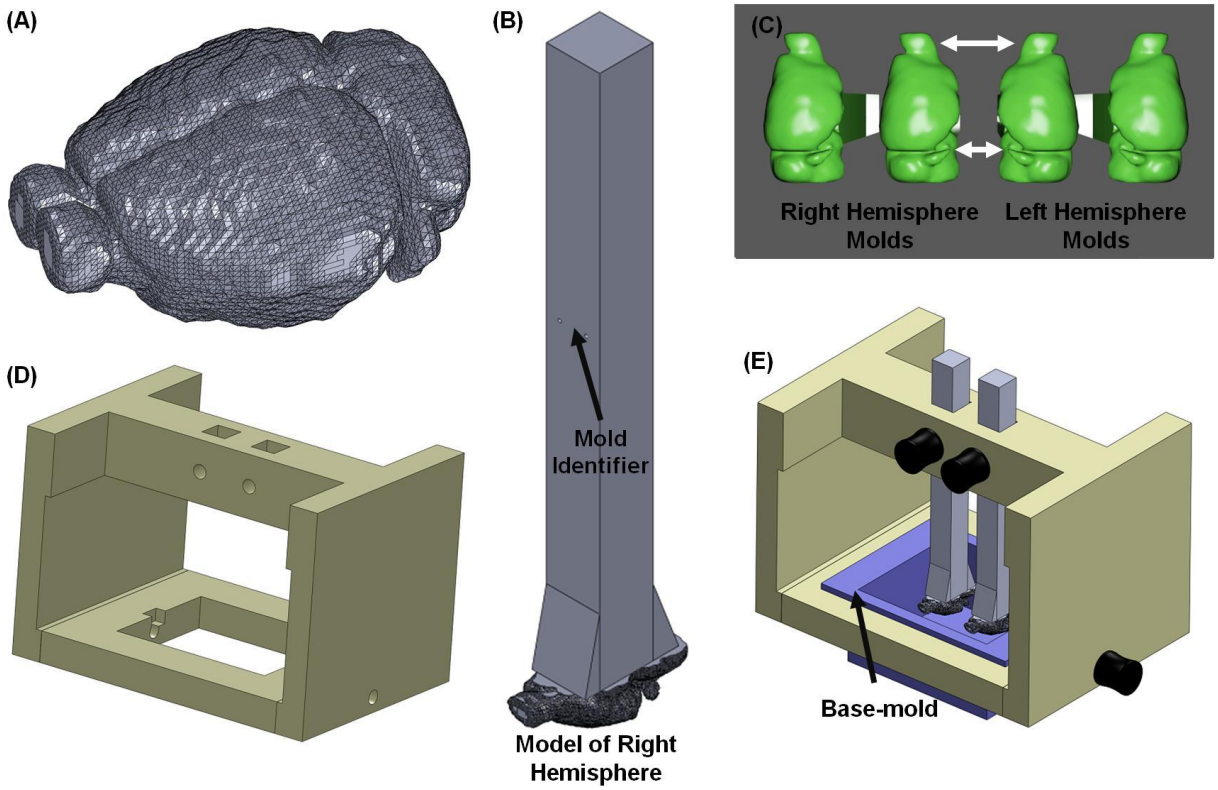

Figure 39: **Brain models and the fixture of the pre-cast mold system**
A 3-D model of a 56-day old C57BL/6 mouse brain is shown in (A). This model was derived from an MRI of the brain used for the Allen Reference Atlas. The left hemisphere of this brain, with a rectangular extrusion is shown in (B). The purpose of this extrusion is to allow for easy control and positioning of the brain model. The black arrow points to two through-holes, which are used to denote that this model corresponds to the left hemisphere of the brain and should be used to cast the left-mold. One-through hole (not shown) is used to denote the model of the right hemisphere, used to cast the right-mold. The bottom view of both models (with extrusions) is shown in (C). The white arrows point to the difference in orientation of the two hemispheres. The fixture used to control the position of the brain models and the base-mold, is shown in (D). The fixture was designed as gantry-frame, to facilitate rigidity and minimize production material. The complete assembly is shown in (E). The thumbscrews are shown in black, the base-mold in blue; the fixture is beige and the brain models in gray.

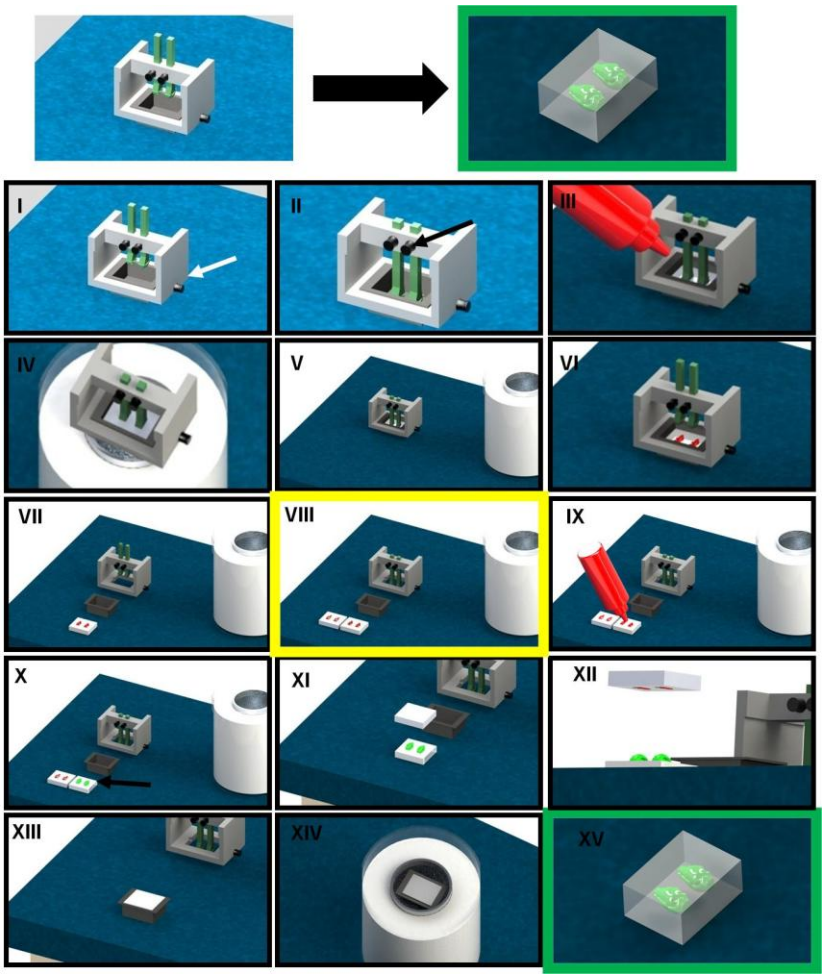

Figure 40: Animated workflow of the freezing process

The freezing method, is a multi-step process, which results in a frozen block of embedding medium that contains two mouse brains (highlighted by a green border), which are both aligned to the rigid edges of the block. The freezing apparatus is assembled by loading the brain models of the left-hemisphere(with extrusion) and the metal base-mold into the fixture. The base-mold is secured using a thumb screw, indicated by a white arrow (I). The brain models are then lowered into the base-mold, to a pre-configured level and secured using two thumbscrews, indicated by a black arrow (II). Embedding medium, NEG-50 (red bottle), is slowly added into the mold, such that it covers the two brain molds (III) . Approximately 3.1 ml of medium is needed. The entire fixture is then frozen, using either the two beaker method, in which dry ice (outer beaker) is used to lower the temperature of isopentane (inner beaker) to around -40C (IV). For this step, the mold can also be placed into a -80C freezer. Once the embedding medium is frozen in the fixture, the fixture is returned to RT and allowed to briefly acclimatize (V). The brain molds are then raised(VI), exposing the formed negative cavities in the mold (shown in red). The base-mold and the cast-mold are removed from the fixture (VII). The cast-mold can either be used immediately or stored in -80C for future use. This cast-mold is the "left mold". The entire process is then repeated (VIII), using brain models that are of the right-hemisphere, resulting in the fabrication of the "right mold". This step is highlighted by a yellow border, to show its importance in the procedure and that two molds, one of each hemisphere, are required to properly freeze the brains. Fresh embedding medium is added to both molds (IX) and the brain is then positioned into the top mold (X), such that the right hemisphere is placed into the mold. The brain is shown in green, indicated by the black arrow. The bottom mold is then positioned over the top mold and pressed together (XI - XII). The two mold halves are then placed back into the base-mold (XIII) and frozen in the two-beaker method (XIV). Once frozen, the resulting block is removed from the base-mold (XV) and can either be used immediately for sectioning, or stored in -80C for future use. The embedding medium is opaque when frozen, so the position of the brains cannot be resolved without sectioning. The block is translucent in XVI to show the expected position of the two frozen brains in the block.

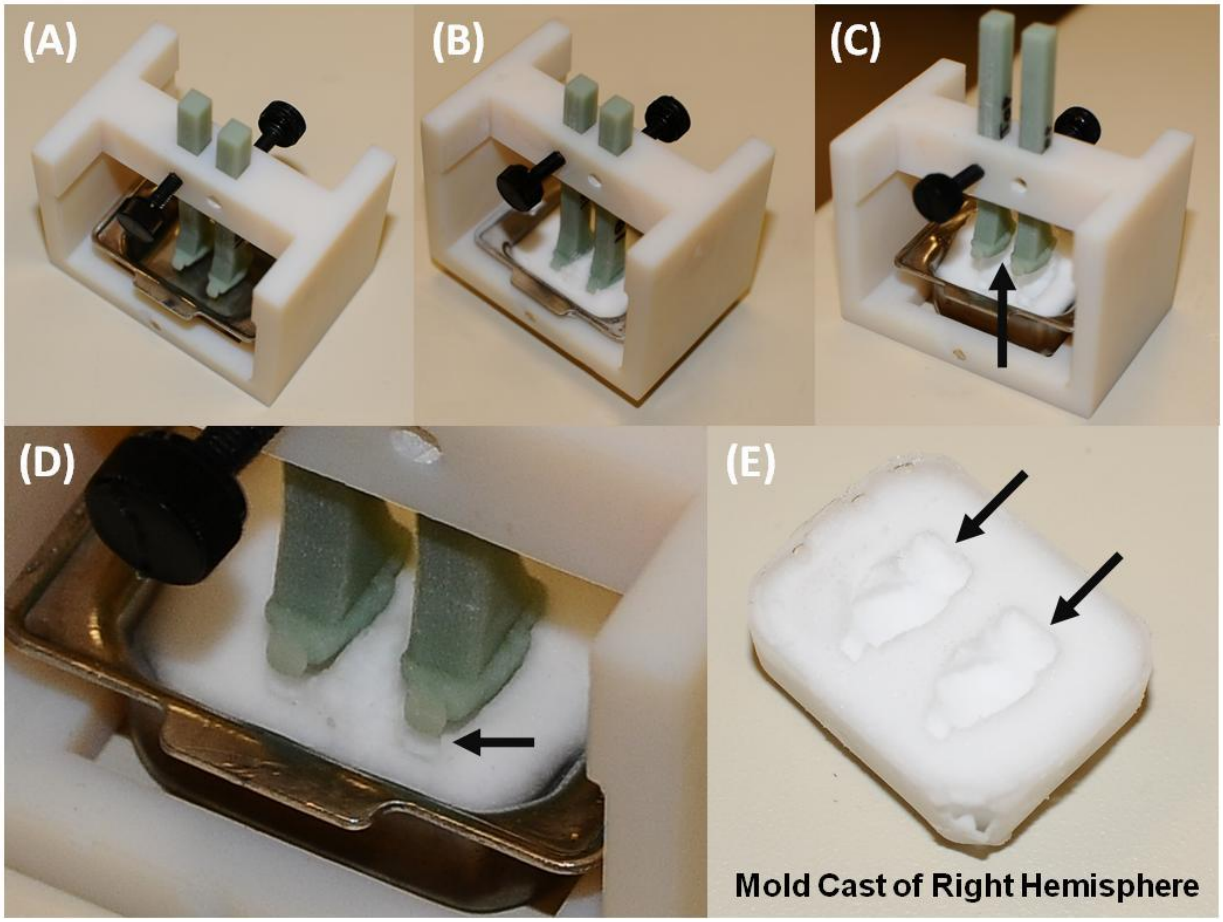

Figure 41: Production of the pre-cast molds
The assembled fixture with two brain models and the base-mold is shown in (A). After adding embedding medium and freezing in -80C, the fixture is allowed to acclimate to room-temperature, as shown in (B). After a few minutes of thawing, the brain models can be raised, while holding the base-mold or rocking it side-to-side. The cast-molds will separate from the brain models, as shown in (C) and at higher-magnification in (D). The black arrows point to the area of separation. The resulting cast-mold is shown in (E). The black arrows point to the formed cavities of the two brains.

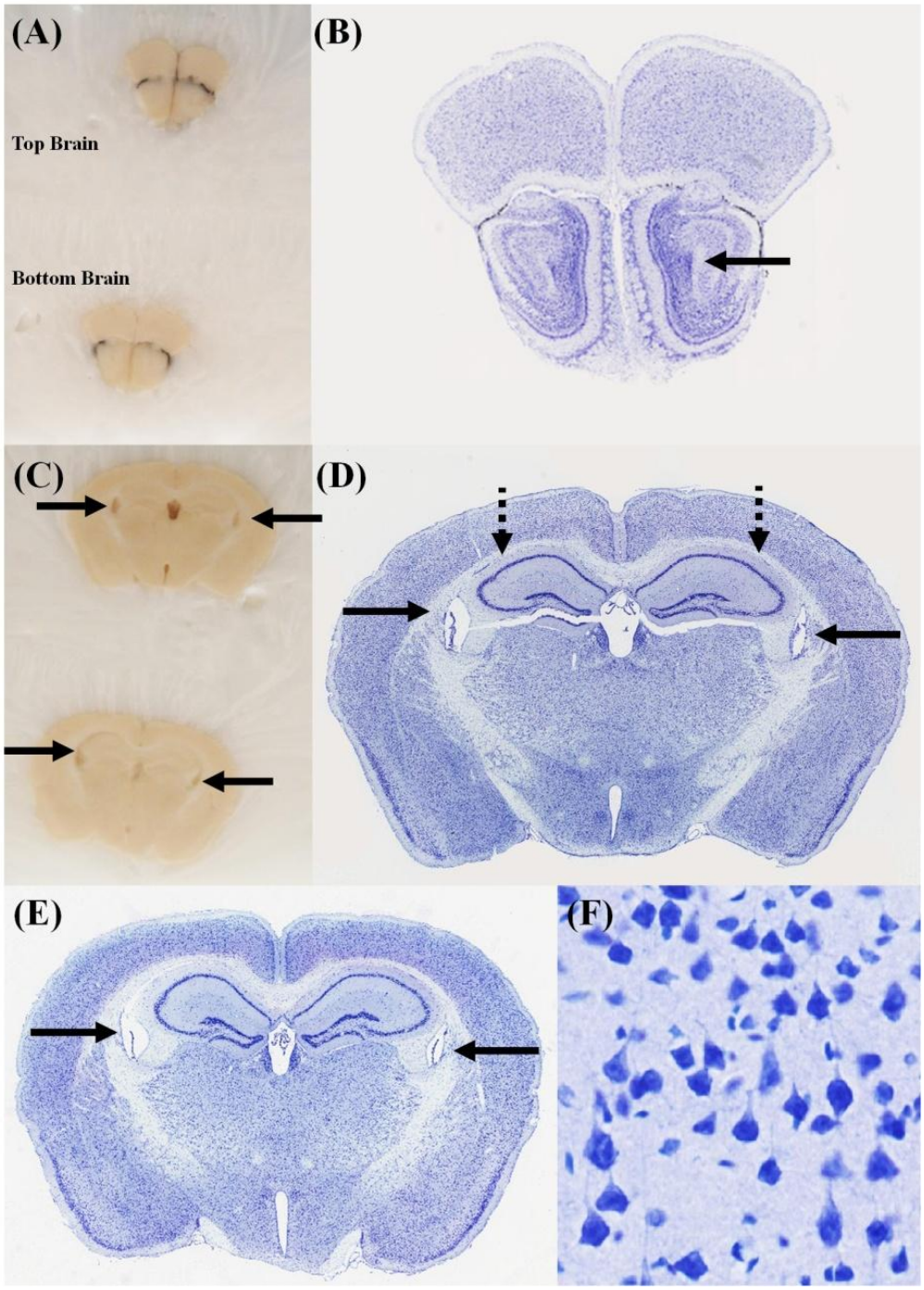

Figure 42: Coronal sections of two brains, frozen using the pre-cast mold system
Blockface images are shown in (A) and (C). The corresponding Nissl stained sections are shown in (B) and (D-F). The "top brain" is shown in (B) and (D). The bottom brain is shown in (E). The solid black arrows point to the lateral ventricles. The dotted black lines point to the hippocampal formation (HPF). All sections appear symmetrical on the blockface, but a closer inspection of the stained sections, shows an offset of about 2-3 atlas plates. This is best seen in the lateral extent of the HPF. One of the advantages of this system, is that two brains can be frozen in the same block, and are cut at the same approximate level, as can be seen in (D) and (E). (F) A high-magnification view of the stained sections shows that the cellular morphology is well preserved.

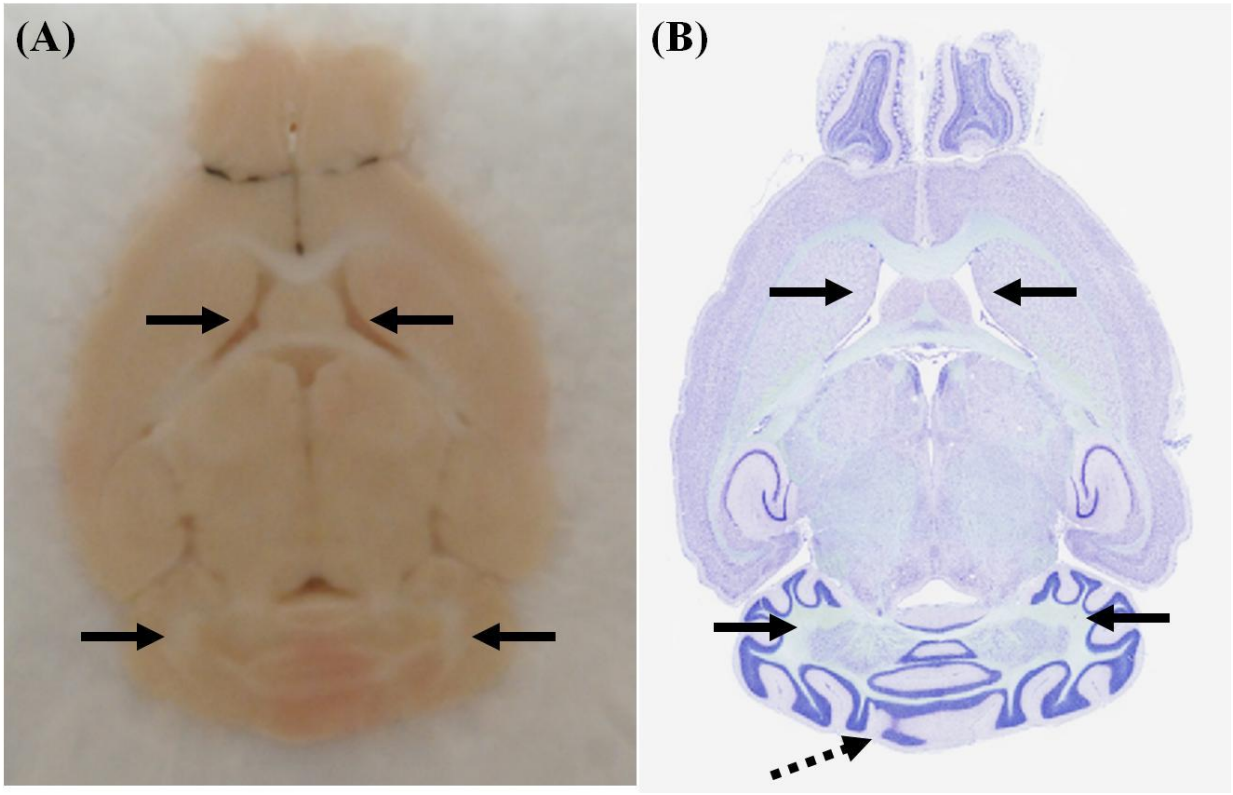

Figure 43: A horizontal section, of a mouse brain, frozen using the pre-cast mold system
A blockface image is shown in (A). The corresponding nissl stained section is shown in (B). The black arrows point to the easily identifiable landmarks on the two images. The section appears symmetrical, but a minor offset of 1-2 atlas plates exists. This is seen in the medial cerebellum, as denoted by the dotted black arrow.

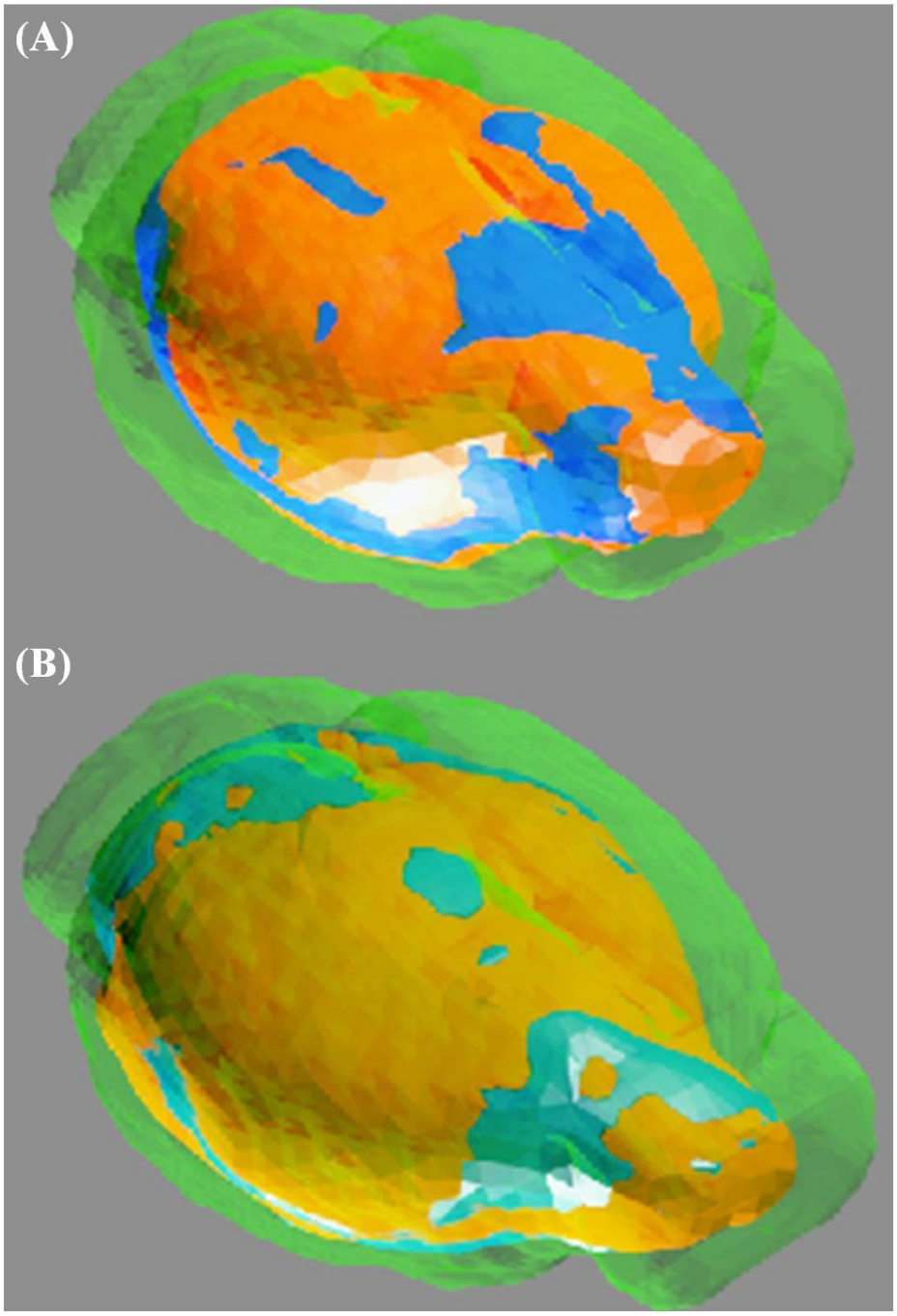

Figure 44: A 3-D scan of two mouse brains are shown, before and after freezing
In both cases, the brains were perfused, post-fixed, frozen using the two-beaker method and then allowed to thaw, through a gradual increase in temperature. The pre-freeze scan of the brains is shown in orange/red; the post-thaw scan is shown in blue; the model brain (with 10% enlargement) is shown in green. The brain in (A) was frozen using conventional methodology, with NEG-50 as the embedding medium. The brain shown in (B) was frozen using the pre-cast mold system. The whole-brain volumetric deformation for the pre-cast mold frozen brain, is approximately equal to that of the conventionally frozen brain. Slight volumetric differences are evident, but these are not significant. There was also no evidence of any obvious damage to the surface of either brain.

CHAPTER 4: TAPE-TRANSFER ASSISTED CRYOSECTIONING

Significance: This paper presents a method that was a key development in this dissertation project and is critical to the data produced by the pipeline. This method was previously believed to be "unfeasible" by senior neuroanatomists. Through extensive development, we were able to find a workable solution and optimize the method for full-production. We improved throughput significantly and reduced the number of failed sections. To our knowledge, this is the first widespread use of a tap- transfer based cryo-sectioning technique to process perfused mouse brains. This paper also shows a detailed compatibility study between the tape-transfer and conventionally cut sections.

Contribution: My role in this project was that of the lead engineer and main author of the paper. I designed, fabricated and extensively tested every component of the method and the system that is presented in this paper. This work required extensive development and resulted in a working system that is more effective than the commercial version, at a fraction of the cost.

Status of Manuscript: The manuscript is currently in the draft form, and is awaiting submission to a journal.

Previous Work: This work was partially presented at the annual meeting of the Society for Neuroscience in 2010. The abstract and the presented poster are included at the end of this chapter.

Title: High-Throughput Method of Whole-Brain Sectioning, using the Tape-Transfer Technique

Authors: Vadim Pinskiy[1,2], Jamie Jones[1], Alexander Tolpygo[1],Neil Franciotti[1],Partha P. Mitra[1]
[1]Cold Spring Harbor Laboratory, Cold Spring Harbor, New York
[2]Department of Biomedical Engineering at Stony Brook University, Stony Brook, NY

Abstract:

Introduction:

Conventional cryostat tissue sectioning is a labor-intensive process, which requires the technician to make constant adjustments to produce good quality sections. As shown in Figure 45, section damage appears in several plates of even the Allen Reference Atlas (ARA)[39]. This damage is in the form of torn and folded sections. This damage is not the product of individual error, but is the byproduct of the technique. This type of damage is common to most cryostat based sectioning. In the case of the Allen Brain Atlas of the mouse[24] and similar whole-brain projects, where serial sections are collected and digitized, this damage is more prevalent because the majority (if not all) of the cut sections are digitized. Instead of a set of a few selected images, which represent a small fraction of the total number of sectioned and stained sections, these projects call for the digitization of all sectioned material.

There are two main methods of collecting cryostat cut sections: (1) Placing the sections into solution using a brush; (2) Directly mounting the sections onto glass slides[54]. Sections intended for free-floating staining, are easier and faster to produce, as the process does not require the use of the anti-roll plate and is independent of tissue curling. Processing of free-floating sections has the downside of requiring the labor and time consuming process of mounting the sections onto glass slides. The mounting is typically performed by "painting" the sections onto the slide, using a fine brush. Most of distortion and damage to the tissue occurs at this step. This process is obviously not compatible with high-throughput neuroanatomy, which requires a reproducible method of sectioning and mounting of the sections. For this reason, a cryostat with an anti-roll plate (and/or a vacuum assist) is typically used to produce uncurled (flat) sections that can be directly mounted on the slide.

Directly mounting the section on the slide, has the advantage of allowing the technician to bypass the free-floating mounting step, but has the downside of being extremely tedious. The problem stems from the need to maintain a constant gap between the edge of the anti-roll plate and the knife that is approximately equal to the thickness of the sections. Since the sections are only 20-100µm thick, this gap is very narrow and susceptible to dust and any other contaminants. Therefore, it requires constant adjustment and cleaning. Beyond the anti-roll plate, obtaining and maintaining uncurled sections is temperature dependent and sensitive to erroneous air currents. If the sections warm, even by a few degrees, relative to the temperature of the knife block (and the chamber of the cryostat), the sections will curl, making it impossible to properly mount them directly onto the slides. To transfer the sections onto the slide, the slide needs to be lowered into the cryostat and positioned over the cut section, such that the thermal differential (the slide is warmer than the sections) facilitates movement of the section on the slide and its adhesion. The slide needs to be rotated to ensure that this movement is uniform and that the section does not wrinkle as it transfers onto the slide.

The above method has merits for low-volume production but is a limiting factor for high-throughput processing. To address these issues, we have optimized a method of utilizing adhesive tape as a means of facilitating the transfer of the sections from the cut block, to the slide. This method is a derivative of the commercial CryoJane system (Instrumedics/Leica Microsystems). Extensive modifications were made to the hardware of the platform and to the protocol for obtaining sections. The CryoJane system utilizes adhesive tape-windows that are attached to the blockface of the tissue block and the block is then sectioned without the anti-roll plate. The cut section remains adhered to the tape and does not curl. The tape and section are then placed onto a glass slide that is coated with a polymer that polymerizes with the application of ultraviolet (UV) light. The polymer is used to secure the cut section onto the slide and allows for the tape to be peeled, without damaging the section. The result is a morphologically intact section that is congruent to the block-face.

The commercial CryoJane system is not well optimized for high-throughput processing of perfused mouse tissue. We addressed this basic limitation through several principle design changes: (1) Use of an array of ultraviolet light emitting diodes (UV-LEDs) to uniformly polymerize the polymer on the slide; (2) User controlled application time, which can be extended for added adhesion strength; (3) Modifications of the tissue preparation procedure and sectioning

temperatures. These changes resulted in a robust system that has been used to section over 1000 brains, as part of the Mouse Brain Architecture (MBA) project. These changes have allowed for a daily throughout of 2-3X higher than possible with the commercial system, with a significantly less number of damaged sections. This system has been primarily used to section mouse brains that have been frozen using pre-cast molds, which allows for 2 brains to be sectioned simultaneously. These brains are sectioned at a thickness of 20µm, in their entirety, resulting in 500+ sections, per brain, all of which are mounted directly on slides and can be used for downstream staining and imaging. We have validated this sectioning method to be compatible with conventional, histochemical (HC) and immunohistochemical staining (IHC). We have also performed extensive fluorescent imaging of sectioned material, and have not detected any significant loss of fluorophore intensity or any other hindrance to transmitted, reflected or darkfield microscopy.

Methods:

Design Elements: The design of the system presented here, has two basic elements. The first is the redesign of the commercial CryoJane system, to address the workflow issues that hinder daily throughput and result in a high-loss of sections. The main problem of the commercial system is that the UV light is underpowered and can only be applied in discrete pulses. Each pulse has a duration of about 50ms, but the pulse-to-pulse interval is 30-60seconds. Multiple pulses of UV are often required for optimal adhesion of the section onto the slide. For this reason, we focused on the use of an array of UV-LEDs. The main advantages of the UV-LEDs is that: (1) The output power is voltage regulated; (2) The LEDs can be arranged in any array configuration, using a common DC power source; (3) The pulse duration can be long; (4) The steady-state operating life is on the order of 1000 hours; (5) The LEDs are stable at low temperatures (up to -30°C); (6) The LEDs are inexpensive, on the order of $5 per LED. Though the irradiance of each LED is low, we overcome this by arranging the LEDs in an array, and increasing the pulse duration. The relatively low cost and size of the LEDs allow for the fabrication of a housing that can accommodate two slides simultaneously, which facilitates the collection of alternating sections per slide.

The second design element, is the use of this platform to section perfused mouse brain tissue. To our knowledge, the majority use of the CryoJane system has been limited to fresh-frozen or paraffin embedded tissue. Perfused tissue is more challenging to section because it has different water content and freezes to a different hardness than fresh tissue. Through extensive empirical testing, we have determined the optimal post-perfusion processing conditions that maximize tissue quality during sectioning. We have also determined the optimal sectioning conditions and present a detailed method of utilizing this platform to maximize tissue quality.

UV-LED Array: The functional unit of the UV platform is the LED model NSPU510CS from Nichia Corporation. This UV-LED is an analog of a common light emitting diode (LED), except that the emitted light has a wavelength of 370-380nm. The optical power of each LED is on the order of 7.5mW with a radiation angle between 20-40°, which corresponds to an effective irradiance of 2.5mW/cm^2 - 0.250mW/cm^2, with increasing distance from the LED. To ensure even distribution of the applied UV, over the surface of the slides, while maximizing the applied UV intensity, the LEDs were formed into a 5 by 13 array. The array was fabricated as a four-layer printed-circuit board (PCB) (Sunstone Corporation). A schematic of the board is shown in Figure 46. The board was pre-wired to arrange the 65 LEDs into a parallel resistor network. Common power and ground terminals were incorporated into the design. The LEDs are soldered to the board, at predestinated terminals using 60-40 rosin core solder. The soldering temperature was maintained at 200°C, to ensure that no damage would be caused to the LEDs (T_{sld}=265°C for 10 seconds). This array has a footprint of 3.5X1.5". This enlargement over the 1X3" glass slide, is intended to allow for variability in the placement of the slide onto the curing platform. The LEDs are arranged with a center-to-center separation of 0.257", which ensures that at a distance of 0.5", the light cone of each LED overlaps.

The LEDs are arranged without serial resistors, as is common in LED array design, because the LEDs are of high-tolerances and are not overly sensitive to erroneous current pulses. The maximum rated voltage and current for this LED model is more than 20% that of the standard. Therefore, we selected a DC power source(Omron Corporation, Model S8VS-03005) with variability less than that limit. A serial resistor was added to the output of the 5V DC source to reduce the voltage to 3.6V. Since the LEDs are of high-tolerance and arranged in a parallel network, the forward voltage and current, are equal for all resistors ($V = I * R$).

Curing Platform: The UV-LED arrays were encased in a static fixture and that was designed to facilitate the placement of sections on the glass slides and the curing of the sections to the slides. An exploded view of the platform is shown in Figure 47. The platform is composed of 7 principle parts: the base enclosure; the PCB with soldered LEDs; a glass plate (McMaster, 8476K141), a top cover; foam spacers (McMaster, 5109K11), a foam pad (McMaster, 8608K311) and a lever door. With the exception of the PCB, the glass plate, the foam spacers and pad, all other components were designed in entirely Solidworks (DAssault Systems Solidworks 2011) and fabricated using polyjet technology (Vista Corporation) in Vero-White. The base of the assembly is the main component and is designed to house two PCB boards, side-by-side. There are side access terminals for the connection cables. Open vents are placed throughout the perimeter of the base, so as to allow for heat dissipation. In steady-state operation, the LEDs do not generate significant heat, therefore passive air circulation is sufficient to maintain operating temperature.

The PCBs inside of the base are encased with a transparent glass plate and secured with a top cover, using screws. The top cover is a shell that has two open regions where the slide is placed. An extra gap is designed on the terminal side of the cover to allow for easy placement of the slide. Foam strips, 1/16th of an inch thick, 1/4" wide, are placed on both sides of each slide position, such that the slide is above the glass plate. These strips allow for variable placement of the slide on the platform and prevent sliding of the slides during section placement and curing. A lever door with a foam pad is then attached to the base using side screws. The door is closed when the UV is applied, to shield the operator from UV exposure. The foam pad is intended to increase pressure on the slides, which facilitates curing of the polymer. The door rotates around the side pivots of the base.

Intended Use and Installation: This system is used in a similar manner as the commercial CryoJane system, with the same basic steps. The only significant procedural difference is that the application of UV is variable and not intrinsically regulated. This feature allows for the technician to vary the amount of UV that is applied to the sections, based on sectioning parameters. The typical UV exposure ranges from 5 to 8 seconds. For thick sections or those with a high-moisture content, it is often best to increase the UV exposure by a few seconds. The application of UV is controlled by the DC power source, which is attached to a serial rocker

switch (DPDT toggle switch) and both units are placed on top of the cryostat. The DC power unit is connected to 110V, to provide the input power. The output of the unit is wired to the PCB boards of the curing platform, via a terminal junction. The curing platform is placed inside of the cryostat, such that it is leveled and that there is enough freedom of motion for the door to open and close. The exact position of the platform in the cryostat is technician specific and empirically determined to optimize performance. For the sectioning of fresh-frozen tissue, this system can be used in an identical manner as the commercial CryoJane. For perfused-tissue, the optimized protocol described below, is best.

Preparation of Perfused Mouse Brains: Mouse brains that have been perfused and extracted from the animal, should be post-fixed in 4%paraformaldehyde (PFA) (perfusion solution) with 10% sucrose (JT Baker, 4072) for 24 hours. The tissue should be further cryo-protected in 20% sucrose in PBS for 24 hours. Thereafter, the tissue should be immediately frozen and kept at -80°C until sectioning.

The tissue should not be kept in sucrose solution longer than 48 hours. For prolonged non-frozen storage, the brains should be kept in PBS solution and should be cryo-protected as described above (without the use of PFA) when ready to freeze and section. We have found it optimal to freeze brains using the two-beaker method, as described below. We have also found it advantageous to freeze the brains using the pre-cast mold system. We have found that Neg-50 (ThermoFisher, 6506) is the preferable embedding medium for this system (and the commercial CryoJane), because it freezes to a similar hardness as tissue and allow for uniformed sectioning of the block. Use of other embedding mediums, like O.C.T, was found to result in micro-damage throughout the tissue. The morphology of the tissue was found to be intact, but when stained and examined at high-magnification (>40X), cell bodies were found to have ruptured. The use of Neg-50 resolved this problem.

Setup and Preparation: The curing platform does not require initialization but the top of the glass plate should be cleaned with ethanol at the beginning and end of each sectioning session. Adhesive tape-windows (LeicaBiosystems, 39475214) should be cut from the roll and placed into the chamber of the cryostat to acclimate. It is best to place the tape-windows onto a thermally insulating surface, which ensures that the temperature of the tape matches the chamber

temperature and not the metal base of the cryostat. One tape-window per section to be cut should be prepared. For a typical mouse brain, 500 such windows should be prepared.

Coated slides should be prepared (discussed below) but maintained at room temperature (RT). Slides should be placed into the cryostat two at a time, no more than 2 minutes before mounting of the sections is to begin. The temperature of the slides should be equal to that of the chamber temperature. If slides are kept for a prolonged period of time, the polymer will not cure properly and tissue damage will result. If slides are warm when mounting begins, sections will melt on the slide and thermal damage will result.

The specimen temperature of the cryostat should be set to -13 to -16°C and the chamber to -15 to -18°C. The cryostat should be given sufficient time to reach the set temperature. It is best to validate the temperature by using an external meter. The cryostat should also be validated against excessive frost buildup that could prevent proper airflow in the chamber. The knife of the cryostat (Thermo Scientific/Shandon MX-35, is recommended, though others of similar quality can also be used) should be replaced after trimming, and at least once per whole brain. The knife platform should be cleaned with ethanol and maintained clean throughout the sectioning. The anti-roll plate can be disengaged for the entire procedure. It can be engaged during the trimming of the block, to validate orientation of the block, relative to the knife.

Temperature and humidity in the room should be adjusted to 16-19°C and 45-60%. These conditions are vital for optimal sectioning quality. If temperature is above 20°C, the chamber temperature of the cryostat could be difficult to maintain and the sections will warm on the slide, before curing, resulting in thermal damage. If humidity is above 65%, excessive frost will begin to form in the chamber, resulting is poor airflow and thermal damage to the sections. If humidity is below 40%, then the sections will dehydrate before curing and fracture.

Sectioning Method for Perfused Tissue: An illustration and a description of the method and use of this system for sectioning perfused tissue is shown in Figure 48 and

Figure 49. Figure 48 shows an animation of the process and is helpful to understand the basic of the system.

Figure 49 shows the use of this technique in production mode.

A frozen brain block should be removed from the -80°C and placed into the chamber of the cryostat for at least 20-30 minutes, and allowed to acclimate. The block should then be mounted onto the chuck, using embedding medium and oriented (tilt and yaw adjustments) relative to the fixed position of the knife. The knife angle should be fixed at 10-12°. The section thickness should be increased to 50µm or the cryostat should be turned to the "trim" mode. The block should then be trimmed until the first sign of tissue. The section thickness should then be changed to the desired thickness, in the range of 10-100µm. All samples presented in this work, were sectioned at 20µm.

Once the desired plane of sectioning is identified, the following procedure should be applied for every set of sections to be collected: (1) Two ready-coated slides should be placed on the curing platform and allowed to acclimate for at least 2 minutes (but no more than 5 minutes). The wet-side of the slides, the side coated with the polymer, should face up. The slide label can be on either lateral side of the chamber. (2) A cooled tape-window should be gently peeled and the covering should be discarded. The tape should be maintained in the cold stream of the cryostat. The adhesive part of the window should be aligned to the blockface of the block, such that the black line on the tape, aligns with the bottom surface of the block and that the midline of the block, aligns with that of the tape. A "hard roller" should be used to smooth the tape onto the block. The blockface or the center portion of the adhesive tape, should *not* be touched with a warm body (like the fingers of the operator). (3) The bottom portion of the tape, which is labeled "THIS TAB OVER KNIFE" should be slightly raised by the technician and held with one hand, as the other is used to rotate the wheel of the cryostat and cut the section. The sectioning motion should be continuous and performed at a steady rate. For the Microm HM550, the semi-automatic advance can be used. The cut section is very susceptible to thermal damage and therefore should be maintained entirely in the cold-stream of the cryostat. The best way to do this is to move the tape-window deep into the cryostat where the temperature is most stable, away from contact with unstable ambient air.

(4) The tape should then be placed onto the slide, such that exposed surface of the section, touches the polymer coating of the slide. The tape should be oriented such that the section is in a pre-defined area of the slide. Once the tape makes contact with the slide, no further movement is possible, without damaging the section. The tape-window and the section should than be smoothed using a "soft-roller". If any air bubbles are apparent underneath the tape, they

should be removed by the rolling motion. The hard-roller should not be used for this purpose, because it can crush the section and cause macro-damage to the morphology. The sections can be placed on the slides in any order or any orientation. To maximize the number of sections that can be placed on a slide, it is best to align the long edge of the tape-window, with the short side of the slide and place the first tape-window closest to the edge of the slide. This is the edge opposite the slide label area. Subsequent tape-windows should be placed relative to this. Slight overlap between the tape-windows is preferable to prevent direct contact between the roller and slide, as long as the sections do not overlap. Steps (1)-(4) should be repeated for a maximum of three tape windows, for a standard 1X3" slide (with a usable region of 1X2.25").

(5) Once each tape segment is smoothed with the soft roller, the lever door of the platform should be lowered and light pressure should be applied to the top surface to press the door down. The rocker switch connected to the DC power supply should be activated. Activation of the UV light should be apparent through the vents of the base. The UV should be applied for 6-8 seconds and then the power switch should be deactivated and the UV should shutoff. The lever door should be raised. Each slide should then be removed from the platform and moved further into the cryostat, into the cold stream. Starting with the tape-window that is closest to the slide label area, the tape should be peeled at approximately a 45°. The peeling motion should be smooth and performed at a steady rate. This peeling should be repeated for all tape windows of both slides. (6) Once the tape is peeled, the slides can be removed from the cryostat and returned to RT. It is best to allow the slides to dry for several hours before staining.

When standardized, the above procedure can be optimized to the rate of 1 slide per minute. This rate is comparable to conventional sectioning, but with the added benefit of reduced section damage. The critical parts of the above procedure can be summarized as follows: (2) The temperature of the specimen should be maintained at -13-16°C and the chamber temperature at -15 to -18°C. These values are relative to RT, which should be maintained at 16-19°C. The humidity of the room should also be carefully maintained at 45-60%; (2) The use of a hard roller to smooth the tape-window onto the blockface, and the use soft roller to smooth the tape-window onto slides. The two should not be interchanged. (3) Once a section is cut from the block, it is very sensitive to temperature changes and thus should always be maintained in the cold stream of the cryostat - it should never be brought close to the exposed area or taken out of the cryostat. (4) Pre-sectioning, slides should be allowed to acclimate for approximately 2 minutes(but no more

than 5 minutes).For serial sectioning, slides can be placed into the cryostat to begin acclimating, while sections are being mounted on other slides.

Slide Preparation: This system is compatible with two types of slides: (1) Pre-coated slides, as purchased from Leica Corporation (Model 39475208) and (2) Those that are self-coated by the operator using polymer solution provided by Leica (Model 39475272). Both methods result in similar sectioning quality. Pre-coated slides are easier to use and advantageous for low-volume sectioning. Coating slides using Solution-B (Model 39475272) is an additional processing step and thus undesirable, but is significantly more cost effective for high-throughput applications. In the case of pre-coated slides, the preparation entails simply removing the protective film from the slide and then the slides can be placed in the cryostat and used for sectioning. In the case of self-coated slides, the process entails two steps: (1) Cleaning the slides with Solution A (Leica Microsystems, 39475270); (2) The cleaned slides need to be coated with the UV-polymer in sets of two, by applying 55µl of Solution-B using a pipette onto the middle surface of one slide and then spreading the solution by placing another slide on top of it. The two slides should than be pulled in opposite directions, resulting in two evenly coated slides that can be placed in the cryostat and used for sectioning.

Two-Beaker Freezing Procedure: To adequately freeze the brains in the embedding medium, without thermally damaging the tissue or cracking the block, we freeze using isopentane, which is chilled by dry-ice. The process involves the use of two beakers, one placed inside of the other. The large beaker (VWR, D10898666) has a volume of 1500 mL; the smaller beaker (VWR, 13977-042) has a volume of 250 mL. Either glass or metal beakers can be used; although metal is preferred due to its superior thermal conductivity (McMaster, 4352T3). Dry ice is crushed to small chunks (¼ - ½ in diameter) and placed inside of just the large beaker, such that surface area contact with the smaller beaker is maximized and air gaps are minimized. Isopentane (Sigma-Aldrich, M32631-4L) is slowly poured into the smaller beaker. After a few minutes of acclimatization, additional solution is added to the beaker to account for rapid evaporation at the initial pour. Once the surface of the solution is calm (minimal bubbling), a few pellets of dry ice are added to the bottom of the smaller beaker. The isopentane solution should be at a temperature of approximately -60°C. A base mold with embedding medium and tissue can then be placed

inside of the isopentane, such that the lip of the base mold is at the surface of the solution. The base mold should not be submerged into the isopentane, until it has frozen. Freezing should occur at a uniform rate from the five sides of the base that are in contact with the isopentane. A standard block that is 32x25x12 mm in size, should freeze in approximately 3 minutes. Thermal gradients in the isopentane are possible, and can lead to macro deformation of the brain. To minimize these, the amount of dry ice around the smaller beaker, should be approximately the same on all sides and on the bottom of the beaker.

Nissl Staining: The sectioned material was allowed to dry overnight at 4°C and was then stained for Nissl bodies, using a thionin based protocol and coverslipped using DPX. The staining and coverslipping was performed in a Sakura Tissue-Tek Prisma & Glas g2. The Nissl protocol was as follows: 1.5 minutes in 0.25% Thionin Solution, two minutes in two solutions of deionized water, five minutes in three grades of ethanol (50%, 75%, 90%), five minutes in two solutions of absolute ethanol, and 5 minutes in two solutions of xylene. Once coverslipped, the slides were manually examined to ensure proper coverage of the mounting medium and allowed to dry overnight at room temperature.

Histochemical and Immunohistochemical Staining: Tape-transfer sectioned material was used for a wide range of staining methods to validate compatibility and compare to conventional sectioning methods. Slides were allowed to dry overnight at 4°C prior to staining. Staining was performed either using the LabVision 720 (Thermo Scientific) or manually using sealed staining trays (EMS, 71397-B). The staining protocol was reagent specific and followed published conventions. For staining comparisons with other sectioning methods (free-floating and conventional on-slide sectioning) an effort was made to use the same protocol for all conditions, as to prevent bias. Free-floating sections were stained in 12-well plates, with inserts; all other sections were stained on-slide.

Biotinylated Dextran Amine (BDA) Detection: The detection of injected BDA entailed: (1) 2X wash in PBS; (2) Incubation in 1% Triton X-100 (Fisher, AC21568) in PBS. (3) Incubation in ABC (Vecastain Elite ABC Kit, Vector Labs, PK-6100) for 18 hours. The solution was prepared per manufacturers protocol of 2 drops of Solution A and 2 drops of solution B, per 5 ml of

buffer; (4) DAB reaction for 5-10minutes. Working solution of0.05% Cobalt Chloride (Sigma, 255599); 0.05% Ammonium Nickel Sulfate Hexahydrate (Sigma, A1827); 0.05% DAB (Sigma, D8001) and fresh 0.0015% Hydrogen Peroxide (Sigma, 2167632); (5) 3X wash in PBS. The slides were then allowed to dry overnight at 4°C and then were counterstained (below) and coverslipped with DPX.

Lectin (WFA), Tyrosine Hydroxylase (TH) and DAPI Staining: The staining protocol for WFA, TH and DAPI entailed: (1) 2X wash in PBS; (2) Incubation in protein block solution: 5% Normal Goat Serum (NRS) (Vector Labs,S-1000), 1% Triton X-100 (Fisher, AC21568), in PBS for 30 minutes; (3) Incubation in primary antibody solution: 5% NGS, 0.3% Triton X-100, 1:500 Lectin, Wisteria (Sigma, L1516) 1:500 Rabbit Anti-TH (Millipore, AB152), for 24 hours; (4) 3X wash in PBS; (5) Incubation in secondary antibody solution: 5% NRS, 0.3% Triton, 1:500 Goat Anti-Rabbit, AF488 (Invitrogen, A11008), 1:500 Streptavadin (Invitrogen, S-32355), for 4 hours; (6) 3X wash in PBS. A select group of slides were counterstained with DAPI. The slides were then allowed to dry overnight at 4°C and coverslipped with Fluoromount-G (EMS, 17984-25).

Myelin Staining: Myelinated fibers were labeled through a silver staining technique, following the protocol published by Gallyas[85]. Empirical adjustments were made to concentrations and incubation times, to produce adequate staining.

Imaging: Imaging of the all data shown in this work, was performed using a NanoZoomer HT system, at a resolution of 0.5µm/pixel. For fluorescence, a standard tri-filter cube (DAPI-FITC-Texas Red filter) was used. All data was uncompressed.

Animals: All animals for this testing were acquired from Jackson Laboratories. The animals were 56±3day old mice, C57BL/6, with a weight of 18.8 – 26.4 grams. The animals were treated per IACUC approved protocols. The animals were perfused with 4%paraformaldehyde (PFA)(JT Baker, JTS898-7) through the heart. Avertine (2.5%) was used as the anesthetic. A saline preflush of 50 mL was used to remove the blood from the circuit, prior to addition of 4% PFA (50 mL). For tracer injection studies, 10% BDA 10,000 MW(Invitrogen, D-1956) at a volume of

15nl, and Adeno-Associated Virus (AAV) at a volume of 5nl were injected into different animals. For AAV, two types: AAV2/1.CB7.CI.EGFP.WPRE.RBG and AAV2/1.CAG.tdTomato.WPRE.SV40, were injected into a single animal. All injections were performed in a dedicated surgical area, inside of an animal facility. A survival period of 1 week was used for BDA and 4 weeks for AAV.

Power Testing: Irradiance measurements were performed using a PM100 Optical Power Meter, with a S121B sensor and an NE01A filter (ThorLabs Corporation).

Results:

Tile images for a mouse brain sectioned in the coronal plane are shown in Figure 50. Similar tile images for brains that were sectioned in the sagittal and horizontal planes, are shown in the supplementary material (Figure 58 and Figure 59). The figures show the thumbnail view of the cut brain sections. We define "a section" as a piece of tissue that was cut from the brain block by adhering a tape-window to the block. Tissue that was intentionally trimmed from the block, is not considered a usable section. Sections that were damaged beyond scanning or those that appear deformed due to imaging artifacts, are not shown in the tile figure. These sections are *all* classified as "damaged" and are included in the numbers below and in Table 9. A total of 570 sections were mounted for the two coronal brains. Of these, 2% of sections are considered totally-damaged and were removed from the tile image; and additional 10% of the sections were structurally sound, but had other forms of damage. The complete damage report for the shown coronal brain and the two sectioned in the sagittal and horizontal planes, is shown in Table 9. The labels in this figure were expanded to show detailed categorization of the damage. In total, 85-90% of all mounted sections are undamaged due to sectioning artifacts. These figures are significantly lower than is common with conventional cryostat sectioning and represent improvement in methodology.

As shown in Figure 51, morphology of the tissue is preserved with this sectioning method, as evident even at high-magnification. No cellular damage is evident in any part of the section. The method also does not hinder Nissl staining or differentiation of cortical layers. One of the principle advantages of the tape-transfer method is that disjoined parts of the brain do not separate during sectioning. This is best seen in the anterior coronal sections, lateral sagittal

sections and ventral horizontal sections, as shown in Figure 52. The mounted sections are a direct representation of what is seen in the blockface, without distortions that are commonly associated by slide mounting.

We have validated and extensively tested that this sectioning method is compatible with downstream staining of the tissue. We performed three different comparisons between this sectioning method, free-floating and conventional direct on-slide sectioning. The first brain was used to validate that the morphology of the tissue was not altered by the tape-transfer method, by staining the sections for Nissl-bodies. The results are shown in Figure 53. No difference in morphology or tissue quality is seen between the three methods. At higher-magnification, individual cortical layers and cell bodies can be seen. The differentiation of the stain, varies across the three conditions, but does not show any biological or morphological differences. Based on this data, it can be said that the tape-transfer produced sections are equivalent to those produced by other sectioning methods, in terms of morphology.

The second brain was injected with AAV into the cortex and then processed to determine if the tape-transfer method resulted in any degradation of the native tissue fluorescence. The results are shown in Figure 54. Two bilateral injections in green and two in red were made into this animal. The green signal is the most prominent in these sections. The red signal is used to show that there is no loss of fluorescence in the fine fibers. No significant difference in intensity between the three methods is seen. There is a slight difference of regional intensity, across the three sections, but this can be attributed to the position of the section relative to the injection site. The absolute intensity level is not as important as the intensity of each fluorophore relative to the background and the ability to use this data to quantify the location of the labeled cells. Based on this data, it can be said that the tape-transfer method does not degrade the native fluorescence of the tissue, affect the intensity or the ability to localize an injected fluorescence tracer. We have also tested this sectioning method with Cholera Toxin Subunit B, conjugated to Alex 488, 555 and 594, with similar results. This data are not shown.

The third brain was injected with BDA into the cortex and processed to determine if the tape-method hindered HC staining. The results are shown in Figure 55. Tape-transfer produced sections have an signal-to-noise ratio that is equivalent to that of free-floating sections. Cell bodies and fibers can clearly be seen in both case conditions. No cellular or tissue distortion is evident. The cell bodies are filled, indicating a complete HC reaction. The label is "black", and

the background is low, indicating that the DAB reaction was complete and did not expose the signal. To show that the compatibility between tape-transfer sectioning and HC staining was not limited to the detection of injected BDA, we have stained for various other biomarkers. In Figure 56 shows the results of c-Fos, Lectin (WFA), Tyrosine Hydroxylase (TH), DAPI and myelin staining. In all cases, the label is of high-quality and can be used quantitative and qualitative analysis.

Besides mouse, we have also validated that this system can be used with other rodent species. Nissl stained, coronal sections, of a perfused rat brain, are shown in Figure 56 (F-G). We have also experimented with the use of the tape-transfer method to simultaneously section tissue without removing the surrounding bone. Figure 57(A) shows a coronal section of a mouse brain, from a 56-day old C57BL/6, with an intact skull. Figure 57 (B) shows sagittal sections of a spinal cord, with the surrounding cervical vertebrae. Tape-transfer sectioning is ideal for this type of material, because it requires only a mild decalcification of the bone (if any). In the case of the spinal cord processing, no decalcification was performed. The mouse skull was decalcified in 0.1 M ethylene diamine tetra-acetic acid (EDTA) for 2 hours (approximately 1/10th the suggested time[86]). The two common problems with sectioning bone and tissue together, is that: (1) the hard bone causes deformation in the soft tissue, as the section is cut from the block; (2) the decalcification process effects the chemical integrity of the tissue and limits downstream staining. Both problems are reduced with the use of tape-transfer sectioning, because the adhesive tape secures and maintains the position of both the bone and the tissue during sectioning, which reduces the needed for decalcification and minimize tissue damage during sectioning.

Discussion:

In this work, we present a redesign of the tape-transfer system and use this system for high-throughput processing of perfused mouse tissue. The redesigned system, allows for the application of higher-UV irradiance in a shorter amount of time, without an extensive pulse-to-pulse wait. The system is also more robust than the commercial variant. With an operating life of 1000 hours and an average application time of 10 seconds, a single LED can be used to cure more than 360,000 slides. The higher irradiance power of this system, combined with optimization of the sectioning methodology, allows for the high-throughput sectioning of

perfused mouse tissue. We have used this system to serially section in a mouse brain in the coronal, sagittal and horizontal planes. As shown in Table 9, on average less than 15% of all collected, 20µm sections are damaged. We definite a damaged section as any section that was intended to be collect and having cosmetic or structural defect. Sections that were intentionally trimmed from the block (<5-10 on average) are not included. The majority of the damaged sections are classified as "torn" or have "missing areas" - this is due to a partial transfer of the section onto the tape or onto the slide. With the exception of knife-damaged sections (<2%), which tends to occur in series, the rest of the damaged sections are not consecutive.

In our testing of free-floating and conventional on-slide cryostat sectioning, the tape-transfer system offers about a 10X reduction in the number of damaged sections. These figures are difficult to directly compare to published results, because such figures are not commonly published. Therefore, we compare to the Allen Reference Atlas, which shows 25µm sections, at a spacing of 100µm (1:4). Out of the 132 sections that comprise the coronal atlas, we count that 16 are damaged (12%). We speculate that the same percentage applies to the sections that are not shown. If the coronal brain shown in Figure 50, was also selected at a frequency of 1:4, with loose spacing, as in the ARA, meaning that some sections would be spaced at 75 or 125µm, instead of 100um, the percentage of damaged sections would be reduced by an order of magnitude, to around 1-2%.

In terms of sectioning rate, a single block can be sectioned at the rate of 100-150 sections for hour, depending on the skill of the operator. A single mouse brain can be sectioned at 20µm, in the coronal plane, in 4-6 hours. When used in conjunction with the pre-cast mold system, a single block can contain two brains, and thus the sectioning rate is reduced to 2-3 hours per brain. This rate is on the same order of magnitude as conventional sectioning.

To show that the tape-transfer method does not hinder downstream staining of the sections, we collected serial sections with three cryostat sectioning methods: free-floating, direct on-slide and tape-transfer. The results showed no significant effects of the tape-transfer method on nissl staining of the sections, the native fluorescence of an injected tracer, or the histochemical detection of injected BDA. In the case of the fluorescence experiment, as shown in Figure 54, an interesting observation is that the tape-transfer system does not result in a reflection of the sections around the mid-plane. The surface of the section that is mounted on the slide, is the distal surface; the surface that is exposed and contacts the mounting

medium+coverglass is the proximal surface, when viewed relative to the blockface. Since the tape secures the position of the sections during cutting, they are transferred onto the block, exactly as they appear on the blockface. No out-of-plane rotation is possible. The advantage of this is that the left and right hemispheres can be identified, throughout the brain, without the need of fixing a marker (often a punch hole) to the sections. This is also advantageous when there is a needed to follow consecutive sections or to account for cells that might be split between two serial sections.

In terms of histochemical and immunohistochemical staining, we have found that the tape-transfer system does not hinder staining. We have not seen evidence of a residue on the surface of the sections, caused by the tape, or any other negative effects of the system on downstream staining. However, this system requires all staining to be performed on-the-slide, which is more challenging that the staining of free-floating sections. The applied volume of each reagent, needs to be monitored to ensure that it covers all of the sections evenly and that the sections do not dry during a long incubation. Since the incubation period for most IHC and HC reactions can be several hours, if not 24+hours, the sections must be maintained in a humid environment, on a leveled surface. If the surface is not leveled, the applied solution will not remain on the slide for the duration of the incubation. These problems are common to all on-slide staining. We address these problems through the use of staining dishes, which are filled with water and sealed to minimized evaporation. We optimized the amount of volume required per section to 100-150µl, which is on the same order as that of free-floating staining. We have also used these sections for automated histochemical processing, using the Labvision720. After adding humidity control to the unit and individual slide leveling, we were able to effectively perform long incubations on-the-slide, using this unit.

One of the advantages of the tape-transfer system for on-the-slide staining, is that the sections are able to withstand higher mechanical agitation that those collected using conventional cryostat sectioning. Since the sections are adhered by the cured polymer, the adhesion force is higher than conventional mounting, which relies on passive adhesion between the slide and the section. This increase in adhesion helps to preserve the integrity of the sections during solution changes and when staining with volatile or corrosive chemicals, like those required for myelin silver staining. We have also found that for counterstaining of HC/IHC processed material with Giemsa, this increase in adhesion, greatly reduces the number of lost sections.

We have predominantly used this system to section mouse brains, in high-throughput, but as shown in Figure 57 , this system can also be adapted for other applications. In both presented cases, the advantage of sectioning the tissue without removing the surrounding bone, is reduced damage to the tissue. Even in the case of mouse brains, which are easier to extract than spinal cord, damage to the brain caused by the rongeurs, forceps or scissors, is very common. The other advantage of sectioning the whole brain, with skull, is reduced macro deformation of the brain, due to freezing. In the case of the spinal cord, the advantage is that the difficult extraction process is avoided and that multiple blocked vertebrate can be sectioned simultaneously. Since the tape secures the position of the blockface, the disjoined tissue segments do not separate or distort during cutting.

Our view is that this technique is most appropriate for the following applications: (1) high-throughput processing of many brains, where the objective is to perform quantitative analysis across the brains. This relates to projects such as the Allen Mouse Brain Atlas, the Mouse Brain Architecture project and similar brain-wide endeavors; (2) where the objective is to section tissue areas that are disjointed and there is a needed to digitally reconstruct the sections into a 3-D volume; (3) where the operator is not a trained histologist, such as students, and there is a needed to collect serial sections or maintain a low failure rate; (4) where the objective is to simultaneously section tissue and the surrounding bone.

Figures:

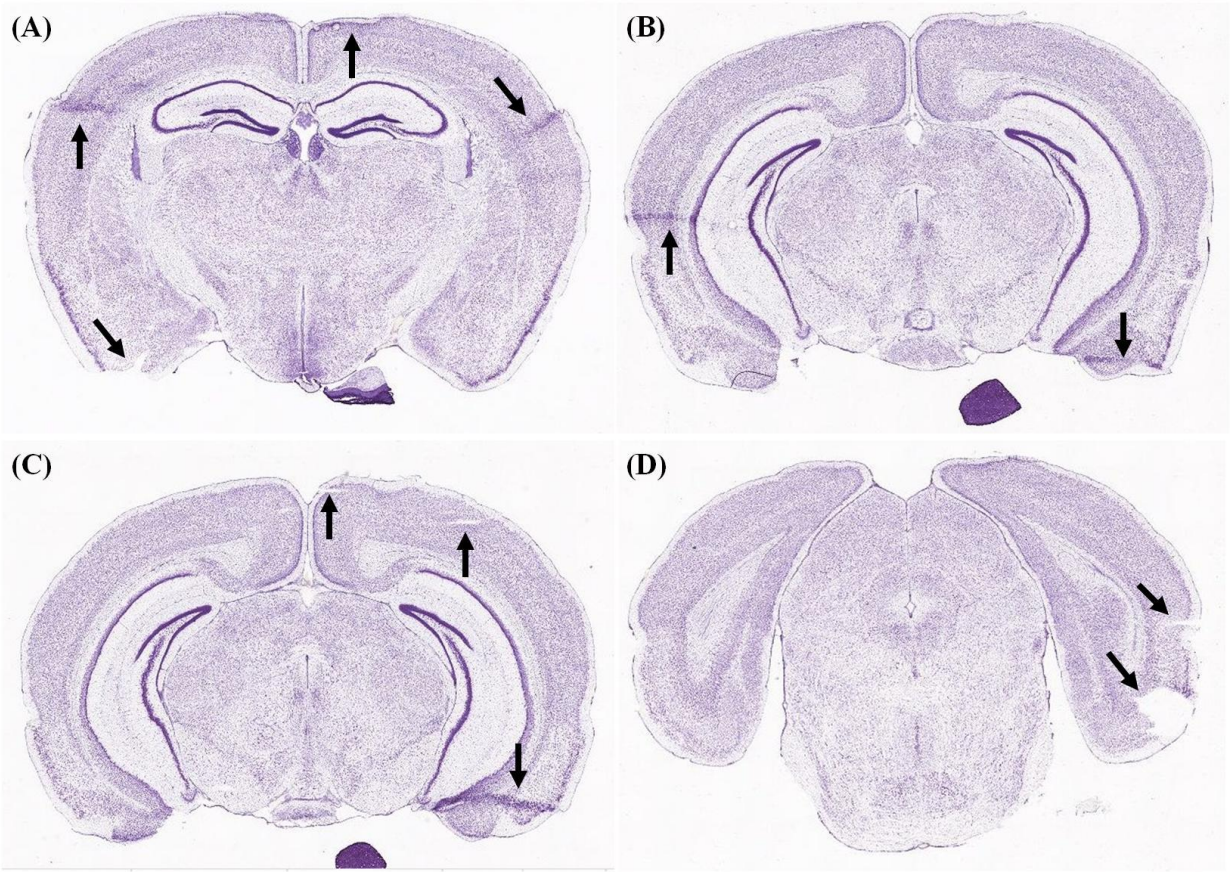

Figure 45: Section damage in the Allen Reference Atlas
Obtaining undamaged cryostat sectioned material is difficult, especially for relatively thin sections (20-25µm). This problem is even evident in the Allen Reference Atlas, which is one of the most commonly used anatomical references of the mouse. The black arrows point to the damage in the sections. The three most common sources of damage are: folded sections areas, as seen in A and B; torn sections, as seen in C and sections with missing areas, as seen in D. Allen Reference Atlas, coronal Level 73 is shown in (A); level 83 is shown in (B); level 84 is shown in (C); and level 96 is shown in (D).

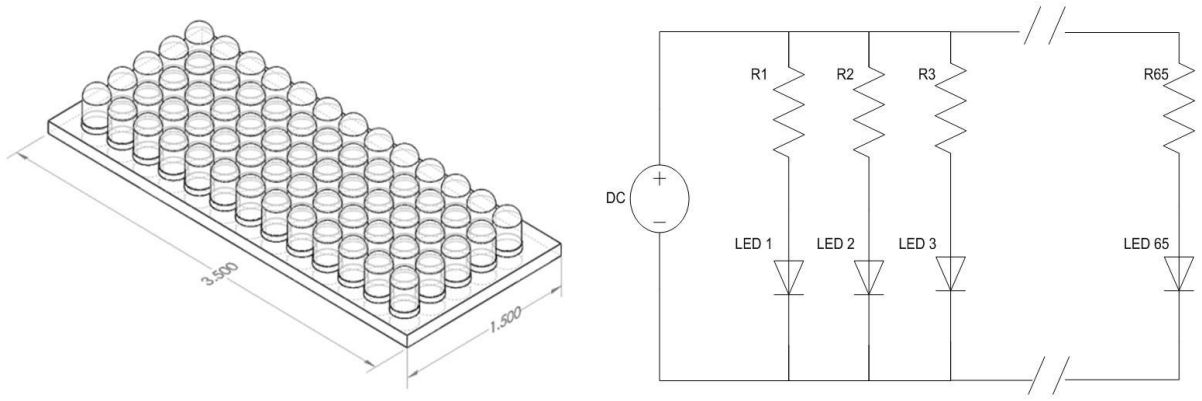

Figure 46: UV-LED array and electrical schematic

The UV-LED array that is used as the principle means of curing the cut sections onto the glass slides is shown on the left. The array is composed of 65 LEDs (Nichia Corporation, NSPU510CS). The LEDs are soldered onto a four-layer, pre-wired, printed-circuit board (PCB) (Sunstone Corporation). Each array is a single unit, with a common ground and power leads. The schematic of the array is shown on the right. Serial resistors (R_1...R_{65}), which are common in most such arrays, were not included, because the UV-LEDs are not overly sensitive to erroneous current pulses.

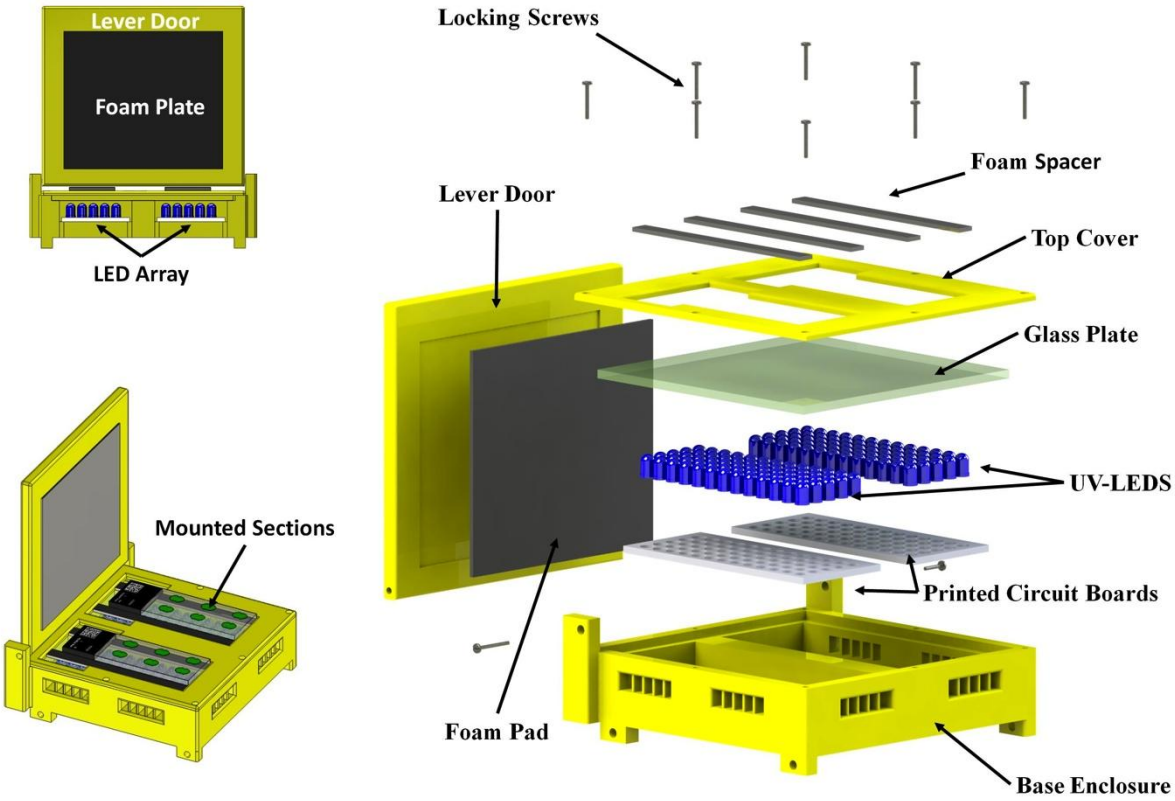

Figure 47: An exploded-view of the redesigned tape-transfer system curing platform
The platform is composed of 7 principle parts: the base enclosure; the printed circuit board with soldered LEDs; a glass plate, a top cover; foam spacers, a foam pad, and a lever door. With the exception of the PCB, the glass plate, the foam spacers and pad, all other components were designed in entirely Solidworks and fabricated using polyjet technology in Vero-White. The fixture is easy to assemble and is secured using machine screws. The base enclosure has side access, to connect the ground and power terminals of the UV-LEDs. The shown enclosure, allows for sections to be collected on two slides simultaneously, as shown on the bottom left. A front view of the platform is shown on the top left. When lowered, the lever door and foam pad are intended to shield the operator from the applied UV and to apply mild pressure onto the slides, which facilitates the curing process.

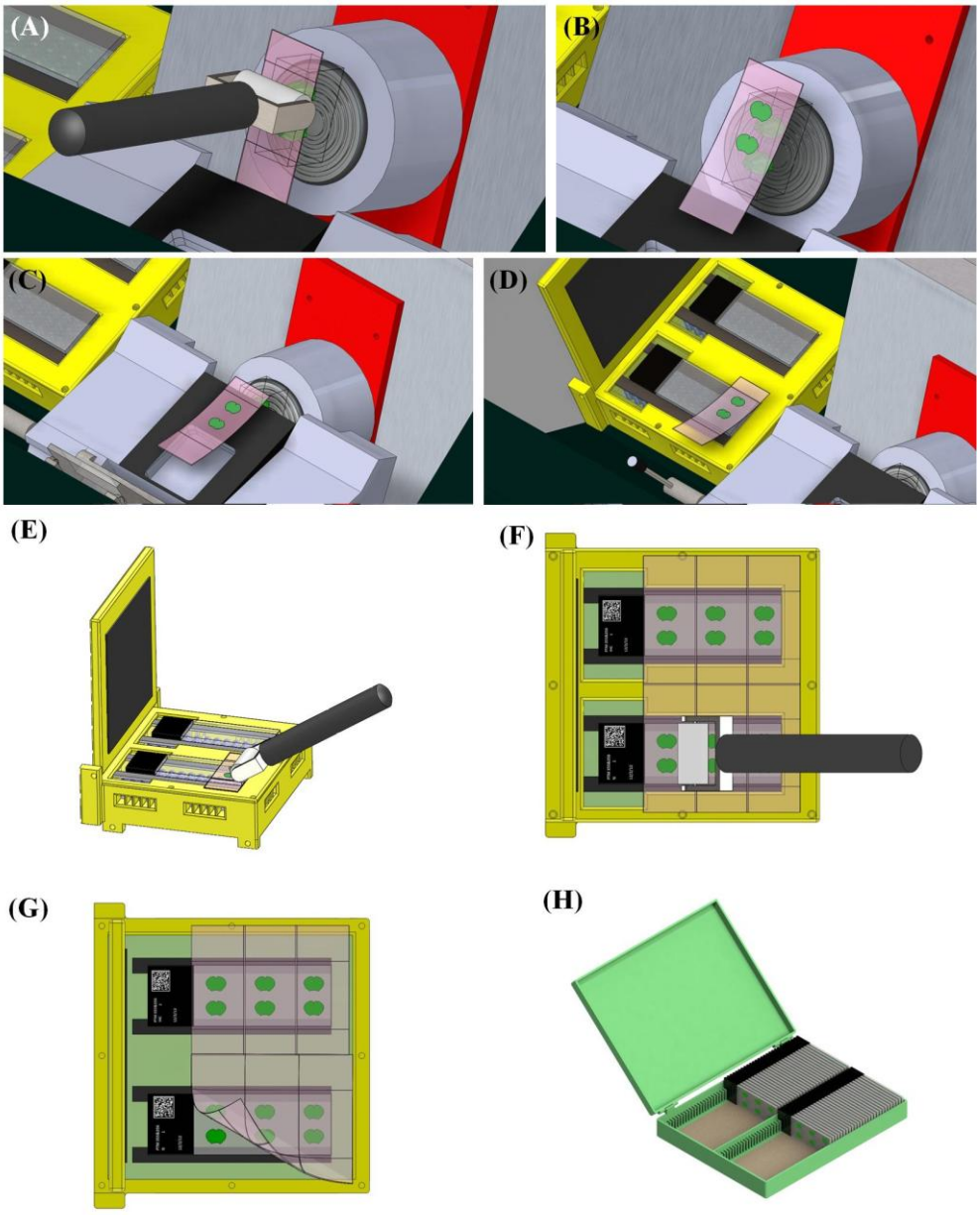

Figure 48: Animated workflow of the tape-transfer system
The tape-transfer method consists of several key steps, which are animated in this figure to provide clarity and full view of the process. Not shown, are the steps of mounting the frozen block on the chuck of the cryostat; trimming the block until the first sign of tissue; removing the protective film from the tape window. The animated brain block is clear, but the frozen brains are shown in green. (A) The first critical step in the process is adhering the exposed tape-window onto the blockface. Only the center region of the tape should contact the block. The bottom tab, which is not adhesive, should be below the bottom of the block. A hard-roller should be used to press the tape onto the block and ensure even adhesion. (B) The block should be sectioned in a single continuous motion. The tape should be supported by the operator, as it is sectioned, such that the tape does not make contact with the knife block. (D) Once sectioned, the tape+section should be moved onto a coated slide (through the cold stream of the cryostat). (E) A soft roller should be used to gently smooth the sections onto the slide. (F) This process should be repeated for all sections. A total of three tape windows can be placed per slide. Once all are adhered, the UV should be applied and the polymer will cure. (G) the tape windows can then be safely peeled from the sections. (H) The slides can then be removed from the cryostat and placed into a slide box, to be stained, coverslipped and imaged.

Figure 49: Production use of the tape-transfer system to section perfused mouse brains
This figure shows the use of this system to collect coronal sections of a perfused mouse brain. (A) The frozen brain block should be removed from -80°C and allowed to acclimated in the cryostat for at least 20-30minutes. The block should then be mounted onto the chuck, such that the surface to be sectioned is pointing up. (B) the block should then be mounted onto the cryostat and trimmed (C). Adjustments to the pitch and yaw, should be made to align the chuck with the knife. (D) The block should be trimmed until the first sign of tissue, as indicated by the white arrow. (E) A tape window, which has been previously maintained in the cryostat to acclimate, should be peeled. Only the center portion of the window should be peeled. (F) The tape should be placed over the blockface, such that the black line is directly below the block. A hard roller should be used to adhere the tape to the block. (G) The block should be sectioned in a single continuous motion. The tape window should be supported during cutting, as not to allow the tape to adhered to the knife block. (H) Once sectioned, the tape window + section, should be moved into the cold stream of the cryostat, away from the open surface, as not to allow the tape to warm. (I) The tape window should be placed onto the slide, and the soft roller should be used to ensure proper adhesion. (J-K) The process should be repeated until three tape-windows are placed per slide. (L) The lever door should be closed and the UV should be activated. Reflections of the UV can be seen in the metal surface of the cryostat and through the open vents. (M) Once the polymer is cured, the slide can be removed from the chamber, and the tape-windows can be safely peeled. (N) The slides can then be removed from the cryostat and used for staining, coverslipping and imaging.

Figure 50: Thumbnails of coronal serial sections, produced using the tape-transfer system

The block was sectioned anterior (top-left) to posterior (bottom-right). The sections were Nissl stained. We define "a section" as a piece of tissue that was cut from the brain block by adhering a tape-window to the block. Tissue that was intentionally trimmed from the block, is not considered a usable section. Sections that were damaged beyond scanning or those that appear deformed due to imaging artifacts, are not shown in the figure. The shown sections have not undergone registration or any other post-processing. A detailed analysis of the sections is shown in Table 9.

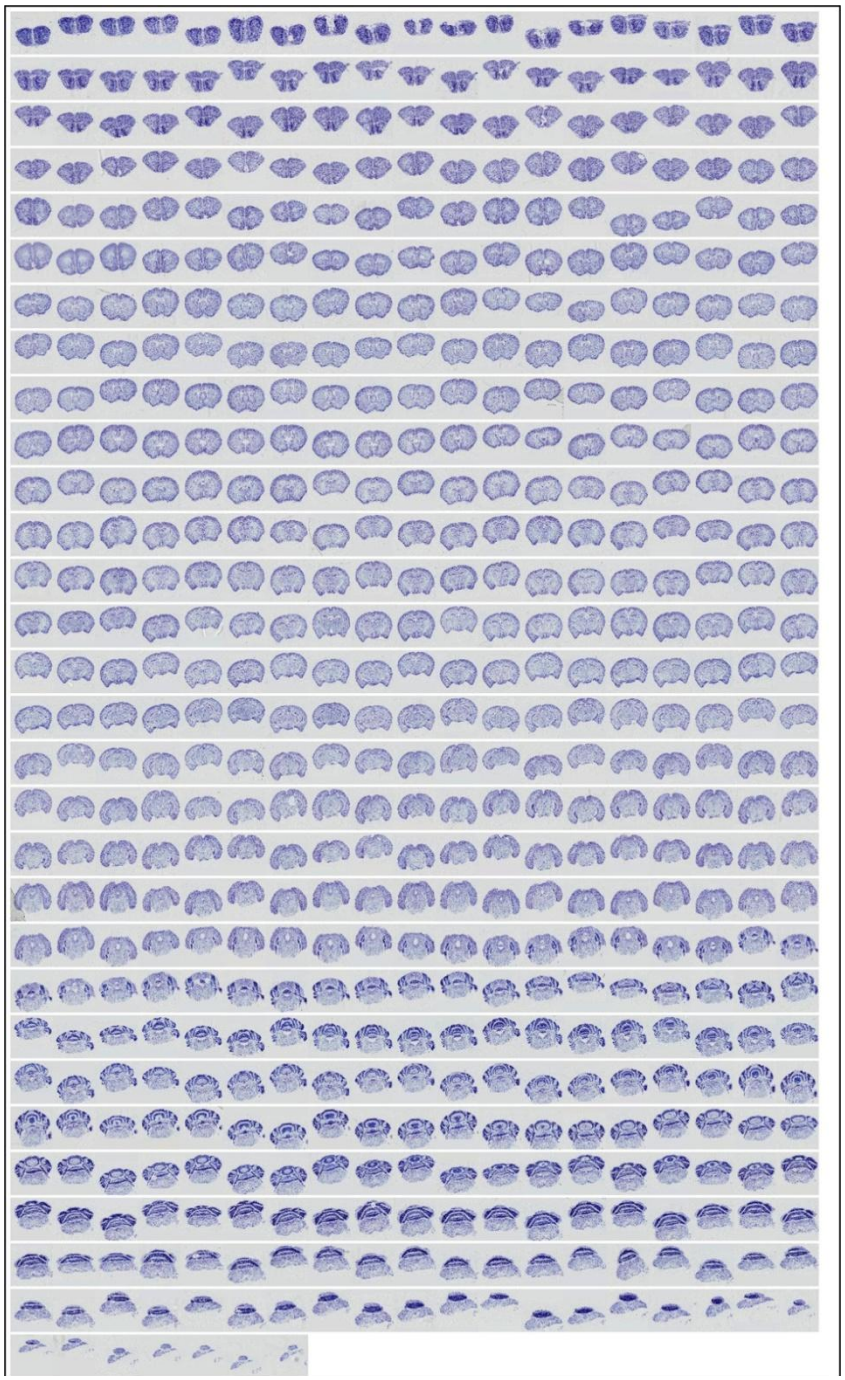

Damage Type	Coronally Sectioned Brain	Sagittally Sectioned Brain	Horizontally Sectioned Brain	Coronal ARA	Sagittal ARA
Torn Sections	23	27	36	7	0
Folded Sections	0	0	1	7	2
Missing Tissue Areas	23	3	0	2	1
Knife Damage	15	5	5	0	0
Mechanical Cellular Damage	0	0	0	0	0
Thermal Damage (Cortical)	4	10	2	0	0
Thermal Damage (Sub-Cortical)	1	0	0	0	0
Tissue Cracking	0	0	0	0	0
Entire Section Missing	0	0	1	0	0
Imaging Artifacts	0	10	0	0	0
Total Number of Damage Sections	66	55	45	16	3
Total Number of Mounted Sections	570	387	300	132	20
Total Percentage of Damage	**12%**	**14%**	**15%**	**12%**	**15%**

Table 9: Categorized damage table for Tape-Transfer sectioned material and that of the Allen Reference Atlas

The above table shows a breakdown of the sections that are considered damaged, for the brains that were sectioned in the coronal, sagittal and horizontal planes, using the tape-transfer system. The same criteria is used to evaluate the coronal and sagittal brains of the Allen Reference Atlas. Most of the categories are self-explanatory. Those that are not, we define as such: "Knife Damage" refers to torn sections that display a periodic "window blind" like pattern, that is parallel to the knife; "Imaging Artifacts" refer to the digitization of the sections. Sections that are out-of-focus, cropped incorrectly, or show foreign contaminants, are grouped into this category. Unlike other sources of damage, these sections can usually be recovered through re-imaging. "Entire Section Missing" refers to instances where the section was intended to be collected, but does not appear imaged. For the Allen Reference Atlas brains, only the sections shown in the atlas have been evaluated. For the coronal brain, these represent ¼ of the collected 25µm sections (100µm spacing).

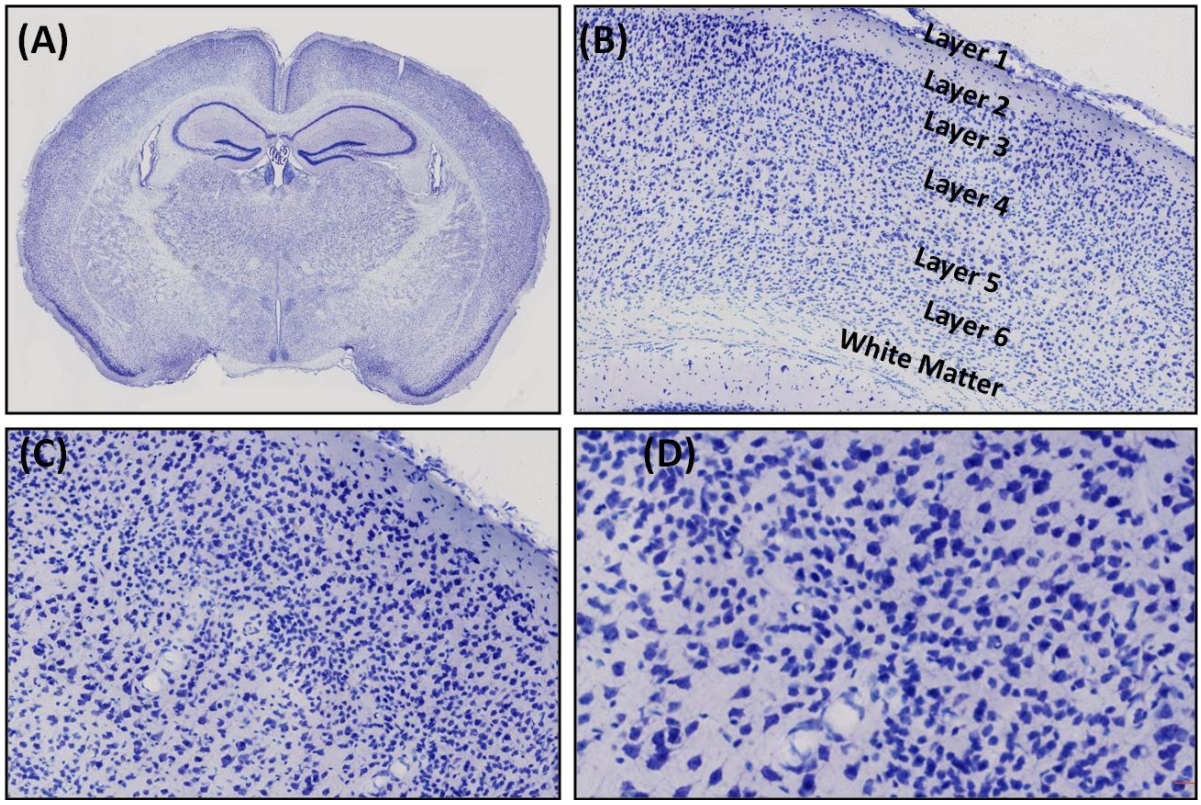

Figure 51: A nissl section of a coronally sectioned brain is shown with increasing magnification
The macro morphology of the Nissl stained section, is seen in (A). The section appears structurally intact, with no obvious signs of damage. At medium-magnification of the cortex, the cortical layers and the white matter can be differentiated from nissl stain. At higher magnification (C and D) the cell bodies are seen. No cellular damage is evident.

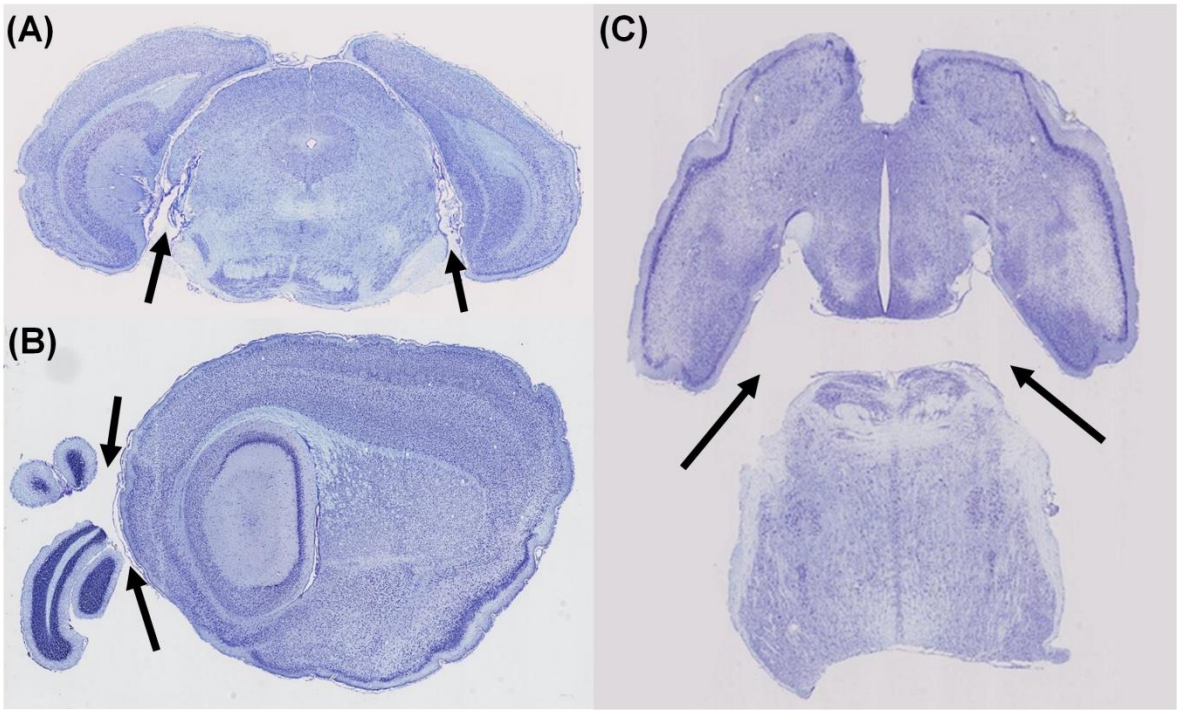

Figure 52: Tape-transfer cut sections are congruent to the blockface
One of the principle advantages of the tape-transfer method is that disjointed tissue in the frozen block, do not separate during sectioning. The position of the cut sections is secured by the tape, which makes the resulting sections a direct representation of the blockface. This is best seen in coronal (A) and sagittal planes (B), where the cortex is separate from the rest of the section. A similar separate is seen in the horizontal plane, shown in (C). The black arrows point to the separation between the tissue entities.

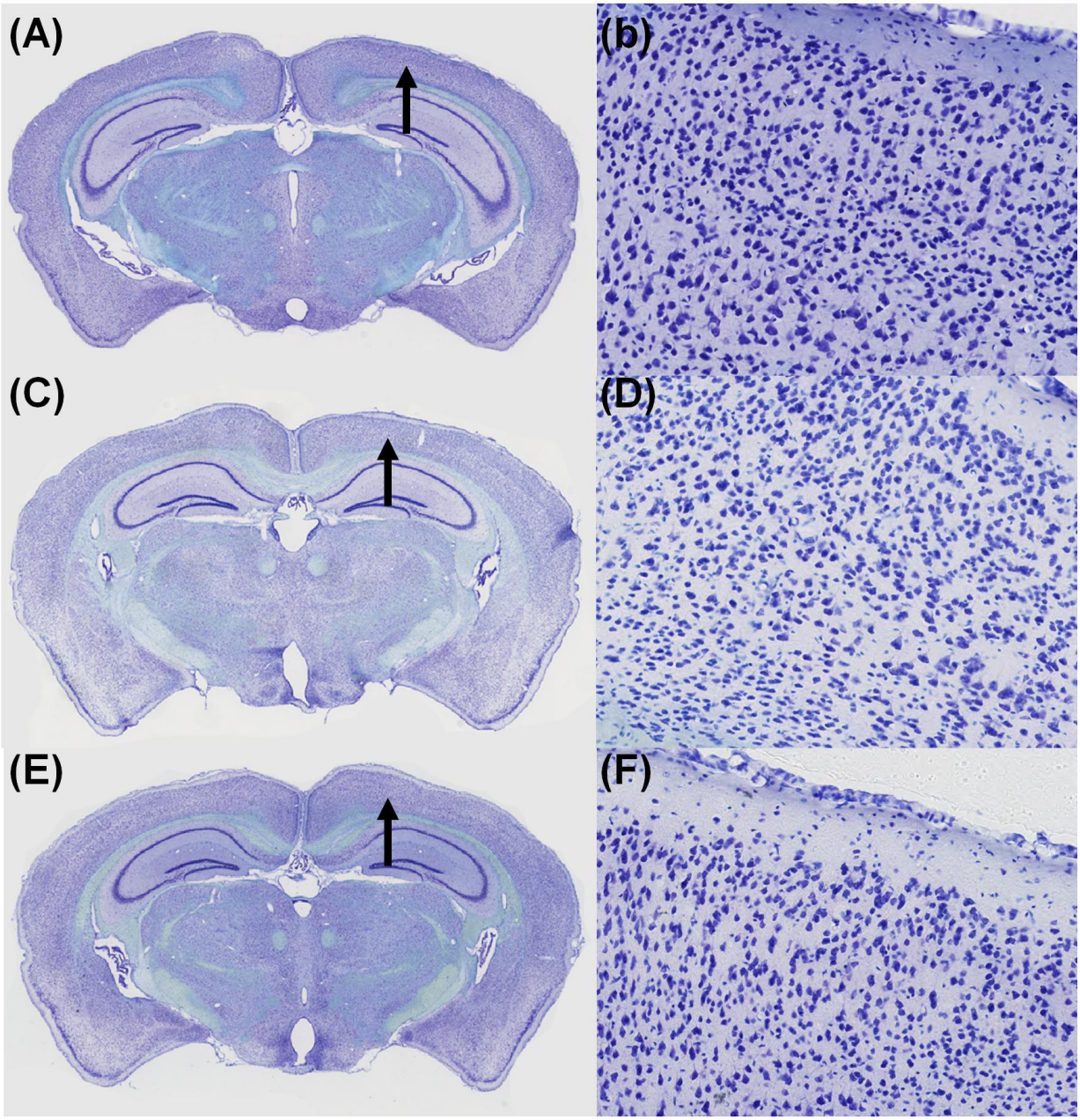

Figure 53: Compatibility of tape-transfer and Nissl staining
Coronal sections of a perfused mouse brain are shown. Serial sections were collected using three methods: free-floating, shown in A and B; direct on-slide mounting, shown in C and D; and using the tape-transfer system, shown in E and F. All sections were Nissl stained, using the same protocol. Though the relative intensity and differentiation varies for the sections, due to the lack of stain optimization, no other significant differences are evident. The tape-transfer produced sections can equivalent to those of conventional sectioning, in terms of nissl staining. The black arrows point to the regions that are shown at higher-magnification, to the right of each section.

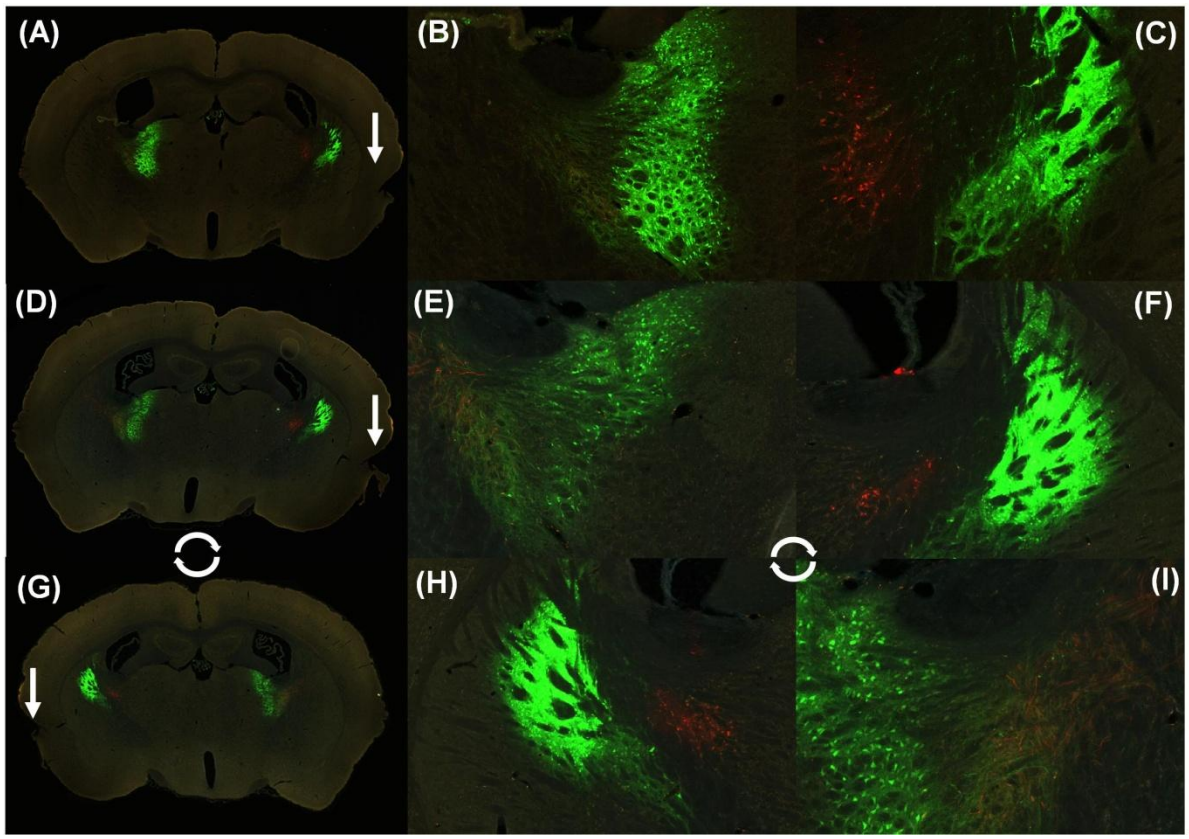

Figure 54: Compatibility of tape-transfer and the detection of injection AAV
Coronal sections of a perfused mouse brain, that was injected with AAV-green and AAV-red are shown. Multiple injections of each tracer was performed to maximize the amount of signal in the sectioned material. Serial sections were collected using three methods: free-floating, shown in A-C; direct on-the-slide mounting, shown in D-F; and using the tape-transfer system, shown in G and I. All sections were coverslipped with DPX and imaged, using the same parameters. No major difference in fluorescence intensity is evident, for either the green or red AAV. The free-floating (A-C) and direct on-the-slide (D-F) sections appear in the same orientation. This occurred by chance, free-floating sections can be mounted in any orientation. This orientation is a mirror image of the blockface. Tape-transfer collected sections, are in the same coordinate system as the blockface. The white circular arrows are used to indicate that a rotation around the vertical should be applied to properly compare the sections. (E) and (B) should be compared to (I); (C) and (F) should be compared to (H). The white arrows point to a source of macro damage that that is common to all sections and is used to verify the alignment.

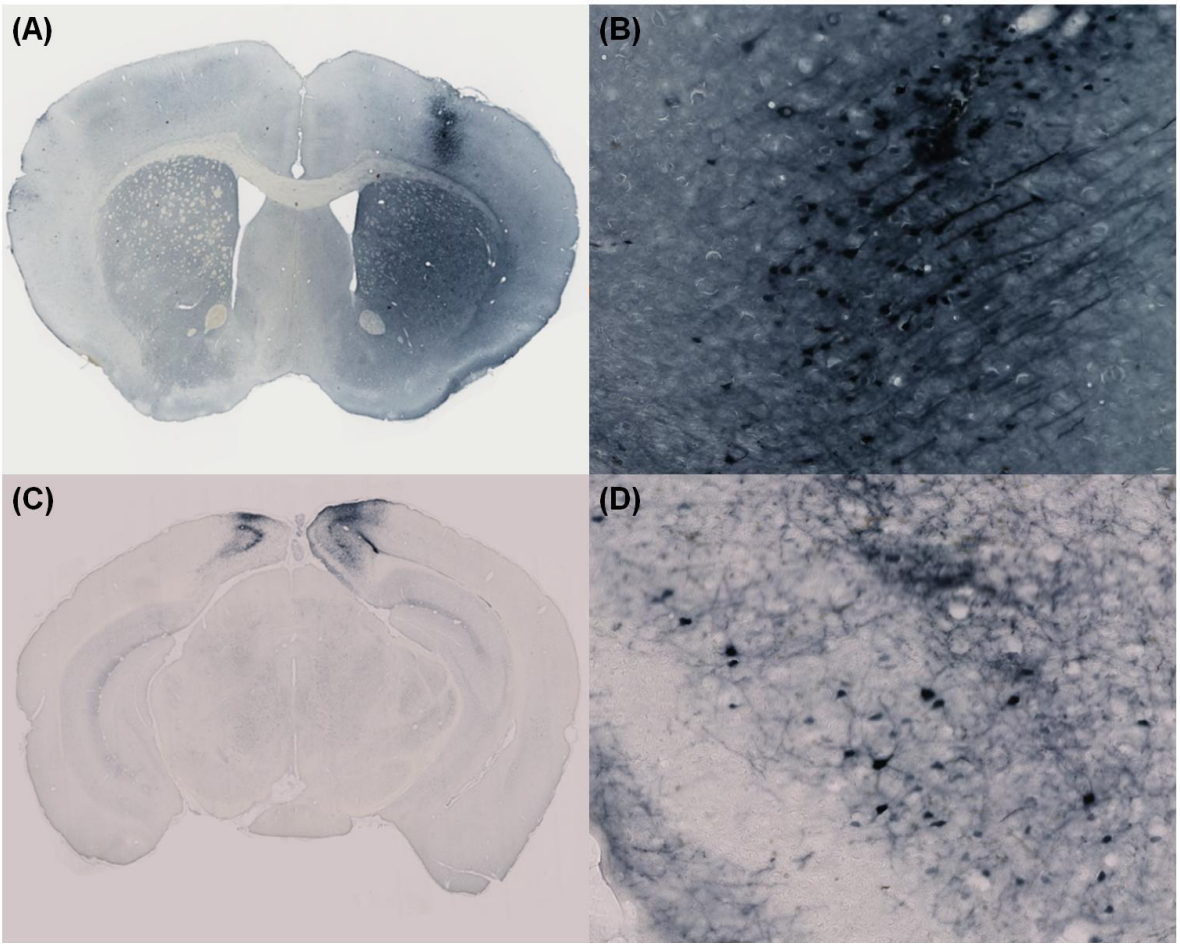

Figure 55: Compatibility of tape-transfer and the detection of injection BDA
Coronal sections of a perfused mouse brain, that was injected with BDA into the cortex is shown. (A and B) were collected as free-floating sections; (C and D) were collected using tape-transfer sectioning. Both sections were stained in a similar manner. The results show that the tape-transfer system does not hinder histochemical detection of injected BDA. Tape-transfer sections need to be stained on-the-slide, which is logistically more challenging to perform than the staining of free-floating sections, but the quality is comparable. Note: this figure is a placeholder, it will be replaced by a more thorough comparison of the three sectioning methods, when data is available.

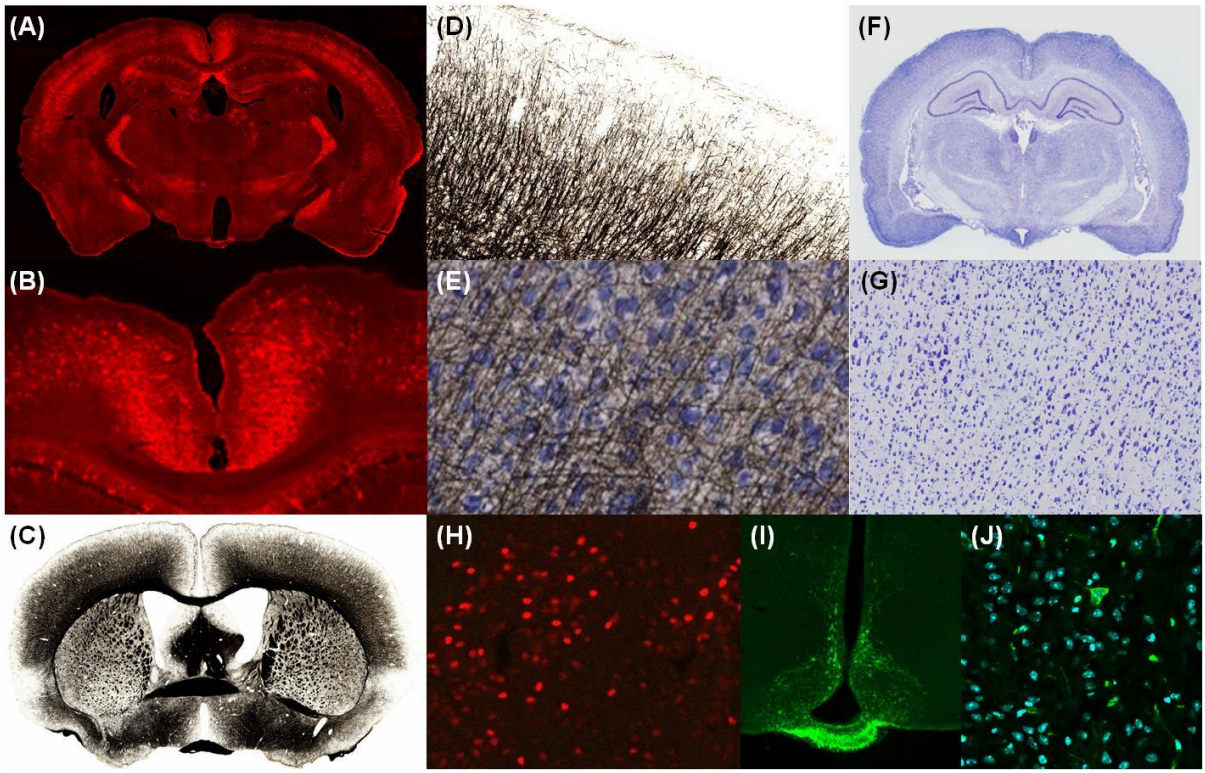

Figure 56: Compatibility of tape-transfer with Lectin, Tyrosine Hydroxylase, DAPI, c-Fos, myelin staining, confocal microscopy and other rodent species

To verify the compatibility of tape-transfer produced sections with immunohistochemical and histochemical staining, we stained for Lectin (WFA), shown in (A) and (B); myelinated fibers, using Gallyas silver stain technique, shown in (C)-(E); c-Fos, shown in (H); Tyrosine Hydroxylase (TH), shown in (I). We have also counterstained the TH material with DAPI and imaged using confocal microscope, to verify the staining, as shown in (J). In all cases, the stain was of high-quality. In (E), a myelin section, counterstained with nissl, is shown. Myelinated fibers and cell bodies can be seen. Aside from mouse, we have also tested this technique with perfused rat tissue, as shown in (F) and (G). The results are similar to that of mouse.

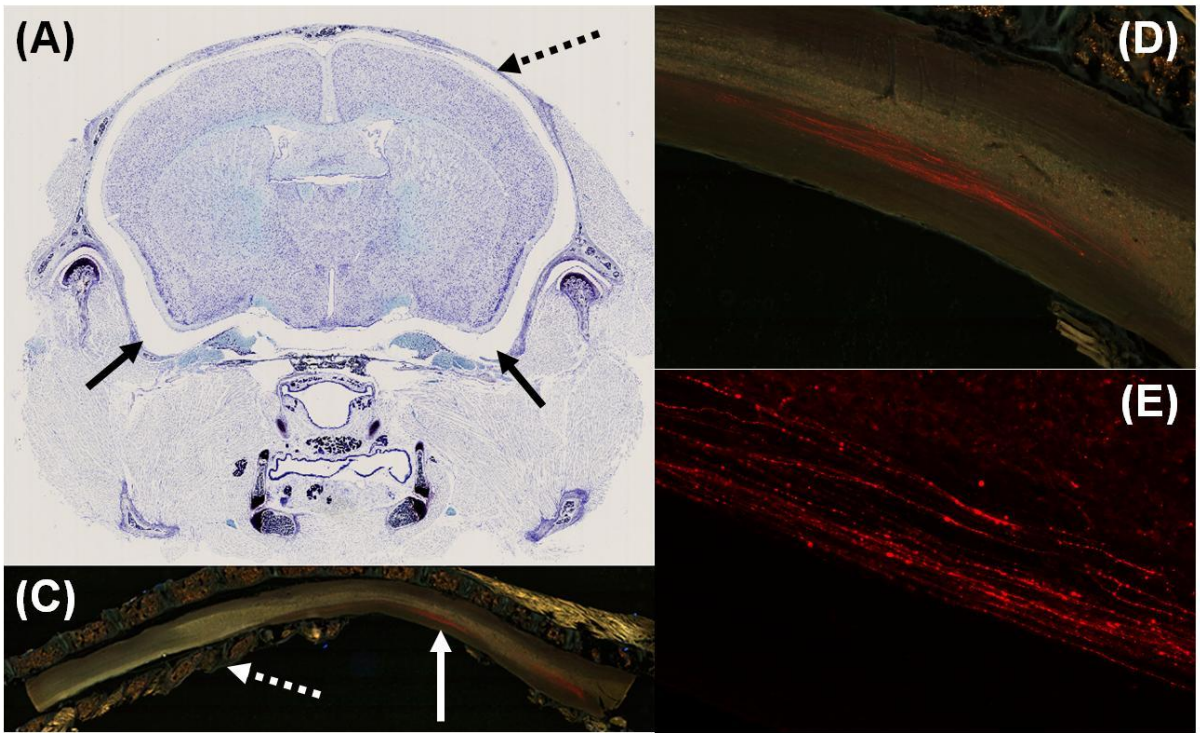

Figure 57: Auxiliary applications of the tape-transfer system to simultaneously section bone and tissue
A perfused mouse brain, with an intact skull, sectioned in the coronal plane, is shown in (A). Post-extraction the skull was briefly decalcified in EDTA. The black arrows point to the gap between the brain and the surrounding bone, to show that the brain did not deform during sectioning. The dotted black arrow points to the dorsal surface of the skull. In (C) a sagittal section of a spinal cord is shown. Cervical vertebrae are at the right and the left leads into the thoracic vertebrae. This spinal cord was extracted from a mouse that was injected with AAV (red) into the cortex. The white arrow points to the label that is shown at higher-magnification in (D) and (E). The dotted white arrow points to the intact vertebrate. The spinal cord was not decalcified. In (E), just the red channel is shown.

Supplementary Figures:

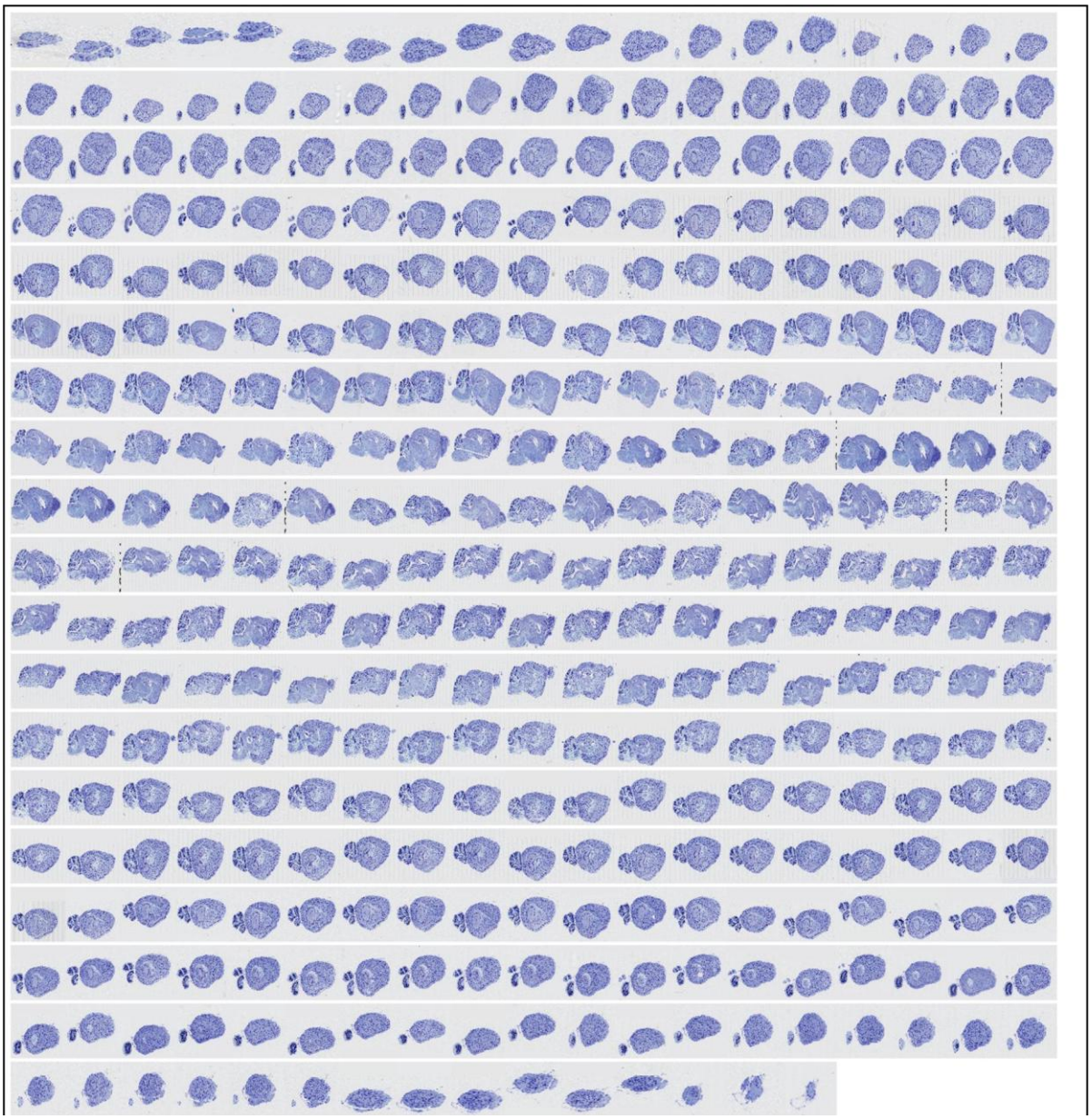

Figure 58: Thumbnails of sagittal serial sections, produced using the tape-transfer system
The sections were Nissl stained. We define "a section" as a piece of tissue that was cut from the brain block by adhering a tape-window to the block. Tissue that was intentionally trimmed from the block, is not considered a usable section. Sections that were damaged beyond scanning or those that appear deformed due to imaging artifacts (cropping artifacts), are not shown in the figure. The shown sections have not undergone registration or any other post-processing. A detailed analysis of the sections is shown in Table 9.

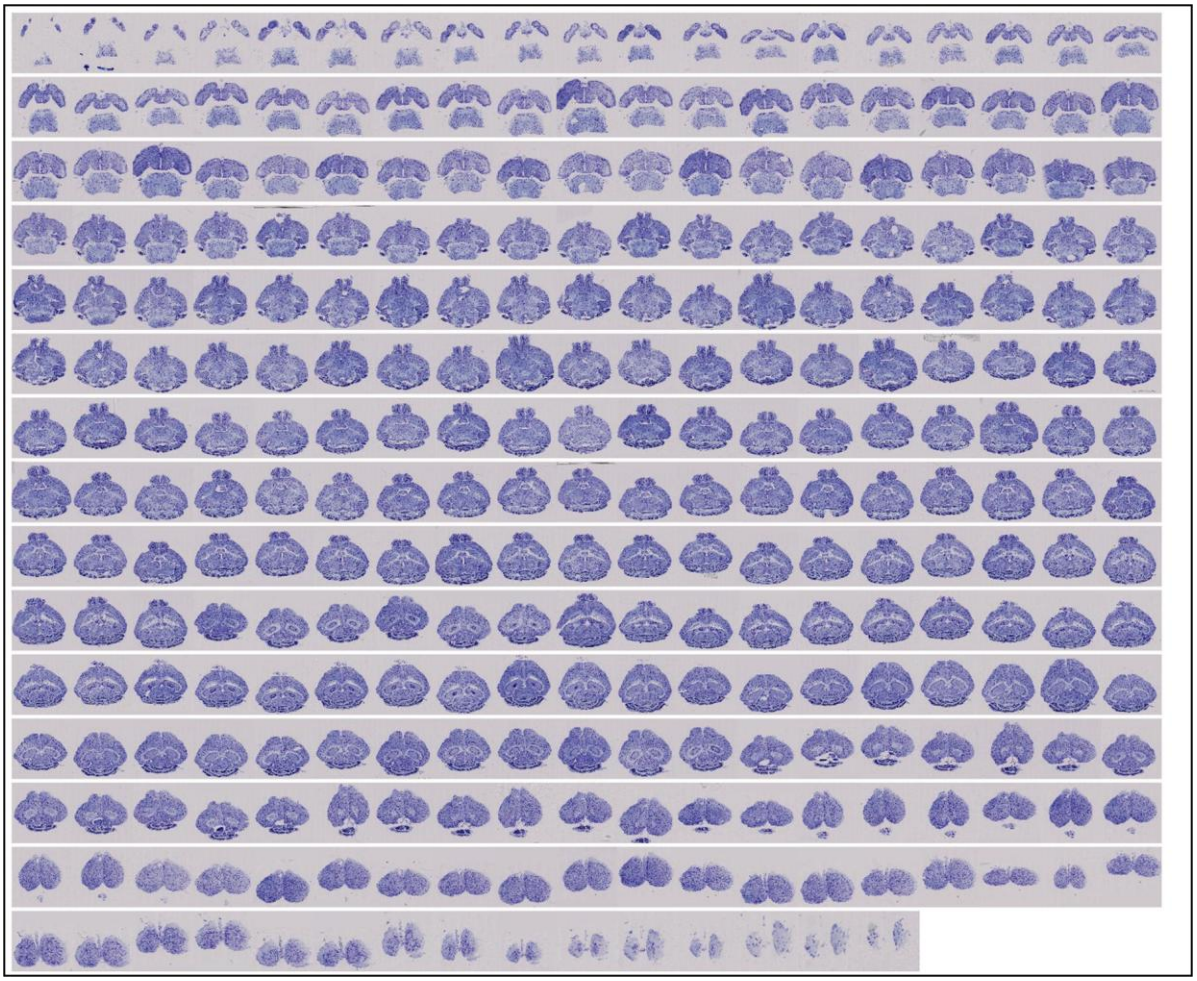

Figure 59: Thumbnails of horizontal serial sections, produced using the tape-transfer system
The block was sectioned ventral (top-left) to dorsal (bottom-right). The sections were Nissl stained. We define "a section" as a piece of tissue that was cut from the brain block by adhering a tape-window to the block. Tissue that was intentionally trimmed from the block, is not considered a usable section. Sections that were damaged beyond scanning or those that appear deformed due to imaging artifacts (cropping artifacts), are not shown in the figure. The shown sections have not undergone registration or any other post-processing. A detailed analysis of the sections is shown in Table 9.

CHAPTER 5: TUTORIAL OF PIPELINE GENERATED MATERIAL

Significance: This chapter is intended to showcase the neuroanatomical data generated as part of this dissertation work. Earlier chapters focus heavily on method development. This chapter shows the culmination of that work. The majority of the data are shown as it currently appears on the project website: www.mouse.brainarchitecture.org. This website is the public repository of the data produced by this pipeline, for the Mouse Brain Architecture project. The tutorial shows sample data for only a handful of brains, with the intent for highlighting the quality, the diversity and the extent of the material generated by the pipeline. Some of the data is similar to that shown in Chapters 3-4, but is formatted in the context of neuroanatomy, rather than method development.

Contribution: I assembled this tutorial for the purpose of this dissertation and to be posted on the project website as a reference document. All presented data was obtained using the methodology discussed in this dissertation work. The analysis of the data was formed in consultation with Dr. Kathleen Rockland.

Mouse Brain Architecture Data Tutorial

Project Data Portal:

The main public data repository for the MBA project is accessible at: http://mouse.brainarchitecture.org/seriesbrowser/. This data portal, lists all of the brains that have been processed as part of this project. The data can be sorted by either the injection region (ARA nomenclature), the injection coordinates (ARA coordinate system) or the tracer type. The user can access the corresponding images for each dataset, by selecting "Section Gallery", which is a link to a Djatoka based image viewer[87]. This image viewer was customized to allow for optimal viewing of this type of neuroanatomical data. The main features of the viewer are: (1) A film strip that shows all images of the brain, referenced to the ARA coordinate system. For coronal sections, the data are arranged anterior (left) to posterior (right); (2) For each selected 2-D image, ability to zoom and pan through the image; (3) Color scales adjustable for each channel, in the range of 0 - 4096 for fluorescent data (12-bit data) and 0 - 255 for brightfield data; (4) Injection metadata and links to relevant material, provided in the Info tab; (5) Ability to access corresponding Nissl-stained sections for each dataset from the Info tab. A screenshot of the viewer is show in the Figure below.

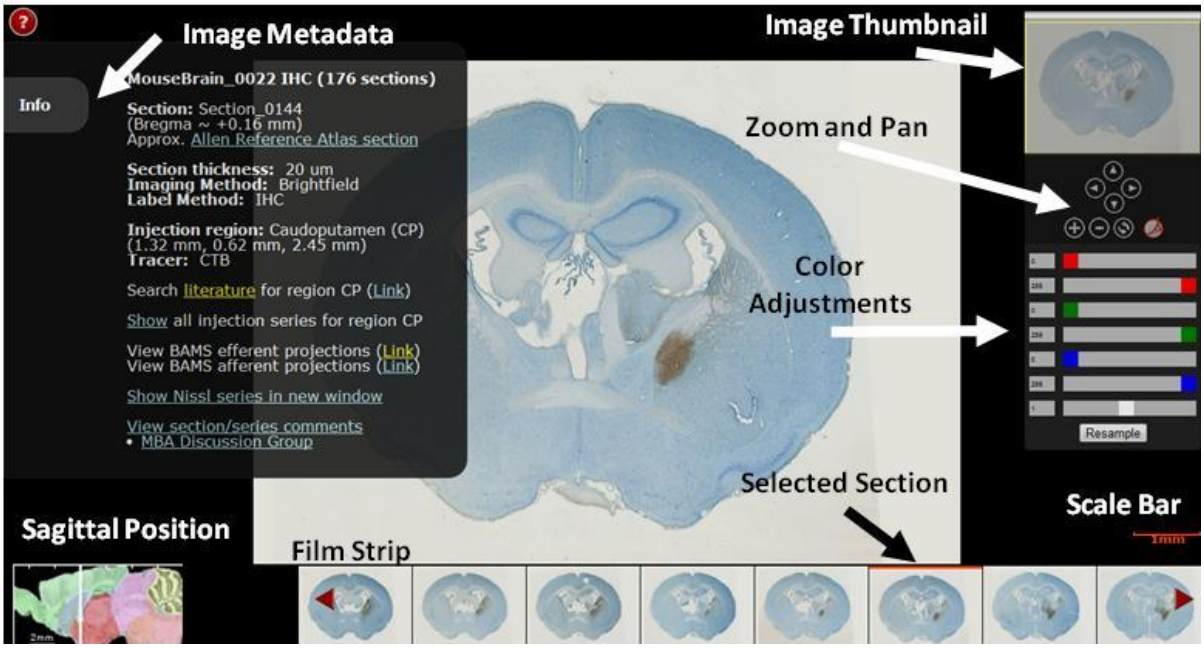

Figure 60: Annotated features of the portal data viewer.
Data for a Cholera Toxin (CTB) injected brain are shown.

In subsequent sections of this Chapter, data from this viewer are supplemented with additional views to present the full picture of the pipeline data. Primary project data are grouped by tracer type: Cholera Toxin subunit B (CTB); Biotinylated Dextran Amines (BDA);Retrograde Rabies Virus; Adeno-Associated Virus (AAV). Auxiliary data are also show, grouped by stain type. The intent with these images is to highlight the quality of the data, the resolution of the images, the diversity of the data and the sheer volume of data that is being made available to the user. One of

the main attributes of this project is the digitization of consecutive sections, throughout all brains. This allows an unprecedented access to the data for a remote user.

Primary Data:

Nissl

The default processing schema for this project calls for alternative Nissl-stained sections to be collected for each sectioned brain (as described in the MBA Technical Whitepaper). These Nissl data are intended to provide regional context for the injection data. These sections can also be used to facilitate the registration of the data onto the Allen Reference Atlas (ARA). To the right, Figure 61, is a tile view of all of the corresponding Nissl images of one brain. Below, Figure 62, is a detailed view of a midbrain coronal section.

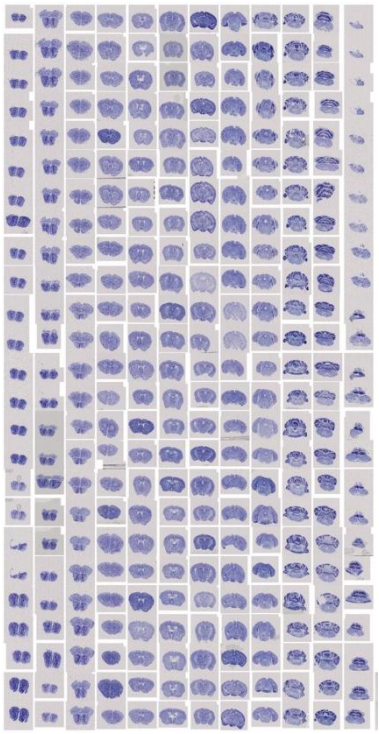

Figure 61: Tile View of all Nissl-stained sections of one Brain.

Figure 62: Portal View of a Nissl-stained section

As for all MBA data, the Nissl images are acquired at a resolution of .5µm/pixel and are posted on the portal in their entirety. No static downsample is applied to the data, but lossy compression with a factor of 10% is applied to minimize the footprint of the data. This allows the user to view the data in low-magnification, as in Figure 62, but also to increase magnification and zoom to select regions of interest (ROIs). As shown in Figure 63, the portal viewer allows for stepwise increase in magnification. A total of 6 magnification levels are possible. At the highest magnification, individual cells are clearly identifiable and the level of resolution and staining is equivalent to that of the Allen Reference Atlas (http://mouse.brain-map.org/experiment/thumbnails/100048576?image_type=atlas).

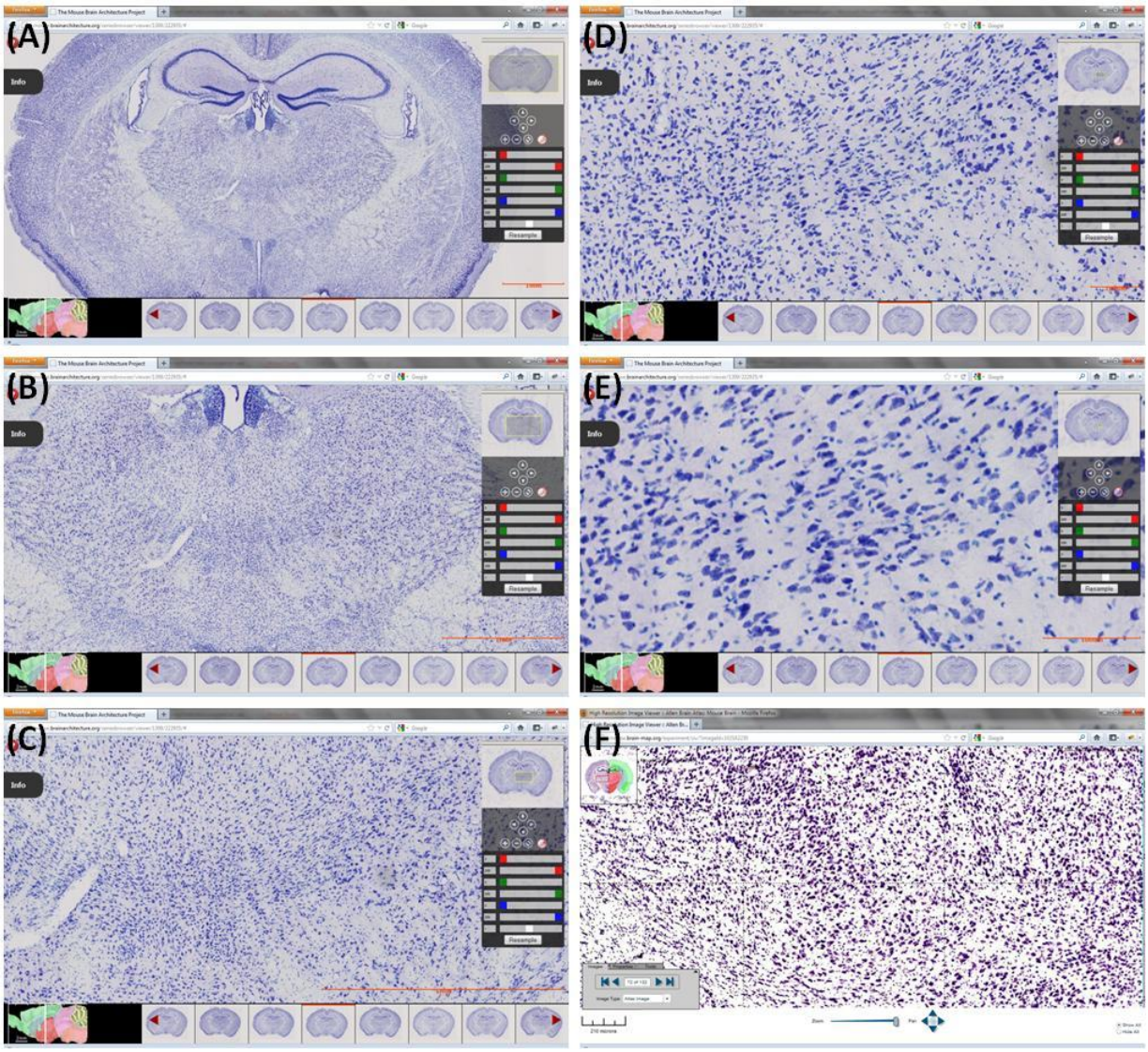

Figure 63: Nissl section at increasing magnification
Increasingly zoomed levels of a Nissl-stained section, from 2-6 (where 6=highest magnification) are shown in (A) through (E). Zoom level 1, macro view of the section, is shown as Figure 2. At the highest magnification, the MBA pipeline data are equivalent to that of the Allen Reference Atlas, shown as (F).

In terms of staining quality, one of the measures of a good Nissl stain is the ability to distinguish cortical layers. As shown in Figure 64(A), this can easily be done with a typical Nissl-stained section, produced by the MBA pipeline. The differentiation of the Nissl stain varies throughout the posted brains, in terms of shading. Ideally, the area identified as Layer 1 should have a white or off-white color; but as shown in Figure 64(A), the color of this region can be darker than optimal. This is not a major problem, as the layers are well differentiated and most Nissl based analysis can be performed. Part of the issue is illumination and whole-slide imaging. As shown in Figure 64(B), the color of Layer1 can be optimized through manipulation of the color channels, without sacrificing other stain related data.

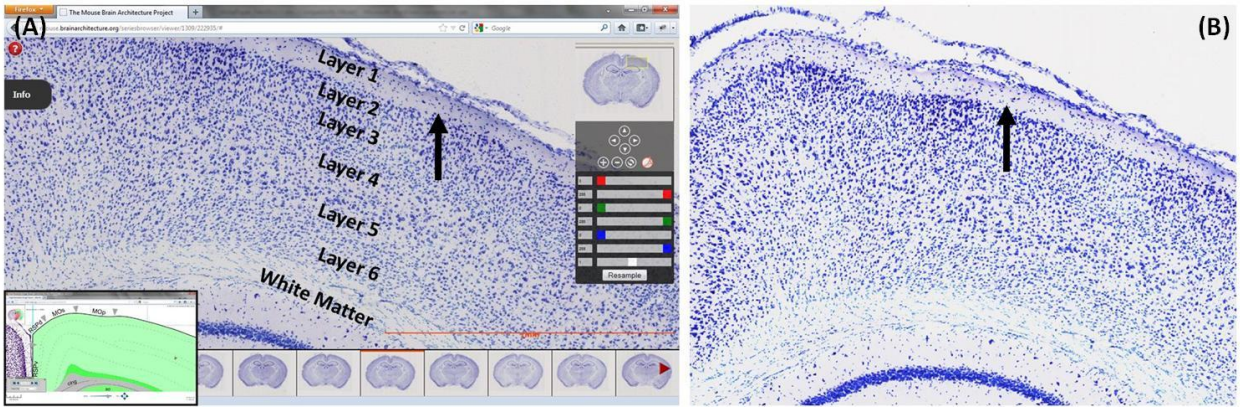

Figure 64: Cortical layer differentiation of a Nissl stained section
(A) Cortical layers are labeled on a MBA pipeline generated Nissl section. The insert on the bottom left, shows the corresponding plate from the Allen Reference Atlas. (B) Contrast and brightness are adjusted to enhance the view of the section and highlight the off-white color of Layer 1. Arrows point to Layer 1.

Giemsa Counterstain

All IHC and HC material processed through the pipeline was counterstained with Giemsa. Giemsa labels neuronal cell bodies and results in a "Nissl like" stain[72]. The differentiation, especially for the cortex, is inferior to that of a Nissl stain. Giemsa should not be considered a replacement for a Nissl stain, but rather a complement. As a counterstain, Giemsa is preferable to Nissl or similar stains because it does not degrade the signal-to-noise ratio of the IHC/HC reaction product. As shown in Figure 65, the Giemsa counterstain maintains the intensity of the label, while staining cell bodies in blue. The Giemsa counterstain also helps to facilitate whole-slide imaging, by increasing the contrast on the section, which allows for robust determination of the focus plane and reduces the background imaging noise.

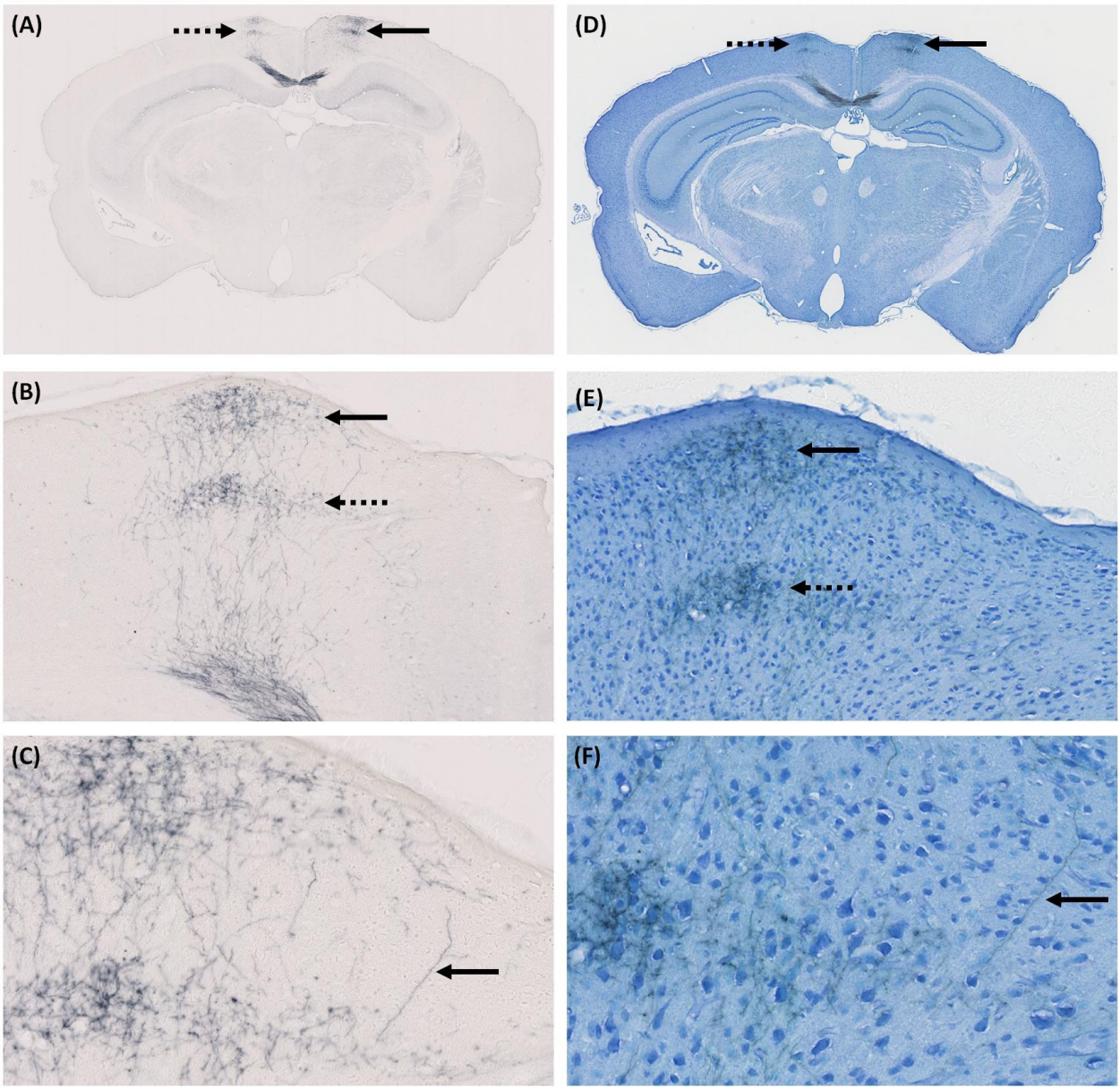

Figure 65: Giemsa Counterstained Tissue
An injection of Biotinylated Dextran Amine (BDA) into the cortex is shown. Following HC staining, the section was coverslipped and imaged, as shown in A, B and C. The coverslip was then removed, the section was washed, counterstained with Giemsa and reimaged, as shown in D, E and F. The injection site (black arrow) and contralateral projections (dotted arrow) through the corpus callosum are seen in both (A) and (D). This correspondence is maintained at medium-magnification (B and E). At medium-magnification (C and F) the projection fibers are clearly seen in layer 1 (black arrow) and layer 3 (dotted arrow). The intensity of label is similar, but the Giemsa counterstain makes the label harder to identify at this resolution. At higher-magnification (C and F), labeled fibers are clearly seen with and without the counterstain. The black arrow points to the same labeled fiber. Labeled cells are clearly seen in (F).

Cholera Toxin subunit B (CTB)

CTB is one of two HC tracers used in the project. The detection of injected CTB requires an antibody step, therefore it is an immunohistochemistry (IHC) reaction. Once the CTB is developed, through a DAB reaction, a Giemsa counterstain is applied.

CTB is primarily considered a retrograde tracer, but is also transported along axons[19]. A typical CTB injection into the primary motor area (MOp) of the cortex is shown in Figure 66. The arrows highlight the label at the injection site, the contralateral projections and the cortical projections to the caudoputamen of both hemispheres. A high-magnification view of the contralateral projections is shown in (B). A high-magnification view of the injection site is shown in (C). Projections from the injection site are apparent. The injection site is very dense, but projection fibers are evident. A clear fiber, medial to the injection site, is denoted by a black arrow.

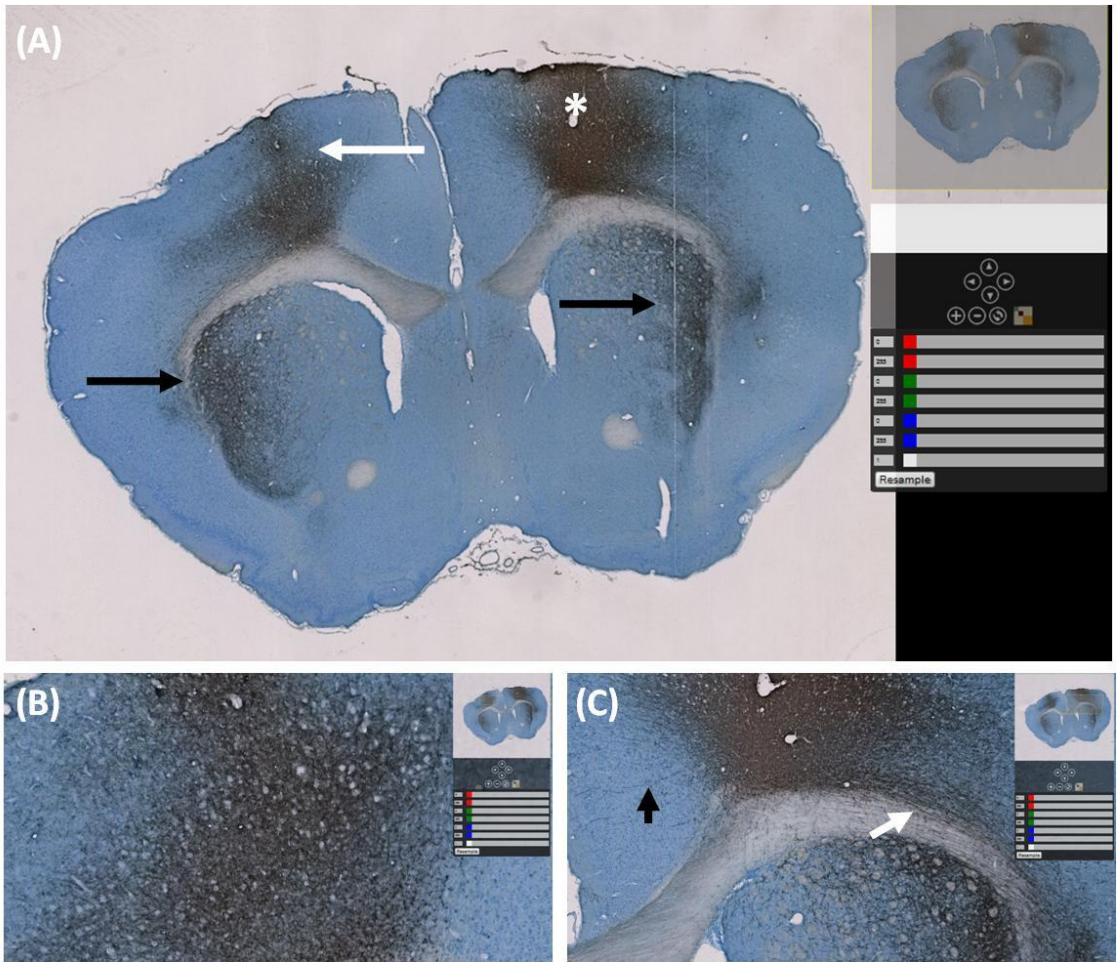

Figure 66: **A portal view of a CTB injection into the primary motor area (MOp) of the cortex.**
In (A) the white arrow points to label in the contralateral cortex. The injection site is indicated by an asterisk. The black arrows point to the label in the caudoputamen. A high-magnification view of the contralateral projections is shown in (B). A high-magnification view of the injection site is shown in (C). Projections from the injection site are apparent. A clearly labeled fiber, medial to the injection site, is denoted by a black arrow.

A mix of cell bodies and fibers is seen at several locations. As a retrograde tracer, cell bodies should be labeled at the projection site, as is shown in Figure 67.

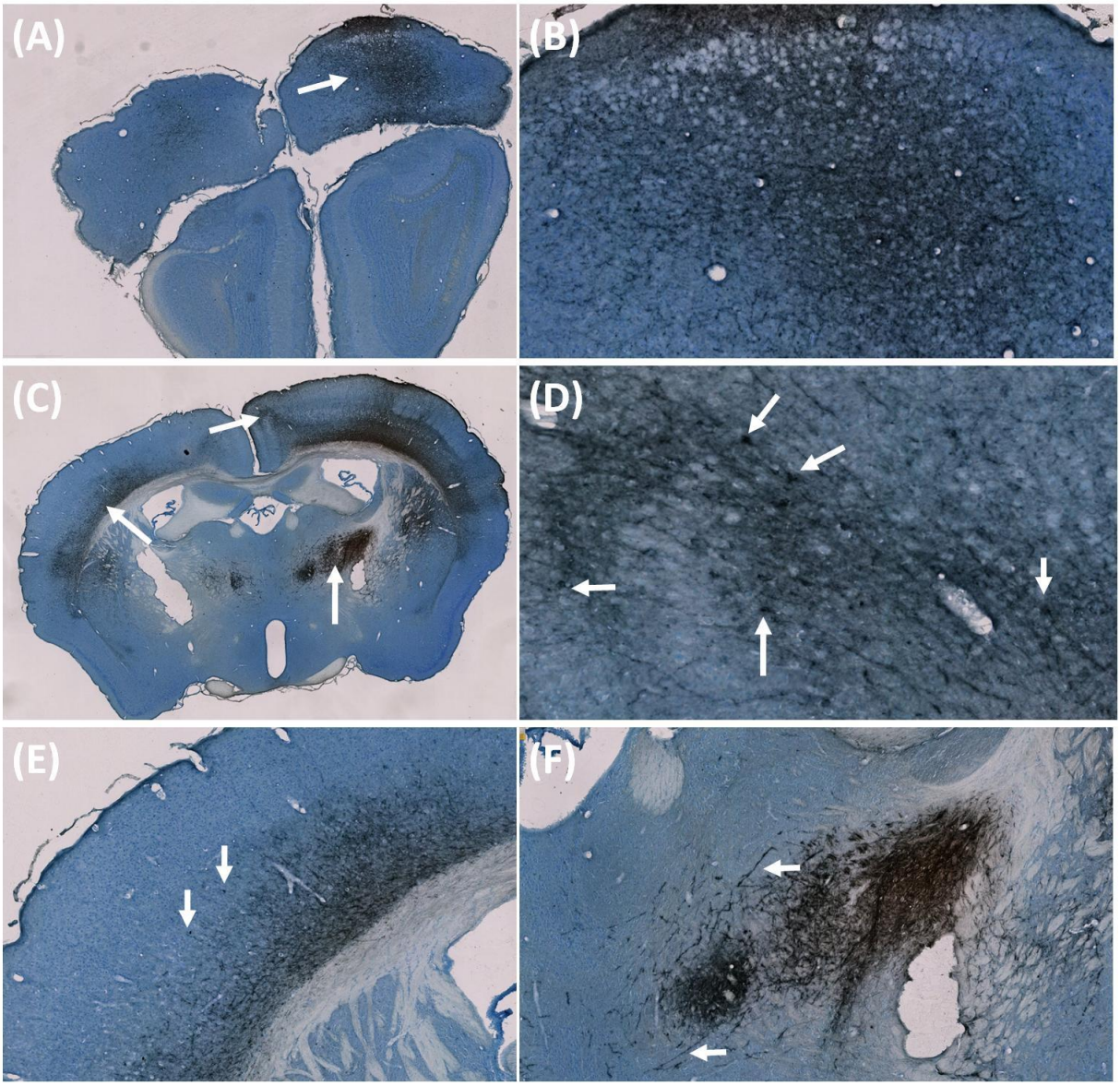

Figure 67: Projection sites labeled from the CTB injection into MOp
Projections to the anterior secondary motor area (MOs), are shown in (A) and (B). Projections to the posterior MOs are shown in (C) and (D). Projections to the lateral somatosensory area (SSp) are shown in (C) and (E). Projections to the thalamus are shown in (C) and (F). In each of the high-magnification images (D, E, F) cell bodies and high intensity fibers are clearly identifiable in the Giemsa counterstain.

The label is also seen in posterior sections of the brain, as shown in Figure 68A. Projection fibers and cells in the midbrain are shown in (B) and in the pons in (C). A few cells are identifiable, contralateral to the fibers in the pons.

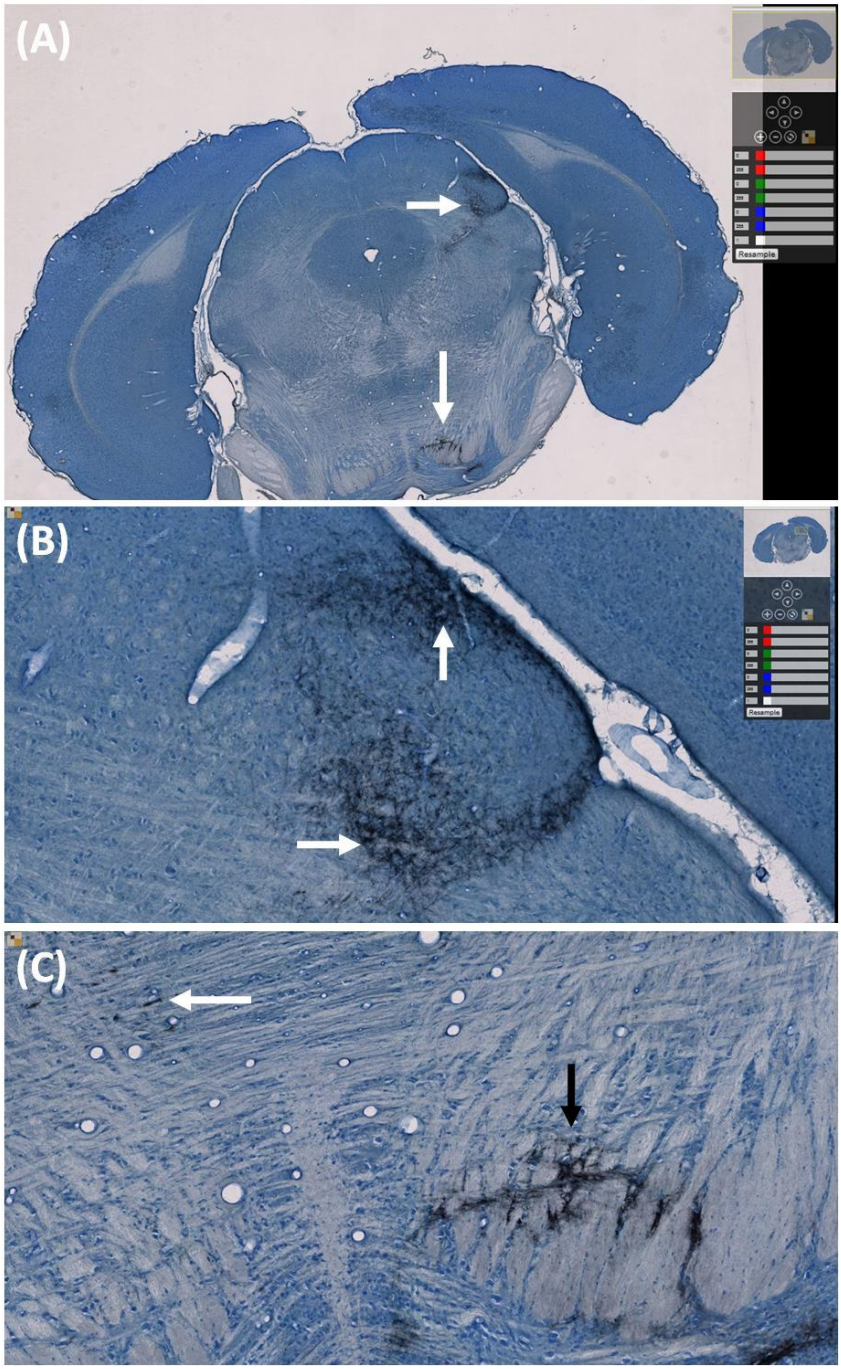

Figure 68: Projections to the midbrain and pons of the CTB injection into MOp
Projections in the midbrain (A and B) and the pons (A and C), resulting from the CTB injection into MOp are shown. (B) and (C) are higher magnification from the arrows in (A). The arrows in (B) point to labeled cells. The arrows in (C) point to a few cells that are contralateral to the fibers in the pons (black arrow).

Biotinylated Dextran Amines (BDA)

BDA is the second HC tracer used in this project. Like CTB, BDA undergoes a Giemsa counterstain, after development of the label with DAB. BDA is primarily an anterograde tracer, and labels fibers and axon terminals (putative synapses)[88]. A typical BDA injection site is shown in Figure 69.

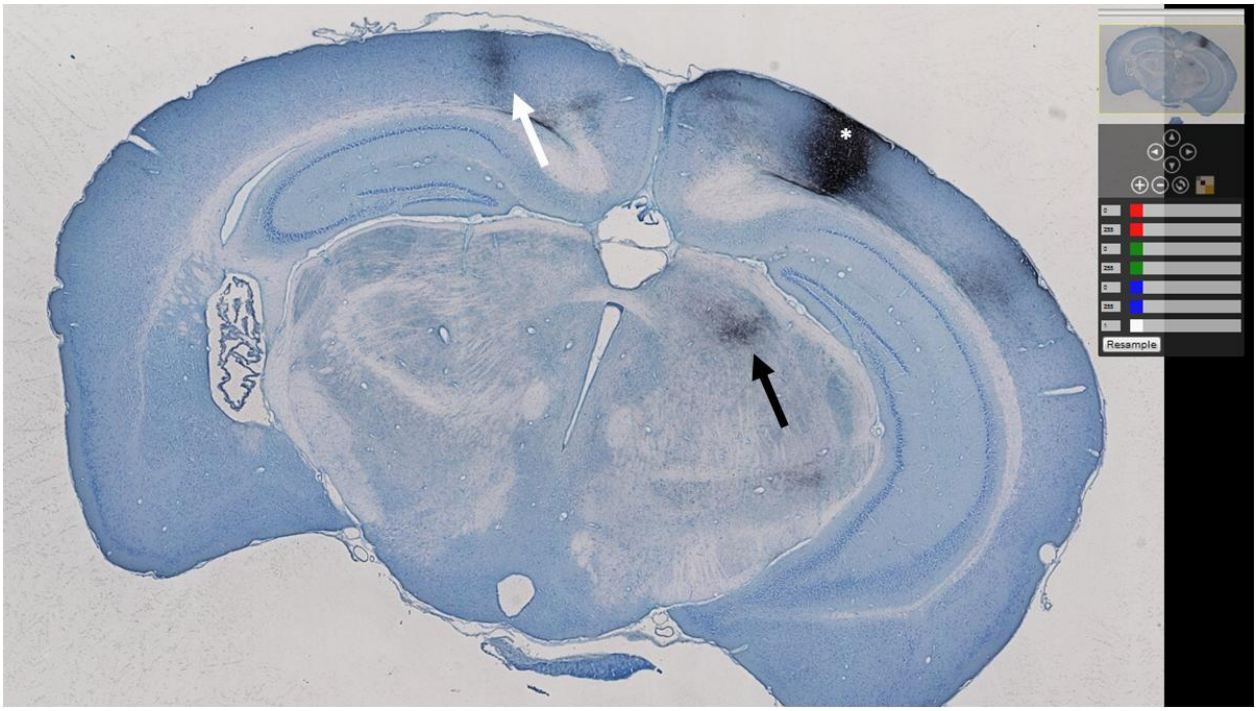

Figure 69: Portal view of a BDA injection into the anteromedial visual area (VISam) of the cortex.
The injection site is indicated by an asterisk (upper right). The white arrow points to the contralateral cortical projections (upper left). The black arrow points to the corticothalamic projections (lower right).

This is an injection into anteromedial visual area (VISam) of the cortex. The thalamic and contralateral projections are indicated by arrows. Each site is shown at higher magnification in Figure 70. The termination fibers are clearly identifiable in the Giemsa counterstain. For both regions, this coronal section shows only a single AP slice of the entire projection region. For the thalamic projection, a more representative image of the label is found anterior to the injection site, as shown in Figure 71. A highlighted view of a single projection fiber is shown on the bottom of Figure 71.

In Figure 70C, a high-magnification view of injection site is shown. Due to the density of the label, identifying individual cells is difficult. Away from the injection site, this identification is easier, as shown in Figure 70D. A different cortical injection is shown in Figure 72. This is an injection into primary motor area (MOp). The same intensity and differentiation of label is evident at the injection and projection sites.

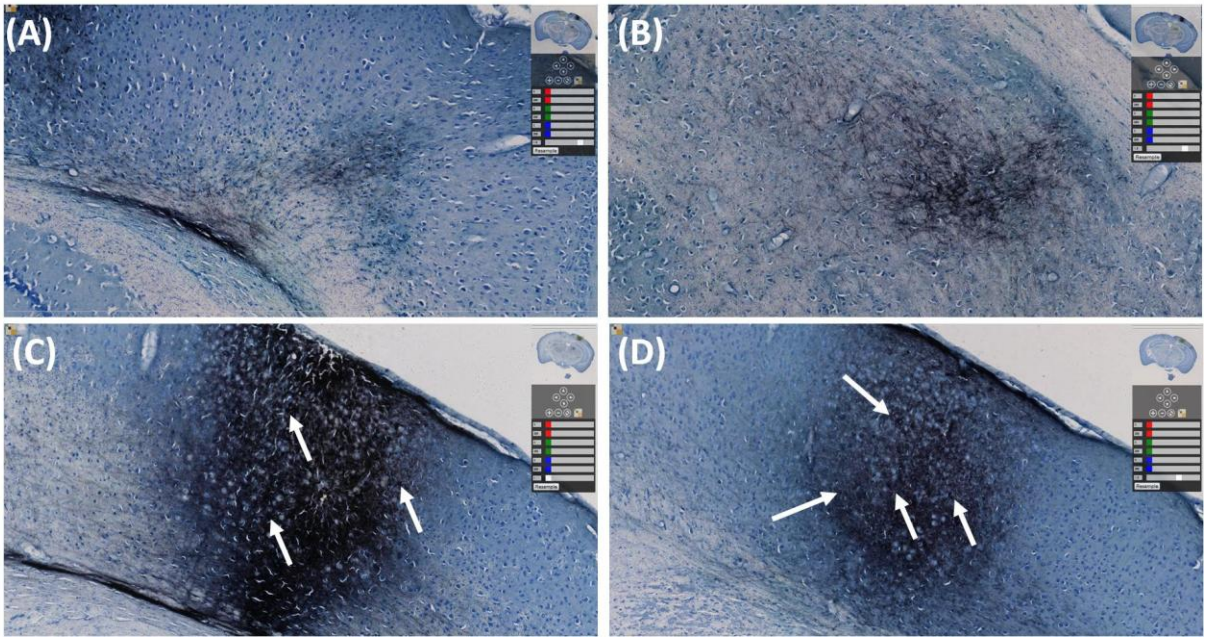

Figure 70: High-magnification views of the injection into VISam.
The contralateral projections are shown in (A). The thalamic projections are shown in (B). The injection site is shown in (C). Cell bodies are difficult to identify at the injection site, due to the density of label. Cell bodies are easier to identify, anterior to the core of the injection site, as shown in (D). A-C are taken from the same AP level as the coronal section as shown in Figure 69. Arrows point to labeled cells.

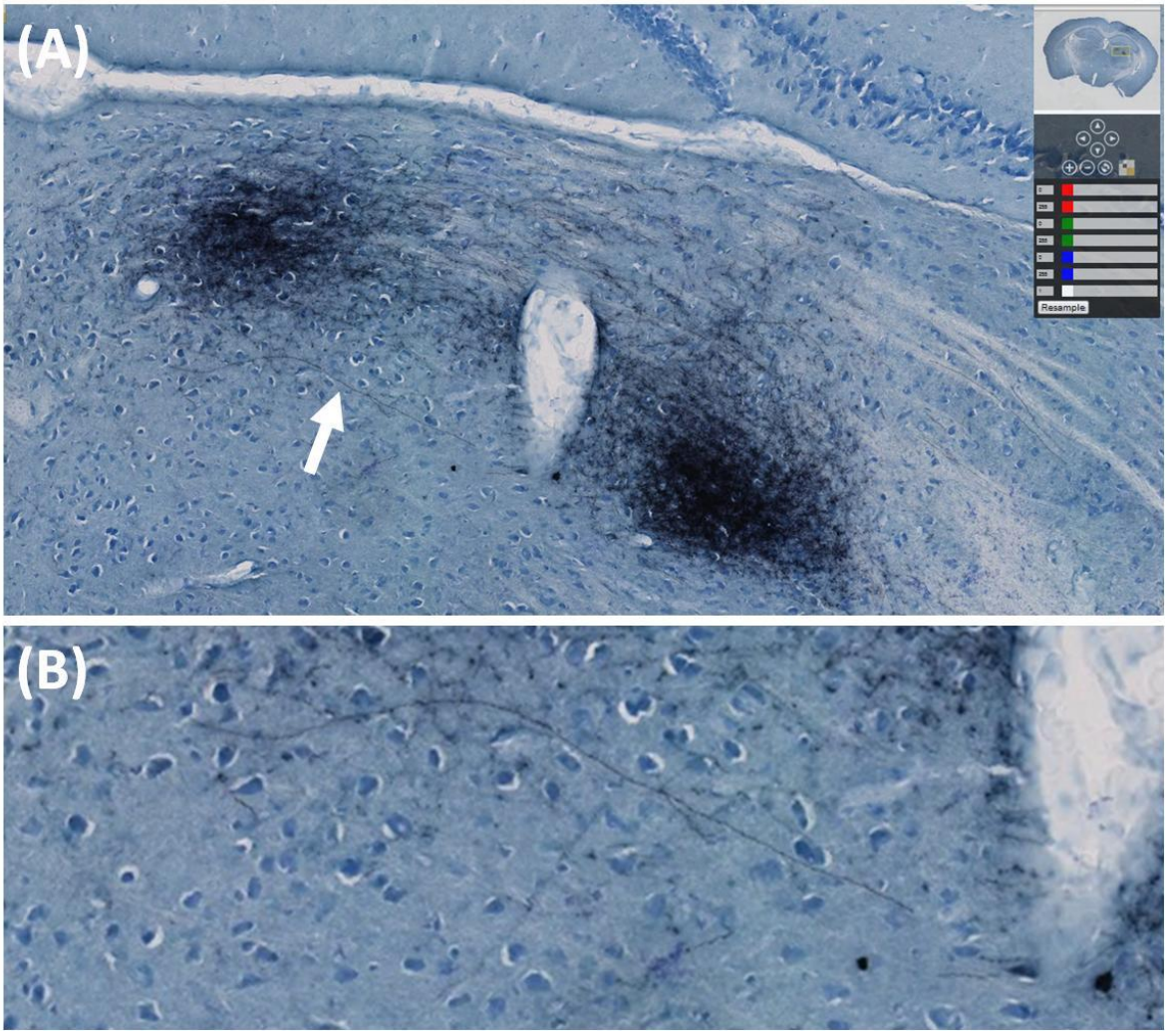

Figure 71: Thalamic projections from the BDA injection into VISam.
The arrow points to a projection fiber that is shown at higher-magnification in (B).

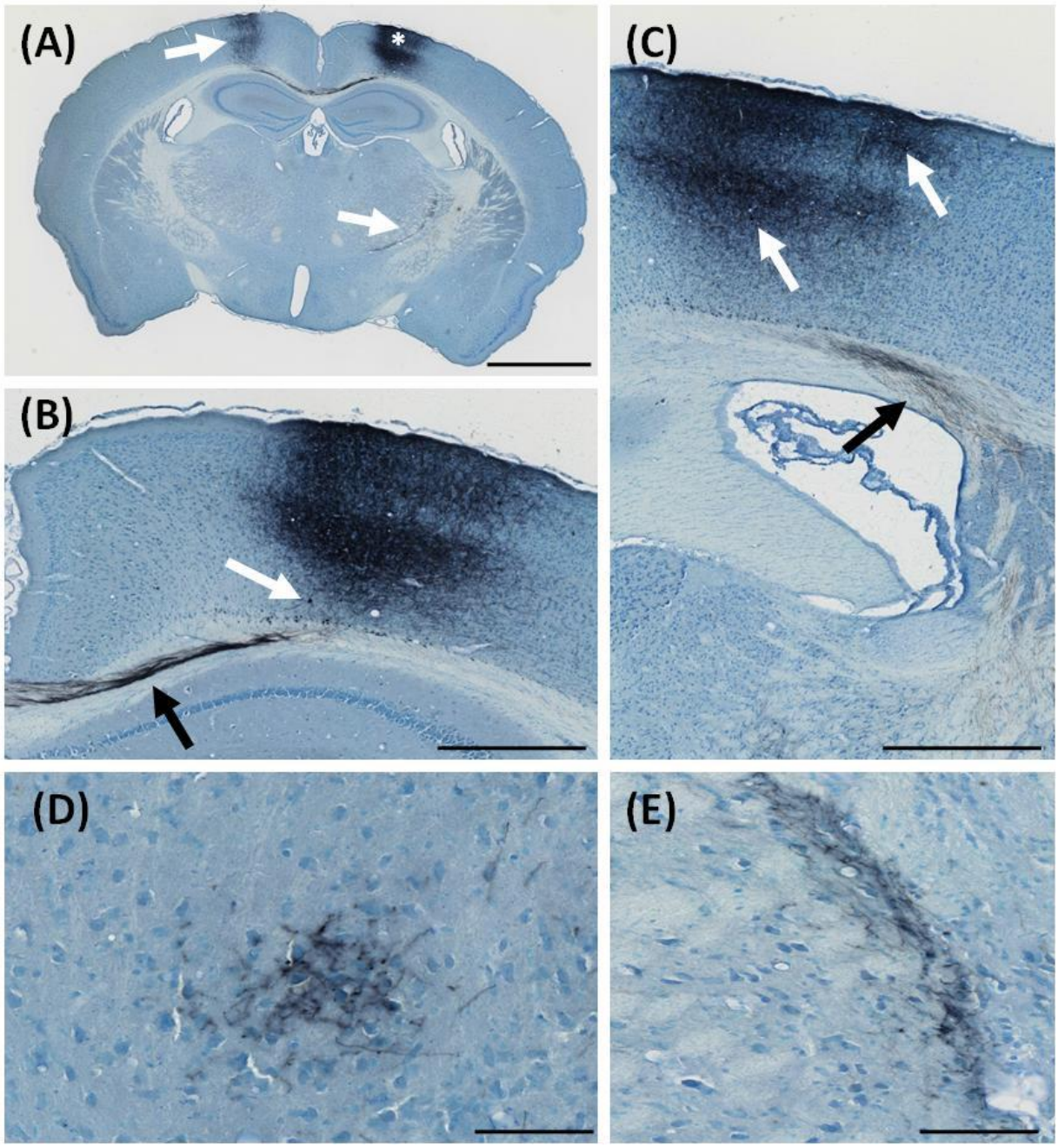

Figure 72: An injection of BDA into Primary motor area (MOp) of the cortex.
A macro view of the injection is shown in (A). The contralateral cortical (upper left arrow) and thalamic projections (bottom right arrow) are evident. The injection site is marked by an asterisk. A higher-magnification view of the injection site is shown in (B). The white arrow points to a clearly labeled cell. The black arrow points to the fibers in the corpus callosum, projecting to the contralateral cortex. Thalamic projections are seen in a section posterior to the same injection, as shown in (C). The white arrows point to labeled cells and the black arrow points to the thalamic projections. Thalamic terminations are shown in (D) and (E). Scale bars are: 2mm, 1mm, 1 mm, 100um, 100um.

Retrograde Rabies Virus (RV-4GFP(B19G))

The Rabies Virus, as produced by Ian Wickersham[89, 90], is available in many forms. For retrograde tracing, the principle form used in this project is that of RV-4GFP(B19G). A typical injection site is shown in Figure 73. The rabies label is easily identifiable versus the background.

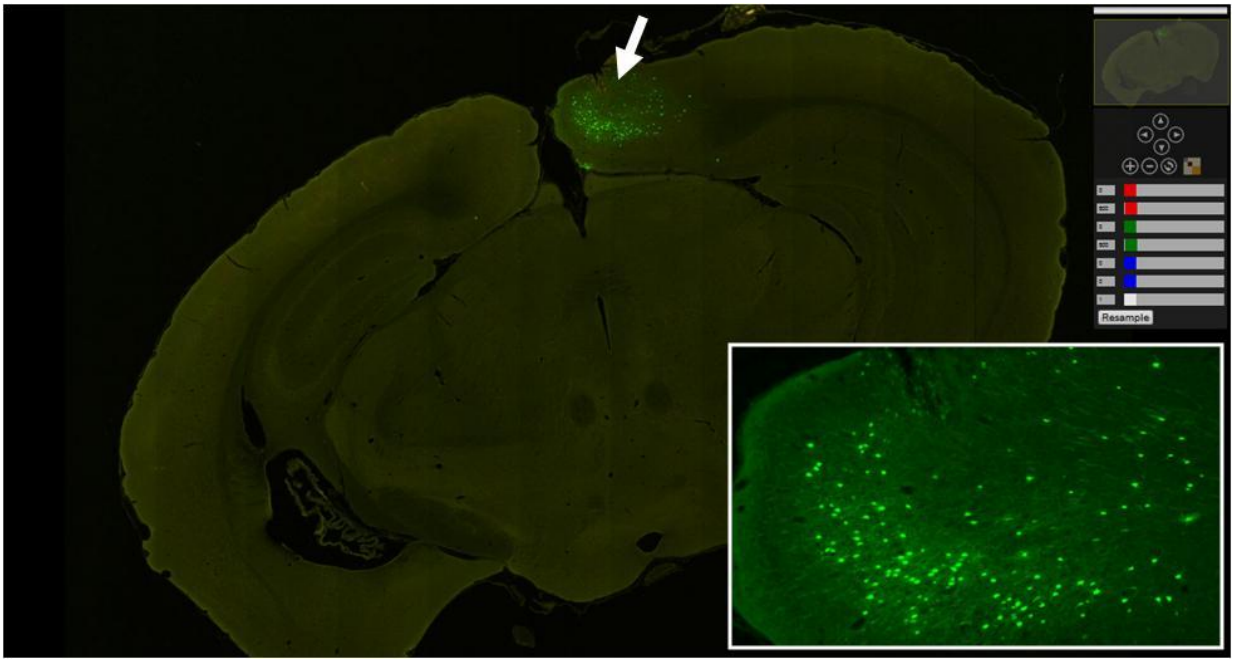

Figure 73: A portal view of a rabies virus injection into the dorsal Retrosplenial area (RSPd) of the cortex. The white arrow points to the injection site. The insert at the bottom right is a high-magnification view of the injection site.

The projection zones to this injection site are shown in Figure 74. As expected for a retrograde tracer, cell bodies are labeled at the projection site. Projections from the thalamus and the hippocampus are shown. In both of these projection zones, the label is of high intensity and easily identifiable. Since whole-slide scanning of fluorescent MBA samples is performed at a dynamic range of 12-bits per pixel, per color channel, the rabies virus does not saturate, even at the injection site.

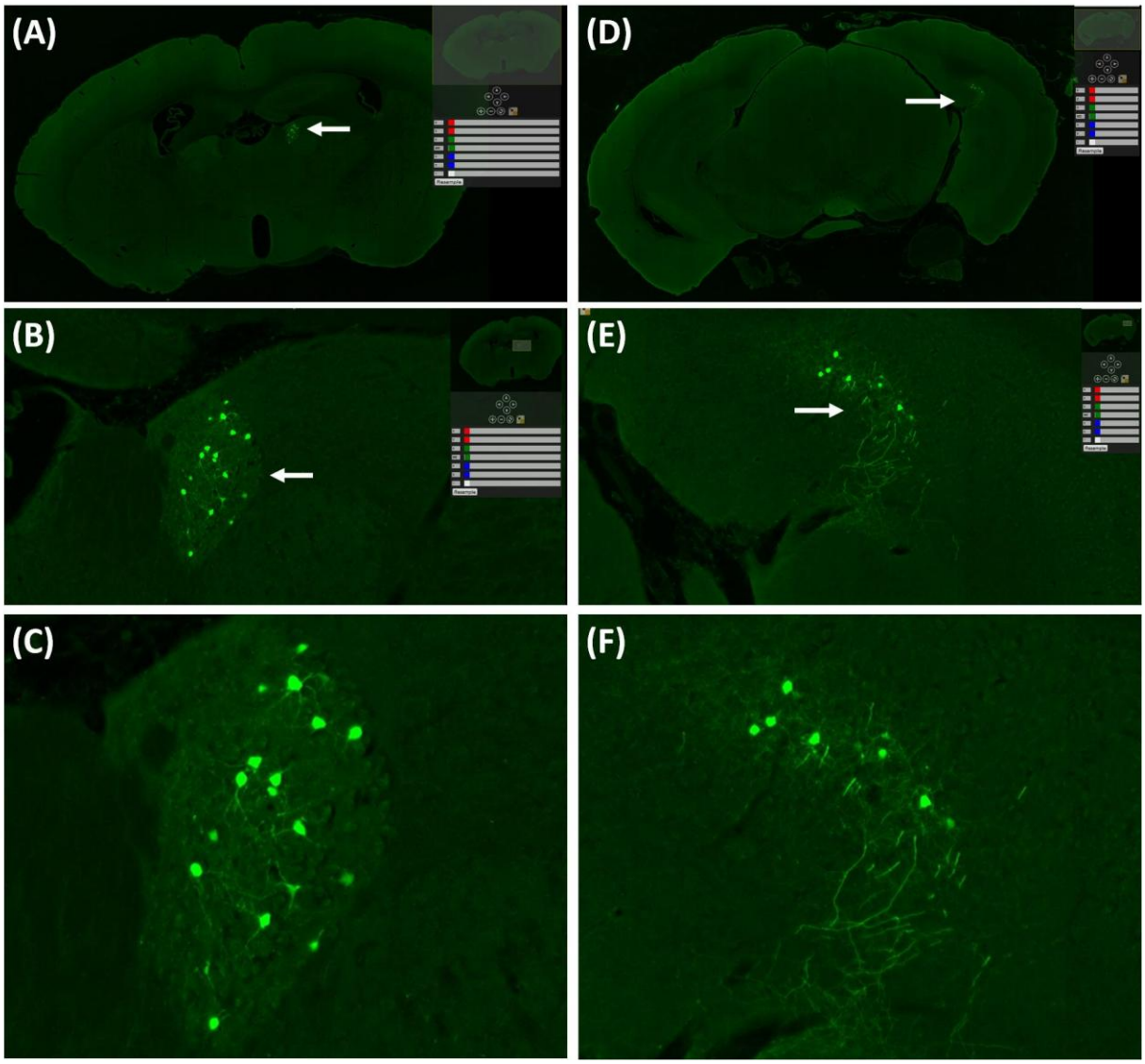

Figure 74: Retrogradely labeled cells, from a rabies virus injection into the RSPd
Labeled cells in the thalamus are shown at low-magnification in (A). The white arrow points to the region of labeling, shown at higher magnifications in (B) and (C). Labeled cells in the hippocampus are shown at low-magnification in (D). The white arrow points to the region of labeling, shown at higher magnifications in (E) and (F).

Adeno-Associated Virus (AAV)
(AAV2/1.CB7.CI.EGFP.WPRE.RBG and AAV2/1.CAG.tdTomato.WPRE.SV40)

Unlike the Rabies virus, AAV is an anterograde tracer[91]. AAV is expected to produce labeling similar to that of BDA. One of the advantages of AAV, is that it is commercially available (University of Pennsylvania) with different reporter genes, such as GFP, RFP, and TdTomato. This allows for two injections to be performed simultaneously per animal, without an alteration of the imaging procedures. Per cortical injection site, superficial layers (1-3) were injected with AAV2/1.CB7.CI.EGFP.WPRE.RBG, so that the resulting label would appear in green; deep layers (4-6) were injected with AAV2/1.CAG.tdTomato.WPRE.SV4, so that the label would appear in red.

A typical two color AAV injection into the cortex is shown in Figure 75.

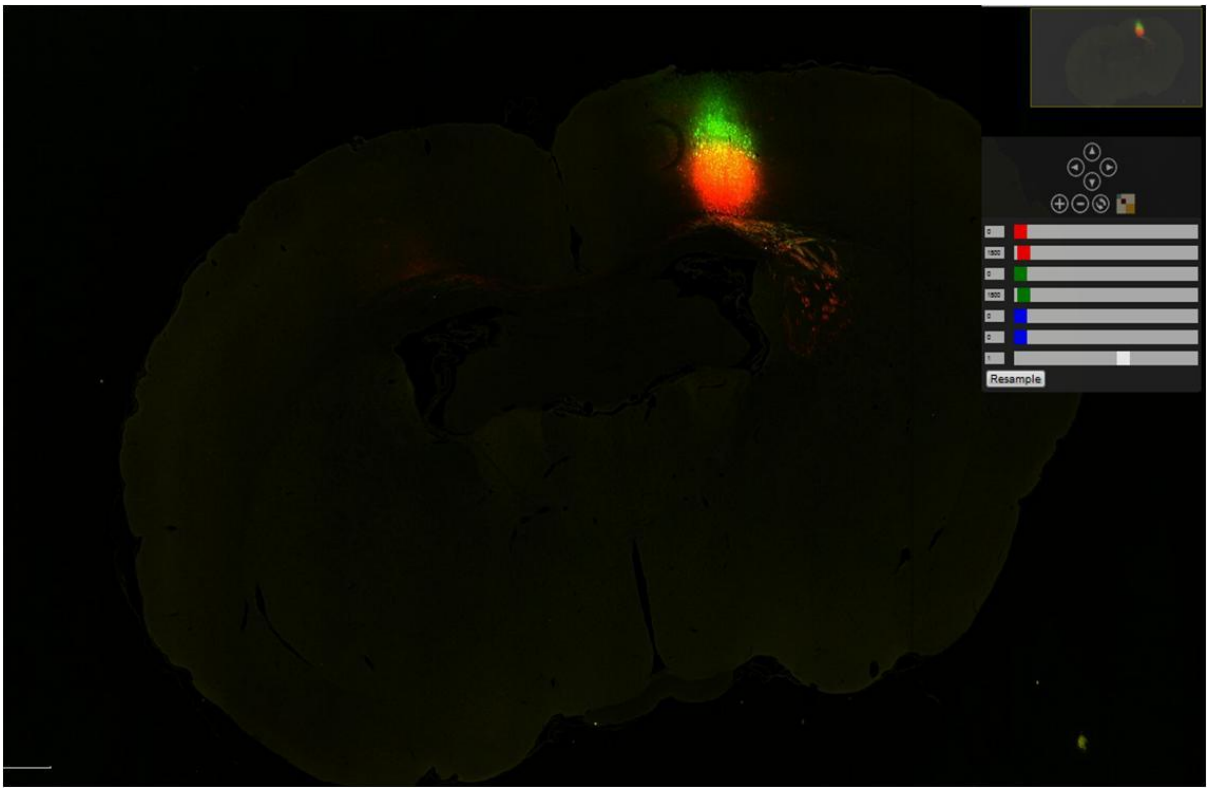

Figure 75: Portal View of two AAV injections into Primary motor area (Mop).
Superficial layers (1-3) are labeled in green. Deep layers (4-6) are labeled in red.

The differential labeling of the superficial versus deep layers is highlighted in Figure 76A. Figure 76B-C show the single color view of the injection site. Figure 76D is a high-magnification view of the injection site. Labeled cells at the injection site and projection fibers in the white matter are evident.

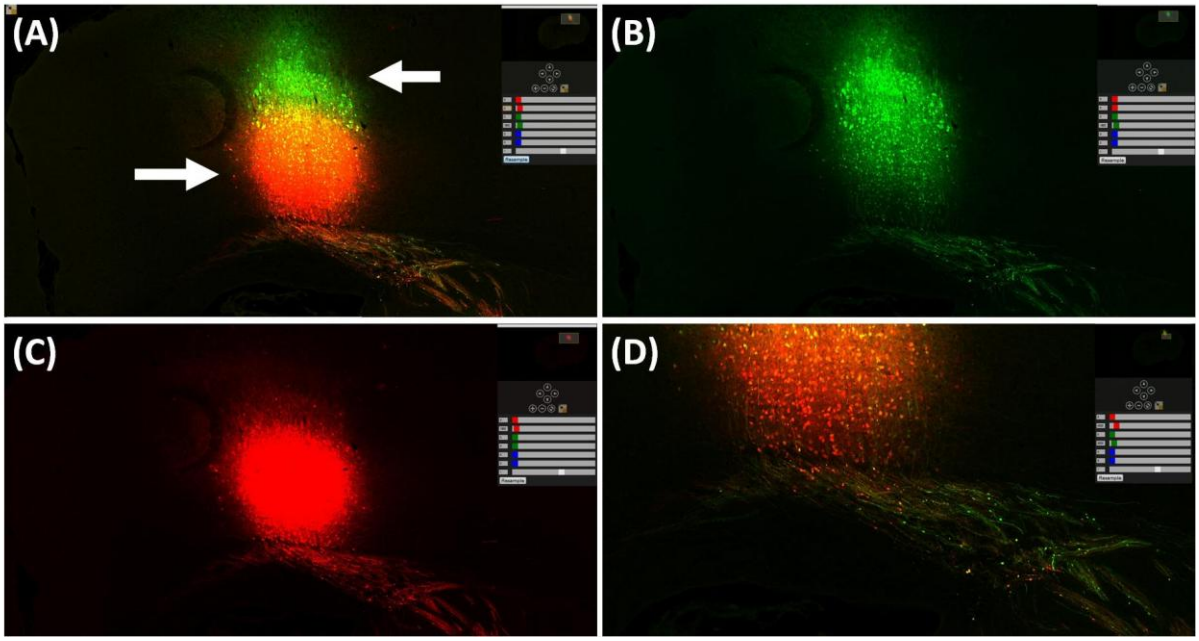

Figure 76: High-magnification view of the two AAV injections to MOp.
The depth-wise differential labeling of cortical layers by the two AAV colors is indicated by white arrows in (A). The right pointing arrow indicates the injection into the superficial layers and the left pointing arrow indicates the injection in the deep layers. In (B) only the green channel is shown, using the color adjustment toolbar of the portal viewer. The green signal is centered at Layers 2-3. In (C) only the red channel is shown. This signal is centered at Layers 4-6. As shown in (D), the labeled cells at the injection site and projection fibers through the white matter are evident.

The terminal projections from this injection to the midbrain and thalamus are shown in Figure 77. In this coronal section, the thalamic label is primarily in red - originating from the deep cortical layers. The midbrain label is apparent in both colors, as is the label in the cerebral peduncle (C).

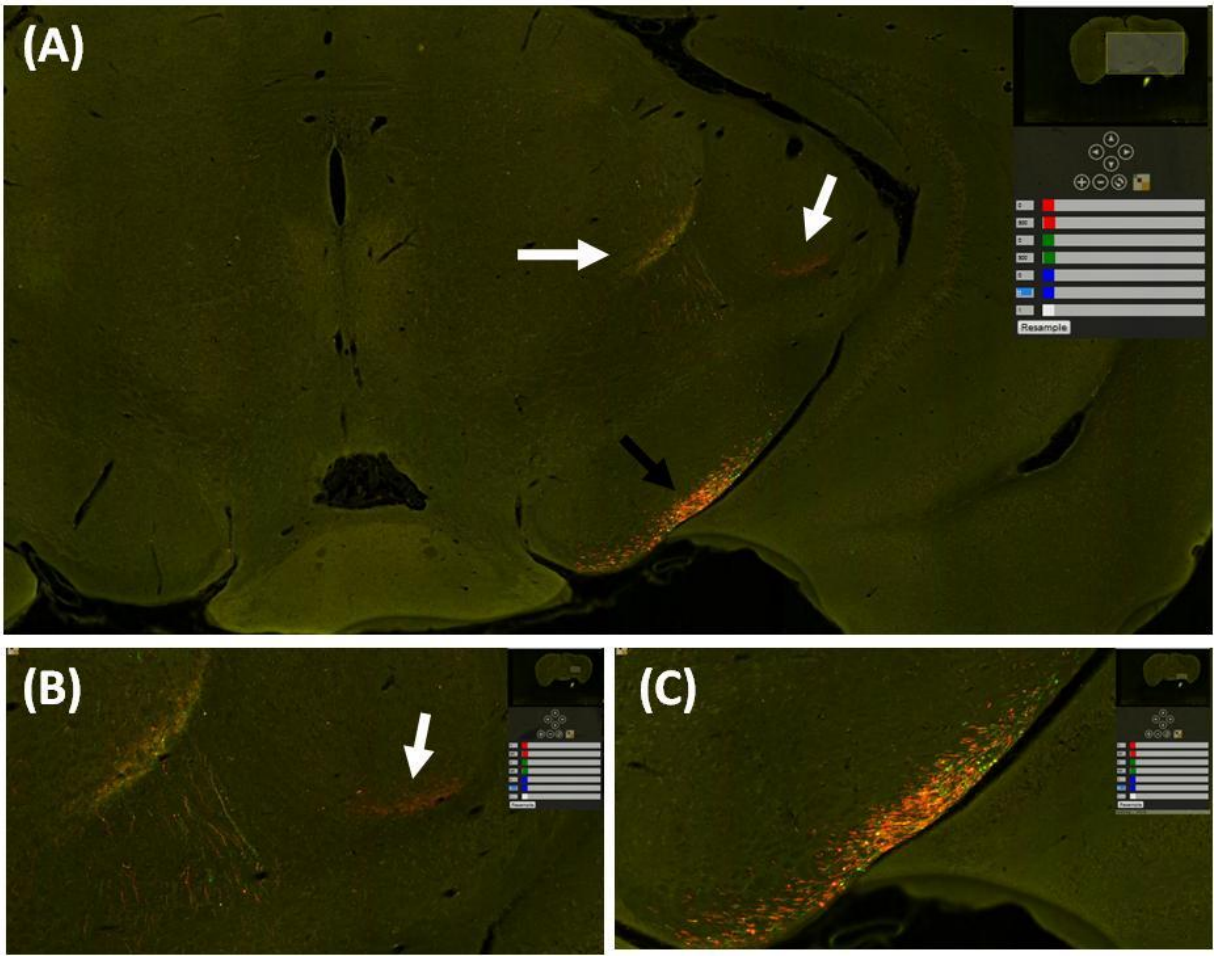

Figure 77: Projections from the AAV injection into MOp
Projections from the AAV injection into MOp, to the midbrain and thalamus are shown. Labeled fibers in the cerebral peduncle are also seen (black arrow). A high-magnification view of the midbrain and the thalamic label is shown in (B). The thalamic label, as indicated by white arrows in (A) and (B), is primarily from the deep structures, in this coronal section. A high-magnification view of the cerebral peduncle is shown in (C).

As part of the MBA pipeline, the whole mouse brain is sectioned and imaged in identical manner. This allows for one to follow the AAV label to the brainstem, as shown in Figure 78. This coronal level is not well represented in the Allen Reference Atlas, but critical structures can be extracted from the neighboring Nissl-stained section in our material. Even at this coronal level, the label is easily identifiable versus the background, as shown in Figure 78C.

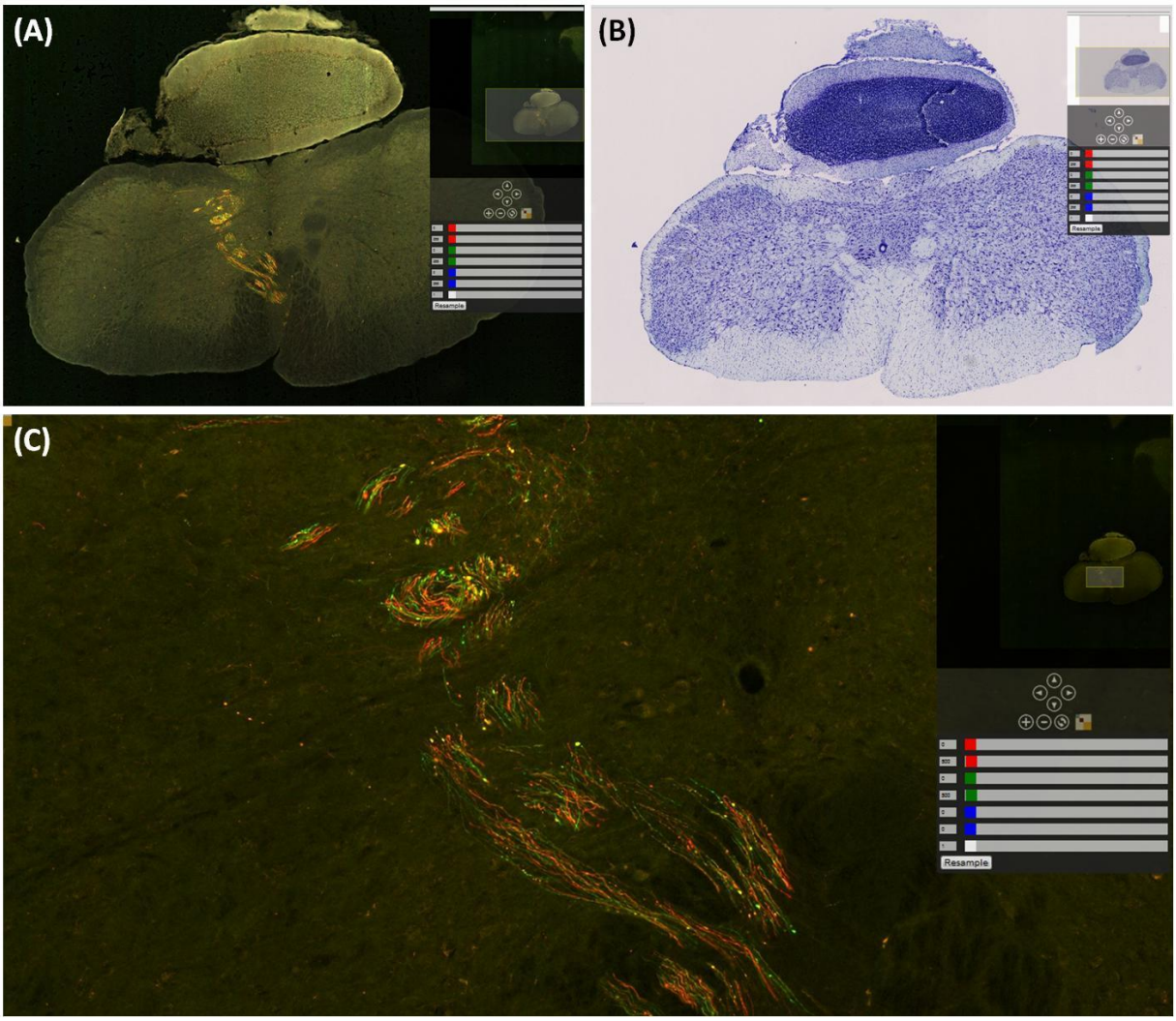

Figure 78: Brainstem projections from the AAV injection into MOp
Brainstem projections from the AAV injection into MOp are shown in (A). The corresponding Nissl –stained section is shown in (B). A high-magnification view of the AAV label is seen in (C).

In addition to the entire brain, the spinal cord from each processed animal is preserved and processed as part of the MBA project. An example of this data are shown in Figure 79. Projection fibers from a single cortical injection of AAV into the MOp are clearly seen. This spinal cord was sectioned using the tape-transfer method[92], as all MBA material, which allows for the sectioning of the entire vertebral column, without extracting the spinal cord or declassifying the bone. The tape-transfer method is successful in preventing damage to the spinal cord, caused by sectioning of the vertebral column, as is evident in the figure.

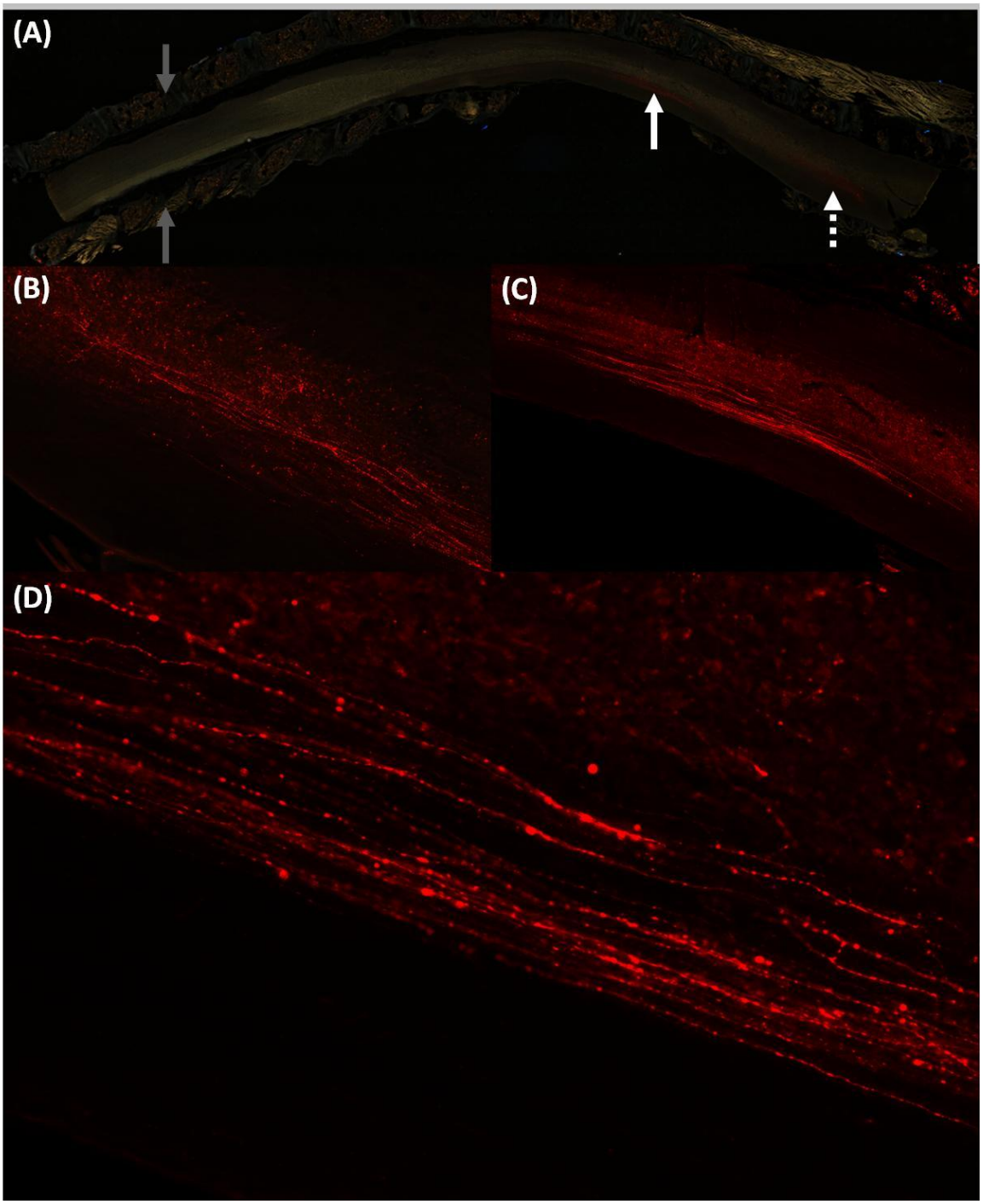

Figure 79: Projection fibers in the spinal cord of the mouse, injected with AAV
A low-magnification image of sagittal section of a spinal cord, extracted from a mouse that was injected with AAV (red) into the primary motor area (MOp), is shown in (A). Cervical vertebrae are at the right and the left leads into the thoracic vertebrae. The dotted white arrow points to the label that is shown at high-magnification in (B). The white arrow points to the area that is shown at higher magnification in (C) and (D). The gray arrows (left) point to the surrounding vertebral column, that was sectioned with the spinal cord, using the tape-transfer system.

A more medial two-color AAV injection to the MOp/MOs is shown in Figure 80. The cortical layer separation is more apparent in this injection than in the above, as the separation is in the medial-lateral plane, along with the dorsal-ventral. The label intensity is similar to that in the above brain. The projections are seen in the same anatomical regions.

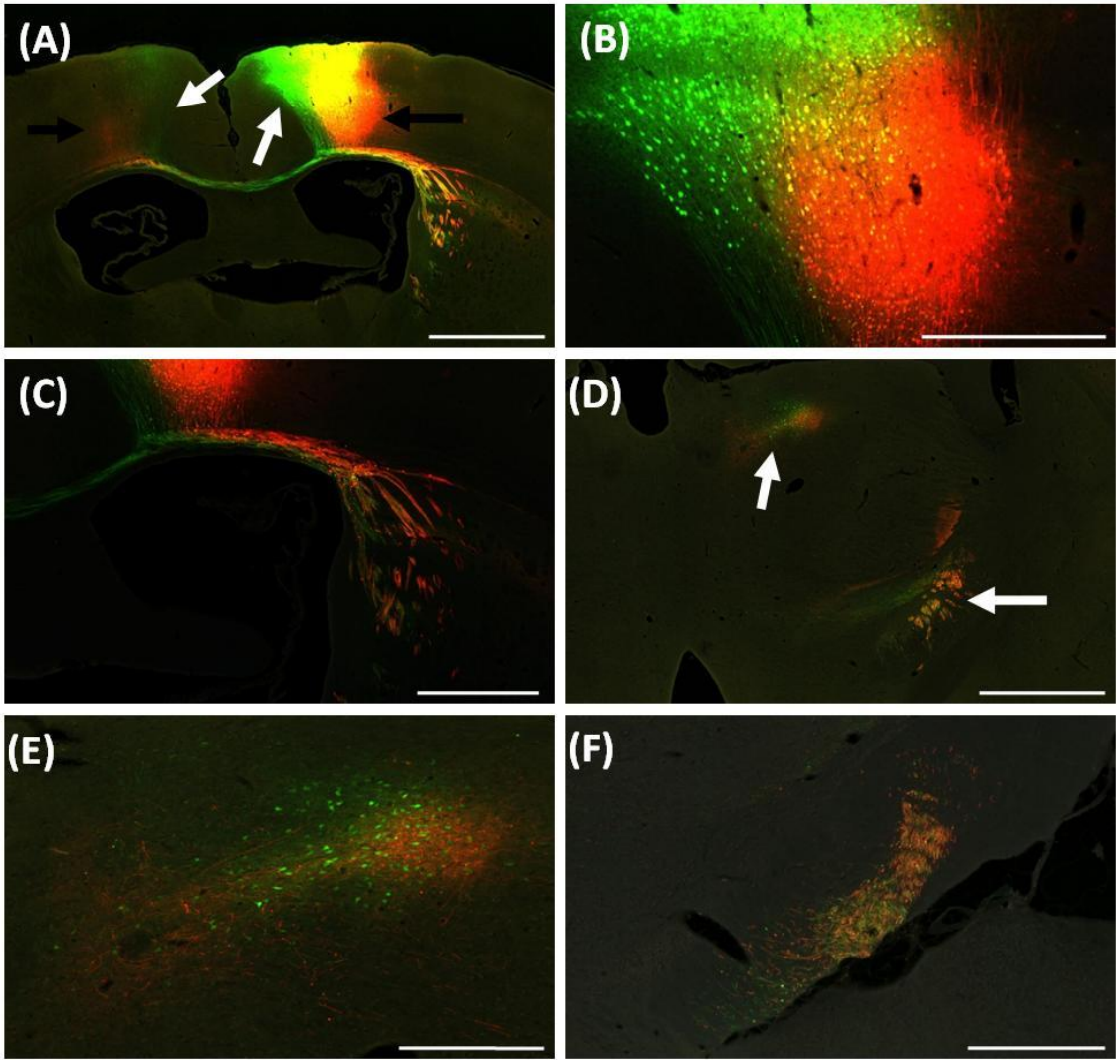

Figure 80: Two AAV injections into the MOs and the MOp
Superficial layers (1-3) in the MOs are labeled in green (white arrows). Deep layers (4-6) of the MOp are labeled in red (black arrows). The differential label of the cortical layers by the two AAV injections is shown in (A) and (B), indicated by arrow. The contralateral label is also highlighted in (A). Projection fibers through the white matter are shown (C). The multiple projection sites from the injection are shown in (D), (E) and (F). At each, the label is easily identifiable. Scale bars are: 1mm, 400µm, 500µm, 1mm, 250µm and 400µm.

Auxiliary Data:

In addition to the primary MBA project, intended for mapping the connectivity in C57BL/6 mouse, the MBA pipeline has been used to collected supplementary neuroanatomical data. A subset of processed material is discussed below. All material will be available through the MBA portal, under the Auxiliary Data section. These data are intended to showcase the use of the MBA pipeline to help answer other neuroanatomical questions and to place the connectivity study in the broader context of neuroanatomy.

Sagittal and Transverse Whole-Brain Nissl

The main portion of MBA processed material is sectioned in the coronal plane. This sectioning plane allows for the continuous processing of the entire brain and the visualization of both hemispheres of the brain on a single section. The brain, however, is a 3-D structure, and to fully capture the inner structure of the brain, other planes of sectioning need to be utilized. For this reason, we have sectioned several brains in both the sagittal (Figure 81) and transverse planes (Figure 82), and prepared Nissl stained sections.

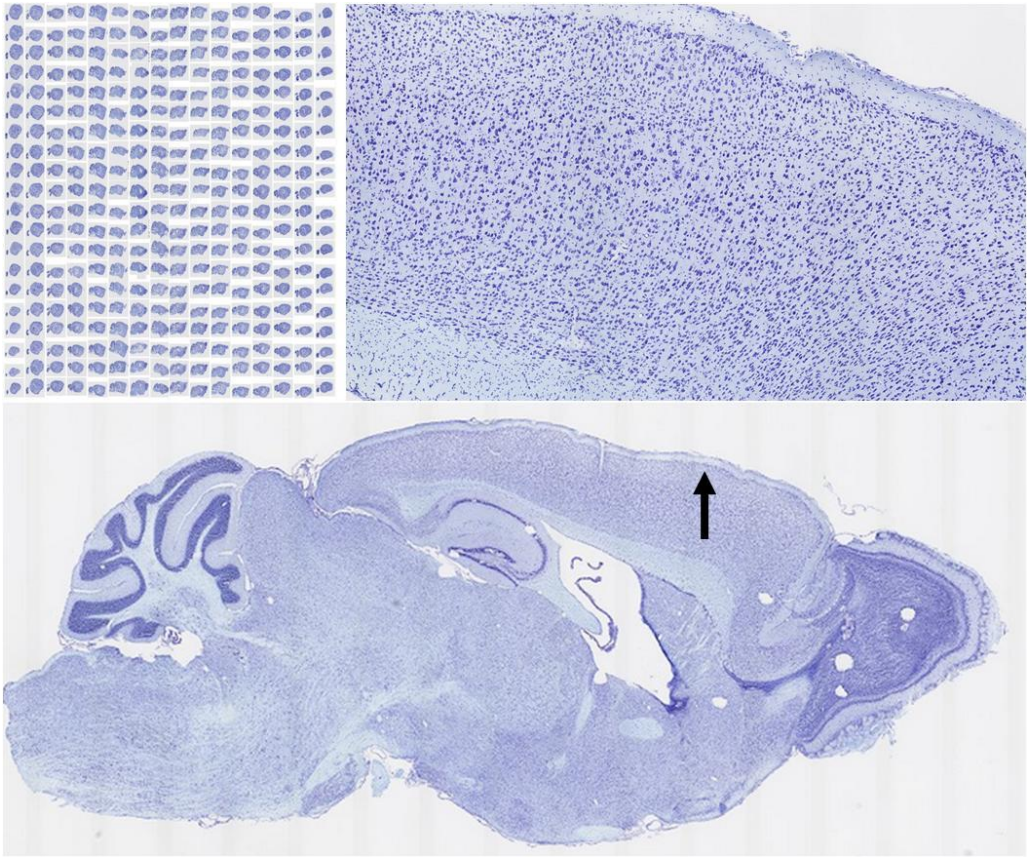

Figure 81: Nissl-stained sections, cut in the sagittal plane
Top-left, is a tile view of all of the sections of the series. Bottom, is a low-magnification view of a typical section. The black arrow points to the cortical region that is shown at higher magnification (top-right).

Because of the tape-transfer method, used for all MBA pipeline material, disjoined regions of the brain do not separate during sectioning, but are transferred onto the section as they appear in the blackface. This allows for an undistorted view of the brain. All sections are 20µm thick and every mounted section was stained and imaged in the same manner, which allows for a continuous view of the entire brain.

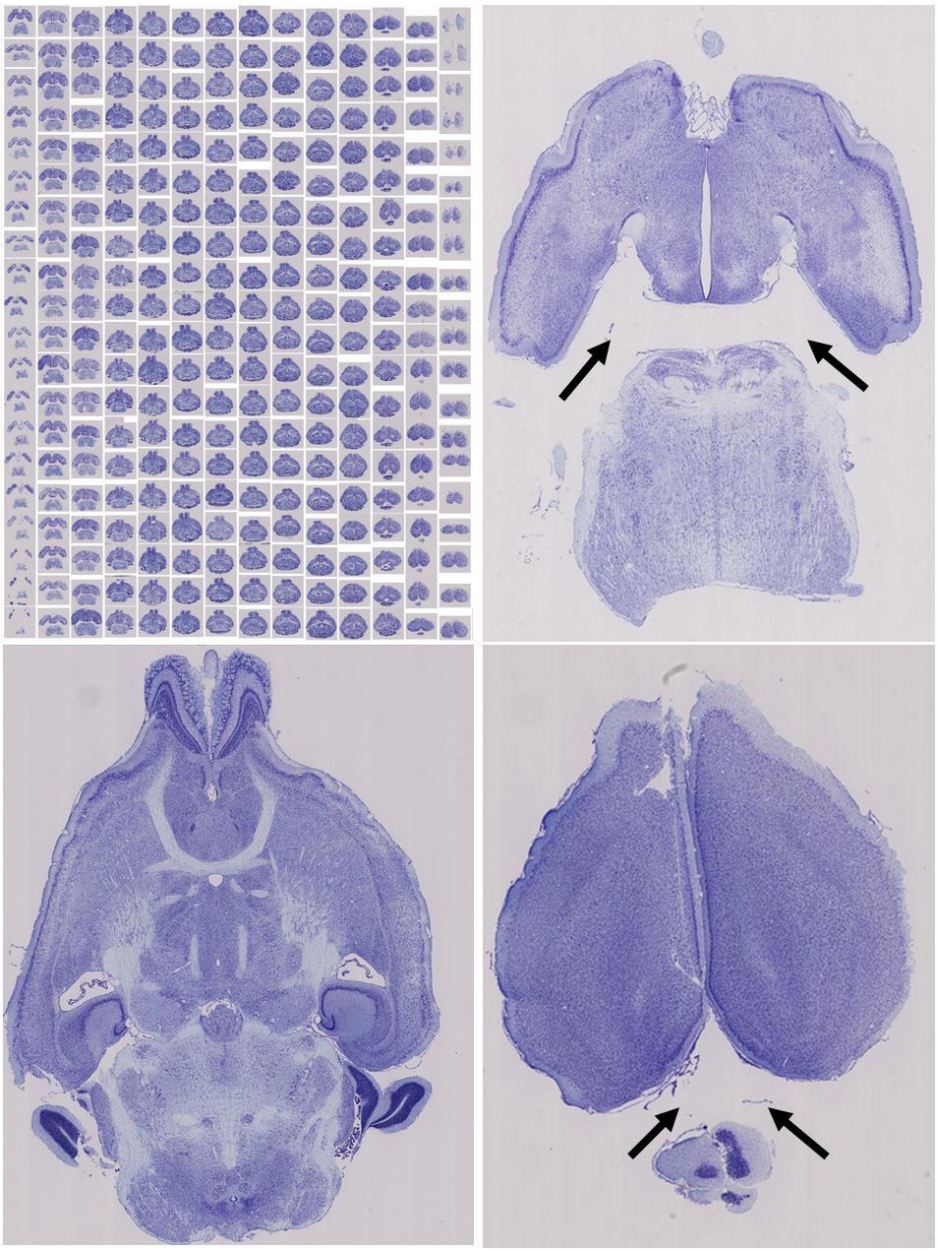

Figure 82: Nissl-stained sections, cut in the transverse plane
Top-left, is a tile view of all of the sections of the series. Top-right is a ventral section. Bottom-left is a mid-plane section. Bottom-right is dorsal section. Black arrows point to the separation between the brain regions. These regions do not separate during sectioning, because of the tape-transfer method.

Fluorescent Nissl

In addition to the conventional Nissl stain, which is imaged through transmitted light microscopy, we have also experimented with a fluorescent Nissl stain (NeuroTrace, Molecular Probes). As shown in Figure 83, this stain is equivalent to Nissl staining with thionin or cresyl violet. Cortical layers are differentiated and can be annotated accordingly. One of the drawbacks of this stain, is that it is not color channel specific. Meaning that the "Blue Fluorescent Nissl Stain" with an excitation and emission wavelength of 435⁄455nm is also prevalent in the Green channel (485/530nm). As a result, this stain cannot be effectively used with GFP based tracers (Rabies virus and AAV) and therefore is not a substitute for conventional Nissl staining of alternating sections.

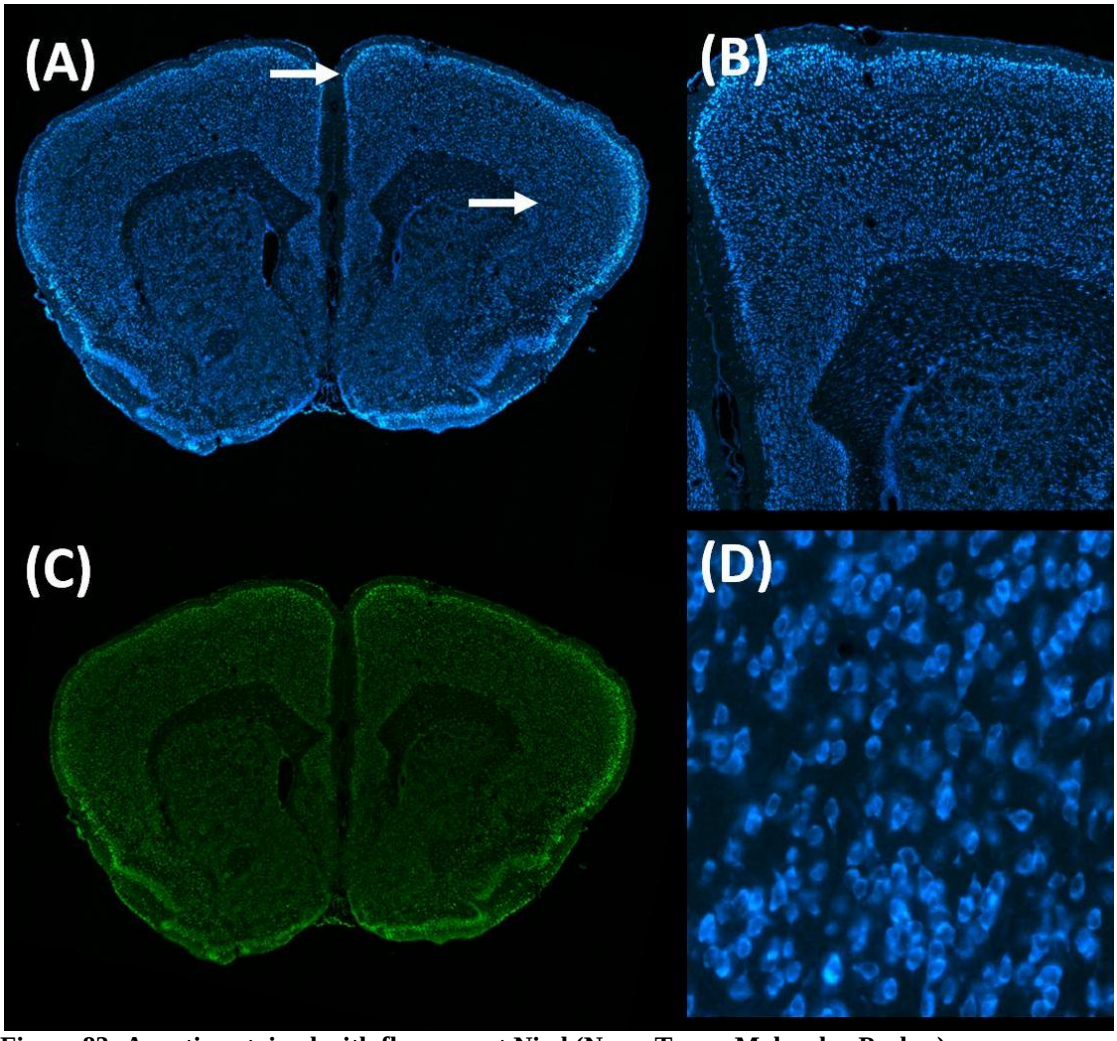

Figure 83: A section stained with fluorescent Nissl (NeuroTrace, Molecular Probes).
The native image is shown in (A). Just the green channel is shown in (B). One of the drawbacks of this stain is that it is not color channel specific and is clearly seen in the green channel. The arrows in (A) point to the regions that are shown at higher magnification in (B) and (D). The cortical layer differentiation is shown in (B) and a higher-magnification view of layer 5/6 is shown in (D). With this stain, individual cells can be identified, as with a standard Nissl stain.

Myelin Staining

Staining for myelinated fibers is a common neuroanatomy technique. We have applied the silver staining technique[85] to MBA processed material, to allow for a high-resolution view of myelinated fibers across the whole brain. As shown in Figure 84, individual fibers are well differentiated. Fibers can be seen throughout the layers of the cortex, including Layer 1 (B, C, E, F). Myelin staining was performed on coronal, sagittal and transverse sections. Per series, one set of alternating slides was coverslipped and imaged directly (A-F); the other was counterstained with Nissl and then imaged (G-I). The purpose of the counterstain was to allow simultaneous visualization of myelinated fibers and cell bodies, as shown in Figure 84I. Myelin data in the transverse plane are not shown below, but will be available through the web portal.

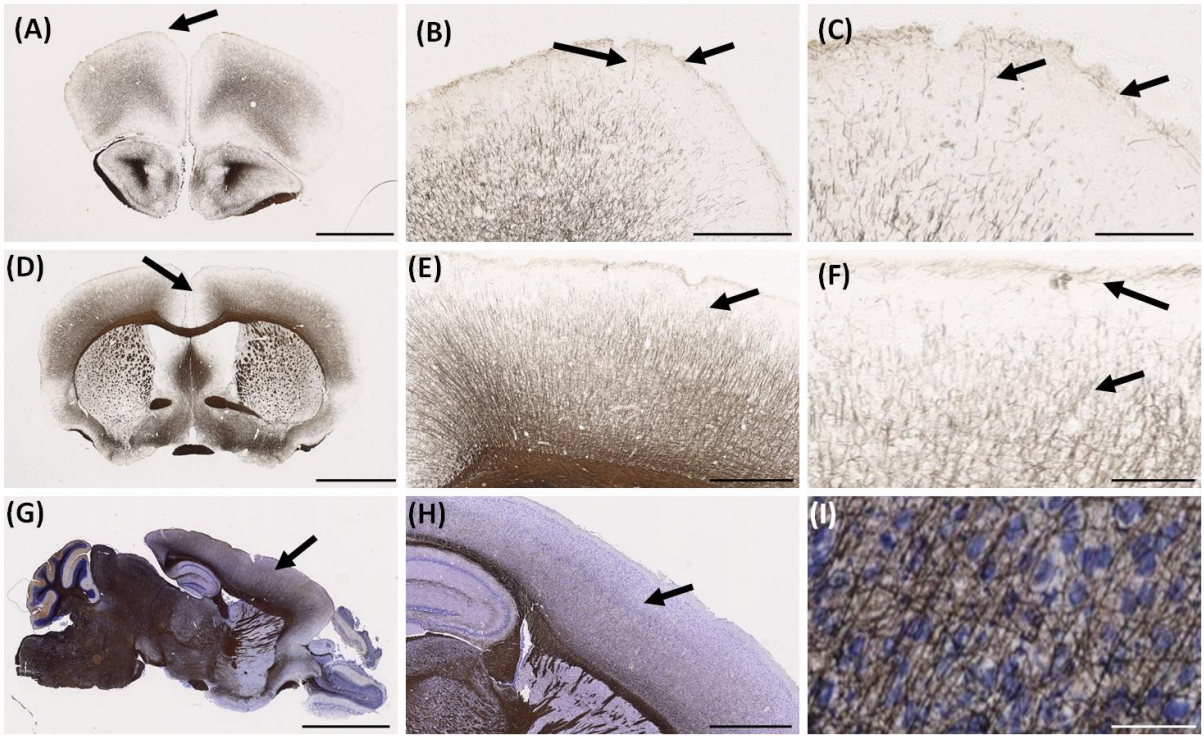

Figure 84: MBA processed material, stained for myelinated fibers
Low-magnification images are shown in (A), (D) and (G). At progressively higher magnifications (B and C, E and F), individual fibers are easily identifiable. Alternating sections were counterstained with Nissl, as shown in a sagitally sectioned brain (G, H and I) to allow for the simultaneous visualization of myelinated fibers and cell bodies. Scale bars are: 1.5mm, 500µm, 20µm, 2mm, 500µm, 135µm, 2.5mm, 1mm, 200µm.

c-Fos Staining

One specifically interesting application of the MBA pipeline has been to study the whole brain expression of c-Fos, an activity related early-immediate gene, in the learned helplessness model of depression in mice to examine the neuronal circuitry underlying helpless and resilient behaviors[93]. Unlike conventional studies that investigate changes only in a few brain regions, or throughout the brain but with very sparse sampling, this study is aimed at a more complete view of c-Fos expression. Sample data from this study are shown in Figure 85. At low-magnification (A) distinct clusters of expression can be seen. At high magnification (B, C, D), individual cells are quite apparent, versus background staining. The intensity of label is region specific. As with all MBA data, staining was performed throughout the brain and the data will be available for browsing and analysis.

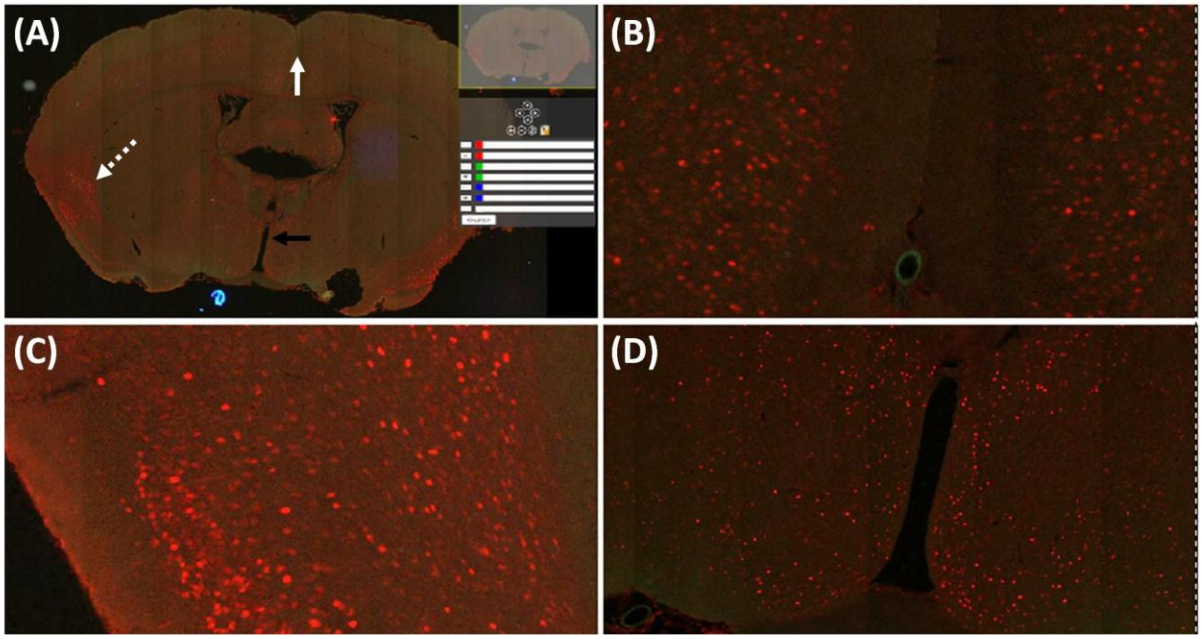

Figure 85: A section stained for c-Fos expression
Low-magnification in (A). The white arrow points to the expression in the anterior cingulate area of the cortex, shown at high-magnification in (B). The dotted white arrow points to the expression in lateral cortex, visceral area, shown at high-magnification in (C). The black arrow points to expression in the hypothalamus, around the third ventricle, shown at high-magnification in (D). Expression of c-Fos is seen in high intensity, against the background.

Tyrosine Hydroxylase (TH), Lectin (WFA) and DAPI Staining

One of the principle extensions of the MBA connectivity project is to obtain whole-brain data for common neuroanatomical biomarkers. In the example shown in Figure 86 and Figure 87, immunofluorescence (IF) staining is performed for Tyrosine Hydroxylase (TH) and Lectin (WFA). A DAPI counterstain is applied to help visualize cellular nuclei. TH staining is shown in green (Alex488); Lectin in red and DAPI in blue. This dataset is a prime example of the quality and volume of data that is produced by the MBA pipeline.

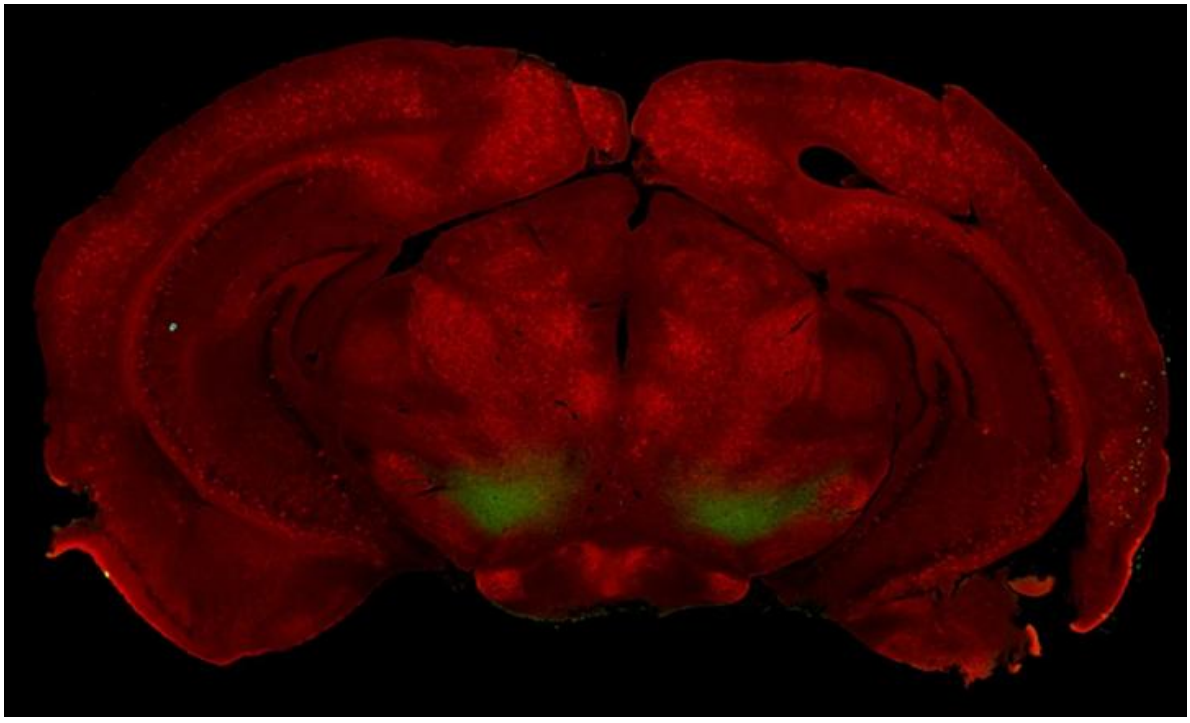

Figure 86: Low-magnification view of a section stained with Lectin and TH.

In Figure 87, a detailed analysis of the TH, Lectin and DAPI staining is shown. Each channel of the native image (A) is shown individually in B, C and E. For each, clear labeling is evident, as highlighted by the high-magnification images in D and F. To further show the cellular integrity of the data, confocal microscopy was performed on this section, using the Zeiss LSM 710. The imaged region is highlighted by a white dotted box in (A). As shown in G, H and I, the TH positive cells and fibers are quite apparent and easily distinguishable versus the background. A single positive TH fiber and cell is shown in (H), along with the DAPI counterstain.

The confocal imaging is able to achieve higher magnification, resolution and signal-to-noise ratio, than is possible with the NanoZoomer HT, but at the sacrifice of scan area. Therefore, it is advantageous to use both techniques to image the data - NanoZoomer to obtain a whole-slide/ whole-brain view of the data and confocal microscopy to focus on selected regions. For this reason, all MBA slides are saved and archived for later use.

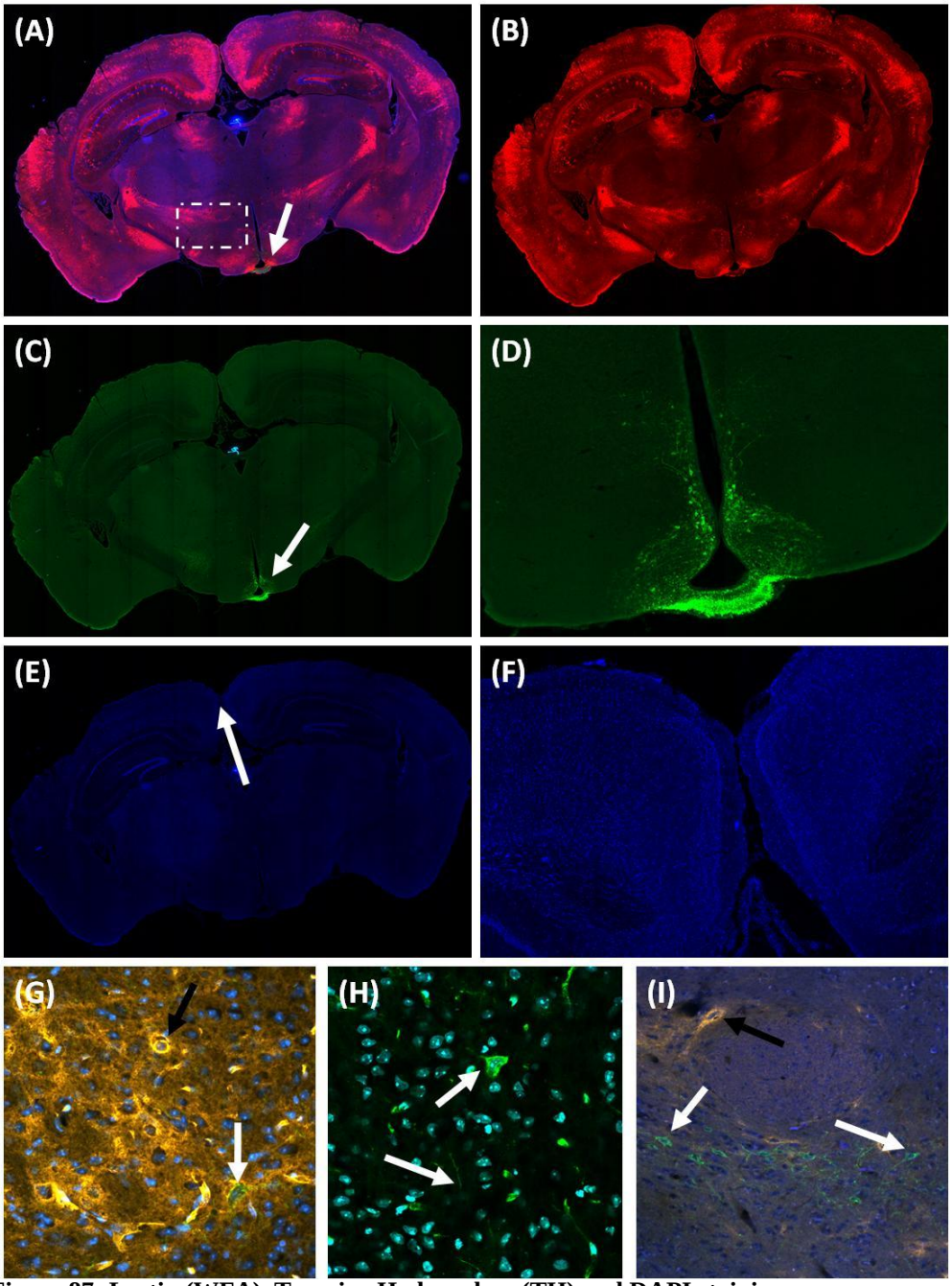

Figure 87: Lectin (WFA), Tyrosine Hydroxylase (TH) and DAPI staining

Low-magnification and high-magnification NanoZoomer images (A-F) are shown, along with confocal images of the data (G-I). TH is in green; Lectin in red and DAPI in blue for all images. The native image, of all three fluorophores is shown in (A). The white arrow indicates the bulk of the TH staining. The dotted white box is the area that was imaged with the Zeiss LSM 710 confocal microscope. Just the red channel (Lectin) is shown in (B). Just the green channel (TH) is shown in (C) and (D). The white arrow in (C) points to the TH staining, which is shown at high magnification in (D). The intensity and quality of the staining is apparent in (D). Just the blue channel (DAPI) is shown in (E) and (F). The white arrow points to the cortical DAPI staining, that is shown at higher-magnification in (F). Confocal images show high-resolution TH and Lectin staining. In (G-I) the white arrows point to TH positive cells and fibers; the black arrow points to Lectin staining (perineuronal nets).

Rattus norvegicus

Though designed for mouse, the MBA pipeline can be retrofitted to process data from other species, such as Rattus norvegicus (rat). The rat brain is about 2X larger than that of mouse, which makes it more difficult and time consuming to process. Nonetheless, the data quality is similar to that obtained in mouse. A typical Nissl stain of a rat brain is shown in Figure 88 (A&B). Cortical layers are identifiable. A myelin stain of neighboring section is shown in Figure 88 (C&D). As in mouse, individual fibers are well differentiated in the cortex, even in Layer 1.

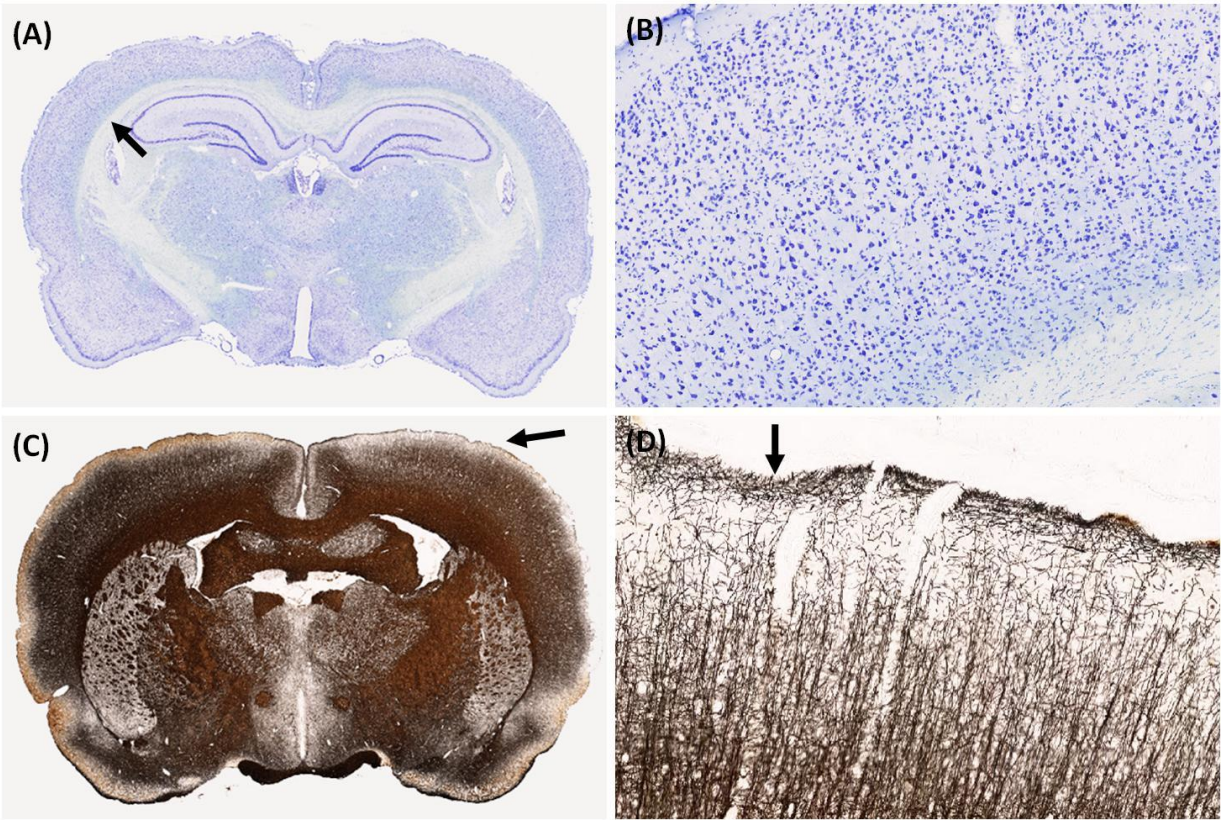

Figure 88: Nissl and myelin staining of a rat brain
Nissl (A) and Myelin (C) sections of a coronally sectioned rat brain are shown. The black arrows in (A) and (C) point to the region that is shown at higher-magnification in (B) and (D). In (D) the black arrow points to the myelinated fibers that are clearly visible in Layer1.

As with mouse, Rattus norvegicus can also be used for connectivity experiments. An AAV injection into the thalamus is shown in Figure 89. This dataset was counterstained with DAPI to aid in the visualization of the label (C). The AAV injection is quite vibrant at both the injection site and the labeled fibers leading to the cortex. Individual fibers can be seen, against the DAPI counterstain (D).

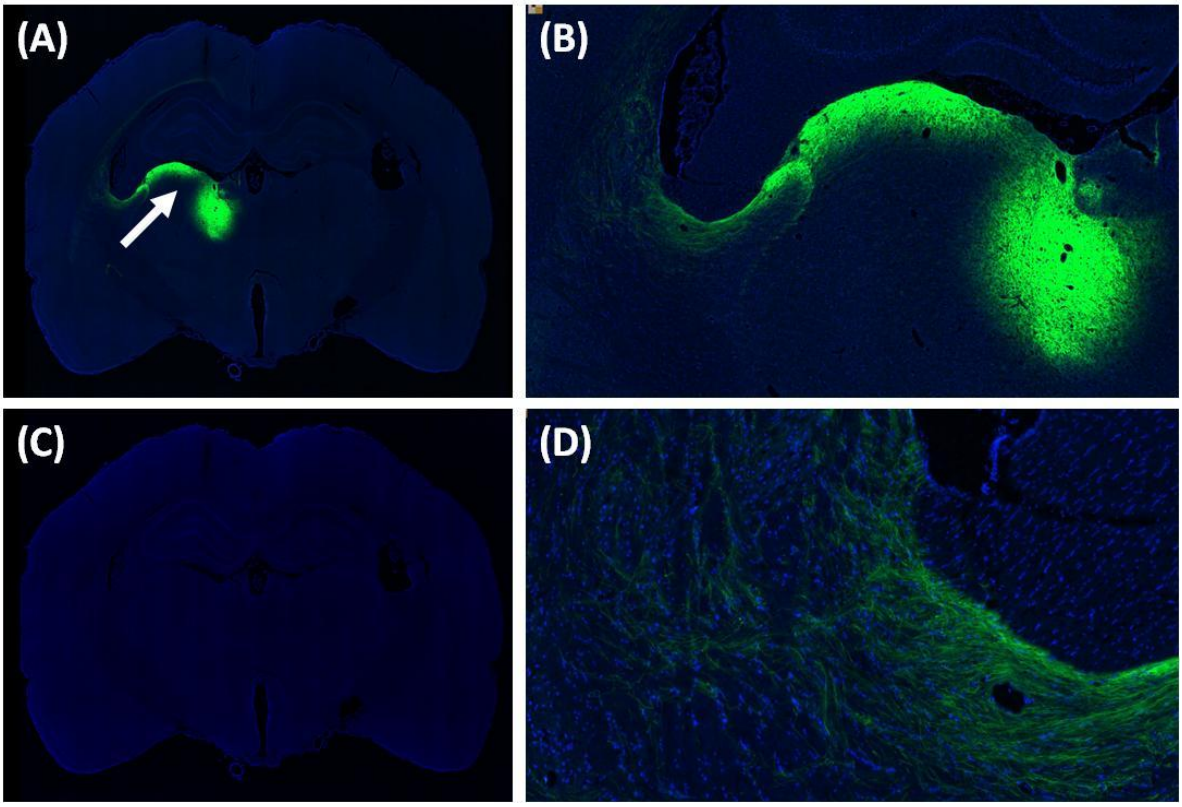

Figure 89: An AAV injection into the thalamus in rat
A low-magnification view of the section is shown in (A). The white arrow indicates the injection region. Projection fibers, through the white matter are seen leading to the cortex. The section was counterstained with DAPI, as shown in (C). At high-magnification (D), the labeled fibers can be easily identified in the DAPI counterstain.

As shown in Figure 90, the terminal projections from this injection can be followed to the cortex. This is anterior to the injection site. As with principle MBA data, all sections of this series are saved and digitized and will be available on the portal for browsing.

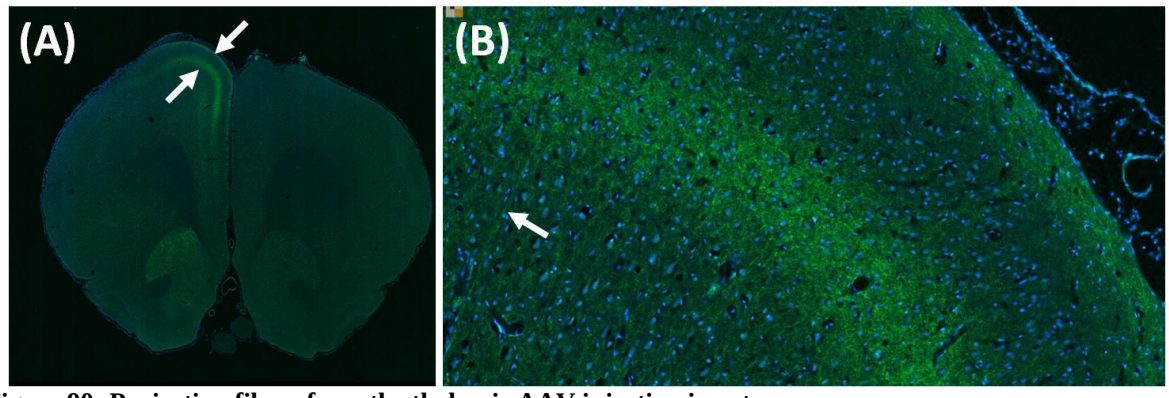

Figure 90: Projection fibers from the thalamic AAV injection in rat
The projection fibers from the AAV injection directed into the thalamus can be seen in the anterior cingulate area (ACad) and the secondary somatomotor area (MOs). Layers 1 and 5 of the cortex are predominantly labeled, as indicated by the arrows. The gap in Layer 2-4 can be seen at higher-magnification (B).

Genetically Engineered Mouse Models

One of the unique applications of the MBA pipeline has been to process mouse models that have been engineered to natively express GFP or a similar reporter in only specific cell types[94]. The MBA pipeline is ideal for this application, because it is a practical means of obtaining a whole-brain understanding of the expression of a specific cell type. The high-resolution imaging of the 20µm thick sections means that the number of overlapping cells per section will be considerably less than with thicker sections (50µm). This is important for whole-brain counting of labeled cells and for use of these models to study conditions such as Autism Spectrum Disorder (ASD)[95]. In Figure 91, whole-section data is shown of GAD2 cells, expressing GFP. As shown in the insert at the bottom right, the nuclear label is very clear and individual cells can be easily identified. As with all MBA material, all sections of the whole-brain are available for browsing and analysis.

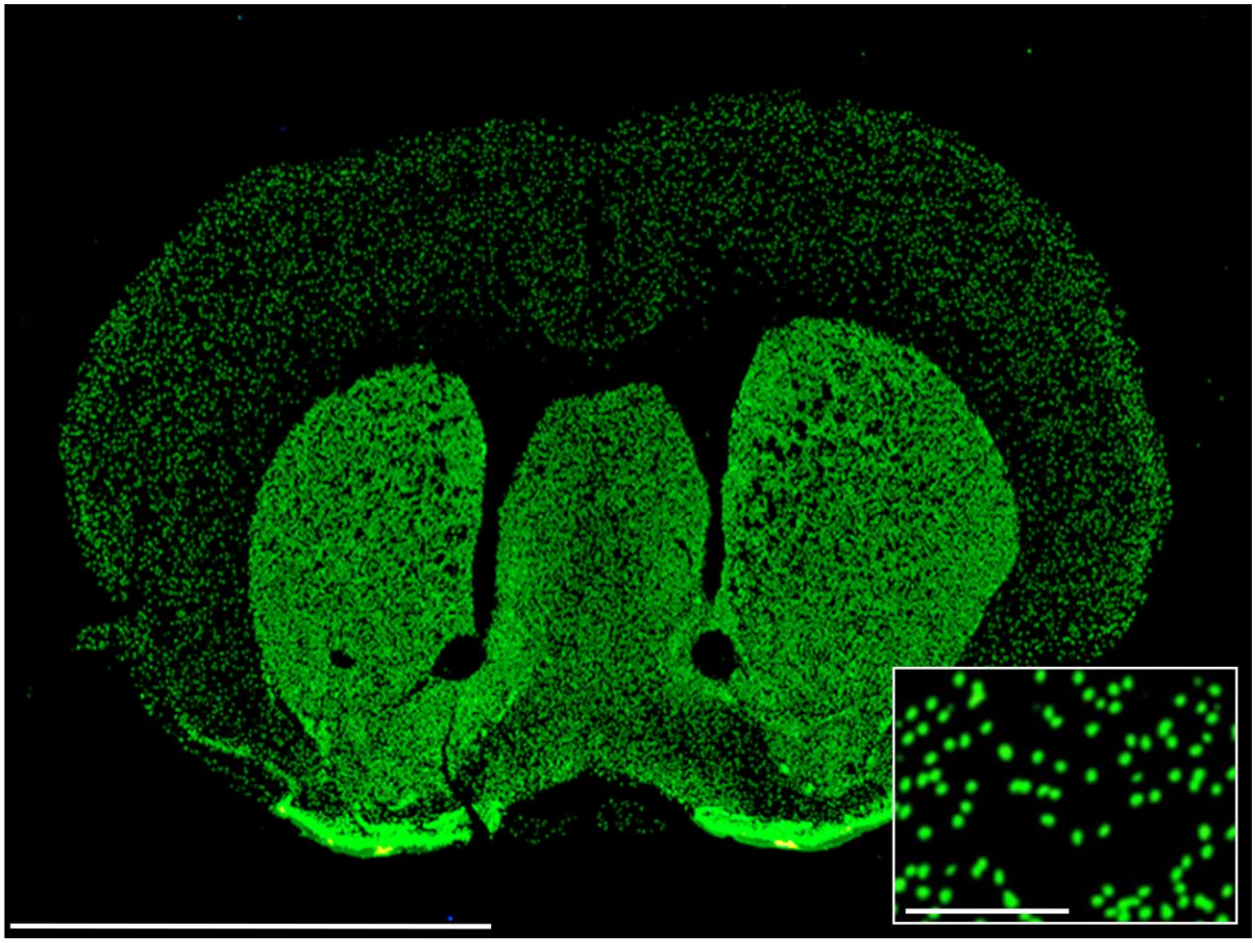

Figure 91: Coronal section of a mouse brain expressing Cre-dependent GFP in GAD2 GABAergic cells. Low-magnification view of a coronal section, acquired on a NanoZoomer HT (in-plane resolution = .5um/pixel). Scale bar is 5mm. High-magnification view of caudoputamen, demonstrating easily identified cell nuclei. Scale Bar is 300um.

Figure 92 - Figure 94 show data for parvalbumin (PV), somatostatin (SOM) and corticotrophin releasing hormone (CRH) positive cells, expressing GFP. In all cases, the 2-D sections are well preserved and the nuclear signal is quite distinct, especially at high-magnification (D).

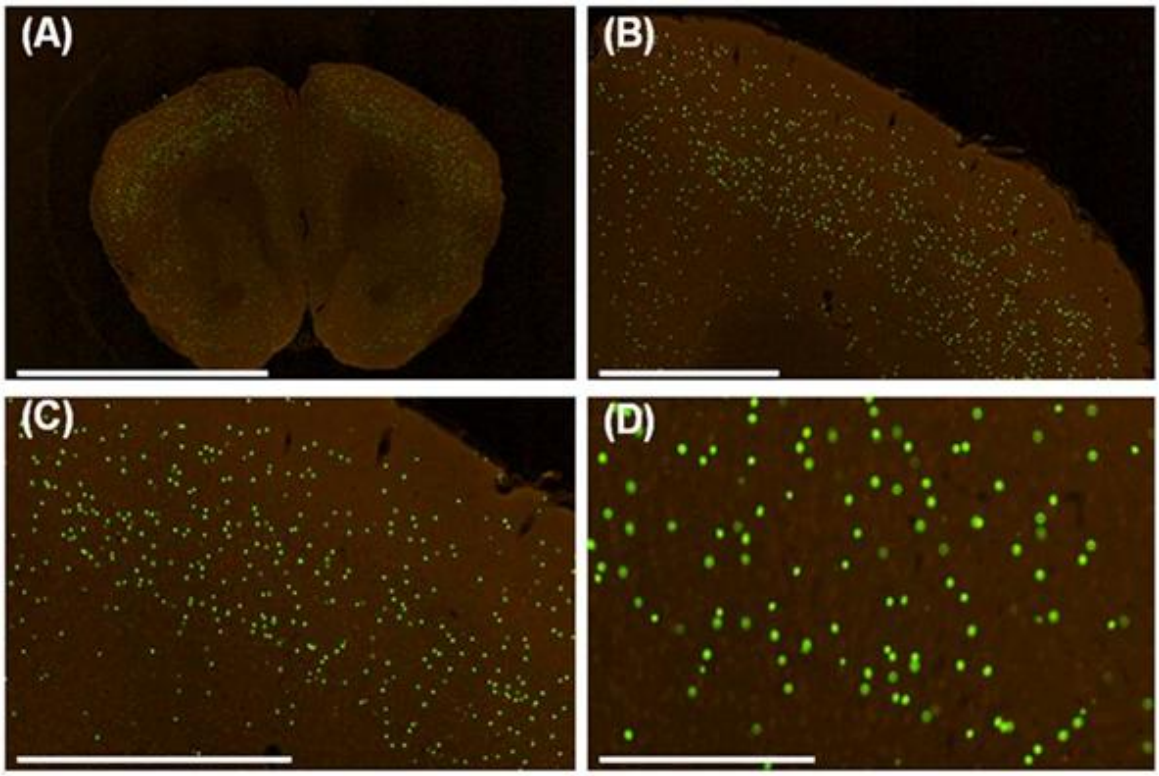

Figure 92: Coronal section of an adult mouse brain (56 day old) expressing Cre-dependent nuclear GFP (H2B-GFP) in Parvalbumin (PV)+ soma-targeting class of GABAergic cells.
Low-magnification view (A, B) of a coronal section, acquired on a NanoZoomer HT, shows PV+ cells distribution in different brain regions including the cortex, striatum and nucleus accumbens High-magnification views (C, D) of cortex, demonstrating easily identifiable individual nuclei. PV+ nuclei are distributed across layers 2-6 of the cortex. Scale bars are 4mm, 1mm; 900um, and 300um.

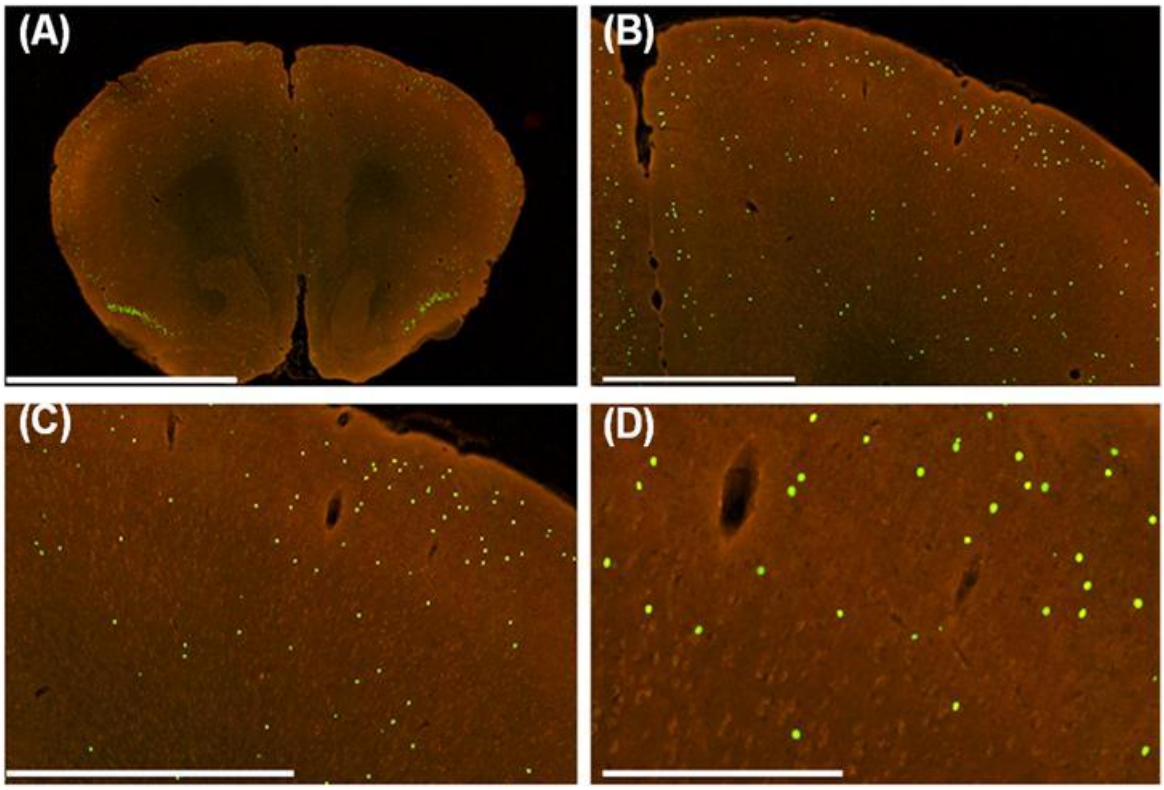

Figure 93: Coronal section of a mouse brain (32 day old) expressing Cre-dependent nuclear GFP (H2B-GFP) in Corticotrophin releasing hormone (CRH)+ GABAergic cells.
Low-magnification view (A, B) of a coronal section, shows the sparse CRH+ nuclei distribution in the brain. High-magnification views (C, D) of cortex, demonstrating easily identifiable individual nuclei. CRH+ nuclei are predominantly distributed in the superficial layers of the cortex. Scale bars are 3mm, 1mm; 800um, and 300um.

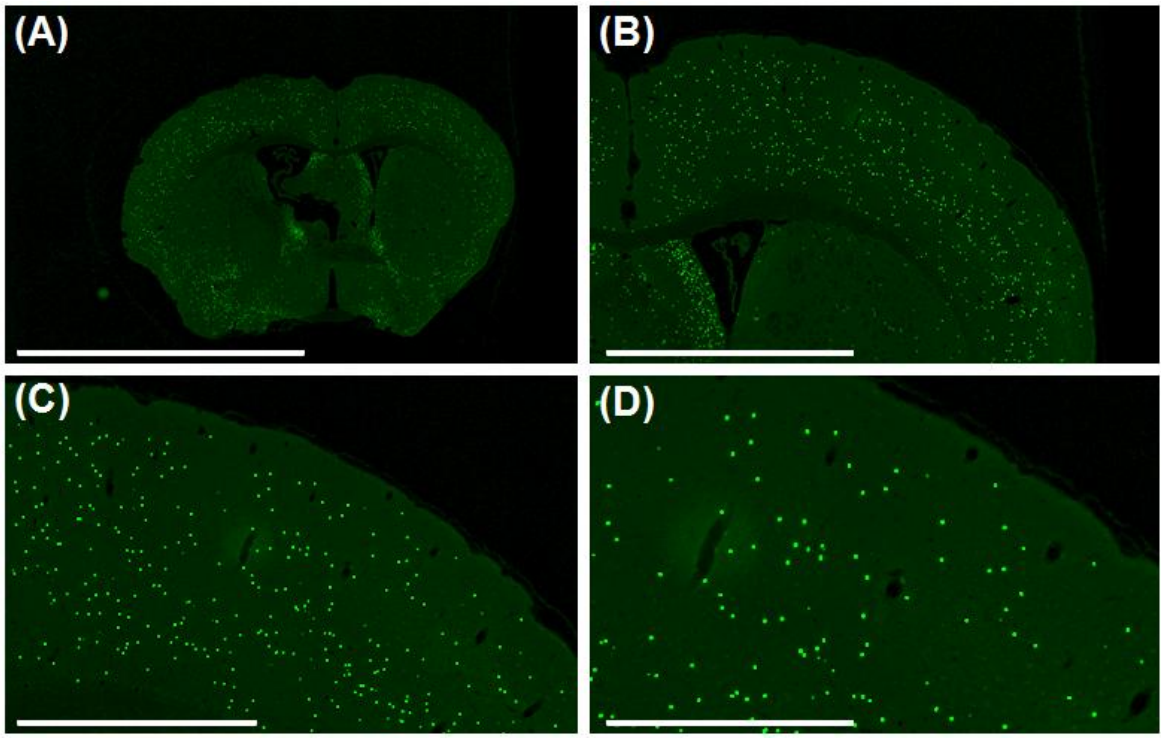

Figure 94: Coronal section of an adult mouse brain (56 day old) expressing Cre-dependent nuclear GFP (H2B-GFP) in Somatostatin (SOM)+ dendrite-targeting class of GABAergic cells.
Low-magnification views (A, B) of a coronal section, acquired on a NanoZoomer HT, shows SOM+ cells distribution in different brain regions including the cortex, striatum and nucleus accumbens. High-magnification views (C, D) of cortex, demonstrating easily identifiable individual nuclei. SOM+ nuclei are distributed across all layers of the cortex. Scale bars are 6mm, 2mm; 1mm, and 600um.

CHAPTER 6: Conclusion

This dissertation focuses on the design, implementation and use of an engineering system to answer a fundamental neuroscience question. This system is a "pipeline" (also referred to as a "machine"), by which a mouse is transformed into a web accessible dataset of 2D histological sections. The role of the pipeline is to optimize each step of this transformation and ensure maximum data quality, in a standardized manner. Though the pipeline can be used for many applications, as discussed in *Chapter 5*, the principle use is to gather the material necessary for the *Development of the First Comprehensive Neural Connectivity Map of the Mouse*. This project is an effort to address the lack of comprehensive understanding of long-range connections in the model organisms. Only 10% of all mesoscale connections in the most studied mammal (rat) have been catalogued and only perhaps one third have been probed at all. To address this problem, the project calls for the injection of neuronal tracers, to be performed in a grid-like manner, spanning the entire brain. The injections are targeted to the left-hemisphere of the mouse brain. A total of 250 injection sites will be probed. The sites are volumetrically distributed across all regions of the mouse brain, as defined by the Allen Reference Atlas. Each site is to be probed four times, across four different animals. Two of the injections are with an anterograde tracer, which labels the output connections; and two with a retrograde tracer, which labels input connections to the site. Per tracer type, one of the injections is with a conventional tracer, such as Cholera Toxin(CTB) for retrograde tracing and Biotinylated Dextran Amines (BDA) for anterograde tracing; the other is with a viral tracer, such as Rabies or Adeno-Associated Virus (AAV). This paradigm helps to ensure that all of the connections from a given site are labeled by at least one of the tracers.

For all injected brains, the tissue is processed in an identical manner, such that the injected tracer can be tracked across the volume of the entire brain. This is a major contrast to conventional neuroanatomy, where the processing of the brain is subject to the region-of-interest. Processing the entire brain, regardless of the injection site, allows for validation of known connections of major regions, and for the labeling of circuits to less-known regions. Revealing connections to regions that would otherwise be unknown, is an central goal of the project. This project is a major effort, with the potential to transform neuroanatomy in the same way that the Allen Mouse Brain Atlas changed rodent neurogenetics.

This project has several major deliverables. *Firstly*, is the release of 2D histological sections, which show the progression of the injected tracer, across the each brain. Once this is accomplished for all 1000 brains (250 injection sites X 4 tracers per site), the data will be computationally and manual curated into connectivity matrix. This matrix will be close in form to that compiled by the Brain Architecture Management System (BAMS), but instead of being just 10% full, the matrix will be complete. The primary intent of this effort is to provide a web-accessible resource that can be used to easily understand the connectivity of a given region. As of now, such a resource does not exist, and if a researcher is interested in the connectivity of a specific region, in order to better design their experiments, the options are to either search the literature or perform the injection into that region. This is especially evident in electrophysiological studies. A literature survey is desirable for practical reasons (time, money, and resources) but often results in an incomplete understanding of the connections, especially for regions that have not been extensively studied. Therefore, the researcher is often tasked with performing injections into the region-of-interest. However, since connectivity investigation is not a simple task and does require extensive expertise, the resulting data is often marked by artifacts and also does not result in a complete view of the connections. As a result, the researcher makes assumptions based on unclear data. In the case of electrophysiology, "without any reference to underlying connectivity it is difficult to interpret measured physiological activity or the effects of microstimulation. Studies that consider the internal dynamics of the brain, including studies of selective attention, often make arguments about top-down or bottom-up processes, which are ultimately contingent on neuroanatomical information that is frequently deficient"[18].

Secondly, this connectivity resource can also be used as a means of validating new anatomical methods. These methods can include new neuronal tracers, or non-invasive imaging technologies. In the case of new tracers, this connectivity dataset can be used to ensure that all the connections for a given region are labeled and not just a subset. This is a critical validation step, which is rarely performed thoroughly, but is essential to ensure that new tools results in the same "anatomical" data, as established methods. Viral tracers are often accepted as face value to have the same efficacy as conventional tracers (those that require histochemistry) but in fact, only some do. This connectivity matrix will allow for a direct comparison on any neuronal tracer, to known standards, across 250 injection sites. In the case of imaging technologies, especially Functional Magnetic Resonance Imaging (fMRI) studies, this connectivity dataset can

be used as ground truth to explain the activity patterns. The overarching limitation of fMRI based research is understanding the complex relationship between correlations in the blood oxygenation level dependent (BOLD) response and physical connections between the neurons indirectly giving rise to that response. This problem, is compounded with the use of non-standardized statistical models to analyze the raw data. This results in subjective findings that need to be structured and validated through different technology. This connectivity dataset can be used to determine if a set of activated regions is known to be inter-connected through either retrograde or anterograde connections. These findings can thereby be used to either refine the experimental parameters of the study or focus on the other physiological phenomenon that is responsible for activation in regions that are known not to be physically connected.

Thirdly, a baseline connectivity map can also serve as a foundation for subsequent study of circuit polymorphisms across genetic mutants. The ability to objectively quantify connectivity alterations in mouse disease models has the potential to transform our understanding of the pathophysiology of neuropsychiatric disorders by helping to close the genotype-phenotype gap that plagues psychiatric genetics. This connectivity dataset will have major impact on the growing number of researchers studying mouse models of disease, and a more general and gradual impact on clinical neuropsychiatry and psychiatric genetics[18].

Fourthly, a major use case of this connectivity database will be for education. One of the persisting problems with neuroanatomy is how to effectively communicate labeled connections to an unfamiliar audience, such as students. This resource will allow for the matrix based visualization of connections, but with the ability to access the raw 2D histological data for each element of the matrix. As a result, the user does not have to accept the matrix at face value, but can validate that each element of a particular injection region, was appropriately populated. This is especially valuable in the case of small brain regions, which are difficult to identify, and their designation depends on which reference atlas is used for the analysis. Along the same lines, this reference can be used as a valuable training tool, to show students the extent of a given injection, and how emphasis should be equally placed on regions with strong and weak label. An inexperienced anatomist will often overlook regions with weak label, as expected, but also falsely classify noise as an abundance of signal. This connectivity reference can be used to train students to not make these common mistakes and to standardize the analysis and annotation of connectivity data. One of the major problems with BAMS and similar resources is the lack of

coherency of language and analysis methods that used throughout published literature. As an example, the same region can be referred to by different names, regardless of the atlas that was sighted as the reference. The same holds for the type of connections that are evident in a given region.

Finally, in addition to the scientific value of the data produced as part of this dissertation, and the connectivity reference that will be compiled out of it, this project can be used as a model of high-throughput experimental neuroanatomy. This project had a tenth of the resources and budget of the Allen Institute for Brain Science, but was able to process a similar number of animals and result in an equally extensive dataset, through with a different purpose. Because of this, the data production pipeline can be replicated in other laboratories and used for analogous connectivity research or adapted for other applications. Two such applications is the use of the pipeline for whole-brain characterization of (1) biomarkers, like cFOS and (2) mouse models of GABAergic cell types. A sample of this type of data is shown in *Chapter 5*. With the exception of the Tracer Injection component, which is not required for these applications, all other elements of the pipeline are unchanged. This results in a fine sampling of the whole-brain distribution of specifically labeled cells. This data can either be used to determine the regional distribution of the labeled cells, and/or correlated directly with the connectivity data, to help understand the brain organization.

Bibliography:

1. Vesalius, A., *De humani corporis fabrica libri septem*1543, Basel: J. Oporinus.
2. Tubbs, R., et al., *The bishop and anatomist Niels Stensen (1638–1686) and his contributions to our early understanding of the brain.* Child's Nervous System. 27(1): p. 1-6.
3. *Ueber eine neue Untersuchungsmethode des Centralorgans zur Feststellung der Localisation der Nervenzellen. Neurologisches Centralblatt, Leipzig, 1894, 13: 507-508.*
4. *Golgi C. "On the cycle of development of malarial parasites in tertian fever: differential diagnosis between the intracellular parasites of tertian and quartant fever. Archivio per le Scienza Mediche. 13: 1730196. 1889.*
5. *Koch R (1878) Untersuchungen über die Aetiologie der Wundinfectionskrankheiten. Vogel, Leipzig.*
6. Marchi, V. and G. Algeri, *Sulle degenerazioni discendenti consecutive a lesioni della corteccia cerebrale.* Revista sperimentale di freniatria e medicina legale in relazione con l'antropologia e le scienze giuridiche e sociali. Reggio-Emilia, 1885. 11: p. 492Â–494.
7. Smith, M.C., *The recognition and prevention of artefacts of the Marchi method.* J Neurol Neurosurg Psychiatry, 1956. 19(2): p. 74-83.
8. Sarikcioglu, L., *Johann Bernhard Aloys von Gudden: an outstanding scientist.* J Neurol Neurosurg Psychiatry, 2007. 78(2): p. 195.
9. Johansen, A., *Staining methods and histochemistry of normal gastric mucin.* Acta Pathol Microbiol Scand Suppl, 1970. 212: p. Suppl 212:57+.
10. Bassetti, C.L. and E.C. Jagella, *Joseph Jules Dejerine (1849-1917).* J Neurol, 2006. 253(6): p. 823-4.
11. Waller, A., *Experiments on the Section of the Glossopharyngeal and Hypoglossal Nerves of the Frog, and Observations of the Alterations Produced Thereby in the Structure of Their Primitive Fibres.* Philosophical Transactions of the Royal Society of London, 1850. 140: p. 423-429.
12. Schmahmann, J.D. and D.N. Pandya, *Cerebral white matter--historical evolution of facts and notions concerning the organization of the fiber pathways of the brain.* J Hist Neurosci, 2007. 16(3): p. 237-67.
13. Dejerine, J., *Anatomie des centres nerveux*1895, Paris: Rueff.
14. Cowan, W.M., et al., *The autoradiographic demonstration of axonal connections in the central nervous system.* Brain Res, 1972. 37(1): p. 21-51.
15. Lavail, J.H. and M.M. Lavail, *Retrograde Axonal Transport in the Central Nervous System.* Science, 1972. 176(4042): p. 1416-1417.
16. Kristensson, K. and Y. Olsson, *Retrograde axonal transport of protein.* Brain Res, 1971. 29(2): p. 363-5.
17. Hsu, S.M., L. Raine, and H. Fanger, *The use of antiavidin antibody and avidin-biotin-peroxidase complex in immunoperoxidase technics.* Am J Clin Pathol, 1981. 75(6): p. 816-21.
18. Bohland, J.W., et al., *A Proposal for a Coordinated Effort for the Determination of Brainwide Neuroanatomical Connectivity in Model Organisms at a Mesoscopic Scale.* PLoS Comput Biol, 2009. 5(3): p. e1000334.
19. Luppi, P.H., P. Fort, and M. Jouvet, *Iontophoretic application of unconjugated cholera toxin B subunit (CTb) combined with immunohistochemistry of neurochemical substances: a method for transmitter identification of retrogradely labeled neurons.* Brain Res, 1990. 534(1-2): p. 209-24.

20. Jennings, B.R., et al., *Use of avidin-biotinylated horseradish peroxidase complex for visualization of spirochetes.* J Clin Microbiol, 1983. 18(5): p. 1250-1.
21. Gerfen, C.R. and P.E. Sawchenko, *An anterograde neuroanatomical tracing method that shows the detailed morphology of neurons, their axons and terminals: immunohistochemical localization of an axonally transported plant lectin, Phaseolus vulgaris leucoagglutinin (PHA-L).* Brain Res, 1984. 290(2): p. 219-38.
22. Casanova, M.F., et al., *Asperger's Syndrome and Cortical Neuropathology.* Journal of Child Neurology, 2002. 17(2): p. 142-145.
23. Mikula, S., et al., *Internet-enabled high-resolution brain mapping and virtual microscopy.* Neuroimage, 2007. 35(1): p. 9-15.
24. Lein, E.S., et al., *Genome-wide atlas of gene expression in the adult mouse brain.* Nature, 2007. 445(7124): p. 168-76.
25. Latham, J. and A. Wilson, *The Great DNA Data Deficit: Are Genes for Disease a Mirage?* The Bioscience Resource Project Commentaries, 2010.
26. Chiang, A.-S., et al., *Three-Dimensional Reconstruction of Brain-wide Wiring Networks in Drosophila at Single-Cell Resolution.* Current biology : CB. 21(1): p. 1-11.
27. Grange, P. and P.P. Mitra, *Algorithmic choice of coordinates for injections into the brain: encoding a neuroanatomical atlas on a grid.* arXiv:1104.2616, 2011.
28. Jacobs, P.F. and D.T. Reid, *Rapid prototyping & manufacturing : fundamentals of stereolithography*. 1st ed1992, Dearborn, MI: Society of Manufacturing Engineers in cooperation with the Computer and Automated Systems Association of SME. 434 p.
29. Lokesh, K. and P.K. Jain, *Selection of Rapid Prototyping Technology* Advances in Production Engineering & Management, 2010. 5(2): p. 75-84.
30. Cetin, A., et al., *Stereotaxic gene delivery in the rodent brain.* Nat. Protocols, 2007. 1(6): p. 3166-3173.
31. Athos, J. and D.R. Storm, *High precision stereotaxic surgery in mice.* Curr Protoc Neurosci, 2001.
32. Instruments, D.K.
33. Riley, W.F., L.D. Sturges, and D.H. Morris, *Statics and mechanics of materials : an integrated approach*. 2nd ed2002, New York: J. Wiley. ix, 723 p.
34. Waldron, K.J. and G.L. Kinzel, *Kinematics, dynamics, and design of machinery*. 2nd ed2004, Hoboken, NJ: J. Wiley. xi, 668 p.
35. McCaman, R.E., D.G. McKenna, and J.K. Ono, *A pressure system for intracellular and extracellular ejections of picoliter volumes.* Brain Res, 1977. 136(1): p. 141-7.
36. Sakai, M., H. Sakai, and C.D. Woody, *Intracellular staining of cortical neurons by pressure microinjection of horseradish peroxidase and recovery by core biopsy.* Exp Neurol, 1978. 58(1): p. 138-44.
37. Messier, C., S. Émond, and K. Ethier, *New Techniques in Stereotaxic Surgery and Anesthesia in the Mouse.* Pharmacology Biochemistry and Behavior, 1999. 63(2): p. 313-318.
38. Paxinos, G. and K.B.J. Franklin, *The Mouse Brain in Stereotaxic Coordinates*. Second Edition ed2003: Academic Press.
39. Dong, H.W. and T.A.I.f.B. Science, *The Allen Reference Atlas*2008: Wiley.
40. Blasiak, T., et al., *A new approach to detection of the bregma point on the rat skull.* J Neurosci Methods, 2010. 185(2): p. 199-203.

41. Chan, E., et al., *Development of a high resolution three-dimensional surgical atlas of the murine head for strains 129S1/SvImJ and C57Bl/6J using magnetic resonance imaging and micro-computed tomography.* Neuroscience, 2007. 144(2): p. 604-15.
42. Dorr, A.E., et al., *High resolution three-dimensional brain atlas using an average magnetic resonance image of 40 adult C57Bl/6J mice.* Neuroimage, 2008. 42(1): p. 60-9.
43. Kiernan, J.A., *Formaldehyde, formalin, paraformaldehyde and glutaraldehyde: what they are and what they do* Microsc. Today 2000. 00-1:8-1.
44. Gerfen, C.R., *Basic neuroanatomical methods.* Curr Protoc Neurosci, 2003. Chapter 1: p. Unit 1 1.
45. Rosene, D.L. and M.M. Mesulam, *Fixation variables in horseradish peroxidase neurohistochemistry. I. The effect of fixation time and perfusion procedures upon enzyme activity.* J Histochem Cytochem, 1978. 26(1): p. 28-39.
46. *Perfusion One- Hand Pumped Instrument for Pressurized Sacriffice Perfusion.* 2007.
47. Goodman, T. and A. Moore, *A simple flow indicator for use in perfusion fixation.* Stain Technol, 1971. 46(1): p. 36-7.
48. Emge, D.J., *Tissue Freezing methods for Cryostat Sectioning* in *Basic Tissue Freezing Methods*.
49. Werner, M., et al., *Effect of formalin tissue fixation and processing on immunohistochemistry.* Am J Surg Pathol, 2000. 24(7): p. 1016-9.
50. Baker, J.R., *Principles of biological microtechnique; a study of fixation and dyeing*1958, London, New York,: Methuen; Wiley. 357 p.
51. Carson, F.L. and C. Hladik, *Histotechnology: A Self-Instructional Text*. 3rd ed2009.
52. Ramos-Vara, J.A., *Technical aspects of immunohistochemistry.* Vet Pathol, 2005. 42(4): p. 405-26.
53. *Brain Block One - Encasement Gels for reproducible Brain Orientation.* 2008.
54. *A Practical Guide to Frozen Section Technique*, ed. S.R. Peters2009: Springer.
55. Jiang, X., et al., *Histological analysis of GFP expression in murine bone.* J Histochem Cytochem, 2005. 53(5): p. 593-602.
56. Jacquet, R., J. Hillyer, and W.J. Landis, *Analysis of connective tissues by laser capture microdissection and reverse transcriptase-polymerase chain reaction.* Analytical Biochemistry, 2005. 337(1): p. 22-34.
57. Salie, R., et al., *A Rapid, Nonradioactive In Situ Hybridization Technique for Use on Cryosectioned Adult Mouse Bone.* Calcified Tissue International, 2008. 83(3): p. 212-221.
58. Watts, G.M., et al., *Manifestations of inflammatory arthritis are critically dependent on LFA-1.* J Immunol, 2005. 174(6): p. 3668-75.
59. Micke, P., et al., *Biobanking of fresh frozen tissue: RNA is stable in nonfixed surgical specimens.* Lab Invest, 2006. 86(2): p. 202-11.
60. Masuzawa, T., et al., *Ultraviolet photodetector using a-Se anode and diamond cold cathode.* Vacuum Nanoelectronics Conference (IVNC), 2011 24th International 2011.
61. Haines, D.M. and B.J. Chelack, *Technical considerations for developing enzyme immunohistochemical staining procedures on formalin-fixed paraffin-embedded tissues for diagnostic pathology.* J Vet Diagn Invest, 1991. 3(1): p. 101-12.
62. Hsu, S.M., L. Raine, and H. Fanger, *Use of avidin-biotin-peroxidase complex (ABC) in immunoperoxidase techniques: a comparison between ABC and unlabeled antibody (PAP) procedures.* J Histochem Cytochem, 1981. 29(4): p. 577-80.

63. Ohara, P., et al., *Anatomy 103: Nissl, H&E and Golgi (Silver) stain*
64. Takahashi, T., *Staining/covering system*, USPTO, Editor 2005, Sakura Seiki Co.
65. Pawley, J., *Handbook of biological confocal microscopy*. 2nd edition ed2005: Springer.
66. Yuste, R., *Imaging: A Laboratory Manual*2011, Cold Spring Harbor, New York: Cold Spring Harbor Press.
67. Espada, J., et al., *Non-aqueous permanent mounting for immunofluorescence microscopy.* Histochem Cell Biol, 2005. 123(3): p. 329-34.
68. Conte, W.L., H. Kamishina, and R.L. Reep, *Multiple neuroanatomical tract-tracing using fluorescent Alexa Fluor conjugates of cholera toxin subunit B in rats.* Nat Protoc, 2009. 4(8): p. 1157-66.
69. Norman K. Rhett, K.K.T., Mark V. Corl, Wai Bun Wong, Ngoc Van Le, Glenn K. Takayama, *Method and apparatus for automatic tissue staining*, O. Ueda, Editor 2001, Lab Vision Corporation.
70. Rockland, K., *Nissl Stain of Cortical Layers*, Massachusetts Institute of Technology.
71. Rockland, K.S. and G.W. Van Hoesen, *Some temporal and parietal cortical connections converge in CA1 of the primate hippocampus.* Cereb Cortex, 1999. 9(3): p. 232-7.
72. Kamino, H. and S.T. Tam, *Immunoperoxidase technique modified by counterstain with azure B as a diagnostic aid in evaluating heavily pigmented melanocytic neoplasms.* J Cutan Pathol, 1991. 18(6): p. 436-9.
73. Scordato, A. and S. Schwartz, *Nikon Microscopy University: Fluorescence Filter Combinations.*
74. Soenksen, D.G., *Fully automatic rapid microscope slide scanner*, USPTO, Editor 2004, Aperio Technologies, Inc.
75. Henderson, C.J., et al., *Slide holder for an automated slide loader*, USPTO, Editor 2002, Leica Biosystems
76. Ludl, H. and D.S. Denu, *Automated slide loader cassette for microscope*, USPTO, Editor 2001, Ludl Electronics Products, Ltd.
77. Pawley, J., *The 39 steps: a cautionary tale of quantitative 3-D fluorescence microscopy.* Biotechniques, 2000. 28(5): p. 884-6, 888.
78. Bernas, T., et al., *Precision of light intensity measurement in biological optical microscopy.* J Microsc, 2007. 226(Pt 2): p. 163-74.
79. Rojo, M.G., et al., *Critical Comparison of 31 Commercially Available Digital Slide Systems in Pathology.* International Journal of Surgical Pathology, 2006. 14(4): p. 285-305.
80. *P. Deutsch, Gzip file format specification, Version 4.3, Technical report, Aladdin Enterprises, 1996.*
81. Technology, P., *Keeping Storage in Mind: When needing to manage petabytes of data, how do organisations decide which storage option is best?* . None, 2011.
82. Corporation, N., *NEC LXFS Filesystem.* 2001-2011.
83. Technology, P. *Vtrak E-Series Enterprise Storage Features and Specs*. 2011 [cited 2011; A general description of the Promise VTrak technology, including technical specs and features.]. Available from: http://www.promise.com/storage/raid_series.aspx?region=en-US&m=576&sub_m=sub_m_2&rsn1=1&rsn3=1.
84. Technology, P., *VTrak data sheet.* 2011.
85. Gallyas, F., *Silver staining of myelin by means of physical development.* Neurol Res, 1979. 1(2): p. 203-9.

86. Cho, A., et al., *A method for rapid demineralization of teeth and bones.* Open Dent J, 2010. 4: p. 223-9.
87. Chute, R. and H.V.d. Sompel, *A Reuse Friendly, Open Source JPEG 2000 Image Server.* D-Lib Magazine, 2008. 14.
88. Reiner, A., et al., *Pathway tracing using biotinylated dextran amines.* J Neurosci Methods, 2000. 103(1): p. 23-37.
89. Callaway, E.M., *A molecular and genetic arsenal for systems neuroscience.* Trends Neurosci, 2005. 28(4): p. 196-201.
90. Wickersham, I.R., et al., *Retrograde neuronal tracing with a deletion-mutant rabies virus.* Nat Methods, 2007. 4(1): p. 47-9.
91. Chamberlin, N.L., et al., *Recombinant adeno-associated virus vector: use for transgene expression and anterograde tract tracing in the CNS.* Brain Res, 1998. 793(1-2): p. 169-75.
92. Pinskiy, V., et al., *Tape-transfer assisted cryosectioning for the Mouse Brain Architecture project.* Society for Neuroscience Annual Meeting, 2010.
93. Perova, Z., et al., *High-throughput brain-wide mapping of neuronal activity in behavioral depression.* Society for Neuroscience Annual Meeting, 2011.
94. Taniguchi, H., et al., *A resource of Cre driver lines for genetic targeting of GABAergic neurons in cerebral cortex.* Neuron, 2011. 71(6): p. 995-1013.
95. Pinskiy, V., et al., *High-throughput whole brain neuroanatomical mapping of gabaergic cell types in C57bl/6 mice.* Society for Neuroscience Annual Meeting, 2011.

Appendix A: Mouse Brain Architecture Technical White Paper

Technical White Paper: Mouse Brain Architecture Project

Project Overview

The *Brain Architecture Project* is an ongoing effort to assemble and integrate information about connectivity in the vertebrate brain. As part of this effort, we previously prepared a position paper[1] that argues for a systematic effort to map neural connectivity brainwide, starting with the mouse. The paper called for comprehensive connectivity assessment using light microscopy, and argues for the use of existing methods rooted in classical neuroanatomy, scaled up, standardized, and modernized for high throughput usage in an experimental and data analysis pipeline. We stressed the importance of integration with existing resources including the Allen Brain Atlas (ABA)[2], and open access to project data, following the model of genome projects. Based on these principles, the Mouse Brain Architecture (MBA) project was started in fall of 2009.

The technical goal of the MBA project is to generate brain-wide maps of neural connectivity in the mouse, which will specify the inputs and outputs of major brain regions. Our approach uses standardized methods to label neuronal projections, followed by light microscopic visualization, and finally computational methods to integrate the results. These steps are integrated into a *pipeline* for performing experiments with high throughput and fidelity, including quality control steps at each stage.

Support

The planning stage of the project, including meetings at the Banbury conference center at CSHL as well as initial informatics work, was made possible by an award from the Keck Foundation. Major funding for the Mouse Brain Architecture project comes from a Challenge Grant from the National Institutes of Health (RC1MH088659) and a Transformative Award from the Office of the NIH Director (R01MH087988). Additional sources of funding include internal funding at Cold Spring Harbor Laboratory.

Process Overview

To determine the outputs of a brain region (i.e., the other regions it projects to), it is injected with a small amount of *anterograde* tracer[3] that is taken up by neurons locally and transported down the axons to the "target" (output) regions. After an appropriate transport period, the brain is perfused, sectioned, suitably stained, and each section digitally imaged. These 2-D images are co-registered into a 3-D computer stack that is subsequently registered to a common reference atlas. The resulting 3-D brain image is largely unlabeled (i.e., contains no signal of interest), except for the connections between the injected region and its target regions. Thus the labeled connections are clearly identifiable. A given region is injected in multiple animals to account for individual variability.

To determine the inputs to the same brain region as above, a *retrograde* tracer (taken up by axonal terminals and transported to neuronal cell bodies[3]) is injected in the same stereotaxic location and the process is repeated.

A systematic grid of injections spanning the brain is used to generate a brainwide connectivity map. Each injection is placed in a different individual mouse and the resulting 3D image volumes co-registered in order to obtain the connectivity atlas.

Pipeline Overview

The MBA histology pipeline is used for all tissue processing in the MBA project. The pipeline consists of several discrete stations, as shown in the figure:
(A) C57BL/6 mice are screened to match specific age and weight requirements. Each selected animal then receives injection of a neuronal tracer (classical or viral) into a predetermined brain region. After the incubation period (tracer specific, but typically 3-21 days), the animal is perfused, and the brain is extracted and frozen in a customized mold that allows for two brains to be frozen side by side (B). The block containing two brains is then serially cryosectioned (C) using the tape-transfer method (specifically engineered for the MBA pipeline), and all sections are mounted directly onto slides. Alternating sections are separated to form two distinct series per brain. One series is processed for conventional cell body staining (D). The alternate slide series is either processed for tracer detection through histochemistry (E) or is directly coverslipped for fluorescent imaging (in the case of viral tracers). Whole-slide digital imaging is performed using an Olympus Nanozoomer HT system that is capable of scanning in brightfield (8 bits per color channel) and in fluorescence (12 bits per color channel) modes. The resulting

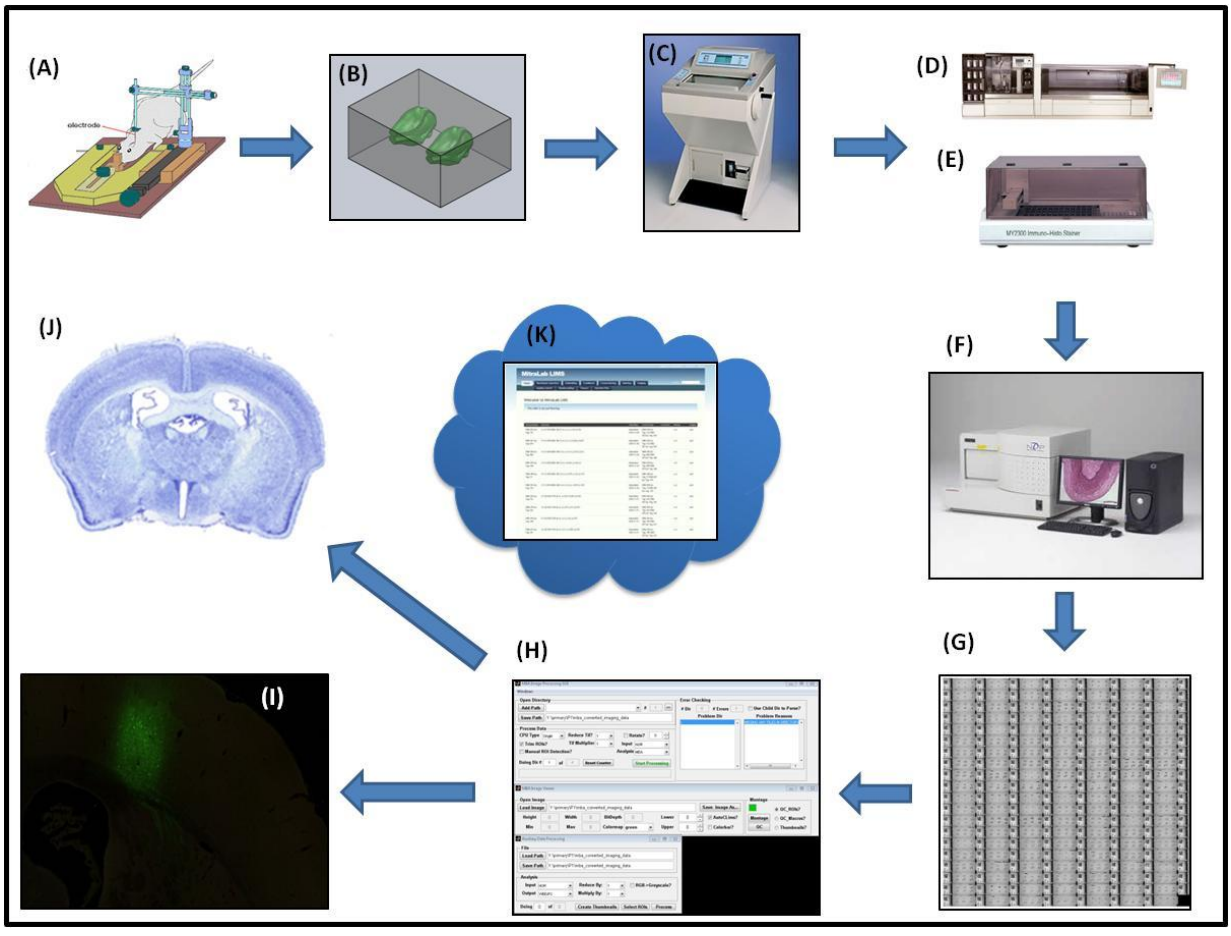

raw data (G) are processed through a custom MATLAB program (H), in which the individual sections are cropped and converted into a specialized file format that is conducive to downstream processing. The result of the experimental pipeline is a large data stack of several hundred sections per brain. Raw image data (0.5µm pixel dimensions) are stored online without lossy compression (I and J). All process metadata, along with investigator observations, are stored in an integrated custom-designed Laboratory Information Management System (LIMS), which helps keep track of all samples and pipeline activities (K).

Inclusion Criteria

The MBA project uses mice purchased from Jackson Labs (Catalog# 664): (1) Strain = C57BL/6; (2) Sex = Male; (3) Age= 53±4 days; (4) Weight= 18.8 - 26.4 grams and (5) Quarantine Period = 7-14 days.

Animal Care

All experiments and procedures were discussed and approved by the CSHL Institutional Animal Care and Use Committee, and conform to all federal regulations, including the NIH Guidelines for *the Care and Use of Laboratory Animals*. Part of our motivation in this project is to generate a community-wide digital database of neuronal circuitry in mouse. Ultimately, therefore, this should result in fewer animals being needed in other experimental protocols, throughout the US (and internationally).

Injection Coordinates

The target injection coordinates for the connectivity dataset were based on the Allen Reference Atlas (ARA). A total of 250 targets were placed in the left-hemisphere of the brain. These injections were volumetrically divided across the structures in the ARA. Regions defined in the atlas that occupied less than 0.4% of the left-hemisphere were subsumed into larger structures (of which they are subdivisions according to the ARA). For each resulting structure, a sphere packing schema was assumed to ensure uniformity of injection spacing, and one injection site is targeted at the center of each sphere. In order to separate the regions, the injection sites are constrained not to be too close to the boundary of the targeted region. For neocortex, we placed injections in a columnar line (normal to the cortical surface).

Classical Neuronal Tracers

Cholera Toxin subunit B (CTB)[4] is used for retrograde tracing and biotinylated dextran amine (BDA)[5] is used for anterograde tracing. CTB (1%) is prepared from a stock solution (List Biological Laboratories) and BDA (10%) is used in the 10,000 MW form (Invitrogen) to ensure primarily anterograde tracing[3].

Viral Neuronal Tracers

Both rabies and adeno-associated (AAV)[6] viral tracers are used as part of the connectivity project. The AAV viral tracers are obtained from the Virus Core Facility at the University of Pennsylvania, in two principle forms: (1) AAV2/1.CB7.CI.EGFP.WPRE.RBG, which expresses green fluorescent protein (EGFP) and (2) AAV2/1.CAG.tdTomato.WPRE.SV40, which expresses red fluorescent protein (tdtomato). For cortical injections, both colors are used, per animal, to target different cortical layers. Modified rabies viruses are used for retrograde tracing

(RV-4GFP(B19G)) as well as for anterograde tracing (RV-1E5nB6SR(VSVG)). These viruses were produced by Ian Wickersham (MIT)[7, 8].

Tissue Sectioning

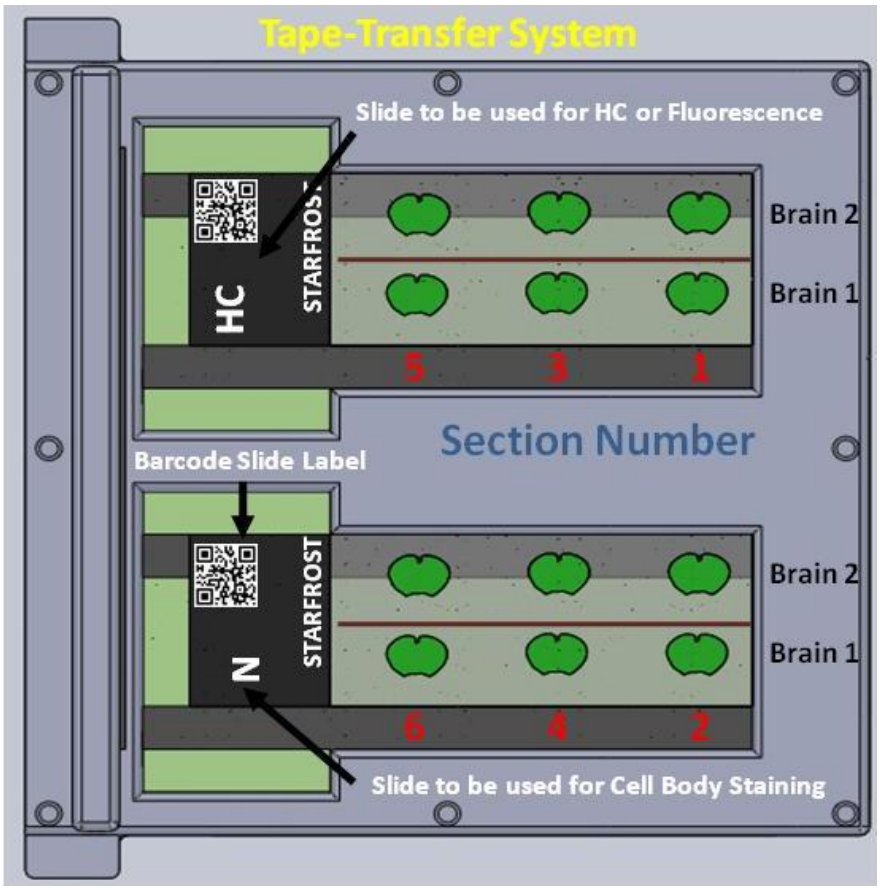

All samples processed through the MBA pipeline are sectioned using a cryostat (Microm HM 550/560) at 20µm thickness, in the specified plane of sectioning. Sectioning is performed using a modified tape-transfer system. The system allows for collections of alternating slides, across two slides. Sections and slides are maintained in the cold stream of the cryostat, to ensure consistency in temperature of the sections. Each brain block is sectioned entirely, and every section is collected onto the slide. Three segments of tape are placed per slide; each segment contains sections from two brains (unless otherwise noted), for a total of six brain sections mounted on each slide. Post-sectioning, all samples are placed in a slide box and maintained at 4°C until staining.

Glass Slides, Slide Coating, Slide Labeling, and Section Order Schema

Standard, uncoated Starfrost slides are used throughout the project. The slides are cleaned and pre-coated in-house. The coating is specific to the intended use of the slides. All slides are barcode labeled (data matrix) with appropriate metadata for each experiment.

Conventional Staining & Coverslipping

Cell Body Staining

Cell body staining is performed using the Tissue-Tek Prisma, Automated Slide Stainer (Sakura). Staining is performed in groups of 60 slides. A Nissl (thionin) staining protocol is used. Staining times were standardized for all samples. All reagents are routinely tested for lot-to-lot consistency.

Dehydration
Fluorescent samples that have undergone immunofluorescence or similar enhancement are dehydrated using the Tissue-Tek Prisma system. Dehydration is performed by passing the slides through a linear ethanol gradient (70%→95%→100%) for several minutes for each step. The slides are then coverslipped.

Giemsa Counterstain
For slides that have undergone enzyme histochemical processing (HC), a Giemsa based counterstain is performed, followed by dehydration of the slides and coverslipping. Giemsa is a cell body stain and also acts to enhance the HC label.

Coverslipping
Slides are coverslipped using the Tissue-Tek Glas g2, Automated Slide Coverslipper (Sakura). A xylene-based mounting medium is used for all samples. After coverslipping, slides are manually unloaded onto a drying rack and examined to ensure that the coverslip does not overhang the edges and that mounting media covers all sections. Slides are allowed to dry for 24 hours before further use.

Enzyme and Immuno-Histochemical Staining

Both enzyme histochemistry (HC) and immunohistochemistry (IHC) are performed on the slide. Staining is performed using a modified LabVision720 (Thermo Scientific) or two parallel Dako Autostainers. Modifications were made to the slide holders of both instruments to facilitate slide-to-slide consistency. A closed-system, forced air, steam humidifier is also connected to the chamber of each unit, and this provides important direct humidity control of the staining chamber.

IHC Detection of Cholera Toxin Subunit B (CTB)
For CTB, the detection protocol consists of a short protein block, prolonged incubation in primary antibody, incubation in secondary antibody, incubation in Avidin-Biotinylated solution (Vector "ABC" Kit), and finally through a DAB histochemical reaction. Slides are hydrated in PBS prior to staining and washed with PBS between each incubation step (with the exception of protein block →1º Antibody).

HC Detection of Biotinylated Dextran Amines (BDA)
BDA is already conjugated with biotin, therefore the detection protocol calls for a prolonged incubation in Avidin-Biotinylated solution (Vector "ABC" Kit), followed by a final DAB histochemical reaction.

Diaminobenzidine (DAB) Histochemical Reaction
The principal form of DAB (Thermo Scientific) used throughout the project is heavy metal enhanced DAB. The solution is prepared fresh, with H_2O_2 added no more than 5 minutes prior to immersion of the slides. Following the incubation, slides are thoroughly washed with PBS to stop the reaction. For some early datasets, an alternative version of DAB was used (Invitrogen).

Image Acquisition

The Nanozoomer HT Virtual Microscopy system (Hamamatsu/Olympus) is used to digitally image all tissue samples resulting from the pipeline. All scanning is performed using a 20X objective (0.46µm per pixel). Brightfield scanning is used for Nissl, IHC, and HC stained slides. Fluorescence scanning at 12-bit depth per pixel, per color channel, using a tri-pass filter cube (FITC/TX-RED/DAPI), is used for all other samples (Rabies and AAV injections). A Lumen Dynamics X-Cite *exacte* light source is used to produce the excitation fluorescence. Cropping boxes are individually positioned around each section and 9-12 focus points are placed per section. Image file names are derived from the barcoded slide name.

Data Conversion and Data Storage

Shortly after image acquisition, the whole-slide data are cropped into individual sections and converted into a custom image data structure. Quality control is performed to ensure that the cropping was done correctly. All data are subsequently transferred to a high-performance storage cluster, through an integrated 10G copper network. Daily backups of the data are created. Data are subjected only to lossless compression; we perform lossy compression for purposes of web display, but raw data is retained in uncompressed form.

Data Presentation Pipeline

Following data conversion, individual brain sections are registered to one another using a rigid-body transformation, and then, using a deformable transformation, are registered to a 3-D digital version of the ARA by custom software developed in MATLAB. Registered 2-D images are placed in a standard bounding box and converted into the JPEG2000 (ISO/IEC 15444-1) image format using custom scripts based on the Kakadu toolkit[9].

The project website has been developed using a combination of technologies, and allows for browsing and viewing high resolution images. The JPEG2000 images are served over the web using a modified version of the Djatoka Image Server[10] and a custom image viewer based on the aDORe Djatoka / IIPMooViewer, which allows for fully interactive zoom and pan, supports online adjustment of RGB dynamic range, as well as gamma adjustment. The website also contains educational units based on the image data and integrates with a variety of other online web tools, such as the Brain Architecture Management System (BAMS)[11].

Laboratory Information Management System (LIMS) and Quality Control

Sample metadata and process-related information are stored in an intranet accessible LIMS system. The system is designed specifically for the pipeline and has dedicated sections for each pipeline station, with multiple fields - each encapsulating an important variable of the process. Status of a sample within the pipeline, priority of processing, reagent control, quality control, and overall pipeline management is performed via LIMS. Investigator observations and general notes are recorded at each pipeline station. Specimens are first entered into the system at the step of stereotaxic injection.

A formal quality control procedure is employed to assess the quality of materials at different stages. This is in order to: (A) Determine possible need to re-inject, re-coverslip, re-image; (B) Correct or improve the pipeline process in an evolutionary operation (EvOp) methodology and (C) Flag unusable sections or materials to reduce unnecessary post-processing. Major QC stages, including examination of slides immediately after coverslipping and after scanning, are formalized into a number of attributes to be checked to ensure consistency across operators and for record keeping.

References:

1. Bohland, J.W., et al., *A Proposal for a Coordinated Effort for the Determination of Brainwide Neuroanatomical Connectivity in Model Organisms at a Mesoscopic Scale.* PLoS Comput Biol, 2009. 5(3): p. e1000334.

2. Lein, E.S., et al., *Genome-wide atlas of gene expression in the adult mouse brain.* Nature, 2007. 445(7124): p. 168-76.

3. Vercelli, A., et al., *Recent techniques for tracing pathways in the central nervous system of developing and adult mammals.* Brain Res Bull, 2000. 51(1): p. 11-28.

4. Luppi, P.H., P. Fort, and M. Jouvet, *Iontophoretic application of unconjugated cholera toxin B subunit (CTb) combined with immunohistochemistry of neurochemical substances: a method for transmitter identification of retrogradely labeled neurons.* Brain Res, 1990. 534(1-2): p. 209-24.

5. Reiner, A., et al., *Pathway tracing using biotinylated dextran amines.* J Neurosci Methods, 2000. 103(1): p. 23-37.

6. Chamberlin, N.L., et al., *Recombinant adeno-associated virus vector: use for transgene expression and anterograde tract tracing in the CNS.* Brain Res, 1998. 793(1-2): p. 169-75.

7. Callaway, E.M., *A molecular and genetic arsenal for systems neuroscience.* Trends Neurosci, 2005. 28(4): p. 196-201.

8. Wickersham, I.R., et al., *Retrograde neuronal tracing with a deletion-mutant rabies virus.* Nat Methods, 2007. 4(1): p. 47-9.

9. Taubman, D.S. and M.W. Marcellin, *JPEG 2000: Image Compression Fundamentals, Standards and Practice*2001, Norwell, MA: Kluwer Academic Publishers.

10. Chute, R. and H.V.d. Sompel, *A Reuse Friendly, Open Source JPEG 2000 Image Server.* D-Lib Magazine, 2008. 14.

11. Bota, M., H.W. Dong, and L.W. Swanson, *Brain architecture management system.* Neuroinformatics, 2005. 3(1): p. 15-48.